Hydrology and hydrochemistry of a High Arctic glacier: Longyearbreen, Svalbard

Master Thesis, 2006 (Revised Edition)

Mette Riger-Kusk

Department of Earth Sciences, University of Aarhus
Department of Geology, University Centre in Svalbard (UNIS)

Acknowledgments

I am extremely grateful to have had the opportunity to study geology in a place like Svalbard. This would not have been possible without financial support from the University Centre in Svalbard (UNIS) and the University of Aarhus.

Water level measurements were kindly provided by Ole Humlum, Adjunct Professor at UNIS, while meteorological data were provided by the Norwegian Meteorological Institute.

I wish to thank all the people who helped me during fieldwork. Karoline Bælum for great teamwork and many enjoyable hours during GPR data acquisition, Henrik Rasmussen and Rico Behlke for scooter assistance, Jannick Schültz for his help with digging snow pits and Helena Grev and Ken Martinussen for their help with water sampling. I also wish to thank all the people who decided to join me on my daily walks to Longyearbreen, and who paid me social calls during periods of camping. It was much appreciated. A special thank you also goes to Marie Kirkegaard Sørensen and Anne Camilla Stavnsgaard Nielsen for always offering a place to sleep during my stays in Aarhus.

Furthermore, I would like to thank the staff at UNIS and Aarhus University, especially Berit Jakobsen, librarian at UNIS, for always finding the references I needed and those I did not know I needed. Fred Skancke Hansen, head of logistics and safety at UNIS, for help arranging the fieldwork and for not naming my fieldwork *the* most stupid fieldwork he had ever heard about. Bente Rasmussen, laboratory technician at the University Aarhus, for guiding me through the laboratory work and Ruth Nielsen, technical assistant at the University of Aarhus, for her map design and technical support.

I wish to thank my supervisor Professor Niels Tvis Knudsen, University of Aarhus and associated Professor Hanne Hvidtfeldt Christiansen, University Centre in Svalbard for advice and encouragement during the fieldwork and writing process. In addition, I wish to thank Ph.D. Jacob Yde, University of Aarhus for his help and support during the entire making of this thesis.

Finally, I wish to express my gratitude to my family, especially my mum, dad and brother, who have been there all the way, as always. And I wish to thank Mark, who made my time on Svalbard so amazing and who continues to inspire me every day.

Front page photograph: Aerial photograph of the study area. The characteristic Sarkofagen mountain separates the two glaciers Larsbreen (furthest to the left) and Longyearbreen. Longyearbreen acts as a major transport routes for snow scooter traffic in the winter and spring and a scooter track is visible on the glacier (photograph: Rico Behlke, April 2004).

Abstract

A detailed study of the hydrology and hydrochemistry of Longyearbreen, a small (2.9 km^2) High Arctic valley glacier on Svalbard, is presented in this master thesis. Sedimentary rocks with a high content of organic matter are present in the study area and plant fossils and coal are abundant on the debris-covered frontal part of Longyearbreen. Fieldwork was carried out in the spring and summer of 2004 and comprised a GPR (Ground Penetrating Radar) survey with 100 MHz antennae and daily sampling of glacial meltwater for future oxygen isotope, solute and suspended sediment analyses. Water samples were collected manually twice a day during most of the ablation period.

The GPR survey showed no indication of zones with temperate ice in the glacier, which was found to have a maximum ice thickness of 110 m. Longyearbreen is therefore thought to be entirely cold-based. However, evidence of a former zone of temperate ice was found in the uppermost parts of the glacier, where unclear ice/bed interfaces most likely reflect a layer of debris-rich basal ice. The glacier has probably undergone a change in thermal regime from polythermal to the present cold-based conditions since the end of the Little Ice Age. Ice-marginal thrust faults, which include the glacier bed, suggest that the marginal areas of the glacier have potentially been cold-based during the entire existence of the glacier. Ice depth differences between two GPR surveys show that during the last 11 years, average thinning of the glacier ice at different altitudes has been comparable to mass balance observations from other ice masses on Svalbard.

The study of suspended sediment concentrations in the glacier meltwater revealed that due to the cold-based conditions, most of the transported sediment was acquired from ice-marginal and proglacial areas. No exhaustion of sediment supply was observed during the ablation period. Discharge measurements showed an early melt period where variations in snowmelt were dampened because of storage of meltwater in the snowpack and within the glacial drainage system. High solute concentrations in the meltwater arose from the preferential leaching of ions from the melting snowpack and the enrichment of the meltwater as it overflowed refrozen solute-rich water in a subglacial meltwater channel. A rapid transition occurred on 30 June from a snowmelt-dominated runoff to a runoff highly influenced by icemelt. Rapid and large discharge fluctuations were observed, reflecting the release of water from storage and a better correlation with air temperature and precipitation events. River meltwater was highly influenced by rapidly draining solute poor and ^{18}O-rich icemelt. During the late ablation period, air temperature and discharge correlated well. Diurnal variations in $\delta^{18}O$ value and solute content were related to diurnal variations in discharge. The variations in $\delta^{18}O$ and Cl^- reflected an increased proportion of snowmelt during low discharge, while a general raise in solute concentration during low ice ablation signified a larger influence of solute-rich pore water from the thawing active layer. Generally, the solute concentrations were high compared to previous studies of glacial meltwater, with SO_4^{2-} as the dominant ion (41%) and HCO_3^- constituting only 5.8% of total solute content. The chemical evolution of the meltwater was from hydrolysis of feldspar and carbonates driven almost entirely by sulphide oxidation. The results suggest that chemical weathering of suspended sediments was of minor importance and that the majority of solutes in the glacial meltwater originated from seepage of solute-rich pore water from the active layer into the ice-marginal drainage channels.

Contents

1. Introduction

In recent years there has been increasing interest in the hydrological and hydrochemical regime of glaciers for two broad reasons. First, a better understanding of glacierized catchments is a prerequisite for exploiting glaciers as energy and drinking water resources. Secondly, research improves knowledge of past glacier response to climatic changes, essential to the ongoing discussion concerning glaciers and present and future climatic change.

The archipelago of Svalbard is located where water and air masses with very different characteristics meet and where sea-ice-extent can vary rapidly. These factors influence the present climate on Svalbard and even the smallest change in any of these can lead to variations in the local climate (Ådlandsvik and Loeng, 1991; Førland et al., 1997; Benestad et al., 2002). Significant temperature variations during the 20th century have been documented on Svalbard (Førland et al., 1997; Duplessy et al., 2001) giving support to the generally accepted theory that the High Arctic is more sensitive to climatic variations than lower latitude areas (Kattenberg et al., 1996; Humlum et al., 2005). This makes Svalbard a key area of glacier study in elucidating potential effects of global warming.

This master thesis investigates the hydrology and hydrochemistry of Longyearbreen, a High Arctic glacier on Svalbard, using GPR, isotope hydrology and meltwater chemistry. Similar studies were conducted on Longyearbreen in 1993-94. Comparisons with these and other relevant studies yield important information about Longyearbreen, High Arctic glaciers in general and how glaciers might respond to a changing climate.

1.1 Outline of thesis

A description of the study area is given in section 2. This comprises a brief introduction to the archipelago of Svalbard, a description of the recent and present climate on Svalbard, the present glaciation and geology in the study area. A detailed description of Longyearbreen and results of former studies of the glacier is also presented in this section. In section 3, a theoretical introduction to the different disciplines applied in this master thesis is given. Here, a general description of the hydrological systems that govern in different types of glacier is followed by an introduction to GPR, discharge variations in a glacial system and the transport of suspended sediments, solutes and oxygen isotopes in glacial meltwater. Data collection and methodology are presented in section 4 where procedures during and following fieldwork are described and evaluated for each discipline. In section 5 results from the fieldwork are presented and related to influencing factors. A discussion of the results in section 6 relates them to previous studies on Longyearbreen and to relevant studies of glaciers, predominantly on Svalbard. The thesis is concluded in section 7.

2. Study area description

2.1 Svalbard

The archipelago of Svalbard has an area of 63 000 km^2 and is located in the northern part of the Barents Sea between 74°N and 81°N, and 10°E and 35°E (see figure 2.1).

Figure 2.1. Svalbard in the Arctic (www.sysselmannen.svalbard.no).

The largest island on Svalbard is called Spitsbergen and has an area of 39 000 km^2 (see figure 2.2). Only two permanent settlements, Longyearbyen and Barentsburg, exist on Svalbard. Longyearbyen (78°13'N, 15°35'E) is the biggest settlement with about 1700, mainly Norwegian inhabitants. The University Centre in Svalbard (UNIS) is situated in this town. The coal-mining settlement of Barentsburg has about 900 inhabitants mainly of Russian and Ukrainian origin. Currently a Norwegian mining settlement and several research stations, run by scientists from all over the world, are also located on Spitsbergen. The glacier studied in this master thesis is called Longyearbreen (78°11'N, 15°30'E) and is located only 2.6 km from Longyearbyen. The locations of glaciers on Svalbard referred to in the text are shown in appendix A.1.

2.2 Climate on Svalbard

Svalbard has a High Arctic climate, which is defined as a climatic environment where insolation and consequently air temperature have small diurnal but large annually fluctuations (French, 1996). Due to its high latitudinal position, Svalbard experiences between about 3 (74°N) and 4 ½ (81°N) months of midnight sun and polar night every year. However, the climate on Svalbard is relatively mild compared to other landmasses located at the same latitude. This is because the final branch of the warm Atlantic current reaches the western coast of Svalbard, thereby raising the temperature of the surroundings. Along the eastern coast of Svalbard cold water leaves the Arctic basin, resulting in a marked temperature difference between the eastern and western parts of the archipelago.

Figure 2.2. Map of Svalbard (http://kart.npolar.no).

The maritime position of Svalbard influences precipitation patterns and the coastal regions are more wet than the arid inner parts of the islands (Humlum, 2002). Generally, the western coastal areas are more arid than the eastern coastal areas (Hagen et al., 2003). The mean annual precipitation measured at the weather stations on Spitsbergen is in the range of 180-440 mm y^{-1}, but values as high as 1200 mm y^{-1} have been reported in the south-eastern parts of the island. A general decrease in precipitation occurs towards the northwest (Hanssen-Bauer et al., 1990).

About 60% of the land area is currently covered by glaciers and ice caps (Hagen and Liestøl, 1990). The largest glaciers are found along the western and eastern coasts, while small valley glaciers (< 5 km^2) are frequent in the more arid central and northern parts of Spitsbergen, where the topography and prevailing wind direction are significant factors in glacier formation (Bamber, 1989; Hagen et al., 1993; Humlum, 2002). Conditions are particularly favourable for glacier growth in the cold north-eastern part of Svalbard where Austfonna, the largest ice mass in Svalbard, is located.

Sea-ice extent around Svalbard can vary a great deal from year to year. In general, sailing around the archipelago is possible during summer, while sea-ice can surround the island during wintertime. The northward drift of warm Atlantic water however, keeps open sea conditions to the west of Spitsbergen even in wintertime. The sea-ice extent is positively linked to the location of cold air masses from the north-east (Isaksson, 2005). During both summer and winter, the weather and temperature can change rapidly on Svalbard because of fluctuations in the physical extent of cold air masses from the Arctic basin and warmer air masses entering the Arctic from the southwest (Hanssen-Bauer et al., 1990). These fluctuations are most evident in the wintertime, where the temperature difference between the two air masses is most distinct (Førland et al., 1997).

Svalbard is located in the zone of continuous permafrost, with thicknesses varying between 200 and 450 meters in the central parts of the island. In the coastal regions permafrost thicknesses approach zero (Liestøl, 1977, www.unis.no/research). Above the perennially frozen permafrost is the active layer, which thaws and freezes seasonally. A maximum average thaw depth of the active layer between 0.1 m and 1 m has been found in the areas surrounding Longyearbyen (www.unis.no/research; Hodgkins, 1998a).

Several meteorological stations are located in Svalbard. Most relevant for this thesis is the station at Longyearbyen airport (78°15'N, 15°28'E) located at 28 m.a.s.l., about 3 km northwest of Longyearbyen and 5-6 km north of the study area (see figure 2.3). A mean annual air temperature of -5.8°C was measured during the period from 1975 to 2000 with February (mean of -15.2°C) and July (mean of 6.2°C) as the coldest and warmest months, respectively (Humlum, 2002). The measured mean annual precipitation is about 190 mm at Longyearbyen (Førland et al., 1997). Humlum (2002) however, modelled precipitation amounts based on 20th century equilibrium lines on glaciers and meteorological observations and suggested precipitation levels as high as 870 mm/year in the study area. The prevailing wind direction in the area surrounding Longyearbyen is from SSE towards NNW (Humlum, 2002). On a local scale however, wind directions are highly dependent on topography.

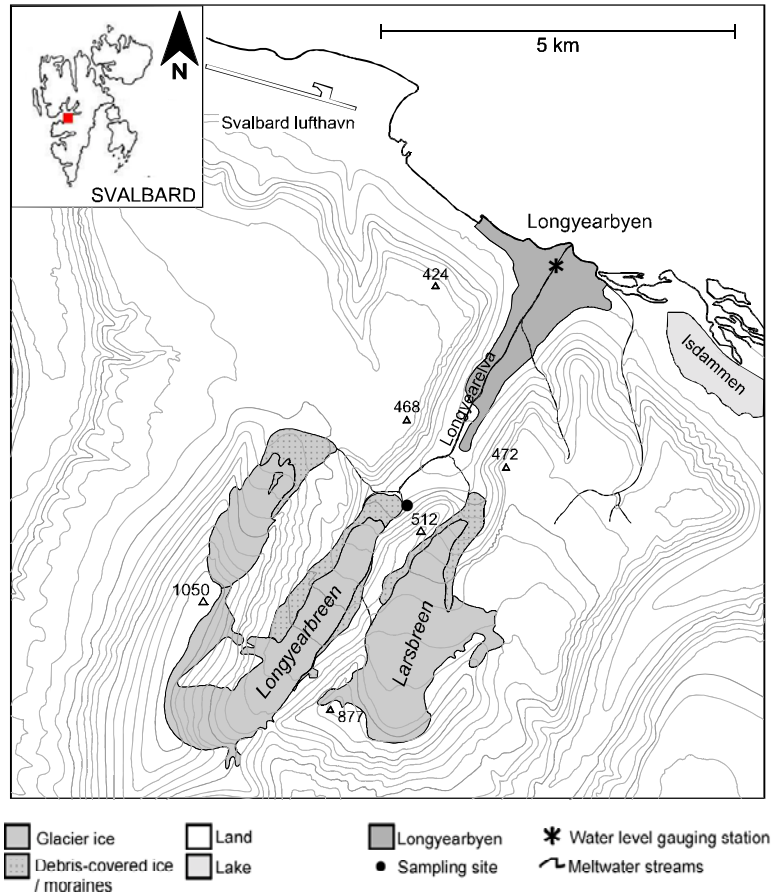

Figure 2.3. Detailed map of the study area. 50 m contour interval.

2.3 Recent climatic variations on Svalbard

The first meteorological station on Svalbard was established in 1912 at Green Harbour, near Barentsburg. Meteorological data collection was initiated in Longyearbyen in 1957 and relocated to Longyearbyen Airport in 1975. In order to reconstruct climatic variations on Svalbard prior to the onset of direct measurements, different methods have been applied such as the study of foraminiferal assemblages in sediment cores (Duplessey et al., 2001), radiocarbon-dating of the warm water mussel, *Mytilus edulis*, found in old beach deposits (Salvigsen et al., 1992; Salvigsen 2002), studies of Svalbard glaciers and their deposits (Snyder et al., 2000; Humlum et al., 2005) and the variations of $\delta^{18}O$ in ice cores (Isaksson, 2005).

The Weichselian ice age ended on Svalbard around 10000 years BP with a deglaciation of the inner fjords as a consequence of the Holocene warming (Svendsen and Mangerud, 1997). Studies indicate a temperature optimum from before 9500 years BP to around 3500 years BP (Salvigsen et al., 1992; Salvigsen 2002), with the biggest influence of warm Atlantic water in the northern Barents Sea between 7800 years BP and 6800 years BP (Duplessey et al., 2001). During the relatively warm early and middle Holocene, glaciers on Svalbard were entirely absent or much reduced in size (Snyder et al., 2000; Humlum et al., 2005). Apart from during the 'Medieval warm period' about 1000 years BP glacier growth on Svalbard has been extensive since 3000 years BP (Humlum et al., 2005). Most glaciers on Svalbard had their maximum physical extent in the Holocene during the Little Ice Age (world-wide from around 1550 to 1860 AD), which on Svalbard, ended with a marked temperature increase of several degrees between 1900 and 1920 AD. This increase was much more pronounced than in northern Scandinavia, emphasizing the sensitivity of the Arctic in relation to climatic variations (Lefauconnier and Hagen; 1990, Hagen and Liestøl, 1990; Humlum et al., 2005). From 1957 to 1968, the mean annual air temperature decreased several degrees, but has since gradually increased (Humlum et al., 2005). In recent years, several specimens of living *Mytilus edulis* have reappeared in waters along the western coast of Spitsbergen and adjacent fjords, possibly indicating a recent increase in sea surface temperatures (Berge et al., 2005).

2.4 Glaciers on Svalbard

Glaciers on Svalbard are either cold based, frozen throughout the entire body, or polythermal, at the pressure melting point in the inner and upper areas but with frozen marginal zones. Often, ice bodies such as icings and pingoes, with periodical running water are observed in front of polythermal glaciers due to leaching of water from under the frozen glacier terminus, and up through the permafrost under increased hydrostatic pressure (Hagen and Liestøl, 1990).

The direct precipitation on Svalbard glaciers is limited (see section 2.2) and other processes such as wind drifting and avalanching of snow are important mechanisms in adding mass to the glaciers during winter (Humlum, 2002). Superimposed ice (frozen, soaked snow) formed in the lower accumulation area between the snowline and the equilibrium line (Paterson, 2001), also play an important role in the mass balance due to the cold surface layers on most of the glaciers. Hagen and Liestøl (1990) found that between 0.1 and 0.2 m of

superimposed ice on average accumulated on the surface of two Svalbard glaciers every year, corresponding to 10-30 % of the total snow accumulation.

Ablation, or the loss of mass from glaciers, mainly depends on mean summer air temperature, and the calving rate for glaciers terminating at sea (Humlum, 2002). Based on long-term monthly mean air temperature data from two meteorological stations in the western coast of Spitsbergen, ablation from glaciers may take place from early June to mid-September (Hodson et al. 2000). Peak discharge from glaciers usually occurs in the late summer where the passage of warm weather systems from the south may result in high air temperatures in combination with precipitation (Sund, 2004).

Glaciers on Svalbard flow with relatively low velocities due to the low ice temperatures (Paterson, 2001) and their frozen margins. Ice velocities are typically around 2 m y^{-1} in the lower ablation area (Hagen et al., 2003). The altitude of the equilibrium line (The line between accumulation area and ablation area on the glacier surface at the end of the ablation period) for glaciers on Svalbard lies above 600 m.a.s.l. in the central parts of Svalbard, between 200 and 300 m.a.s.l. in the eastern coastal areas and between 300 and 400 m.a.s.l in the western coastal areas (Hagen et al., 2003). These variations are mainly caused by differences in precipitation patterns (Humlum, 2002; Hagen et al., 2003).

If a glacier is in equilibrium with the present climate, the amount of ablation equals the amount of accumulation (mass balance equals zero) (Paterson, 2001). On Svalbard fluctuations in glacier extent has been shown to occur throughout the Holocene (Lefauconnier et al., 1990; Hagen and liestøl, 1990; Hagen et al., 2003; Humlum et al., 2005). Humlum et al. (2005) for example dated old vegetation frozen in situ at the glacier bed of Longyearbreen on Svalbard, and found that the glacier had expanded by about 2 km during the last 1100 years. Glaciers on Svalbard and smaller low-lying glaciers in particular (Hagen et al., 2003) are not considered to be in equilibrium with the present climate (Hagen and Liestøl, 1990). Studies of mass-balance on glaciers on Svalbard during the last 30 years have shown that the glaciers have had a constant negative mass balance probably since the end of the Little Ice Age (Lefauconnier and Hagen, 1990; Hagen and Liestøl, 1990; Hagen et al., 2003).

Surging glaciers are common on Svalbard, and estimates of the proportion of glaciers that have surged in the past have been as high as 90 % (Hagen and Liestøl, 1990), although other studies suggest a more moderate percentage of 36 % (Hamilton and Dowdeswell, 1996). As this thesis is being written, a glacier on Svalbard called Paulabreen, has been surging since the beginning of 2005 and an advance of about 1 km in the period from 21 April to 15 August has been documented by UNIS (www.forskning.no/Artikler; www.unis.no/research).

2.5 Geological setting of study area

Longyearbreen (2.9 km^2), Larsbreen (3.0 km^2) and a smaller unnamed glacier (0.3 km^2) are located in the inner part of Longyeardalen (see figure 2.3). Longyeardalen terminates in Adventfjorden, which opens into Isfjorden, the largest SW-NE oriented fjord on Svalbard (see figure 2.2). Longyearbyen occupies most of outer Longyeardalen and is still expanding,

while a smaller part of the settlement called Nybyen is located about 3 km up the valley. Longyeardalen is flanked by plateau mountains about 500 meters in height (figure 2.5).

In the outer part of Longyeardalen the Cretaceous Carolinefjellet Formation is visible (green colour on figure 2.4), a marine sequence of shales, siltstones, and sandstones. The overlying formations are of lower Tertiary origin and in total they constitute a thickness of about 1000 m (yellow colours on figure 2.4). The oldest section, the Firkanten Formation, is in level with the glacier terminus of Longyearbreen. It is overlain by the Basilika Formation, the Sarkofagen Formation, the Gibsonryggen Formation, the Battfjellet Formation and lastly the Aspelintoppen Formation (Major and Nagy, 1972; Hjelle, 1993). This latter formation is visible at Nordenskiöldtoppen (~1050 m.a.s.l.), the highest mountain in the area.

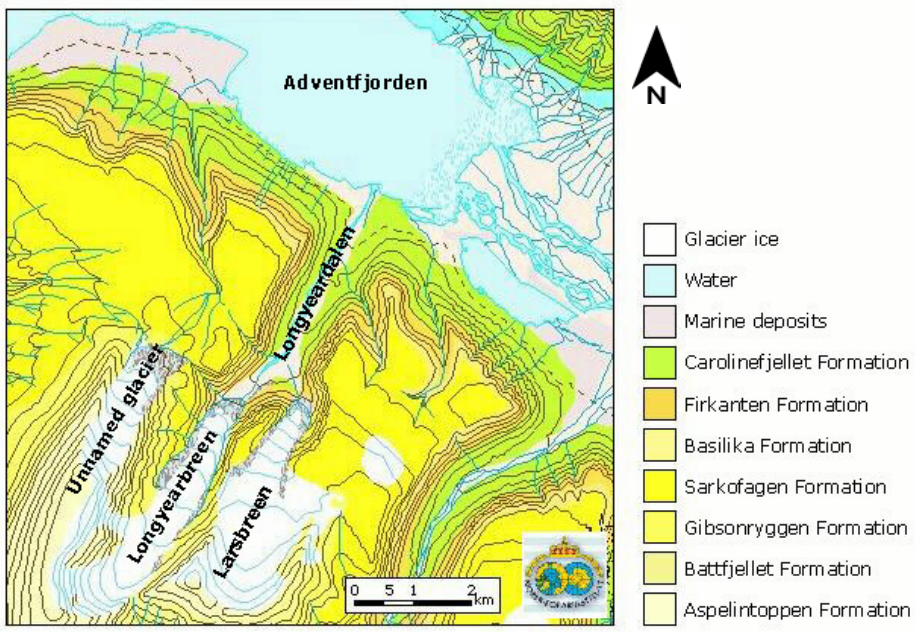

Figure 2.4. Geological map of the study area. 50 m contour interval (http://kart.npolar.no).

The tertiary sequence consists of marine, estuarine or terrestrial facies of mainly sandstone and shale deposits. Five coal seams are present in the lower part of the Firkanten Formation and several coal companies have had mining operations in these layers. Another prominent feature of the tertiary sequence is the abundance of plant fossils in the Aspelintoppen Formation (Major and Nagy, 1972; Hjelle, 1993). This formation is heavily weathered and mass wasting and avalanching on the mountain sides, transport eroded rocks onto the surface of Longyearbreen where they are incorporated into the ice. Beautiful fossils can therefore be found on the debris-covered glacier terminus and it is a popular tourist site during summer.

2.6 **Longyearbreen**

Longyearbreen is a small valley glacier with an area of about 2.9 km^2. The glacier is approximately 4.8 km long, about 520 meters wide and it located between 210 and 850 m.a.s.l. (Bringedal, 2004). The glacier has a relatively flat main body of ice with two small accumulation basins expanding towards the south-western and western mountain sides

(Etzelmüller et al., 2000; Tonning, 1996; Bringedal, 2004). In 2001 the equilibrium line altitude (ELA) was estimated to lay at about 615 m.a.s.l. (Bringedal, 2004).

The photograph in figure 2.5 is taken from the opposite side of Adventfjorden showing Longyeardalen and the two glaciers, Larsbreen (left) and Longyearbreen (right). The glaciers are separated by the 512 m high Sarkofagen mountain and behind it, the 877 m high Lars Hierta mountain. Permafrost thicknesses in the area vary between 150 m under the glacier to about 450 m under the surrounding mountains (Justad, 1997).

Figure 2.5. Longyearbyen and the two glaciers Larsbreen (left) and Longyearbreen (right) (photograph: Karoline Bælum, August 2003).

Like most of the glaciers on Svalbard, Longyearbreen is thought to have experienced its maximum physical extent during The Little Ice Age. The glacier has since thinned considerably and old trimlines suggest that the glacier was 20-30 meters thicker in some places around 1920 AD (Humlum et al. 2003). Mass-balance measurements were carried out on Longyearbreen from 1977 to 1982 showing a constant mean annual net balance of -0.55 m water equivalent per year (Hagen and Liestøl, 1990). Due to the debris-covered terminus, Longyearbreen has not retreated significantly since the Little Ice Age. To date, no evidence of past surging behaviour of Longyearbreen has been discovered (Etzelmüller et al., 2000; Humlum et al., 2005).

Due to the proximity of Longyearbreen to an urban area, it has been the subject of numerous studies. Ice-flow velocity of the glacier was measured in a geodetic survey from 1993 to 1995 and was found to vary between 2 and 4 m y^{-1} in the accumulation area, decreasing to less than 1 m y^{-1} at the glacier terminus (Etzelmüller et al., 2000). Evidence of velocity variations perpendicular to the flow direction can clearly be observed from the sediment-rich, convex shaped ice layers on the glacier surface (see figure 2.6). These layers occur when airborne dust particles are transported to the glaciers from the dry autumn river

beds. Along the glacier margin where the ice is frozen to the sides and ice velocity is low, bands are almost parallel with the flow direction. Conversely the bands are perpendicular along the centreline where friction to the surroundings is less significant.

Figure 2.6. Sediment-bands within the ice give evidence of differences in ice velocity across the glacier. Supraglacial channels are seen meandering down glacier (August 2004).

In April 1993 a GPR survey conducted on the glacier, found the depth along the central flow line to be about 80 m and the total volume of the glacier to be around 0.122 km^3 (Etzelmüller et al., 2000; Tonning, 1996). The survey also revealed patches of temperate ice with thicknesses largely below 10 m and covering about 75% of the glacier bed. The strongest evidence of temperate ice was found in the uppermost parts of the glacier where ice thicknesses reached 115 m (Tonning, 1996). The subglacial relief below Longyearbreen was found to be V-shaped, indicating limited rates of basal erosion possibly due to subzero conditions at the glacier bed (Etzelmüller et al., 2000). Humlum et al. (2005), found vegetation frozen in situ at the glacier bed in a subglacial channel about 2 km from the glacier front and 150 m from the lateral glacier border, indicating that the glacier at this location has been cold based since it advanced over the vegetation. There are no pingos or other indications of water leaving Longyearbreen during winter. If temperate ice does exists under Longyearbreen, it is therefore most likely in the form of thin, isolated patches.

A large debris-covered terminus characterizes Longyearbreen. This has previously been described as an ice-cored moraine complex (Etzelmüller et al., 2002), but was redefined because of the large amounts of active ice under the debris cover, the lack of glacier retreat since the Little Ice Age and the subzero ground temperature conditions (Bringedal, 2004). Lateral moraines are present on both sides of the glacier towards the ELA. The glacier surface is smooth and crevasses are only seen as bergschrunds at the uppermost part, towards Nordenskiöldtoppen. A single moulin is present on the western part of the glacier, about 1.3 km from the glacier snout. In summer, melt water is lead to the glacier bed through this structure.

Longyearbreen drains a catchment with an area of 10.68 km^2 where 43% is glacierized (based on map from Tonning, 1996). Of this, 1.3 km^2 covers the upper western area of Larsbreen, from which meltwater is routed through lateral moraines on Sarkofagen mountain towards Longyearbreen. Furthermore, water is drained from the unnamed glacier, towards the western meltwater stream emanating from Longyearbreen. 43% of the catchment is glacier covered. Snowmelt from the glacier-free areas of the catchment is usually complete by the end of July, after which meltwater originating from the glaciers and precipitation events dominate the river runoff (Grønsten, 1998).

On the upper and middle section of Longyearbreen, most meltwater drains the glacier surface supraglacial. Supraglacial channels are present in the middle of the glacier towards the debris-covered glacier snout, where they confluence (see figure 2.6 and figure 2.7). However, the majority of the supraglacial channels are directed to the margins of the glacier where they become increasingly incised and subsequently englacial upon reaching a depth of 8-12 meters due to ice deformation (Hansen, 2001; Humlum et al., 2005). The western lateral channel is more incised and drains englacial and subglacial for a considerable distance, while the eastern lateral meltwater channel disappears into the glacier ice just before reaching the debris-covered glacier snout (figure 2.7).

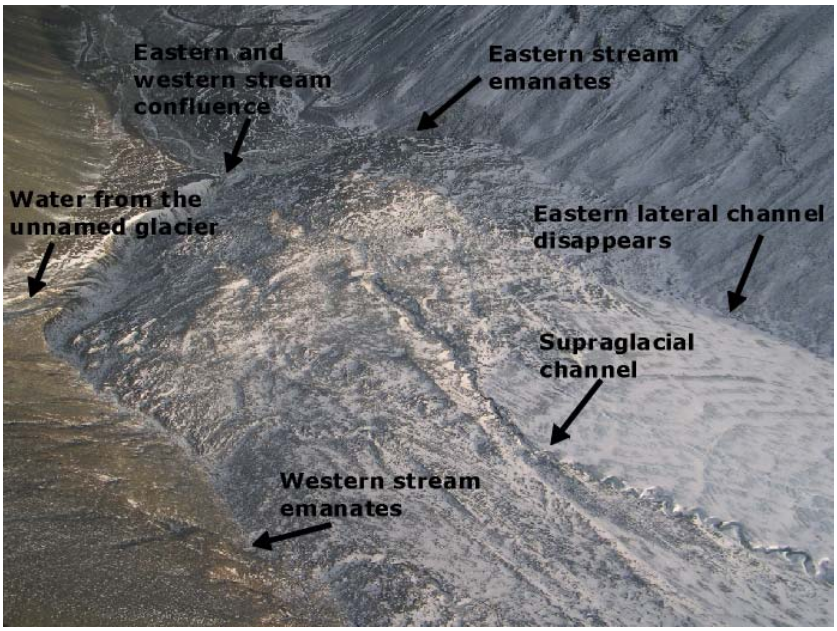

Figure 2.7. Photograph of the debris-covered frontal area of Longyearbreen with indications of major hydrological features (Photograph: Anders, September 2004).

The western lateral channel is accessible during winter, giving a unique opportunity to study the structure of the glacier ice and the evolution of the hydrological system first hand (figure 2.8). The channel reaches the glacier bed 20-50 meters below the surface, allowing the meltwater to come into contact with the underlying sediment (Etzelmüller et al., 2000; Hansen, 2001; Humlum et al. 2003). The channel is continuously evolving, and a net incision rate of approximately 1 m y^{-1} was found by Hansen (2001) about 2 km from the terminus.

Figure 2.8. Englacial channel found in extension of the incised western lateral channel. Channel height is about 1.2 m.

Two main meltwater streams leave the glacier along each margin. The western stream emanates from the side of the debris-covered frontal ice, while the eastern stream emerges from below the debris-covered terminus. The western meltwater stream runs along the edge of the debris-covered glacier snout and is joined by some of the meltwater from the unnamed glacier on Nordenskiöld. In front of the debris-covered terminus, the western meltwater stream confluences with the eastern meltwater stream and several smaller meltwater streams, which run on the surface or emanate from within the debris-covered glacier terminus (see figure 2.7). The meeting of streams forms Longyearelva. Further downstream, Longyearelva flows together with meltwater from Larsbreen (Larselva) (see figure 2.3).

Sægrov (1995) studied the solute and suspended sediment transport in river meltwater from Larsbreen and Longyearbreen. Suspended sediment load carried by the meltwater emanating from the glacier was similar to values for temperate and polythermal glacier. The sediment was thought to be derived primarily from the debris-covered terminus but also from lateral moraines and subglacial water contact with sediments (Etzelmüller, 2000; Hodgkins, 1997a). The amount of solutes in meltwater from Longyearbreen suggested a high input of sea-salts, comparable to previous studies of glaciers on Svalbard. Sægrov (1995), argued that meltwater from Longyearbreen acquired solutes from the underlying glacier bed and within the sediment-rich frontal ice.

3. Theoretical background

3.1 Glacial hydrology

Glaciers can, according to their temperature regime, roughly be divided into the following three categories: temperate glaciers, where the entire ice body is at the pressure melting point; polythermal glaciers, that have cold (temperature below melting point) marginal regions but an inner and upper region of temperate (temperature at the pressure melting point) ice; and lastly cold glaciers which are frozen throughout the entire body (Paterson, 2001).

The physical properties of cold and temperate ice differ, and glaciers with different thermal regimes have, among other things, different drainage systems. The chemical signature of the bulk meltwater from a glacier is the result of the origin of the meltwater, routing of the water through different drainage structures and accessibility of geological materials during drainage (Hodson et al. 1997). These factors all relate to the drainage system of the individual glacier. A basic understanding of glacial hydrology is therefore necessary when working with meltwater chemistry. The hydraulic systems that exist in temperate, polythermal and cold glaciers are closely related, and in order to provide an understanding the mechanisms governing meltwater drainage, all three types are described below.

3.1.1 Temperate glaciers

Temperate glaciers (see figure 3.1) are at the pressure melting point throughout the entire glacier body, except for a thin surface-layer, which can be frozen during winter (Benn and Evans, 1998). The temperature regime of temperate glaciers is mainly a result of thick ice depressing the melting point, effective insulation of the glacier ice by a thick snow-cover and lastly the release of heat from meltwater penetrating the snow, firn (partially melted one year old snow, with granular texture) and ice. Temperate glaciers are abundant in Scandinavia, East Greenland and the Alps, where mean annual air temperature is relatively high and precipitation levels large. Temperate glaciers are fast moving ice masses because of the high ice temperature, and are therefore characterized by a relatively large number of crevasses and moulins (Paterson, 2001).

Meltwater on temperate glaciers originates mostly from surface melting of snow and ice. The majority of the ablation therefore takes place during summer, where air temperatures above zero result in extensive surface melting. Frictional heat released from the deforming ice and geothermal heat flux from the underlying rocks can also melt considerable amounts of ice (Bennet and Glasser, 1999). Icemelt therefore takes place all year and water is often observed leaving temperate glaciers during winter.

Snowmelt is the first water to leave the glacier surface in the spring. The water percolates through the snowpack where it either refreezes, subsequently raising the temperature of the residual snow, or eventually reaches the underlying firn (only present in the accumulation

area) or glacier surface. The release of latent heat as water freezes is an important mechanism in raising temperature of snow, firn and glacier ice. The transient snowline (the line between snow and glacier ice or firn) moves up-glacier as the summer progresses and more and more icemelt consequently contributes to the bulk meltwater (Benn and Evans, 1998).

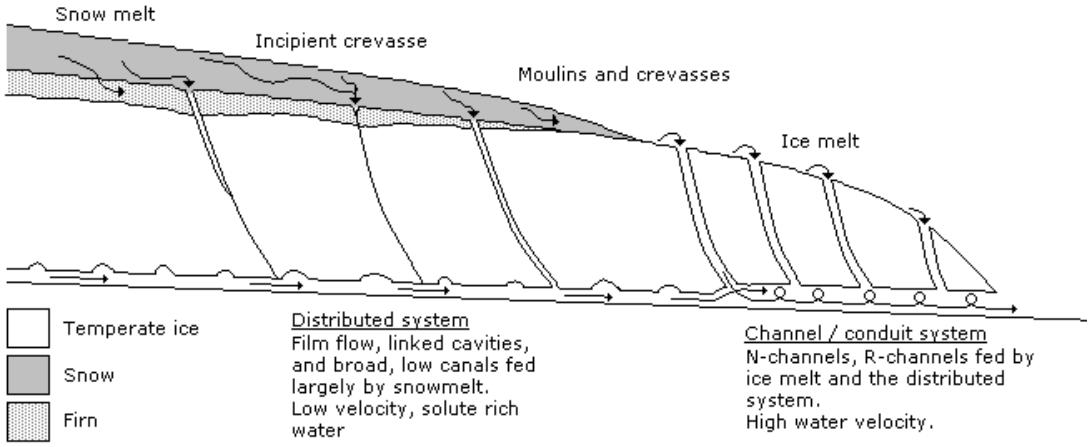

Figure 3.1. Schematic representation of possible drainage systems in temperate glaciers (after Brown, 2002)

The melting of snow is slower than the melting of ice due to the higher albedo of ice (Hodgkins, 1997a; Benn and Evans, 1998). Different hydrological systems therefore govern above and below the transient snowline. Above the snowline, the snowmelt slowly and constantly percolates first the snowpack and then the permeable firn layer. Considerable amounts of water can be stored within the snowpack and firn resulting in a damping of the diurnal variations in surface melting (Jansson et al., 2003). When reaching the ice surface, the water is routed either in supraglacial channels or along the firn-ice boundary to crevasses and moulins which englacially, through enlarging of intergranular veins, drain the water to a subglacial distributed hydraulic system. The distributed system consists of small cavities created in the lee side of obstacles on the glacier bed and small N-channels cut into the basal till, both connected by intergranular veins in the ice. The system is characterized by low flow velocity and thus by high residence time for the water (Fountain and Walder, 1998). This water mass was first recognized by Collins (1977) and has been referred to as delayed flow (Tranter et al., 1993) and as the base flow (Paterson, 2001) of a glacier. The delayed flow is very solute-rich because of the abundance of subglacial sediments and the long water:rock contact time in the slow draining distributed system (Collins, 1977 and 1979; Paterson, 2001; Tranter et al., 1993).

Below the snowline, in the ablation area, different conditions prevail. The icemelt is more responsive to meteorological conditions than snow and no significant storage of meltwater takes place. A larger amount of meltwater is therefore rapidly routed in supraglacial channels to well developed crevasses and moulins that englacially lead the water towards the glacier bed (Collins, 1977). In the subglacial hydraulic system under the lower part of the glacier, water is drained rapidly through large, stable R-channels cut into the ice and mainly kept open by frictional heat from the meltwater. This conduit system is much more efficient than the distributed system (Fountain and Walder, 1998). Tranter et al. (1993) referred to this ice-melt derived water mass as the quick flow component. Water:rock

contact time of the conduit system is low and access to erodible subglacial sediments is limited due to the confined channel structure. Quick flow will therefore contain fewer dissolved ions than the delayed flow (Collins, 1977 and 1979; Paterson, 2001; Tranter et al., 1993).

The delayed flow and the quick flow mix in the channelized hydraulic system and the water emanating from the glacier will therefore be a mix of the two components. The largest fraction of delayed flow meltwater occurs during low discharge when ice ablation is low but temporarily stored water still percolates through the snow and firn layers above the transient snow line (Collins, 1977 and 1979). Temperate glaciers are highly erosive agents, due to the well-developed subglacial drainage systems that exist under the entire glacier (Bennet and Glasser, 1999).

3.1.2 **Polythermal glaciers**

Polythermal glaciers (subpolar glaciers) with temperate inner and upper regions are abundant on Svalbard where precipitation is relatively sparse and temperatures low (see figure 3.2). The temperate zones occur where the glacier is thick enough to reach the pressure melting point, the insulation snow-cover is thick and where latent heat is released from meltwater in a firn-layer during the melt season. Subzero temperatures are found along the margins of the glacier and in the accumulation area where the ice is thinnest and heating of the glacier ice during summer takes place through inefficient heat conduction (Björnsson et al., 1996; Hodgkins, 1997a). Polythermal glaciers in general, move with lower velocities than their temperate counterparts due to both the subzero temperatures in the marginal regions and a lower mass balance gradient caused by lower accumulation and ablation. As a result, fewer crevasses and moulins are usually present (Hodkins, 1997a). The changing temperature regimes in polythermal glaciers result in a complex drainage system. In the temperate ice on the polythermal glacier, drainage structures are similar to those present in temperate glaciers (see figure 3.2).

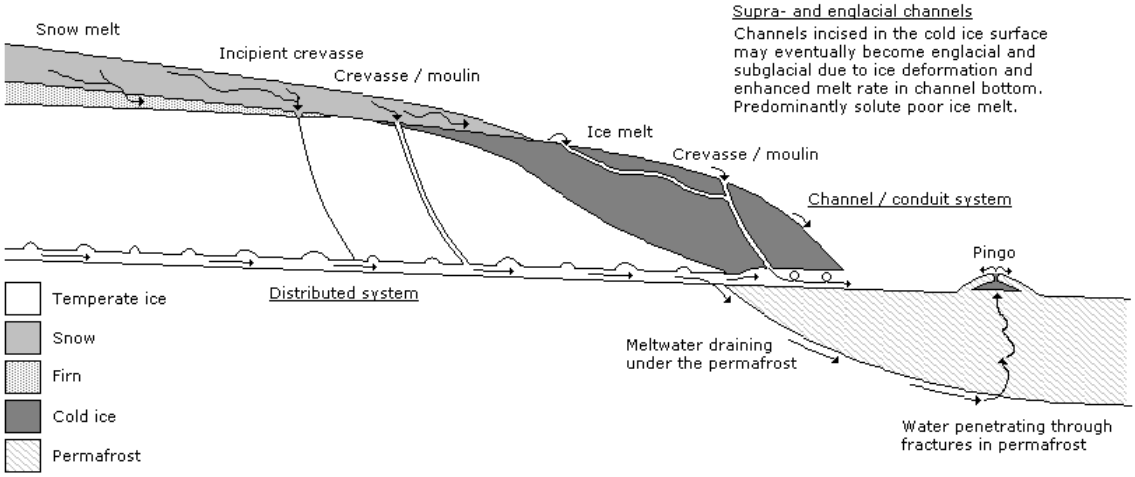

Figure 3.2. Schematic representation of possible drainage systems in polythermal glaciers (after Wadham et al., 1998). See also figure 3.1.

In the cold part of the glacier, englacial and subglacial drainage structures are limited. This is because fewer crevasses and moulins exist to lead the water into the glacier, and because of the refreezing of meltwater upon contact with cold ice, leading to the sealing of potential drainage structures (Hodgkins, 1997a). Meltwater therefore primarily drains the glacier surface through supraglacial channels that tend to be driven towards the glacial margins by the ice surface slope (Wadham et al., 1998). Supraglacial channels can become deeply incised into the glacier ice due to enhanced melting of the channel floor as heat is transferred from the meltwater to the ice (Etzelmüller et al., 2000; Hansen, 2001). When reaching a certain depth, ice deformation closes off the upper part of the channel and the supraglacial channel becomes englacial. Down cutting of channels in cold ice is slow but may eventually result in the channel reaching the base of the ice. Crevasses and moulins may also drain water from the cold glacier surface if in contact with an englacial or subglacial drainage network (Hodgkins, 1997a; Etzelmüller et al.; 2000, Hansen, 2001; Boon and Sharp, 2003). Drainage structures in cold ice are therefore not necessarily limited to supraglacial channels and water may be routed through the cold ice in both englacial and subglacial channels, although limited in extent. However, this is only possible if the rate of water flow through the cold ice is sufficient to prevent the channels from freezing in (Tranter et al. 1996; Hodson et al., 1997). If subglacial drainage is present under the cold ice, the water is thought to be confined to a few large and stable channels which, together with the presence of permafrost, limit the erosive powers of this type of glacier (Hodgkins, 1997a).

Pingos are abundant in front of polythermal glaciers, because subglacial meltwater from the temperate part of the glacier may penetrate into the thawed ground below the permafrost in the frontal area of the glacier. The water then rises to the surface under high hydraulic pressure through weaknesses in the permafrost, before contributing to pingo formation (Liestøl, 1977; Wadham et al. 1998). If no channels connect the distributed system with the conduit system, seepage of water through the permafrost is the principal way of draining water from the temperate part of the glacier and no evidence of the distributed system will be found in the bulk meltwater (Wadham et al., 1998).

3.1.3 **Cold glaciers**

The third and last category, and most important for this thesis, are the cold glaciers (polar glaciers). Here, the whole glacier is frozen to its bed and consists of ice with temperatures below the pressure melting point (see figure 3.3). Movement is therefore entirely driven by internal deformation (Benn and Evans, 1998). Cold glaciers can be found in Antarctica, the Canadian Arctic and on Svalbard, where temperatures are low and precipitation very sparse. These conditions result in thin glaciers unable to reach the pressure melting point at depth with thin insulating snow- and firn-layers causing a high penetration depth of the winter cold wave.

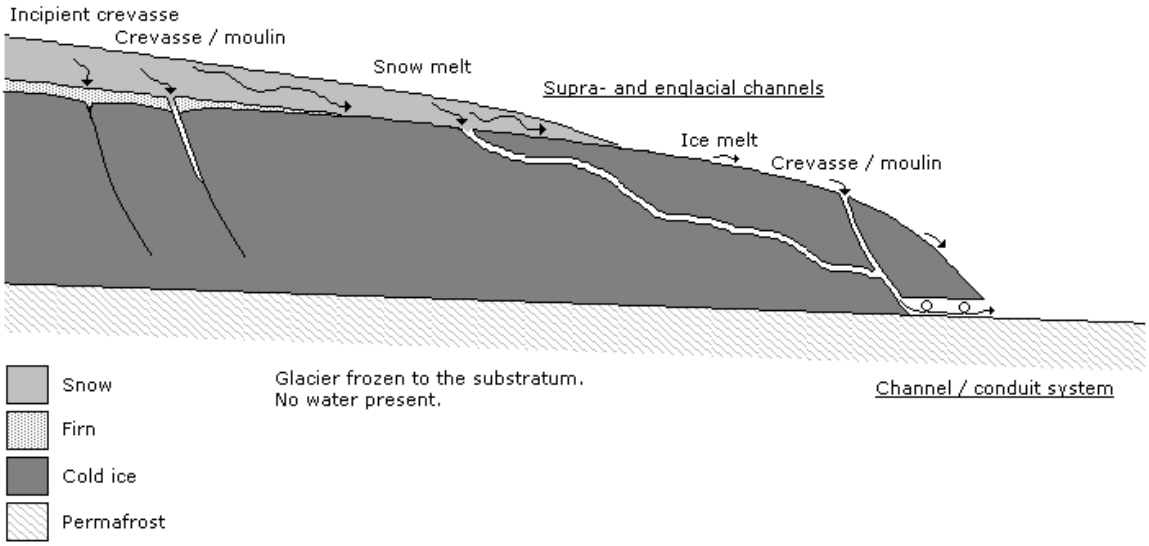

Figure 3.3. Schematic representation of possible drainage systems in cold-based glaciers (see also figure 3.1 and 3.2).

Drainage of meltwater in cold ice has been described in section 3.1.2. The dynamics of cold glaciers is very limited as the deformation rate of ice decreases with temperature (Paterson, 2001). Crevasses and moulins are therefore rare compared to on temperate and polythermal glaciers, but also more permanent for the same reasons (Etzelmüller et al., 2000). Studies on cold glaciers on Svalbard indicate that crevasses and moulins may act as sinks for large amounts of supraglacial meltwater, leading it through englacial and possibly subglacial channels toward the glacier snout (Sægrov, 1995; Hansen, 2001; Boon and Sharp, 2003). If meltwater reaches the glacier bed, drainage to the front takes place in large confined channels (Hodgkins, 1997a). Another important issue when investigating hydraulic systems on cold glaciers is, that glaciers in general have been retreating and thinning since the end of the Little Ice Age, possibly leading to shifts in their temperature regimes. Therefore, polythermal glaciers, which have evolved to cold glaciers, may contain relict hydraulic systems due to the slow deforming cold ice (Hodgkins, 1996 and 2001; Etzelmüller et al., 2000).

Contrary to the temperate and polythermal glaciers, no subglacial delayed flow component exists for cold glaciers and the bulk meltwater is exclusively a result of one type of hydraulic system. However, cold glaciers still experience diurnal variations in meltwater origin, with a greater proportion of snowmelt during low discharge periods, due to storage of snowmelt in the snowpack (Hodgkins, 2001).

Of the three categories of glaciers, cold glaciers exhibit least erosional strength. This is because fresh subglacial sediment is sparse due to the cold base of the glaciers, but also because the meltwater has limited contact with sediment sources before it reaches the moraine area. Large quantities of sediment in the meltwater is therefore not necessarily an indicator of intensive subglacial erosion but more likely shows, that the glacier has access to extensive amounts of sediment in the moraine areas (Hodgkins, 1997b and 2001; Etzelmüller et al.; Hodson et al., 2002).

3.2 Ground Penetrating Radar (GPR)

GPR is the most utilized method when mapping dimensions and internal structures such as those in glaciers and ice caps. The initial building blocks for developing the system, as it is known today, were already laid in 1904 by the German scientist, Heinrich Hertz. However, it was not until the mid-1970s that GPR was widely employed for geological purposes (Plewes and Hubbard, 2001). Currently, aside from uses in ice-covered areas, GPR is also widely applied in locating contaminated soil, mineral explorations, mapping of saltwater intrusions and groundwater investigations in sandy soils.

3.2.1 GPR theory

Radar is short for *ra*dio *d*etection *a*nd *r*anging. Basically, an antenna transmits electromagnetic waves of frequencies between 1 and 1000 MHz into the ground and the intensity (amplitude) and shape (phase) of the reflected signal is recorded by a receiving antenna (see figure 3.4). Different geological materials have different propagation velocities resulting in different two-way travel times (TWT) for the electromagnetic wave. Furthermore, the amplitude and phase of the reflected signal provides useful information about the underlying reflector (Annan, 1992).

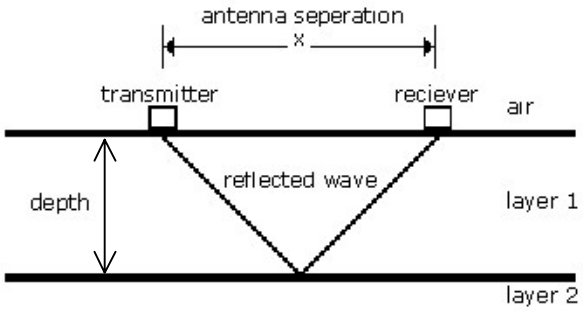

Figure 3.4. Basic GPR setup over a two-layer ground.

The depth of a reflecting layer can be calculated if the radar velocity of the material is known (equation 1). Since the distance x on figure 3.4 is normally significantly smaller than the distance to the reflector, it is assumed that the antennae are located in the same surface point.

$$depth \approx \frac{TWT \cdot velocity}{2} \quad (1)$$

The velocity of the electromagnetic wave depends on the conductivity (σ), the dielectric constant (κ) and the magnetic permeability (μ) of the material in question. For the frequencies used in GPR surveys, the magnetic permeability for a geological material is assumed equal to the value in vacuum. Both the dielectric constant and the conductivity will, for each individual geological material, be treated as constants in this thesis, even though this is not always the case (Plewes and Hubbard, 2001). The influencing factors are however secondary and a more detailed review of these is beyond the scope of this thesis.

Conductivity is a measure of how efficient an electric current is conducted through a material when an electric field is applied. The dielectric constant describes the capacity of a material to store an electric charge. The former refers to conductive currents, while the latter is concerned with displacement currents. The two forces both contribute to the total current flowing in a material when affected by an electric field. This relationship changes with the frequency of the electric field and conductive currents dominate at low frequencies while displacement currents are more important at high frequencies. Where conductive currents prevail, the electromagnetic pulse will attenuate rapidly and a different method than GPR should be applied (Annan, 1992; Plewes and Hubbard, 2001). In table 3.1 examples of electrical properties of some geological materials are shown.

Table 3.1. Dielectric constant, electric conductivity, radar wave velocity and radar wave attenuation of some geological materials (Annan, 1992).

Material	Dielectric constant κ	Conductivity σ [mS/m]	Velocity v [m/ns]	Attenuation α [dB/m]
Air	1	0	0.3	0
Distilled water	80	0.01	0.033	$2*10^{-3}$
Fresh water	80	0.5	0.033	0.1
Sea water	80	$3*10^{3}$	0.01	10^{3}
Dry sand	3-5	0.01	0.15	0.01
Saturated sand	20-30	0.1-1	0.06	0.03-0.3
Limestone	4-8	0.5-2	0.12	0.4-1
Shales	5-15	1-100	0.09	1-100
Silts	5-30	1-100	0.07	1-100
Clays	5-40	2-1000	0.06	1-300
Granite	4-6	0.01-1	0.13	0.01-1
Dry salt	5-6	0.01-1	0.13	0.01-1
Ice	3-4	0.01	0.168	0.01

The electromagnetic wave will be reflected if it encounters changes in the dielectric constant. Large dielectric contrasts result in a large reflection coefficient and lesser energy is, as a consequence, transmitted further into the ground. As the radar wave travels through the ground it attenuates due to absorption in the materials, scattering of energy when reflected from objects or layer boundaries and a loss of wave energy as the rays are geometrically spread in the ground. High frequency radar waves attenuate faster than low frequency waves, but also have the best vertical resolution. When designing a GPR survey, it is therefore vital to balance the resolution with the penetration depth desired (Annan, 1992; Plewes and Hubbard, 2001).

3.2.2 **GPR in glacial settings**

The electric properties of ice listed in table 3.1 clearly illustrates why GPR is an efficient tool when working with glaciers; the dielectric constant and conductivity is extremely low for ice, resulting in low attenuation of the electromagnetic wave. Variations in conductivity and dielectric constant of glacier ice may be caused by density differences, the presence of water bodies and impurities (acids and salts), spatial temperature variations and changes in ice crystal size and their orientation (Bamber, 1987).

Due to the transparency of ice to electromagnetic waves, GPR has widely been used as a tool in determining thicknesses of ice masses. In cold ice, penetration depths as high as 4000 m have been surveyed, compared to 1500 m in temperate ice where water inclusions scatter the electromagnetic signal (Plewes and Hubbard, 2001).

On Svalbard numerous GPR studies have been carried out on glaciers, with different objectives. GPR has proven successful when investigating snow thicknesses (Maijala et al., 1998), firn distribution (Maijala et al., 1998; Moore et al., 1999), the thermal regimes of glaciers through the presence of cold and temperate ice (Bamber, 1987, 1988 and 1989; Jania et al., 1996; Björnsson et al, 1996; Ødegård et al., 1997; Moore et al., 1999), water content in the glacier ice through changes in radar velocity in the ice (Hamran et al., 1996; Moore et al., 1999; Murray et al., 2000), the presence of water at the glacier bed through changes in the power of reflection coefficient (Bamber, 1989; Copland and Sharp, 2001), the existence and extent of debris-bands within glacier ice (Murray et al., 1997) and the presence of water- or air-filled englacial meltwater tunnels in both cold and temperate ice (Bamber, 1987 and 1988; Hagen and Sætrang, 1991; Moore et al., 1999; Bælum, 2006).

3.3 Discharge variations

Quantities of water melting from glaciers vary a great deal both on a diurnal and seasonal scale. Diurnal discharge variations are a reflection of changing meteorological conditions, primarily the air temperature (Gurnell et al., 1994; Hodgkins, 2001). Seasonal variations in discharge reflect the seasonal changes in air temperature. However, they also give indications about changes in meltwater sources through changes in the size of diurnal variations and the development of the drainage system through the observed time lags between ablation and discharge variations (Bennet and Glasser, 1999).

3.3.1 Seasonal evolution of the glacial drainage system

During winter, the hydraulic system is subjected to degradation. Crevasses, moulins and supraglacial channels are blocked with snow, while the refreezing of captured meltwater as subzero temperatures penetrate the glacier ice, may seal off englacial drainage structures. Subglacial hydraulic drainage systems are exposed to heavy stress loading from the deforming ice. The distributed system may survive without much damage, since the drainage structures are mainly kept open by basal sliding. The conduit system on the other hand, collapses where ice deformation rates are high because the channels are primarily kept open by the melting of ice due to frictional heat from flowing meltwater (Fountain and Walder, 1998). Ice deformation for cold ice is low and drainage structures in cold ice may therefore, unlike those in temperate ice, experience little alternation during winter (Vatne, 2001).

When snowmelt initiates in the spring, large volumes of water are stored in the residual snowpack, especially on cold glaciers where ice lenses in the snow and on the ice surface prevent the meltwater from reaching the supraglacial channels (Hodgkins, 1997a). Along with the state of the hydraulic system described above, this results in long travel times for the water, smoothing out discharge variations to meteorological conditions in the early melt

season. As the melting increases, the drainage system of the glacier develops. Conduits enlarge and a new channelized system is established, capable of evacuating the growing volumes of meltwater. The progression is largest for temperate glaciers since they are subjected to the greatest breakdown of drainage structures during winter (Vatne, 2001).

The transient snowline moves up-glacier as the season progresses and icemelt becomes more and more important. This results in a gradual change in the hydraulic system and the drainage patterns for the glacier, since little storage of the meltwater occur below the snowline and the melting rate of snow is slower than that for ice. Discharge patterns therefore change towards a more meteorological driven system, with clearer diurnal cycles of predominately icemelt superimposed on a baseflow component consisting of both snowmelt and icemelt (Bennet and Glasser, 1999).

For temperate glaciers the slow distributed system governs above the transient snowline, while the more efficient conduit system drains predominantly icemelt below the line. The conduit system therefore moves up-glacier as the melt season advances. For polythermal and cold glaciers, a complex drainage system of supraglacial, englacial, and possibly subglacial channels efficiently evacuate the large volumes of meltwater (Hodgkins, 1997a; Fountain and Walder, 1998). There are indications that the transition from snowmelt dominated runoff to runoff highly influenced by icemelt, occurs non-progressively and rapidly for cold glaciers. This is due to the enhanced storage of water in the snowpack, combined with a rapid decay of the soaked snow and an efficient evacuation route for the water through ice-marginal channels (Hodgkins, 2001).

Diurnal variations in bulk meltwater are often observed in late season, where the snowline is near its maximum height. This is clearly illustrated on figure 3.5, which shows discharge curves in fine weather from a temperate glacier near Zermatt, Switzerland (Elliston, 1973). It is seen that as the season advances and the proportion of icemelt to snowmelt increases, diurnal variations in discharge progressively become more and more pronounced. It is also seen that the time lag between maximum melting from the glacier (at noon) and maximum discharge decreases during the summer as the hydraulic system becomes more efficient in routing the meltwater to the glacier snout (Bennet and Glasser, 1999).

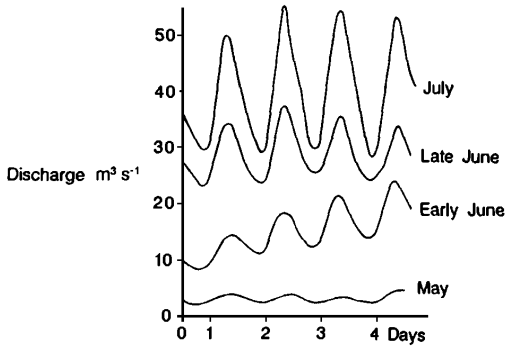

Figure 3.5. Discharge fluctuations in meltwater from a temperate glacier in Switzerland. Diurnal variations become more and more pronounced as the ablation period proceeds (From Bennet and Glasser, 1999, after Elliston, 1973).

An example of the evolution of the glacial drainage system is shown in figure 3.6 where measured discharge (solid line) is compared to simulated discharge (dashed line) estimated from air temperature and precipitation. In the early ablation period discharges are overestimated and meltwater is thought to be temporarily stored, mainly in the snowpack. For the intermediate period, the measured discharge highly exceeds the calculated discharge due to the release of water from storage. The only time where a good correlation exists between the measured discharge and the discharge calculated based on meteorological parameters is in the end of the ablation period, where the transient snowline is approaching its maximum altitude and the drainage system is fully developed (Bennet and Glasser, 1999).

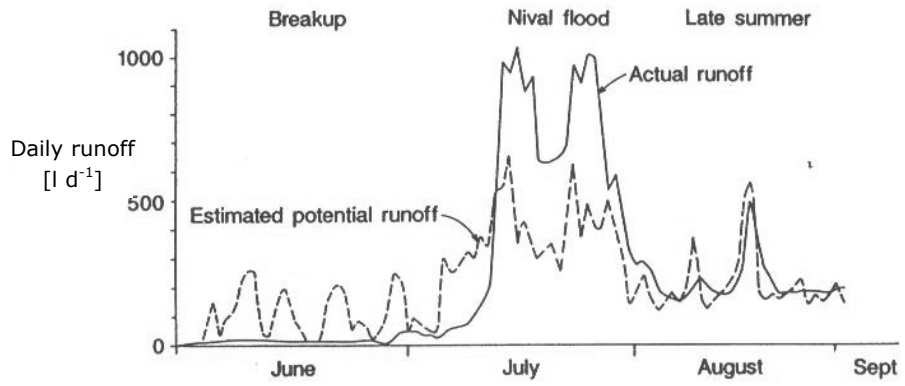

Figure 3.6. Seasonal fluctuations in discharge (from Bennet and Glasser, 1999; after Stenborg, 1970).

3.3.2 **Glacial discharge studies on Svalbard**

Discharge variations of glaciers have been a key research area on Svalbard for the last 30 years and measurements have been conducted at numerous localities by universities from all over the world. Since 1989 the Norwegian Water Resources and Energy Directorate have carried out long-term hydrological investigations on several localities on Spitsbergen (Sund, 2004).

Figure 3.7 shows fluctuations in bulk meltwater from a study made by Wadham et al. (1998) on the polythermal glacier Finsterwalderbreen. The hydrograph has been divided into three different periods. Early melt period, where discharge is low and snowmelt dominates, a peak flow period, where melting of the residual snowpack, icemelt and rain events result in significant discharge fluctuations, and a late season flow recession, where clear diurnal fluctuations are observed due to a lower influence of snowmelt and a well-developed drainage system. In this latter period, clear diurnal variations of icemelt are superimposed on a base flow with a larger proportion of snowmelt.

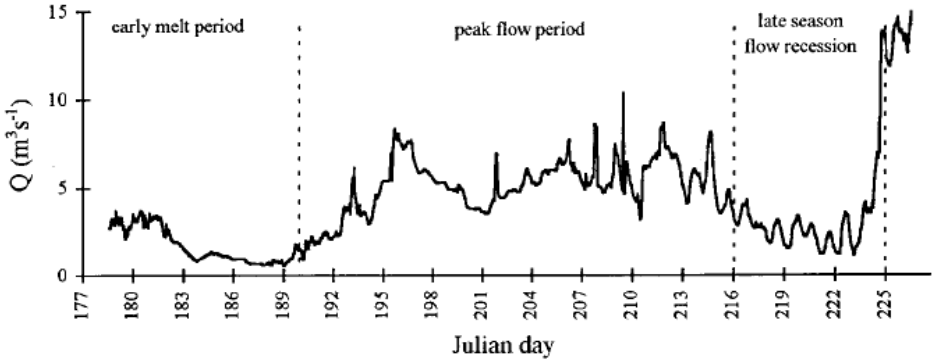

Figure 3.7. Seasonal variations in bulk meltwater from Finsterwalderbreen on Svalbard (Wadham et al., 1998)

Both Tranter et al. (1996) and Wadham et al. (1998) found that the time lags in polythermal glaciers on Svalbard were longer than those seen for temperate glaciers, and that the diurnal variations later in the season were smaller. Chemical analysis of the meltwater suggested that a lesser proportion of the water from polythermal glaciers originated from the snow derived delayed flow component.

Hodgkins (2001) studied the cold-based glacier, Scott Turnerbreen, in the summer of 1992. Unlike for temperate and polythermal glaciers, Hodgkins (2001) found that evolution in the meltwater system for the glacier was non-progressive. Before the 4 August discharge was high and variable and a net loss in meltwater from storage took place. The net loss was shown to be equivalent to the meltwater temporarily stored in the snowpack during the early periods of melting. After 4 August discharges were low and invariable and a small net gain in storage occurred as water refroze in the drainage channels. The rapid change was explained as a fast depletion of stored water in the snowpack caused by a collapse of ice lenses in the snow and on the glacier surface. Clear diurnal variations in discharge were not recognized until the snowmelt had decreased considerably, i.e. after the 4 August 1992. The time lag between maximum melt and maximum discharge was short after the 4 August 1992, indicating an effective and well-developed drainage system (Hodgkins, 2001).

3.4 **Suspended sediment transport**

From observing the muddy meltwater that emanates from a glacier, it is evident that glaciers act as impressive erosional agents. The loud, rumbling sound of rocks being transported by the water as bedload by sliding, rolling or saltation, also makes it clear that suspended sediment concentration (SSC) is not a measure of the total sediment load transported by the water. SSC therefore, does not equal the total amount of erosion caused by the glacier, but merely represents the amount of non-dissolved sediment held in suspension in the water. SSC varies on both a seasonal and diurnal scale and can be used as an indicator of the thermal regime of the glacier, because it reflects the availability of sediments during transport of meltwater through the glacier, and thus the structure of the drainage system (Hodgkins, 1997a; Hodson et al., 1997).

3.4.1 **Sediment transport as an indicator of thermal regime**

A large amount of suspended sediment in the meltwater indicates a well-developed subglacial drainage system with access to abundant amounts of fresh erodable sediments. This is often the case for temperate glaciers, where the bulk meltwater is transported to the glacier snout subglacially over thawed sediments. For polythermal and cold glaciers, subglacial drainage is limited and permafrost makes the sediments less accessible (Gurnell et al., 1994). For these two types of glaciers, and for cold glaciers in particular, much of the entrained sediment is thought to derive from the ice-marginal areas, thereby representing denudation of the marginal moraines rather than erosion caused by the glacier (Hodgkins, 1997a).

In table 3.2, discharge and SSC weighted in relation to discharge, are listed for three glaciers on Svalbard with different temperature regimes (Hodson and Ferguson, 1999). Mean discharge-weighted SSC is, as expected, highest for the largely warm-based Finsterwalderbreen. This is in contrast to the mainly cold-based Austre Brøggerbreen, which has the markedly lowest value, a whole order of magnitude lower than even the intermediate polythermal Erdmannbreen.

*Table 3.2. Discharge and suspended sediment concentrations (SSC) for three Svalbard glaciers. *relative to discharge (Hodson and Ferguson, 1999).*

Glacier	Temperature regime	Mean discharge [$m^3 s^{-1}$]	Mean SSC* [$g l^{-1}$]
Finsterwalderbreen	Largely warm-based	4.0	2.0
Austre Brøggerbreen	Largely cold-based	2.1	0.1
Erdmannbreen	Polythermal	2.2	1.5

Studies have shown that the SSC for temperate glaciers decrease during a melt season indicating an exhaustion of the subglacial sediment supply. This is explained by the gradual replacement of the distributed drainage system with a channelized system where access to subglacial sediments is more restricted (Gurnell et al., 1994; Hodson and Ferguson, 1999). The opposite is the case for cold glaciers, where SSC increase continuously as the ablation season advances. Enhanced degradation of lateral and marginal moraines and proglacial sediment sources as the active layer thaws, are thought to explain the seasonal pattern in SSC in meltwater emanating cold glaciers (Sægrov, 1995; Hodgkins, 1996 and 1997a; Hodson et al., 1998; Hodson and Ferguson, 1999; Etzelmüller et al., 2000). Like cold glaciers, polythermal glaciers are known to have an increase in SSC during the ablation season (Gurnell et al., 1994; Hodson and Ferguson, 1999). A possible explanation to this phenomenon could be the gradual development of a subglacial drainage network (Gurnell et al., 1994).

3.4.2 **Suspended sediment studies on Svalbard**

Several studies of SSC have been conducted on Svalbard, emphasizing the variations between trends seen for glaciers with different temperature regimes. Hodson et al. (1997) compared the polythermal, Finsterwalderbreen to the largely cold-based Austre Brøggerbreen. He found marked differences between the two glaciers. Austre Brøggerbreen had relatively low mean daily SSC compared to Finsterwalderbreen. This was explained by

the absence of a subglacial drainage system under the cold-based parts of the glacier, limiting the access of water to fresh sediment. The suspended sediment in the meltwater emanating from Austre Brøggerbreen, was thought to originate from ice-marginal sediment sources such as lateral moraines and other supraglacial sediments. During high discharge, mass wasting from the sides of the surrounding mountains was thought to contribute to the sediment load. The relatively high SSC of Finsterwalderbreen gave indications of a well-developed stable subglacial drainage system, even though the marginal areas of the glacier are frozen to the ground (Hodson et al., 1997).

Hodgkins (1996) examined discharge and SSC for the cold glacier, Scott Turnerbreen on Svalbard. Like Hodson et al. (1997) he found that the primary source of sediments was in the ice-marginal meltwater channels where sediments were brought to the drainage system by mass wasting from the sides. A progressive increase in SSC in the glacial meltwater was observed during the ablation period illustrating the inexhaustible sediment source (Hodgkins, 1996).

3.5 **Glacier Hydrochemistry**

The chemical composition of meltwater emanating from a glacier front can give valuable information about meltwater sources, different drainage pathways, and availability of ions in these. Both seasonal and diurnal changes in chemistry can be observed as a result of changes in these parameters. Changes in water chemistry from one glacier to another can be immense due to differences in the chemical composition of meltwater sources, in the underlying bedrock geology, in drainage structures, and in the thermal regime of the glaciers. Water chemistry is therefore an important tool when investigating and classifying glaciers (Collins, 1977 and 1979; Tranter et al., 1993 and 1996; Hodson et al., 2000).

The dissociation of dissolved CO_2 from the atmosphere is an important way of supplying protons for chemical weathering to the glacial meltwater (Tranter et al., 1993). Chemical denudation in glacial environment may therefore play an important role in the event of climate change. Enhanced denudation rates brought on by increased melting and suspended sediment load would promote CO_2 drawdown from the atmosphere acting as a negative feedback process (Raiswell, 1984; Sharp et al., 1995). This effect is not to be overlooked since studies have shown that the global mean of CO_2 drawdown for glacierized basins is comparable to some of the world's largest river basins (Hodson et al., 2000).

3.5.1 **Solute provenances**

Glacial meltwater acquires solutes from two principal sources: the atmosphere and sediments within the glacial system. The atmosphere contributes with sea-salts (dominated by Cl^- and Na^+) and other atmospheric aerosols (fx SO_4^{2-} and NO_3^-). Contact with sediments and rocks within the drainage system, gives rise to a wide variety of cations (Ca^{2+}, Mg^{2+}, Na^+ and K^+) and anions (HCO_3^- and SO_4^{2-}) (Tranter et al. 1993; 1996, Hodgkins, 1998b).

Table 3.3 shows mean concentrations of solutes in snow, superimposed ice, glacier ice and rain for the polythermal Finsterwalderbreen on Svalbard (Wadham et al., 1998). The

chemical composition of snow and rain is dependent on the moisture source and air mass trajectory of the precipitation cloud (He and Theakstone, 1994; Raben and Theakstone, 1994). Glaciers located in populated areas can be contaminated by ions originating from anthropogenic activity, whereas maritime glaciers have a higher input of sea-salts compared to continental glaciers. The content of sea-salts in precipitation is expected to reduce during the winter as the presence of sea-ice results in increased distance to the source area, i.e. the open sea (Humlum et al., 1995).

Table 3.3. Solute concentrations [µeq/l] of snow, superimposed ice, glacier ice and rain for Finsterwalderbreen, Svalbard (Wadham et al, 1998). In brackets are shown standard deviation and number of samples.

	Cl^-	SO_4^{2-}	HCO_3^-	Na^+	K^+	Mg^{2+}	Ca^{2+}
Snow	73 (87, *41*)	15 (23, *41*)	12 (50, *41*)	61 (70, *41)*	2.9 (4.7, *41)*	18 (23, *41*)	16 (40, *41)*
Rain	94 (65, *4*)	81 (73, *4*)	46 (46, *4*)	79 (34, *4*)	18 (10, *4*)	22 (10, *4*)	54 (13, *4*)
Glacier ice	13 (9.6, *6*)	4.5 (4.2, *6*)	79 (64, *4*)	11 (4.9, *5*)	3.8 (1.3, *5*)	7.2 (5.4, *5*)	56 (56, *5*)
Superimposed ice	69 (53, *8*)	13 (8.6, *8*)	22 (26, *8*)	69 (45, *8*)	2.5 (2.7, *8*)	15 (12, *8*)	20 (20, *8*)

After the snow has precipitated onto the glacier, melting and refreezing events may change the original chemical stratification of the snowpack, while wind transport of dust particles can raise the ion concentration in the top snow layer. However, studies have shown that vertical variations in the snowpack on Austre Okstindbreen in Norway are greater than horizontal variations, and that only a little, if any, altitude dependency of the ion content can be seen (He and Theakstone, 1994; Raben and Theakstone, 1994). Rainfall events supply ions to the glacial meltwater due to its original chemical composition, and because rainfall from elsewhere in the catchment is enriched with ions when running over rock and sediments prior to entering the glacial drainage system (Theakstone and Knudsen, 1996b). As seen in table 3.3, glacier ice is relatively solute-poor compared to both snow and rain. This is a result of leaching of ions from the snowpack when temperature in the snow approaches 0°C, a process that will be explained in more detail in section 3.5.2. As a distinct contrast to the generally solute-poor ice, colourful, ion-rich bands of ice or firn layers may exist in and on the glacier as a result of autumn wind transport of dust particles when melting ceases and river beds dry out. This is the case on Svalbard, where vegetation is sparse, river beds widespread and wind-forces high (Hodgkins et al., 1997b).

A major supply of ions to the meltwater derives from contact with bedrock and sediments when water flows through the glacial drainage system. The amount and type of chemical weathering produced by the meltwater, highly depends on the chemical composition of the lithologies present in the system. Bluth and Klump (1994) studied the chemical denudation rates of different rocks and presented the following relationship: sandstone > granite > basalt > shale > carbonate, with sandstone showing the least susceptibility to chemical weathering and carbonate rocks the greatest. Hodson et al. (2000) however, found basalt and carbonates to show equal weaknesses to chemical weathering, whereas shales proved to be more resistant than both. Also evaporites and sulphides have high chemical denudation rates (Raiswell, 1984; Tranter et al., 1996). Other factors that increase the

magnitude and rate of chemical weathering are small particle size (due to their larger surface areas by mass), the availability of fresh material and water, the reactivity of the water (the presence of protons and oxygen), and the amount of time the water is in contact with the material (Raiswell, 1984; Tranter et al.; 1996, Brown, 2002).

3.5.2 **Drainage and acquisition of solutes by glacial meltwater**

When the temperature in the snowpack approaches zero degrees in the early ablation period, metamorphism in the snow enlarges the snow crystals. During this process, a differential exclusion of ions from the snow crystals takes place, resulting in the ions being located as a coating on crystal surfaces. Therefore, when the snowpack starts to actually melt and the meltwater penetrates down through the snowpack, ions are rapidly leached. An example of the elution of a snowpack can be seen in figure 3.8, where the change in ionic composition of snow samples collected from Austre Okstindbreen in Norway is shown (Raben and Theakstone, 1994).

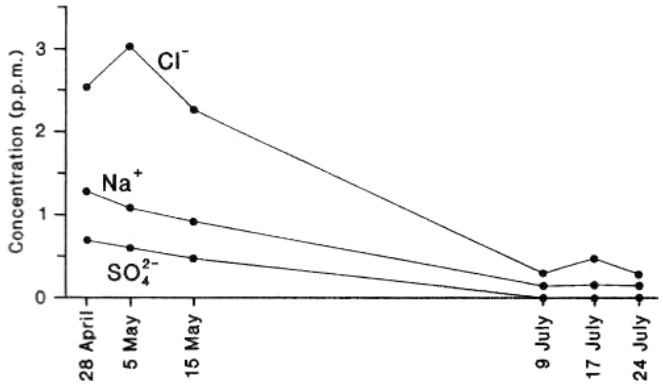

Figure 3.8. Seasonal change in the mean ionic concentration in the snowpack at Austre Okstindbreen in Norway (Raben and Theakstone, 1994).

Studies suggest that SO_4^{2-} is the first ion to leave the snowpack followed by Na^+ and lastly Cl^- (Raben and Theakstone, 1994; Theakstone and Knudsen, 1996a). The preferential leaching of ions with the first meltwater may result in high concentrations of snow pack derived ions in glacial meltwater in the early ablation period. Hodgkins and Tranter (1998b) observed a three to five fold concentration of Cl^- in meltwater compared to the snow pack in the beginning of the ablation period for the maritime, cold-based glacier, Scott Turnerbreen. Ice layers in the snowpack and superimposed ice on the glacier surface, act as impermeable barriers for the first meltwater. High concentrations of ions are therefore, often found just above ice layers and a pulsation of the first snowmelt has been observed as a result of melting ice layers collapsing and releasing solute-rich water to the system (Hodgkins and Tranter, 1998b). Considerable amounts of water can be temporarily stored in the snowpack as a consequence of ice layers and an impermeable glacier surface (He and Theakstone, 1994; Raben and Theakstone, 1994).

As more and more snow melts, the transient equilibrium line moves up-glacier resulting in a fast-growing proportion of the meltwater originating from the more dilute icemelt. Although some chemical weathering may occur within the snowpack (Tranter et al., 1993; Hodson et

al., 2002), the majority of solutes are absorbed after water leaves the snowpack and comes into contact with rock materials in supraglacial, englacial and subglacial drainage structures.

Simple dissolution reactions can take place wherever highly reactive materials such as sea-salt, aerosols from the snow or evaporitic minerals are present. These reactions take place without the use of protons (Tranter et al., 1993). Chemical weathering by acid hydrolysis is the most important mechanism in adding solutes to meltwater. One of the most important ways of supplying protons to the meltwater is by diffusion of CO_2 from the atmosphere into the meltwater where it is dissolved and dissociated (Raiswell, 1984).

Dissociation of CO_2:

$$CO_2(aq) + H_2O(l) \leftrightarrow H^+(aq) + HCO_3^-(aq) \quad (2)$$

Another way to add protons to glacial meltwater is by oxidation of sulphides in the bedrock such as pyrite.

Oxidation of sulphides:

$$\underset{Pyrite}{2FeS_2(s)} + 7O_2(aq) + 2H_2O(l) \leftrightarrow 4SO_4^{2-}(aq) + 2Fe^{2+}(aq) + 4H^+(aq) \quad (3)$$

Diffusion of CO_2 from the atmosphere is a relatively slow process and requires an atmospheric CO_2 source to take place. Oxidation of sulphides is a more rapid reaction that is dependent on the presence of oxygen in the water and of course sulphides in the rocks eroded by the glacier. The anions (HCO_3^- or SO_4^{2-}) present in the meltwater reflect the type of acid source used in the dissolution (Raiswell, 1984).

The partial pressure of CO_2, $p(CO_2)$, in the water, is a reflection of the rate of supply of H^+ to the meltwater by CO_2 drawdown from the atmosphere, and the rate of consumption of protons by chemical weathering. If $p(CO_2)$ is equal to the atmosphere ($p(CO_2) = 10^{-3.5}$ bar), the system is in an equilibrium state where supply of CO_2 equals the removal. This is referred to as an open system. A closed system is where $p(CO_2)$ in the meltwater differs from $p(CO_2)$ in the atmosphere. A low-$p(CO_2)$ system ($p(CO_2) < 10^{-3.5}$ bar), occurs when CO_2 removal exceeds CO_2 supply either because chemical weathering takes place where there is limited access to the atmosphere, or because highly reactive sediments consume protons faster than CO_2 can diffuse into the water to form new. The opposite is the case for high-$p(CO_2)$ systems ($p(CO_2) > 10^{-3.5}$ bar). Here, chemical reactions, such as the coupling of sulphide oxidation and carbonate dissolution (equation 4), supply HCO_3^- to meltwater and consequently enable the formation of CO_2 (equation 2 from right to left) in parts of the drainage system where degasification is limited (Raiswell, 1984; Tranter et al., 1993; Sharp et al., 1995; Hodgkins, 1997b).

Coupled sulphide oxidation-carbonate dissolution:

$$\begin{aligned}&\underset{Pyrite}{4FeS_2(s)} + 16\underset{Carbonate}{Ca_x(Mg_{1-x})CO_3(s)} + 15O_2(aq) + 14H_2O(l) \leftrightarrow \\ &16xCa^{2+}(aq) + 16(1-x)Mg^{2+}(aq) + 8SO_4^{2-}(aq) + 16HCO_3^-(aq) + 4Fe(OH)_3(s)\end{aligned} \quad (4)$$

Chemical denudation in the supraglacial system is relatively sparse (Collins, 1977 and 1979) and predominantly limited to feldspar and carbonate dissolution driven by carbonation (equation 5, 6 and 7) (Tranter et al., 1993 and 1998; Wadham et al., 1998; Hodson et al., 2002).

Carbonation of feldspar:

$$\underset{Albite}{NaAlSi_3O_8}(s) + CO_2(aq) + H_2O(l) \leftrightarrow Na^+(aq) + HCO_3^-(aq) + HAlSi_3O_8(s) \quad (5)$$

$$\underset{Anorthite}{CaAl_2Si_2O_8}(s) + 2CO_2(aq) + 2H_2O(l) \leftrightarrow Ca^{2+}(aq) + 2HCO_3^-(aq) + H_2Al_2Si_2O_8(s) \quad (6)$$

Carbonation of carbonates:

$$\underset{Carbonate}{Ca_x(Mg_{1-x})}CO_3(s) + CO_2(aq) + H_2O(l) \leftrightarrow xCa^{2+}(aq) + (1-x)Mg^{2+}(aq) + 2HCO_3^-(aq) \quad (7)$$

The low denudation rates in supraglacial environments are a reflection of restricted access to weatherable materials, and the fact that the material present may be protected by a coating of low reactive weathering products having spent considerable time on the glacier surface. The residence time of the water is small (hours), leaving very little time for chemical reactions to take place. The supraglacial system is an open system with free access to atmospheric CO_2 and low consumption of protons for weathering (Raiswell, 1984).

The englacial drainage system shows similar characteristics to the supraglacial system. The water velocity is high and the sediments available for chemical denudation are sparse and again carbonation reactions dominate. Even though access to atmospheric CO_2 is limited, englacial channels show open system behaviour due to low chemical weathering (Raiswell, 1984; Wadham et al., 1998).

Most chemical weathering takes place in the subglacial drainage system. In temperate, and to some extent polythermal glaciers, snowmelt reaches a subglacial distributed network of small-scale drainage structures (see section 3.1.1 and 3.1.2). In these structures, the sediment sources are abundant, the suspended sediment load is high, the residence time of the water is high (days), and fresh material is continuously added to the system by abrasion and crushing as the glacier erodes and deforms the bed. The distributed drainage system is a closed system ($pCO_2 \neq 10^{-3.5}$ bar) with no access to atmospheric CO_2 and, even though some carbonation takes place, the majority of protons for chemical weathering are supplied by oxidation of sulphides (Collins, 1977 and 1979; Raiswell, 1984; Tranter et al., 1993). Below three examples of hydrolysis are shown.

Hydrolysis of feldspar:

$$\underset{Albite}{NaAlSi_3O_8}(s) + H_2O(l) \leftrightarrow Na^+(aq) + OH^-(aq) + HAlSi_3O_8(s) \quad (8)$$

$$\underset{Anorthite}{CaAl_2Si_2O_8}(s) + 2H_2O(l) \leftrightarrow Ca^{2+}(aq) + 2OH^-(aq) + H_2Al_2Si_2O_8(s) \quad (9)$$

Hydrolysis of carbonate:

$$\underset{Carbonate}{Ca_x(Mg_{1-x})}CO_3(s) + H_2O(l) \leftrightarrow xCa^{2+}(aq) + (1-x)Mg^{2+}(aq) + OH^-(aq) + HCO_3^-(aq) \quad (10)$$

As the water drains towards the glacier terminus, it enters the more dynamic ice-marginal basal channels. Solute- and suspended sediment-rich water from the distributed drainage system mixes with fast flowing dilute water masses from the englacial channels. The englacial water holds protons due to low rates of weathering, and the subglacial water most likely still carries weatherable material in suspension. Mixing processes of the two water masses might therefore result in further chemical weathering within hours and a change in the partial pressure of CO_2 (Raiswell, 1984; Tranter et al., 1993).

In the conduit system, chemical weathering is lower than that of the distributed system. This is because of shorter residence time for the water and poor access to subglacial sediments due to the larger and more confined meltwater channels. For the polythermal and cold glaciers the availability of fresh sediment sources is also limited because of subzero temperatures at the glacier bed. The partial pressure of CO_2 is higher in the conduit system and carbonation processes dominate (Raiswell, 1984).

For both temperate and polythermal glaciers, the distributed drainage system is where the majority of the chemical weathering takes place. The chemical denudation rate for cold glaciers is significantly smaller since no distributed network is present. Instead, chemical weathering of sediments in ice-marginal channels are an important solute source. Carbonation reactions have been found to dominate this environment while oxidation of sulphides is restricted, primarily because erodible sediments are less abundant in the ice-marginal channels (Hodgkins, 1997a, Hodgkins et al. 1997b, Etzelmüller et al., 2000, Hodson et al., 2000 and 2002). However, studies have shown that the chemical signature of meltwater from cold glaciers may resemble that of water from the distributed system under temperate and polythermal glaciers. This is thought to be due to the slow seepage of solute-rich meltwater into the ice-marginal channels from the thawing active layer in moraines and mountainsides (Hodgkins, 1997b and Hodgkins et al., 1998a).

3.5.3 **Seasonal changes in solute concentrations of bulk meltwater**

As the ions in the snowpack are preferentially leached with the first water draining the snow, the bulk meltwater is dominated by dissolved ions from the snowpack in the early melt period. As the melt season advances snowmelt becomes progressively more dilute and as the transient equilibrium line moves up-glacier, the proportion of rapidly draining dilute icemelt increases. A general trend towards more dilute bulk meltwater is therefore often observed as the melt season progresses (Hodgkins et al., 1997b). Later in the season, when englacial and subglacial drainage systems have developed, diurnal variations in solute concentrations in bulk meltwater are expected. Daytime is dominated by a fast responsive drainage system, which leads icemelt through supra- and englacial channels, whereas slower travelling solute-rich snowmelt derived water from the distributed system constitutes a larger proportion of the bulk meltwater during night time where ice ablation is reduced. The amount of solutes in bulk meltwater is therefore expected to rise during low discharge and decrease during high discharge (Theakstone and Knudsen, 1996b; Hodgkins, 1997a and Hodgkins and Tranter, 1998b). Different chemical processes govern in the different drainage systems, which can be recognized in the bulk meltwater. Carbonation reactions will dominate during high discharge of water from the supraglacial and englacial drainage system, while hydrolysis reactions are more widespread when a larger proportion of the water originates from the slower, distributed drainage system (Tranter et al., 1996).

3.5.4 **Hydrochemistry studies of glacial meltwater**

Collins (1977) was the first to use meltwater chemistry in glacierized catchments to separate bulk meltwater into two components: a solute-rich, subglacial water mass derived

from snowmelt, and a dilute englacial ice-melt component. Since then, several detailed studies of hydrochemical behaviour of glacial meltwater have been conducted on temperate, polythermal and cold glaciers. Two studies conducted on Svalbard will be mentioned here.

Hodgkins et al. (1997b) studied meltwater emanating from the cold-based glacier, Scott Turnerbreen on Svalbard and found that 25% of the solutes originated from sea-salts, resulting from the maritime location of Scott Turnerbreen. 71% of all solutes were crustally derived, while 4% originated from aerosols and atmospheric sources. Significantly lower chemical denudation estimates, compared to temperate glacierized catchments, were explained by the shorter ablation period and the lower specific runoff for the High Arctic glacier, rather than differences in chemical weathering rates. The results showed that solute acquisition of the bulk meltwater was controlled by varying inputs of solutes from snow- and icemelt, solutes released from a proglacial icing as the water overflowed it and finally entrainment of solute-rich water from the thawing active layer of an ice-cored lateral moraine (Hodgkins et al., 1998a). High $p(CO_2)$ in the bulk meltwater was explained by significant sulphide oxidation taking place within the moraine areas where the abundant amounts of sediments had a high organic and sulphide content (Hodgkins et al., 1997b).

Chemical denudations rates of five glaciers in Western Spitsbergen were compared by Hodson et al. (2000). Specific annual discharge was found to be the most important factor in explaining the different denudation rates, while the different lithology under the glaciers acted as a secondary control. Similarly, rates of atmospheric CO_2 drawdown were found to vary with specific annual discharge, and also with the different underlying rock types, showing highest drawdown in areas with carbonate rocks and low values when plutonic and metamorphic rocks prevailed. The magnitude of chemical denudation and CO_2 drawdown was found to lay within the range of other glacier basins in the northern hemisphere (Hodson et al., 2000).

3.6 **Oxygen isotope hydrology**

Isotope hydrology is based on the fact that liquid water consists of a mix of slightly different molecules, and that these molecules differ in physical properties. The three most important molecular structures in water are $H_2{}^{16}O$, $H_2{}^{18}O$ and HDO and they have the approximate relationship of 997680:2000:320 parts per million (ppm) respectively. This relationship varies with temperature, and has therefore been widely used to reconstruct past climate fluctuation based on isotope measurements from ice cores from Greenland, Antarctic and Svalbard for example (Simões, 1990; Andersen et al., 2004; Isaksson et al., 2005). The isotopic signature of rain, snow, firn, ice and water differs due to isotopic fractionation. Changes in the relationship between the individual stable oxygen isotopes have thus successfully been exploited when studying the original provenances of glacial meltwater and variations in these (He and Theakstone, 1994; Raben and Theakstone, 1994; Theakstone and Knudsen, 1996a and 1996b; Theakstone, 2003; Yde and Knudsen, 2004).

3.6.1 **Oxygen isotopes in precipitations**

No accurate method has been found to measure the absolute value of ^{18}O. Instead all samples are compared to a standard that is calibrated towards the theoretically defined SMOW (Standard Mean Ocean Water). SMOW is based on values from 6 Atlantic, 11 Pacific and 2 Indian Ocean samples. $\delta^{18}O$ can therefore be defined as:

$$\delta^{18}O = \frac{^{18}O/^{16}O_{sample} - ^{18}O/^{16}O_{SMOW}}{^{18}O/^{16}O_{SMOW}} \quad (11)$$

From this equation it is seen that large values of $\delta^{18}O$ reflects enrichment in ^{18}O while low $\delta^{18}O$ reflects depletion of ^{18}O compared to SMOW (Dansgaard, 1964).

$H_2{}^{16}O$ has a smaller mass than $H_2{}^{18}O$ and the molecule is therefore more volatile. This results in isotopic fractionation when water evaporates and in all condensation processes. The $\delta^{18}O$ values of precipitation depend mainly on the condensation temperature, but other factors in conjunction such as original composition of water vapour, the type of cooling of the air mass (at constant pressure = isobaric, or without heat exchange = adiabatic), distance travelled from source area and from coast, the amount of precipitation and geographical parameters such as latitude and altitude of the area where precipitation falls (Dansgaard, 1964; Simões, 1990; Theakstone, 2003). With all these factors in play, difficulties easily arise when interpreting variations in stable oxygen isotopes. Some general guidelines can be concluded though. A positive relationship can be found between mean annual air temperature and $\delta^{18}O$ values. This behaviour is most pronounced in high latitude, non-continental regions, where mean annual air temperature is similar to mean annual condensation temperature, precipitation is formed at low temperatures and altitudes, and falls as snow. These factors all minimize the effect of isotopic fractionation by re-evaporation as the condensate falls through the air. In the warmer tropical regions, evaporation from falling drops is much more important and correlation between air temperature and $\delta^{18}O$ values is normally not possible (Dansgaard, 1964).

Seasonal variations in $\delta^{18}O$ in precipitation are normally seen, and reflect variations in air temperature, changes in vapour source areas or the amount of re-evaporation from falling drops. At low latitudes summer precipitation is more depleted in ^{18}O than the winter precipitation due to higher re-evaporation from falling drops during the dry winter. The opposite is the case in high latitudinal areas, where the cold winter results in a depletion of ^{18}O compared to the summer values. An altitudinal decrease in $\delta^{18}O$ is observed as a consequence of falling temperature and a preferential release of the heavier $\delta^{18}O$. Studies have also revealed an inland decrease in $\delta^{18}O$ as moisture is released when uplifted over land (Dansgaard, 1964).

3.6.2 **Oxygen isotopes in glacial meltwater**

Isotopic fractionation results in different $\delta^{18}O$ for rain, snow, firn and ice. The relationship between stable oxygen isotopes in glacier meltwater and variations therein, gives valuable information about the original provenances contributing to the runoff (He and Theakstone, 1994; Raben and Theakstone, 1994; Theakstone and Knudsen, 1996a and 1996b;

Theakstone, 2003; Yde and Knudsen, 2004). Table 3.4 shows range and mean $\delta^{18}O$ values of sources contributing to glacier meltwater at the Norwegian glacier Austre Okstindbreen in the period from 1980 to 1990 (Theakstone and Knudsen, 1996).

Table 3.4. Range and mean $\delta^{18}O$ values (‰) of sources of glacier river water collected at Austre Okstindbreen, Norway from 1980 to 1990 (Theakstone and Knudsen, 1996b). n = number of samples.

Source	Minimum	Mean	Maximum	Median	*n*
Glacier ice	-12.78	-11.61	-10.79	-11.57	39
Ice meltwater	-12.72	-11.94	-10.49	-11.78	31
Snow (May)	-21.84	-12.79	-7.23	-12.14	112
Snow (July)	-15.60	-11.54	-8.66	-11.38	250
Snow meltwater	-13.75	-12.10	-10.46	-12.08	16
Firn	-12.05	-10.91	-10.30	-10.73	35
Rain water	-15.53	-10.52	-6.49	-10.16	38

The isotopic composition of snow and rain varies according to the factors mentioned above. Horizontal layers with different $\delta^{18}O$ values, representing the different precipitation events, therefore initially build up the snowpack. During cold winters, the snowpack will be more depleted in $\delta^{18}O$ than in warm winters. As shown in table 3.4, the $\delta^{18}O$ values for snow and rain cover a wide range and can vary significantly from one precipitation event to the other, with rain less depleted in $\delta^{18}O$ due to the higher condensation temperature (He and Theakstone, 1994; Raben and Theakstone, 1994; Theakstone and Knudsen, 1996b).

When snowmelt starts, water percolating through the snow will result in a homogenization of the snowpack as illustrated in table 3.4 by the smaller range of $\delta^{18}O$ values in the snowpack in July. Due to isotopic exchange between the meltwater and the snow, the snowmelt will be depleted in ^{18}O, leaving the residual snowpack more enriched (Raben and Theakstone, 1994; Theakstone, 2003). The seasonal change occurring in the snowpack is illustrated in figure 3.9.

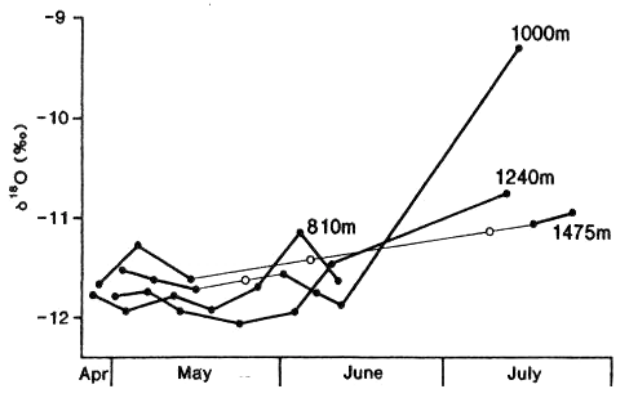

Figure 3.9. Seasonal change in isotopic composition in the snowpack at Austre Okstindbreen in Norway. The lines represents the change occurring in individual snow pits at different altitudes on the glacier (Raben and Theakstone, 1994).

Snow meltwater passes slowly through the underlying dense firn layer and isotopic exchange during densification results in an isotopically homogeneous firn layer with

relatively high $\delta^{18}O$ values (Theakstone and Knudsen, 1996b). Glacier ice also exhibits a low isotopic variability and relatively high $\delta^{18}O$ values (table 3.4). No isotopic fractionation occurs when ice melts, and ice meltwater therefore has similar isotopic composition as ice. During refreezing processes though, isotopic changes take place. Rain generally has high $\delta^{18}O$ values and a raise in $\delta^{18}O$ of the meltwater can often be recognized during or immediately after rainfall events (Theakstone, 2003).

Distinct variations in isotopic composition of the meltwater occur during the ablation period. Initially snowmelt dominates the meltwater, reflected by low $\delta^{18}O$ values in the bulk meltwater. When ice-melt starts, snowmelt above the transient equilibrium line on the glacier still maintains the low $\delta^{18}O$ base flow component of bulk meltwater, while diurnal increase in $\delta^{18}O$ values are seen in periods with warm weather, demonstrating enhanced icemelt. Towards the end of the melt season, the residual snowpack has relatively high $\delta^{18}O$ values, as does the water leaving the snowpack (Theakstone and Knudsen, 1996a and b; Theakstone, 2003).

3.6.3 **Oxygen isotope studies on Svalbard**

A detailed study of $\delta^{18}O$ values in meltwater has never been conducted on Svalbard. Instead, studies have concentrated on $\delta^{18}O$ variations in precipitation and the application of this when interpreting ice cores. Both Dansgaard (1964) and Simões (1990) found that on Svalbard, the seasonal variation in $\delta^{18}O$ values is very small (~2‰) and only recognized over a longer periods of time. Precipitation on Svalbard is related to frontal activity and sometimes during winter, the cold Arctic air is broken by warmer mid-latitude cyclones. It is therefore not unusual that winter precipitation shows high $\delta^{18}O$ values (Simões, 1990).

An extensive study of $\delta^{18}O$ values in precipitation in Longyearbyen was carried out from 1999 to 2003. A total of 291 samples were collected during all seasons and compared with the meteorological conditions at the time of precipitation. The following linear relationship was presented for $\delta^{18}O$ values and temperature in Longyearbyen:

$$\delta^{18}O = 0.59T - 12.05 \qquad (12)$$

The data set however had a large spread, and for several precipitation events no correlation with temperature was found. No evident seasonal trend could be established, emphasising the importance of source area when interpreting isotope data on Svalbard. A minimum $\delta^{18}O$ value of -35.21‰ was measured on 2 April 2003 at a temperature of -18.4°C while the maximum $\delta^{18}O$ value ever measured on Svalbard, -3.54‰, occurred on 21 September 2000 at an air temperature of 3°C (Bringedal, 2004).

4. Data collection and methods

4.1 GPR

A 100 MHz Ground penetrating radar (GPR) was applied for mapping the size and shape of the glacier, possible areas of temperate ice, debris bands within the ice and if possible, locate major englacial and subglacial meltwater channels. Fieldwork for this part of the thesis was done in co-operation with Karoline Bælum who used GPR in a study of the nearby Tellbreen (Bælum, 2006). April and May 2004 was spent planning and preparing the fieldwork, familiarisation and setting up of the GPR instruments, adjusting and developing equipment and carrying out the data acquisition.

Figure 4.1 shows the GPR field set-up showing the snow scooter and wooden sledge, the position of the transmitter and receiver with associated antennae, control console, computer and odometer wheel. The computer enabled data display and data storage to take place in field, and the connected odometer wheel measured the travelled distance and triggered measurements at a fixed length interval. The transmitting and receiving antennae were placed as far back on the sledge as possible to reduce noise from the snow scooter in the collected data. The antennae were orientation perpendicular to the survey line so that maximum power was transmitted parallel to the survey direction (Annan, 1992)

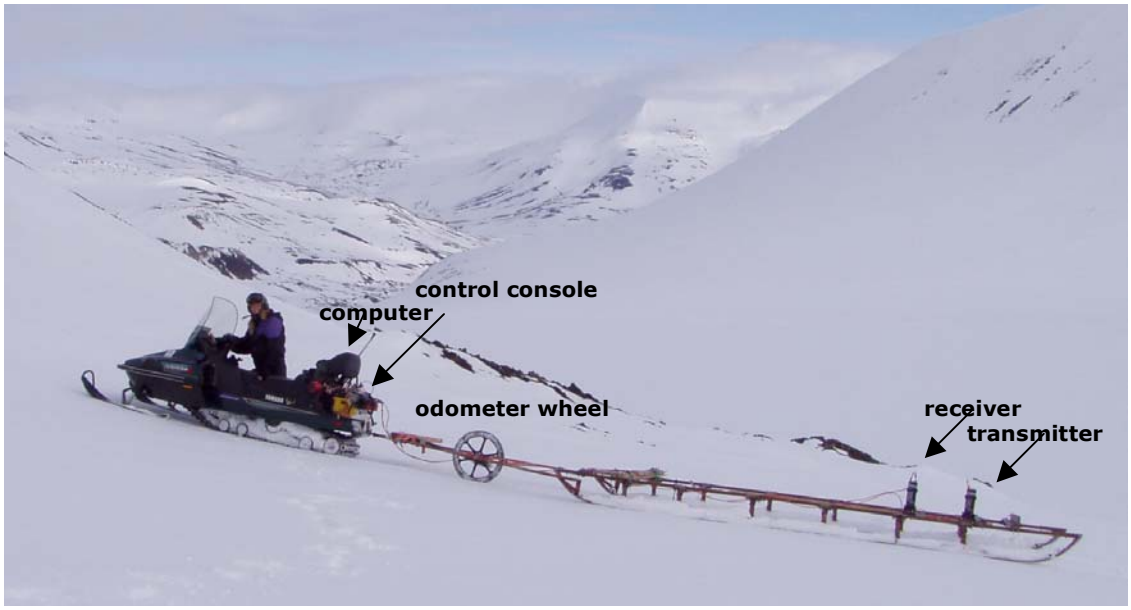

Figure 4.1. Data acquisition of GPR on Tellbreen, May 2004. The same set-up was used on Longyearbreen.

The GPR equipment turned out to be very unstable and the data collection was consequently problematic. The two computers that were available were old and infected with computer viruses making both of them unstable and at times completely unable to communicate properly with the GPR. Two new computers were later purchased by UNIS in an attempt to

solve this problem. Unfortunately they too had problems and later proved unable to cope with the low air temperatures. The GPR itself was also marked by several years of being transported great distances behind snow scooters, a history of multiple users with varying knowledge of GPR and the exposure to extreme weather conditions on Svalbard. The data acquisition was therefore challenging and more time-consuming than expected. By the end of May poor snow conditions made it impossible to access the glaciers on snow scooters resulting in an only partly completion of the planned fieldwork. In the autumn of 2004 several attempts to collect additional data failed due to the poor state of the GPR and the field computers.

Presented in this thesis is a reflection mode GPR survey carried out with 100 MHz antennae and a common midpoint survey for velocity determination of the glacier ice (see figure 4.2). A planned survey with 200 MHz antennae and a detailed mapping of the frontal area of the glacier were unfortunately abandoned due to equipment malfunction and the mentioned spring snow conditions of 2004.

The GPR used for the survey was a pulseEKKO 100 system (Sensors and Software Inc., Canada) with a peak voltage of 400 volts for the transmitter. The pulseEKKO 100 system is a digital radar with two separate identical resistivity loaded dipolar antennae. This makes it possible both to conduct reflection profiling with a fixed antenna arrangement, and CMP studies where the antennae are moved independently (see figure 4.2). CMP surveys can be used for velocity determination of the underlying material since the increase in distance to the reflector can be calculated based on the increasing antennae separation.

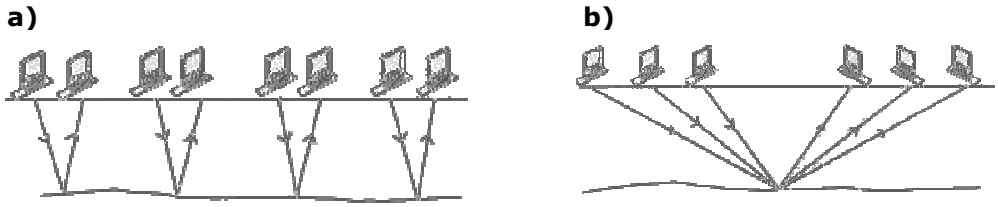

Figure 4.2. An illustration of two different antenna setups, a) reflection mode with common-offset and b) common midpoint survey (CMP), (Sensors and Software, 1992-1999).

Antennae with the frequency of 100 MHz were chosen for the reflection profiling. This was because 100 MHz antennae have previously been shown to successfully receive reflections of glacier beds in studies of glaciers of similar size (Murray et al., 1997). A GPR survey on cold glacier ice with 100 MHz antennae will reflect structures with thicknesses down to 0.1 m (Murray et al., 1997). The antennae were strapped onto the wooden sledge with a separation of 1 m. The total time window for each measurement was set at 2000 ns corresponding to the two-way time for 170 meters of ice, which was far more than anticipated at Longyearbreen. Two measurements (traces) were taken for every 0.5 m and stacked by the GPR in order to eliminate noise. Number of points per trace was set at 2500.

GPS coordinates from the starting and ending points of the profiles driven on Longyearbreen in 1993 (Tonning, 1996), were transferred to a handheld GPS and the survey lines were driven with starting and ending points similar to these. It proved impossible to conduct a complete replica of the previous study because of safety issues in the marginal areas of the glacier, where deep lateral meltwater channels exist. The locations of the individual survey

lines generally had an accuracy of ± 25 m, and a maximum uncertainty of 50 m compared to the 1993 survey. The endpoint of one profile was connected with the starting point of the next. GPS waypoints of starting and ending positions were stored in the handheld GPS in European 1950 datum. In figure 4.3 a map of Longyearbreen is shown with the location of the 13 GPR survey lines in May 2004. Lines A, B, C, D, E, F and G correspond to the lines previously collected on Longyearbreen (Tonning, 1996). A total of 6.75 km GPR was collected.

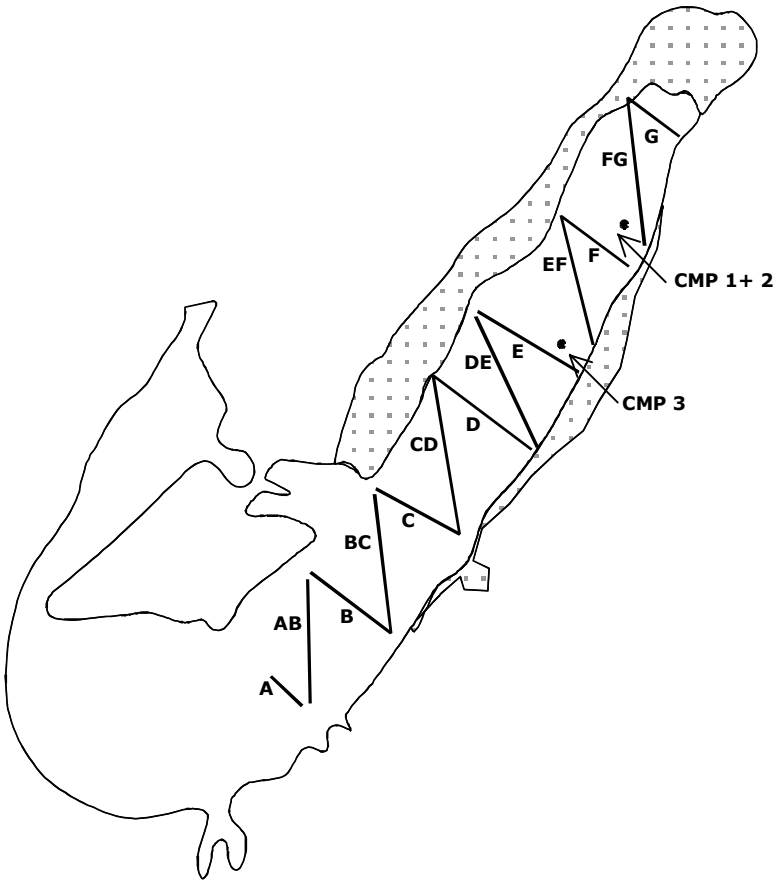

Figure 4.3. Positions of GPR lines and the three CMP surveys on Longyearbreen, May 2004.

Three CMP surveys were conducted on Longyearbreen with 100 MHz antennae. All surveys were performed perpendicular to the ice flow and the first two at the same location (see figure 4.3). The starting position of the antennae was 0 m and for each measurement the individual antenna was moved 0.2 m away from the midpoint of the line. Traces were stacked 16 times in order to eliminate noise in the data.

4.1.1 **Data processing**

Processing of the GPR data is essential in achieving a good interpretation of the profiles. The program Reflex-Win 3.5.7 (Sandmeier Software) was used for processing and interpreting the GPR data, using the same techniques as for seismic data. Generally, the same processing flow was applied to all profiles.

Each GPR line has an associated file that contains the parameters for the survey (the header file). Time zero was found for the individual profiles and corrected in the header file. The odometer wheel proved to be very unstable resulting in considerable differences between the lengths of the lines measured by the wheel and those obtained from the handheld GPS. For some of the lines, the length of the survey lines measured by the odometer wheel was only half that of the GPS. No major jumps in the basal reflector were observed within the profiles and the error in length measured by the odometer wheel is thought to have been constant within each survey line (for more details see Bælum, 2006). The GPR lines were therefore assigned the GPS lengths in the header file, resulting in a change of the 0.5 m step size. In figure 4.4 the new trace increment for the individual lines is seen. Line E to G correlated well with the length obtained from the odometer wheel, while the discrepancy continuously enlarged from line DE to line A.

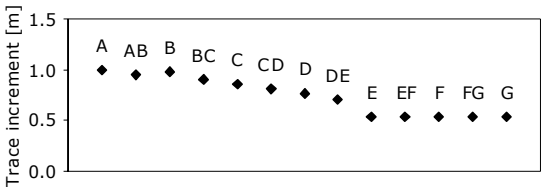

Figure 4.4. The trace increments for the individual GPR lines after being assigned the length obtained from the handheld GPS.

GPR lines with one-letter names were surveyed from east towards west, while lines with two letter names were surveyed from west towards east. For presentation purposes, the profiles with two letters were flipped in the opposite direction so that all profiles are presented from east towards west.

The glacier ice was assigned a radar velocity of 0.17 m ns^{-1}. A similar radar wave velocity of 0.168 m ns^{-1} has previously been applied to cold glacier ice on Svalbard (Ødegård et al., 1997; Murray et al., 2000). This velocity was supported by analyses of the CMP surveys and diffraction hyperbolas observed in the profiles (see appendix A.2 for the CMP surveys).

The electromagnetic signal attenuates with increasing distance from transmitting and receiving antenna (Annan, 1992). A reflector at a shallow depth will therefore appear with a higher intensity (amplitude) than a similar reflector at greater depth. By applying a gain function to the GPR profiles, the electromagnetic signal is strengthened with increased time (depth). The technique called Automatic Gain Control (AGC) was chosen for all the profiles. The AGC function equalizes the signal strength on each trace of the line within a chosen time window. Weak signals will therefore be emphasised more than strong signals. All original amplitude information is consequently lost (Annan, 1992). Figure 4.5 illustrates the effect of AGC on a section of profile D.

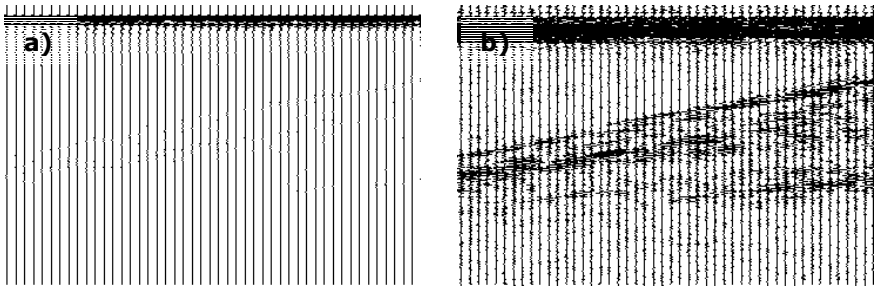

Figure 4.5. The effect of AGC on a section of profile D. a) shows the section before applying the gain function while b) shows the section after application (window length: 30ns, scaling value: 1).

Low-frequency noise from instrument drift or radios sources obstruct the GPR signal resulting in an off center flow in the traces with time (Murray et al., 1997). This effect is compensated for by applying a subtract-mean (dewow) filter to the individual traces. For every trace, the filter calculates a mean value within a specified time window and subsequently subtracts this value from the central point. Traces subjected to a flow will be realigned along the centre line after the application of the dewow filter. An example of the effect of the filter on a section of profile D is shown in figure 4.6.

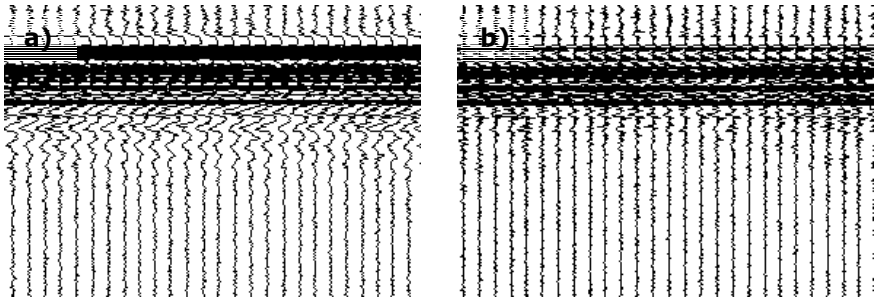

Figure 4.6. A section of profile D a) before and b) after the application of the dewow filter (time window: 10ns).

When plotting GPR data it is assumed that the reflection observed in the radar image originates from an object located directly under the receiving and transmitting antennae. This is not always the case, and abrupt changes in electromagnetic properties (due to for example faults, debris within the glacier ice or meltwater channels) and steeply dipping structures (for example at the glacier margin) may result in false reflections (diffraction hyperbolas) and an incorrect positioning of the structures. Diffraction hyperbolas occur because reflections from a point source are received before and after the antennae are directly above it. Since distance traveled on the surface is known, the diffraction hyperbolas consequently give valuable information of the velocity of the material between the antennae and the point source. The processing step, migration, collapses diffraction hyperbolas by centering the reflected energy in the correctly positioned top point, while steeply dipping reflectors are placed in the true geometrical location (Annan, 1992). The migration technique called diffraction stacking was applied to most of the GPR profiles. Input parameters to this technique are velocity, obtained from the diffraction hyperbola itself, and a summation width of traces larger than the width of the individual diffraction hyperbolas. Figure 4.7 shows the effect of migrations by diffraction stacking on a diffraction hyperbola in profile F.

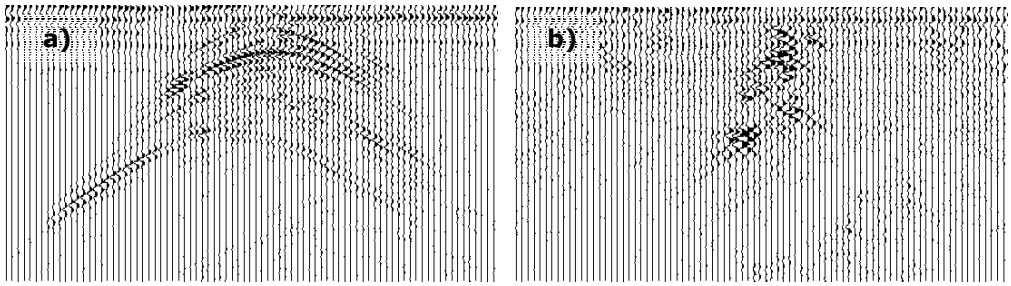

Figure 4.7. A section of profile F a) before and b) after migration by diffraction stacking (summation width: 64, velocity: 0.17 m ns^{-1}).

An example of the effect of migration on an entire profile is shown in figure 4.8. The migration has resulted in a slightly steeper inclination of the bottom reflector in the marginal areas. However, the most pronounced effect of the diffraction stacking is seen in the deepest part of the bottom reflector where diffraction hyperbolas prior to migration formed a "bow-tie" pattern obscuring the actual reflector. This is seen in narrow synclines where reflections are received at the surface from several points on the structure.

A clear reflection of the ice/bed interface was observed subsequent to data processing in most profiles. Where the ice/bed interface was very weak or absent, the most likely position of the reflector was chosen based on the radar image. All GPR profiles are shown in appendix A.3 before and after migration.

A contour map of the ice thicknesses of Longyearbreen was constructed in Surfer 8.04 (Golden Software Inc.) using the Natural Neighbour gridding method. The Natural Neighbour method constructs a grid of polygons using a weighted average of the neighbouring data points. The total volume of glacier ice was consequently computed based on the ice thickness grid.

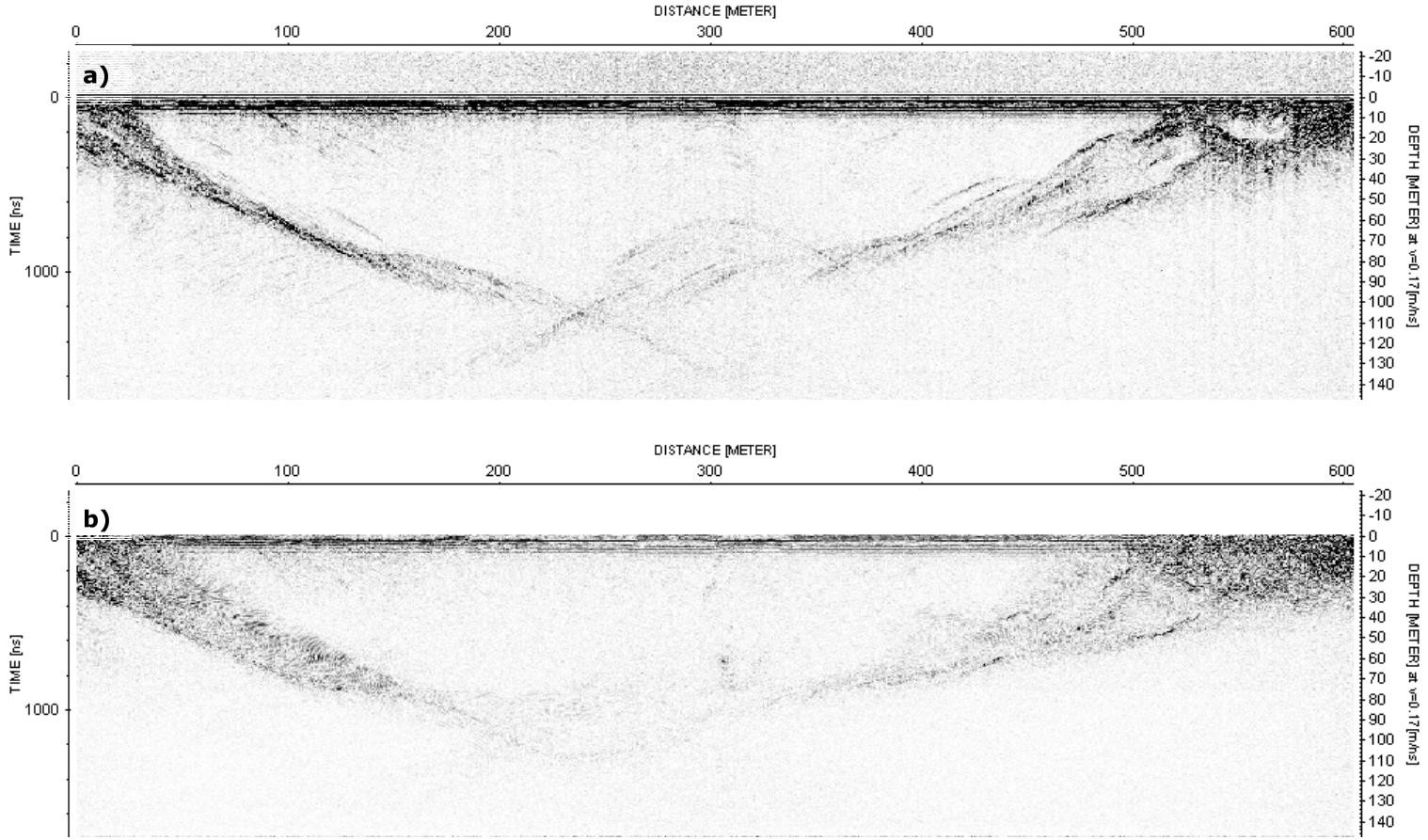

Figure 4.8. Profile D a) before and b) after migration by diffraction stacking (summation width: 64 from 0-900 ns and 128 from 900-1700 ns, velocity 0.17 m ns^{-1}). Before migration the deepest point on the bottom reflector was obscured by diffraction hyperbolas forming a pattern often referred to as a "bow-tie" event. This is seen in narrow synclines where reflections are received at the surface from several points on the structure.

4.1.2 **Source of error**

Most power from the transmitting antenna is radiated downwards (Annan, 1992), but since the antennae for the pulseEKKO 100 system are not shielded, the signal will be affected by conductive materials in the surroundings. It is therefore not optimum to have a snow scooter pulling the sledge, but unfortunately necessary with the type of large-scale study conducted for this thesis. Noise from the snow scooter can clearly be seen in the uppermost 100 ns of the time window, obscuring whatever reflection that may occur in this area.

In order to transform time into depth in the radar image, a velocity for the electromagnetic wave in the glaciers is applied. The velocity varies however within the ice as mentioned in section 3.2, and firn, superimposed ice and snow have velocities that differ from that of the pure ice. The snowpack on Longyearbreen is less than 2 m thick and would lead to a maximum error in depth estimates of about -0.5 m of ice, assuming a snow velocity of 0.22 m ns^{-1} (Moore et al., 1999) and an radar wave velocity of 0.17 m ns^{-1}. The uncertainty when picking the basal reflector from the radar images may result in some error in the ice thickness estimates. All reflectors were manually picked and a maximum uncertainty of 10 ns is estimated in areas of a weak basal reflector. This corresponds to an error of about 1 m in ice thickness estimates. The overall accuracy of the ice depth estimates of the basal reflector is thought to be 5 to 10 m, which is similar to previous GPR studies (Hagen and Sætrang, 1991; Björnsson et al., 1996; Tonning, 1996).

Starting and ending points of the radar profiles were found through handheld GPS. The uncertainty of the global positioning system on Svalbard in the horizontal plane is less than 9 m on an average day and usually about 5 m. The altitude measurement is slightly more uncertain with an accuracy of about 9-15 m. For each profile, a waypoint was stored at the starting and ending points. Between the two points it is assumed that the profiles were driven in a linear line on a flat surface. Looking back on the scooter tracks in field supported this assumption. A direct comparison with the GPR study from 1993 is thought to be realistic.

As mentioned above, the GPR system proved very unstable. One of the major concerns was the odometer wheel, which failed to trigger with the desired length interval. The individual GPR lines were therefore assigned the lengths derived from the handheld GPS since they appeared to be more accurate (section 4.1.1 and Bælum, 2006). The uncertainty associated with the GPS coordinates are therefore also reflected in the lengths of the survey lines.

4.2 **Exploration of cave**

Channel exploration of the glacial drainage system of Longyearbreen is possible during winter and spring. Every spring, tourist companies locate the western incised supraglacial channel and dig their way through the overhanging snow bridges, opening the channel (also known as the ice cave) to access. The shape and accessibility of the channel varies from year to year but in general it is possible to reach both englacial channels and the glacier bed of Longyearbreen. Water running in this channel therefore has access to both local sedimentary bedrock and soils rich in organic matter as was documented by Humlum et al. (2005). Where the eastern meltwater stream emanates from the debris-covered glacier

snout it is possible to enter the frontal marginal subglacial drainage system. This locality is referred to as the moraine cave. This meltwater channel is also excavated in the spring and it is possible to walk several hundred meters under the debris-rich ice. During explorations of the ice cave and moraine cave, samples of snow, ice (in May) and water (in September) were collected. This was done in order to determine the source of the ions found in the bulk meltwater.

4.3 Meteorological parameters

The Norwegian Meteorological Institute provided detailed meteorological data from May to September 2004. Wind speed, wind direction, cloud cover, precipitation, air temperature and air humidity were recorded every three hours by the meteorological station at Longyearbyen Airport, approximately 6 km from the sampling site (see figure 2.3). Air temperature was measured manually every time a sample was collected and weather conditions were noted.

4.3.1 Source of error

The fact that the meteorological station at Longyearbyen Airport is 6 km away, at a different altitude and situated close the open sea constitutes some uncertainty. However, Sægrov (1995) compared temperature data from Longyearbreen Airport with temperatures measured at a local weather station in the debris-covered glacier snout of Longyearbreen, and found a good correlation between the two. However, variations in precipitations levels between Longyearbyen Airport and the sampling site may be significant and values measured at the airport should therefore be applied with caution.

4.4 Water level measurements

A gauging station was located on the road bridge on Strandveien about 4 km downstream from the sampling site, just before Longyearelva runs into Adventfjorden (see figure 2.3). Due to the concrete bridge construction, the flow undergoes critical condition and a relationship between water level and discharge can be obtained (Grønsten, 1998). An Aanderaa gauging station with a pressure sensor (Pressure Sensor 4017) measured water level every 10 minutes. Data was provided by Ole Humlum, Adjunct Professor at UNIS.

Some calibration of the raw data was necessary since measured water level was constantly too high. A value of 0.238 m was subtracted from the measured value in order to correlate with the actual conditions in Longyearelva. This value was obtained by comparing known zero water level in the river with measured value. The gauging station was out of order in the period from 27 July to 3 August and water levels therefore had to be estimated based on notes from field work, photographs taken at the sampling site and comparison with earlier periods with similar meteorological parameters.

Grønsten (1998) studied Longyearelva catchment from 1995 to 1997 and had a water level sensor located at the same locality as the one used for this study. A relationship between

water level and discharge was found by Grønsten (1998) by comparing measured water level, h [m], with calculation of water flux obtained through the use of direct measurements of the mean water velocity. The following equations for discharge, Q [$m^3 s^{-1}$], were found:

$$Q_1 = 200h^{3.64} \qquad \text{for h} < 0.39 \text{ m} \qquad (13)$$

$$Q_2 = 22h^{1.29} \qquad \text{for h} \geq 0.39 \text{ m} \qquad (14)$$

Equation 13 was based on 18 direct measurements of discharge and water level. Equation 14 on the other hand relied only on one measurement and an estimated value of maximum discharge under the bridge (Grønsten, 1998). The relationship between water level and discharge was applied to the data from the ablation period of 2004.

An estimate of the magnitude of different water sources to Longyearelva was made based on personal observations and direct measurements of water amounts in different tributaries, conducted by Sægrov (1995) and Grønsten (1998). It was therefore possible to give an estimate of the total amount of water flowing in the river at the sampling site (see figure 2.3) during the ablation period of 2004, together with a total estimate of meltwater draining through the drainage system of Longyearbreen.

4.4.1 **Source of error**

Water levels and calculated discharges were utilized in order to explain variations in water chemistry and suspended sediment transport in the water flowing at the sampling site. Furthermore an estimate was provided of the total amount of solutes and suspended sediment transported by meltwater from Longyearbreen in 2004. The optimum situation would result in measurements of water level and discharge at the sampling site and where the meltwater streams from Longyearbreen confluence. This was not possible due to problems finding a stable profile where these measurements could take place and the lack of appropriate instruments. Water levels were instead obtained from a gauging station in Longyearbyen, where different tributaries without connections to Longyearbreen contribute to the water levels measured. Estimates of the different tributaries were made in order to determine the quantities of water flowing at the sampling site and from Longyearbreen in total. Even though these estimates are based partly on studies conducted as much as 10 years prior to the field work for this thesis, proportions of the individual water sources are not thought to have changed considerably. Another complication in using data from the bridge in Longyearbyen is that the variations in water levels in Longyearelva do not only originate from Longyearbreen and uncertainties arise when using them in this way. Meltwater from the catchment of Longyearbreen does however constitute the largest proportion of water source in Longyearelva (50%) and the signal from the glacier is thought to be clear in the water level data from Longyearbyen.

The gauging station is located about 4 km downstream from the glacier snout and travel time of the water from the glacier terminus to the gauging station changes with discharge. If the water travels with a velocity of 1 $m s^{-1}$, the delay in discharge signal from the glacier terminus to the bridge in Longyearbreen will be about an hour and is therefore thought to be of little importance when discussing diurnal discharge variations.

Water level measurements conducted in glacial environments are associated with many difficulties. The system is extremely dynamic on both a diurnal and seasonal scale with water levels experiencing large fluctuations depending on meteorological factors and the release of stored water within the glacial drainage system. The river path may therefore change within hours in an attempt to adjust to the new conditions, making it very difficult to find a stable profile to conduct the measurements. These influencing factors are minimised at the river profile in Longyearbyen due to its cemented construction. Furthermore, water on Svalbard ceases to flow in the autumn and river beds become filled with ice and snow. In early melt season this snow and ice will affect the measured water levels in the early ablation period.

Discharge was calculated from the water levels by using the equations provided by Grønsten (1998). Equation 13 is well described by 18 measured points. Equation 14 on the other hand, is only established on the basis of two discharge values of which one is a rough estimate of maximum discharge during a peak flow event. Moreover, the direct discharge measurements were conducted by Grønsten (1998) in the summer of 1997. Even though the river profile is a manmade construction that has not experienced changes during this time, alternations in the river path up- and downstream from the bridge may cause changes in the discharge relationship. Applying the equations derived by Grønsten (1998) to the water levels from the ablation period of 2004 therefore offers some uncertainty. It was however beyond the scope of the fieldwork for this thesis to obtain new direct discharge measurements and the equations have therefore been applied.

4.5 Suspended sediment concentrations and meltwater chemistry

Two sets of samples were collected during fieldwork. 250 ml pre-rinsed polypropylene bottles for future analyses of solute content and SSC, and 20 ml plastic bottles for $\delta^{18}O$ determination. To prevent any form of contamination, disposable gloves were used during sampling and bottle and lid were rinsed twice with meltwater before collecting the sample. Samples of meltwater were filled to a maximum leaving no space for air, while the majority of the snow, ice and rain samples were not completely filled. After sampling, the bottles were stored at 4°C in a dark refrigerated space for 2½ to 6 month before analyses.

Collection of samples began in the middle of April 2004 with sampling of ice from the ice cave and the moraine cave and snow samples from four snow pits dug on the glacier. Sampling points in the catchment area are indicated in figure 4.9 and the number of samples collected is shown in table 4.1. Not all samples are presented in this thesis. Snow and ice samples for solute determinations were collected in polypropylene bottles and subsequently thawed when put into storage. Samples for $\delta^{18}O$ analysis were collected in plastic bags and transferred to bottles after thawing. The four snow pits were dug at three different occasions at three different places during a two-week period at end of April. Snow was collected from 0.10 m intervals and snow temperature and snow densities were measured for every 0.10 m down the snow pack until reaching the glacier surface.

The majority of meltwater leaves Longyearbreen through two meltwater streams (see section 2.6). A western meltwater stream that emanates from the side of the glacier in the debris-rich frontal ice and an eastern stream that springs from beneath the debris-rich ice

(see figure 4.9). The aim was to collect water samples as close to the glacier terminus as possible. The eastern meltwater stream was chosen as sampling site, due to logistic reasons. Water samples were collected in turbulent water between 20 and 50 m after leaving the moraine cave (labelled "sampling site" in figure 4.9, see also figure 4.10). During high discharge, water sampling at the glacier front was too dangerous and the sampling site consequently moved 100 m downstream. Water sampling commenced 29 May 2004 when water started flowing in the river bed and ended 11 September when water ceased to flow under the thickening surface layer of ice. Samples were collected twice a day for most of the summer during assumed lowest and highest discharge. Until 9 June samples were collected at 00:00 and 12:00. This was then changed to 06:00 and 18:00 on the basis of the measured water level fluctuations. Water level measurements from previous seasons had shown a gradual change in discharge patterns at the end of the season and in order to accommodate this possible change, time of sampling was changed back to 00:00 and 24:00 on 10 August.

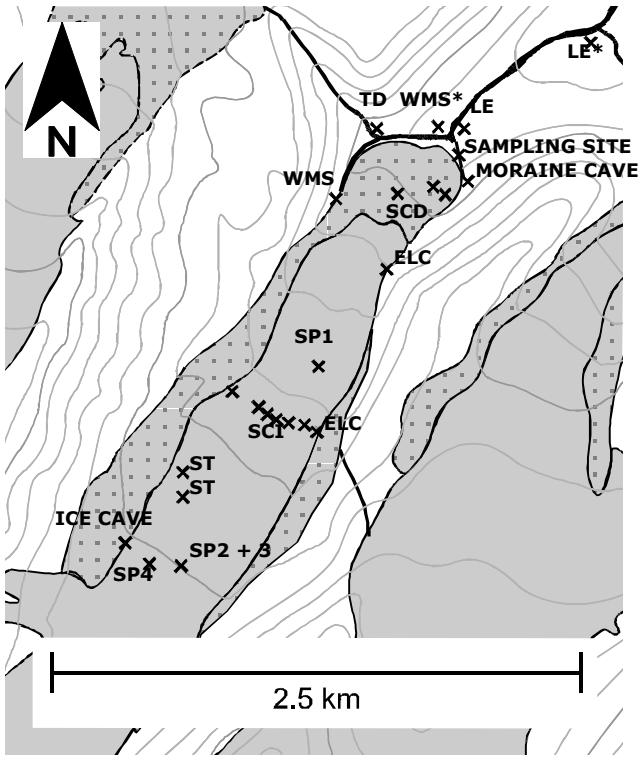

Figure 4.9. Detailed map of the study area. LE = Longyearelva, TD = Tværdalen, WMS = western meltwater stream, SCI = supraglacial channels on ice, SCD = supraglacial channels on debris, ELC = eastern lateral channels, WLC = western lateral channels, SP = snow pit, ST = scooter track.

On two occasions more frequent water sampling took place over two periods of three days in an attempt to resolve diurnal variations in the meltwater. The first three-day period started 21 June at 21:00 and ended 23 June at 20:00. Samples were taken every hour for the first 24 hours and every four hours thereafter. The second period was conducted between 27 July at 06:00 and 30 July at 06:00. Four-hour samples were taken at the beginning and end of the period and the hourly samples during the middle 24 hours.

On 18 August, samples were collected from different water sources contributing to total runoff from Longyearbreen in order to investigate the provenance of solutes, isotopes, and suspended sediments measured in the water from Longyearbreen. Water was therefore sampled from lateral meltwater streams, supraglacial streams, from the western meltwater stream leaving Longyearbreen and from Tværdalen, the valley contributing with water from the unnamed glacier on Nordenskiöldtoppen (see figure 4.9).

Table 4.1. Number of samples collected during the fieldwork for SSC, solute and oxygen isotope analyses. The number written in italic shows number of samples collected for isotope analyses. Not all samples are presented in this thesis.

Description	Time of sampling	Number of samples
Snow from snow pits	24.04.04-01.05.04	50, *51*
Ice	06.05.04-16.05.04	5, *10*
Freshly precipitated snow	04.06.04-12.09.06	5, *8*
Rain	26.07.04-29.07.04	2, *4*
Water from the sampling site	29.05.04-11.09.04	221, *236*
Water from different sources	29.05.04-11.09.04	54, *77*
Total	24.04.04-11.09.04	337, *386*

An automatic water sampler was purchased by UNIS both to reduce the workload of manual sampling and to obtain a more detailed dataset (figure 4.10). Unfortunately, this equipment was incompatible with the nature of the Longyearbreen meltwater. During the highest discharge recorded over the summer, the rock, that the hose was attached to, was displaced and the automatic sampler was drawn into the river ending up 1½ km downstream. The automatic water sampler had suffered serious and irrevocable damage in the process. This event occurred just after testing of the water sampler had finished and before the instrument had contributed with samples to the dataset. Therefore, all samples presented in this thesis are sampled manually.

Figure 4.10. Picture from the sampling site (photograph: Hanne H. Christiansen, 22 June, 2004).

During the ablation period, water samples were collected at different places in the catchment. Every time a water sample was collected, electric conductivity and water temperature were measured using a HACH sensION156 portable pH- and conductivity-meter. In the early stages of the sampling, pH was also measured. However, the measurements were not successful since high concentrations of suspended sediment in the water disturbed the electrodes. Readings were unstable and measuring was stopped as a consequence.

The samples for oxygen isotope determination were sent to the Niels Bohr Institute in Copenhagen where the $\delta^{18}O$ values were determined by mass spectrometry, with an accuracy of ±0.04‰. Analyses of the solute samples were carried out in a laboratory of the University of Aarhus. All samples were filtered through a 0.7 µm Whatman glass microfibre filter. The filters were dried in a warm oven and then weighed for determination of suspended sediment concentrations in the water. Prior to analysis, the samples were filtered again through 0.45 µm cellulose nitrate membranes and several water samples were diluted since they contained higher concentrations than the instruments were capable of detecting. Solute concentrations of major anions (Cl^-, NO_3^- and SO_4^{2-}) were determined by using a Perkin-Elmer ion liquid chromatography. The concentration of major cations (Na^+, K^+, Mg^{2+} and Ca^{2+}) and Si were determined by a Perkin-Elmer 5100 PC and an autosampler.

4.5.1 **Source of error**

When dealing with meltwater samples, there is always the possibility of contaminating the samples either during sampling or later in the laboratory. For the rain samples, no pre-rinsed container big enough to collect the required amount of water was found and these samples may therefore have been contaminated.

No direct measurement of HCO_3^- was conducted and concentrations of this ion have therefore been calculated based on the measured concentrations of all other ions. The concentrations therefore also reflect the uncertainties for the other ions.

The samples were kept in storage for 2½ to 6 months before filtration. This carries the inherent possibility that reactions between suspended sediment and water may have taken place during this time. However, these reactions are thought to have been kept to a minimum since the samples were stored in a cool and dark place.

The precision of the analyses was ±5% for the anions, ±5% Na^+ and Mg^{2+} and ±10% K^+ and Ca^{2+}. All concentrations were above detection limit at all times, except for NO_3^- that occasionally fell below the limit of 0.8 µeq l^{-1}. Due to very high concentrations of some of the ions in the glacial meltwater, the water had to be diluted prior to analyses. This concerned SO_4^{2-}, Na^+, Mg^{2+} and Ca^{2+} in samples of meltwater in the early and late ablation period. The concentrations for these samples may therefore be related with an additional error of maximum 5%.

5. Results

5.1 GPR

The glacier ice was assigned a velocity of 0.17 m ns^{-1} similar to what has previously been assigned to cold ice (Ødegård et al., 1997; Murray et al., 2000). The results from the CMP surveys were not convincing and velocities within a wide range seemed to match the shape of the basal reflector. Hyperbolas from most of the GPR lines however clearly indicated velocities of about 0.17 m n s^{-1} except for profiles C (0.12 m ns^{-1}), DE (0.12 m ns^{-1}) and FG (0.25 m ns^{-1}). These fairly large differences are most likely caused by the problems with the odometer wheel mentioned in section 4.1. Figure 5.1 shows a section of profile F where clear diffraction hyperbolas are observed. The red hyperbolas indicate modelled diffraction hyperbolas assuming a radar wave velocity of 0.17 m ns^{-1}. The calculated hyperbolas correspond very well with the measured hyperbolas indicating a correct assigned step size.

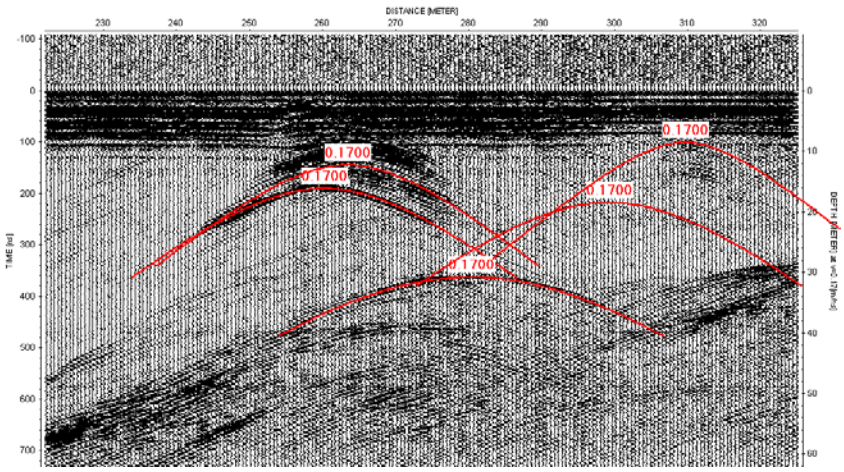

Figure 5.1. Diffraction hyperbolas in profile F compared to modelled hyperbolas (red lines) assuming a radar wave velocity of 0.17 m ns^{-1}.

The thickness of the glacier ice was calculated from the TWT to the ice/bed interface (equation 1). This interface is very clear in most profiles although at times obscured by diffraction hyperbolas, especially in the deepest and western parts of the glacier (marked with a thin line on figure 5.2). Figure 5.2 shows the measured ice thicknesses for the survey lines positioned perpendicular to the glacier flow. The view is up-glacier (towards south-west) with the ice thicknesses plotted from east to west. The locations of the survey lines are shown in figure 4.3. All GPR profiles can be seen in appendix A.3. In figure 5.2, relatively thin ice thicknesses are visible in both the lower and the upper parts of the glacier with maximum ice thickness of 65 m in profile A and 52 m in profile G. The largest ice thickness is 110 m in profile D but profile C and E also have thicknesses above 100 m. The only time ice thicknesses approach zero is in the end of profile D and G. This is because great care was taken in approaching unknown marginal areas of the glacier due to the presence of deep snow covered lateral meltwater channels. A distinct synclinal is observed in the deepest parts of profile D, E, and F. This is not the case for the up-glacier profile B

and C where the boundary appears smoother. The discontinuous basal reflection in profile B will be discussed in more detail later.

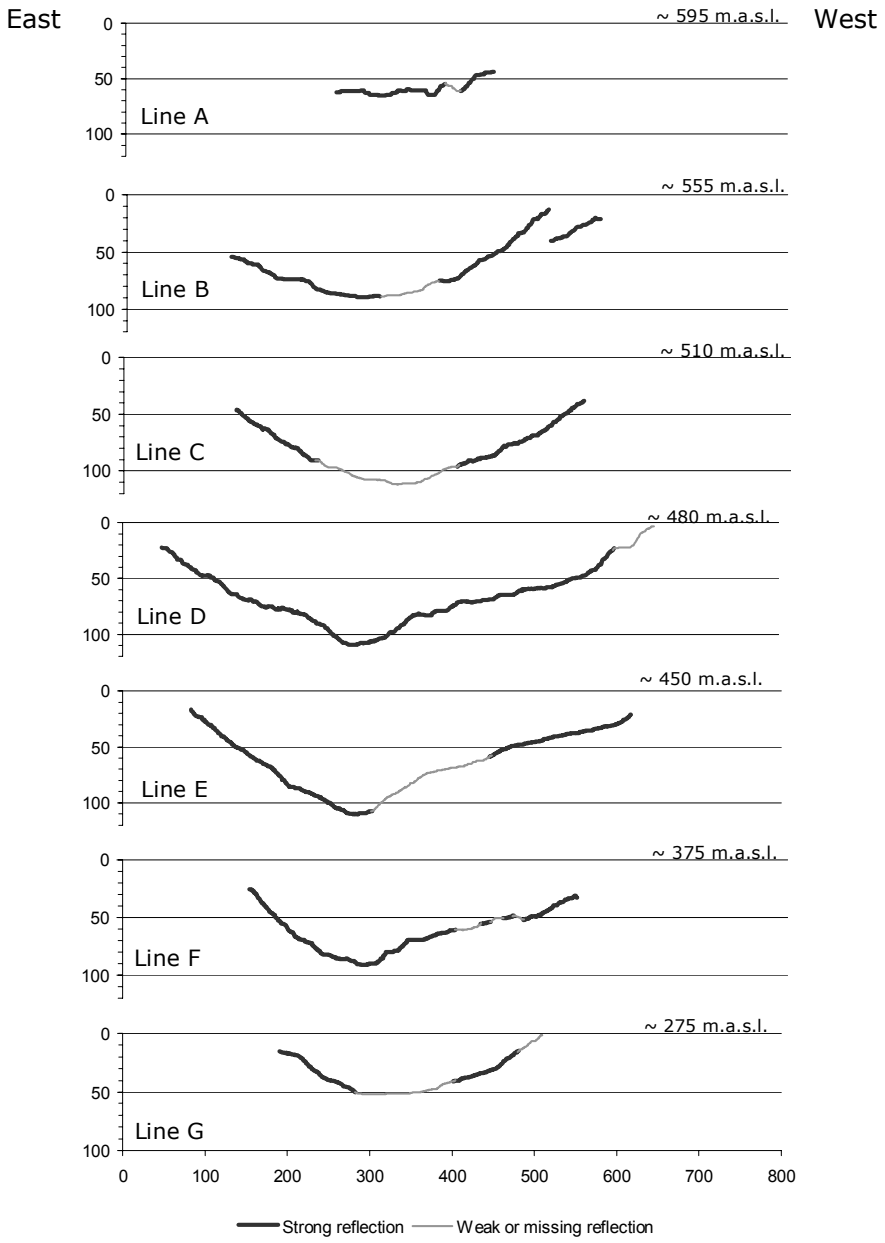

Figure 5.2. Ice thicknesses measured in survey lines perpendicular to the glacier flow. The approximate altitude of the individual line is stated for each plot.

A contour map of ice thicknesses determined from all survey lines is shown in figure 5.3. The figure shows a subglacial terrain, non-symmetrical around the glacier's centre flow line with the thickest ice located towards the east, especially in the lower part of the glacier. A narrowing of the subglacial terrain occur down-glacier.

The volume of the glacier ice was computed based on the contour map, excluding ice outside the grid. A volume of 0.08 km^3 was calculated for the surveyed part of Longyearbreen. No estimate of ice volume was calculated for the entire glacier.

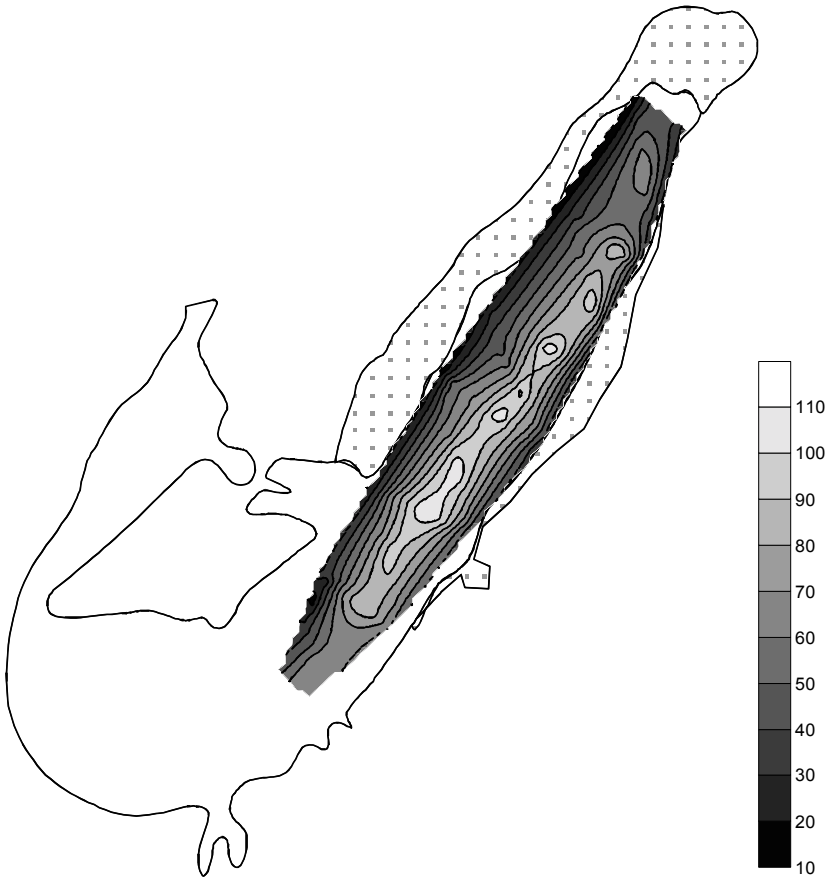

Figure 5.3. Contour map of ice thickness variations on Longyearbreen based on 9748 point measurements distributed on 13 GPR profiles.

Figure 5.4 shows the glacier altitude (obtained from GPS coordinates of the data points) and ice/bed interface in the points of maximum ice thickness measured in the 13 GPR cross sections. The glacier surface is slightly steeper than the underlying topography in the frontal areas, while the opposite is the case in the upper parts of the glacier. Overall, the glacier surface seems to follow the underlying topography well.

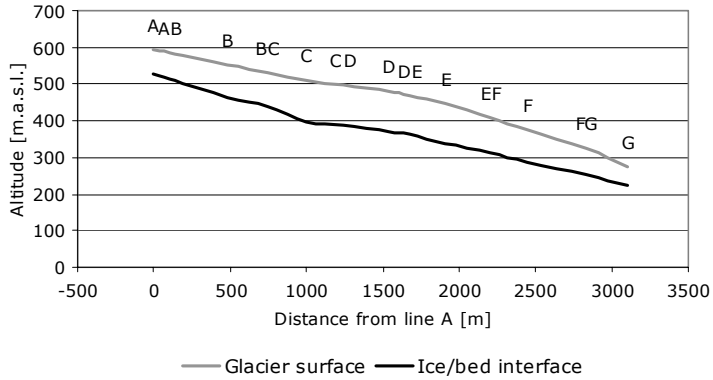

Figure 5.4. Topography [m.a.s.l.] of the glacier surface and the ice/bed interface for the point of maximum ice thickness measured in the 13 survey lines. X-axis shows distance from line A.

In all profiles the upper 100 ns were almost completely obscured due to noise from the instruments and the snow scooter. Interpretations of reflections caused by surface features therefore mostly rely on multiple diffraction hyperbolas. Many of the reflectors observed in the radar profiles are related to surface features. This is illustrated by comparing figure 5.5 and 5.6.

Figure 5.5 shows the position of lines G, FG, F, EF, E and DE on an aerial photograph of Longyearbreen (Norwegian Polar Institute, 1990). The aerial photograph was taken in 1990 but when comparing it to the picture taken in the summer of 2004 (figure 2.6) it is evident that little change in the geometrical position of the surface features have occurred. The numbers on figure 5.5 indicate surface features that are thought to relate to reflectors observed in the radar cross sections.

Figure 5.6 shows the radar image of profile G, which is the survey line nearest to the debris-covered glacier snout. Several dipping reflectors are observed in the cross section. The magnitude of these, the continuity with depth and the appearance of sediment-bands on the aerial photograph (number 1) suggest that the features are sediment-rich thrusts perhaps of basal origin. Some of the debris-bands in the eastern part of the profile may have thicknesses close to the radar detection of 0.1 m, explaining why the bands are observed on the glacier surface but not continuously in the radar image. Isolated diffraction hyperbolas are seen in the center of profile G in 20 m depth. These reflections are not associated with structures observed on the surface and are not identified in any of the other profiles. Outcropping debris bands are present in the middle of the glacier towards the debris-covered glacier snout. The diffraction hyperbolas are therefore probably related to thrust features perpendicular to the profile direction. The largest supraglacial channel on Longyearbreen (number 2 on figure 5.5 and 5.6) is clearly reflected on profile G. It is also apparent from profile G that the supraglacial stream runs through an area where debris-bands are traceable about 40 meters into the ice.

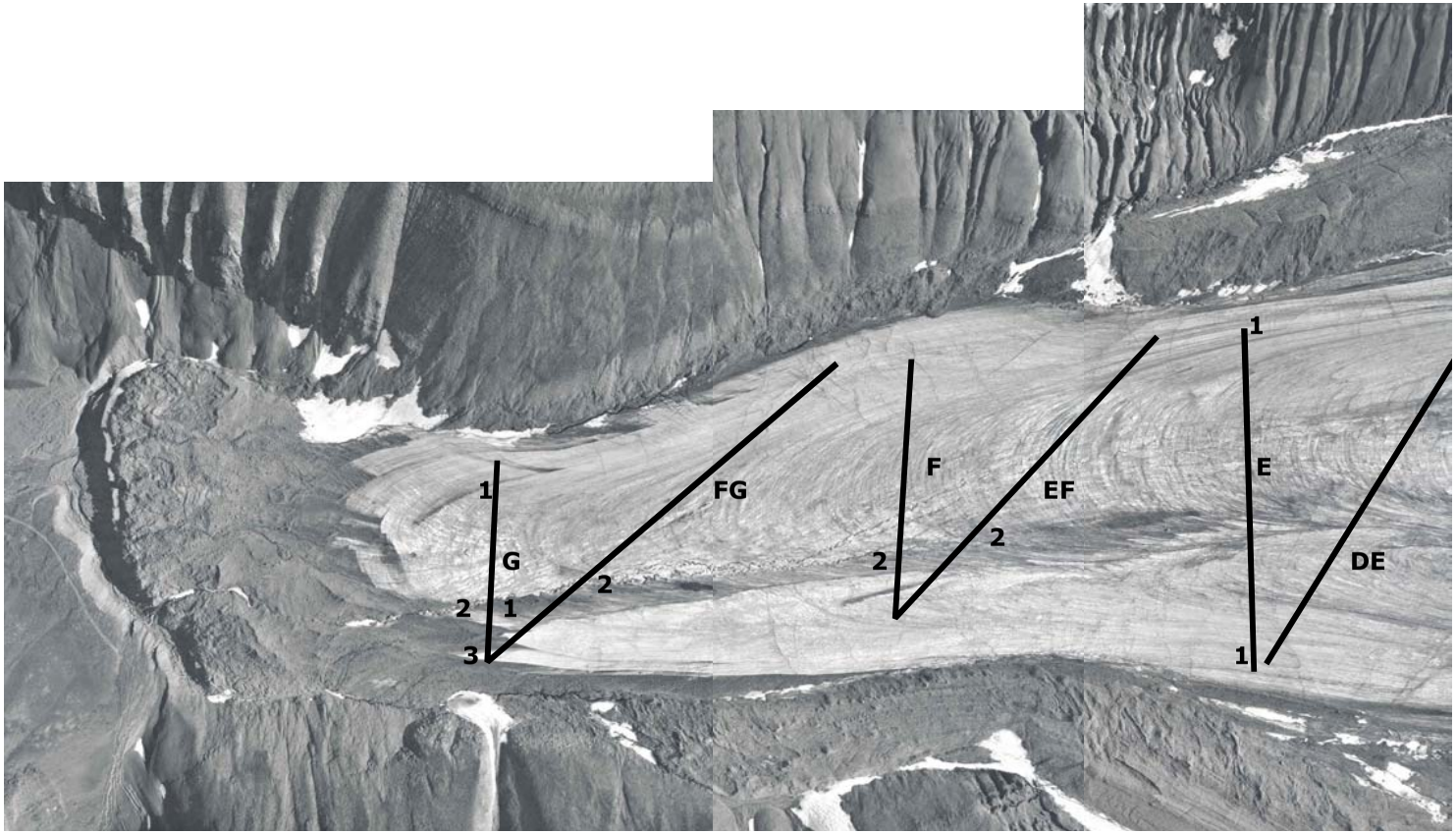

Figure 5.5. Aerial photograph of the glacier terminus of Longyearbreen (Norwegian Polar Institute, 1990) with the location of survey line G, FG, F, EF, E and part of line DE. Numbers indicate features recognized in the radar image for the particular line. 1: sediment-bands within the ice, 2: supraglacial channel and 3: moraine material.

The supraglacial meltwater stream is also clearly detected by the radar in profiles FG, F and to a lesser extent in profile EF (appendix A.3). No debris-bands are related to the supraglacial channel in these radar profiles. The intense scattering of the radar signal in the end of profile G and FG is thought to be caused by the moraine material observed on the aerial photograph. The basal reflection is unclear in the center of profile G. This is also observed in several of the other profiles especially in profile FG, E and C (appendix A.3).

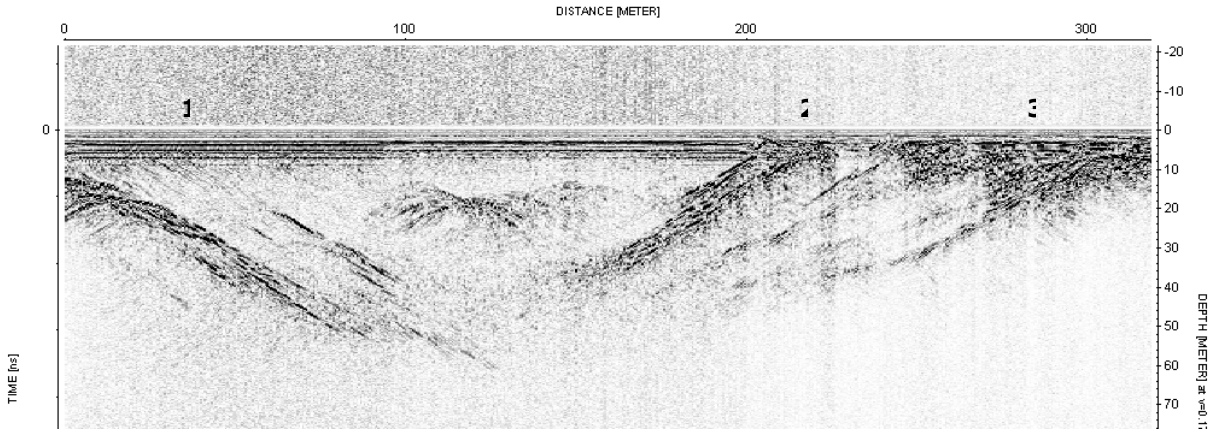

Figure 5.6. Profile G with numbers associated with surface features observed on figure 5.5. 1: sediment-bands within the ice, 2: supraglacial channel and 3: moraine material.

The western lateral channel on Longyearbreen is deeply incised, becoming englacial and subglacial as it approaches the glacier terminus. The channel is in general 10 to 15 m deep (Bælum, 2006) and crossing it with the GPR was expected to give clear reflections. A comparison of GPS coordinates from line D with coordinates from a mapping of the meltwater channel (Bælum, 2006) showed that survey line D crossed the western lateral channel at about 525 m. A section of the profile is shown in figure 5.7. Several diffraction hyperbolas can be seen between 510 and 550 m. Assuming that the top points of the hyperbolas indicate the upper and lower boundaries of the channel and that the channel is filled with air, the reflection free void (indicated with the red arrow on figure 5.7) is equal to a channel height of about 6 m (equation 1, v_{air} = 0.3 m ns^{-1}). The roof of the channel is located in about 9 m depth resulting in a distance of 15 m from the glacier surface to the channel floor. Mapping of the geometry of the meltwater channel in May 2004 showed that the channel floor is positioned at about 20 m depth at this location and that ice deformation has sealed off the top of the channel (personal observation, Bælum, 2006). This correlates well with the dimensions of the channel observed in radar profile D. Diffraction hyperbolas that are thought to relate to the presence of lateral meltwater channels incised in the glacier ice, are seen in both the eastern and western ends of the profiles D, DE, E, EF and F and in the western end on profile CD and F (appendix A.3).

Diffraction hyperbolas appear within the clear ice on most of the radar profiles. It is not possible however, to state whether or not these reflections originate from air inclusion in the ice or blocks of sediments.

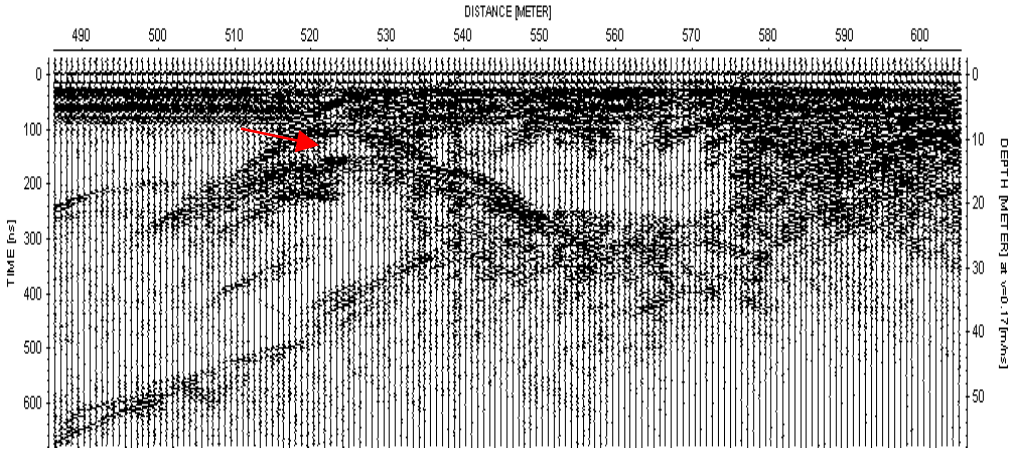

Figure 5.7. Enlarged section of profile D. Clear diffraction hyperbolas indicate the presence of the western lateral channels. The red arrow indicates a possible air filled void.

Figure 5.8 shows the discontinuous basal reflector observed on profile AB and B in detail. Several similar features were encountered in many of the radar images, although to a lesser extent. Thrust faults like these are often found in glaciers where frozen margins restrict glacier movement (Murray et al., 1997). The very strong reflections observed in profile AB and B signifies the large amount of sediment uplifted by the frozen base to an englacial position.

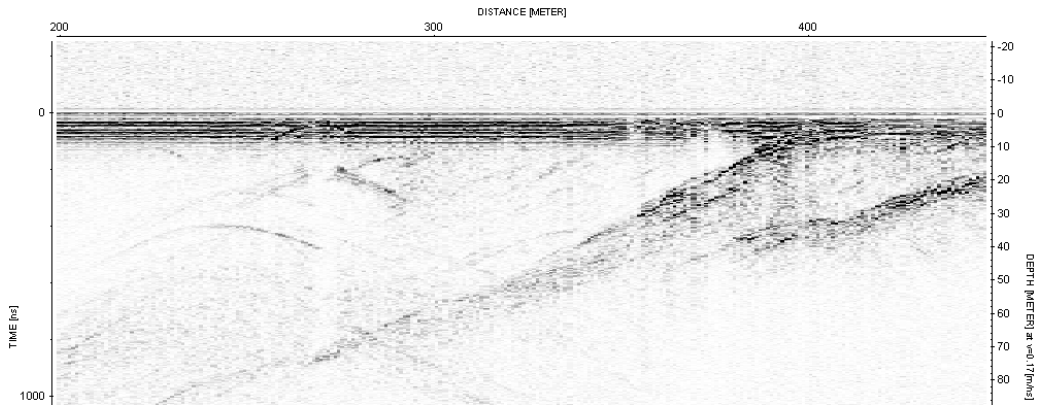

Figure 5.8. Enlarged section of profile B. Clear thrust feature in the basal reflector in the western marginal area of the glacier.

5.2 **Weather data**

A comparison between the monthly air temperature and precipitation amounts from October 2003 to September 2004, and the "normal" values derived from the average monthly mean from 1961 to 1990 (http://met.no) is presented in figure 5.9. All values are from the meteorological station at Longyearbyen Airport (for location see figure 2.3).

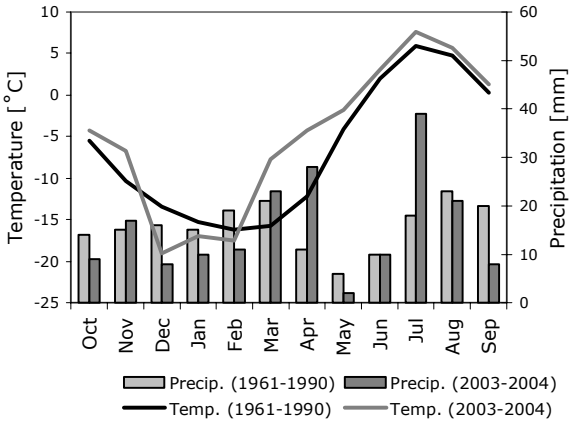

Figure 5.9. Monthly temperature and precipitation data from the meteorological station at Longyearbyen Airport. Values from October 2003 to September 2003 are compared to the monthly average from 1961 to 1990 (http://met.no).

The temperature curves in figure 5.9 show that December 2003 in particular, and January and February 2004 to a lesser extent, were slightly colder than normal. March and April 2004 were considerably warmer than usual with mean temperatures about 8°C higher than normally recorded. The summer of 2004 was slightly warmer than normal. The precipitation data show a relatively dry winter followed by a spring with values above normal. The most distinct feature in an otherwise dry summer is the value from July, which was more than twice the normal value. More detailed meteorological data of precipitation level, air temperature, cloud cover and air humidity were provided by the Norwegian Meteorological Institute from 15 May to 30 September 2004 (appendix A.4 and figure 5.10).

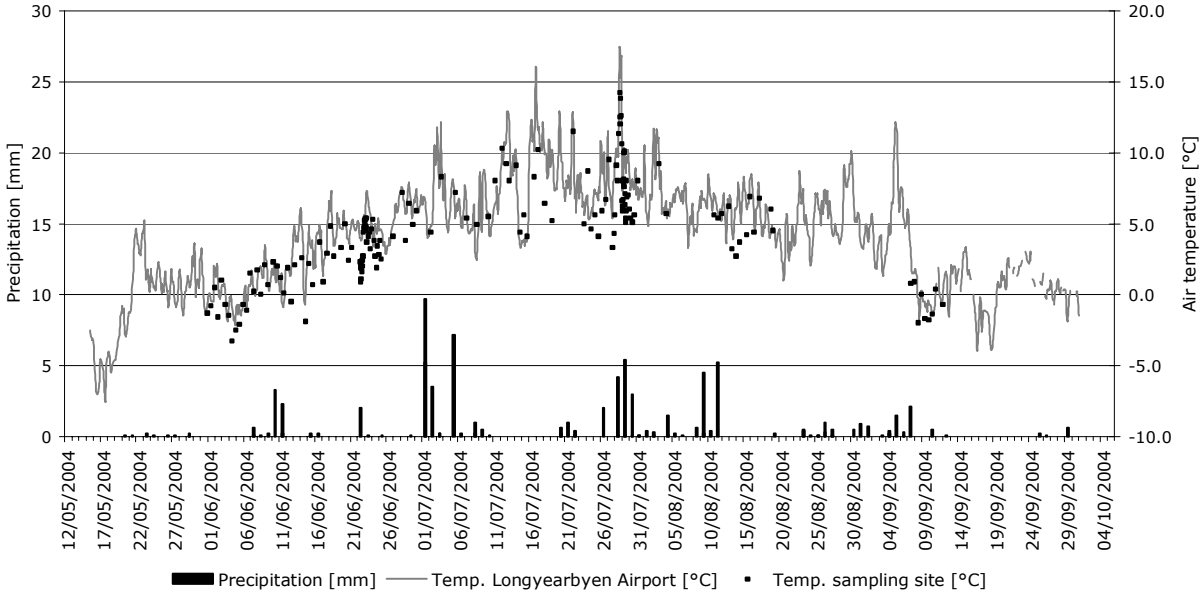

Figure 5.10. Temperature and precipitation record from Longyearbyen Airport in the period from the 15 May to 30 September 2004 compared to temperatures manually measured at the sampling site.

In figure 5.10 temperatures and precipitations levels (measured every three hours) at Longyearbyen Airport is shown together with temperatures measured at the sampling site when collecting water samples. Temperatures were in general above 0°C after 20 May and below the freezing point after 8 September. Maximum summer temperature of 17.3°C was measured at Longyearbyen Airport on 28 July at 04:00 in the morning. Several major precipitation events took place in the beginning and end of July resulting in an unusually high level for this period. Air humidity varied from 60 to 100% throughout the summer (appendix A.4). Temperature measured at the sampling site clearly related well with temperatures measured at Longyearbyen Airport.

Figure 5.11 shows the correlation between temperature measured at the sampling site and air temperature at Longyearbyen Airport from 15 May to 30 September. Temperatures correlated well ($R^2 = 0.84$) with a maximum deviation of 4.9°C. Temperatures at the sampling site, which was located about 100 m higher and further inland than the station at Longyearbyen airport, were generally lower than the temperature measured at the airport. The trend line suggests a temperature difference of –1.4°C between the meteorological station at Longyearbyen airport and the sampling site. This difference appears to be larger on warm days than on cold days. In the following sections, temperatures from Longyearbyen airport will be used because the data set is more comprehensive and reflects the temperature conditions at the sampling site well.

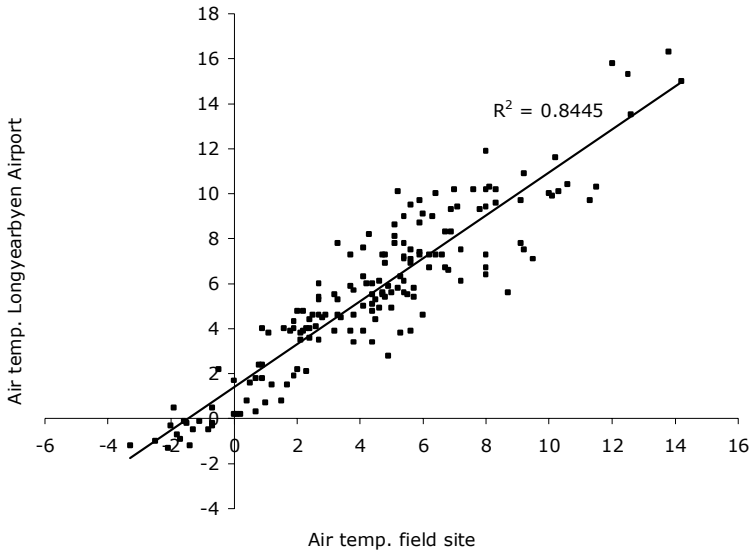

Figure 5.11. Correlation between air temperatures recorded at the meteorological station at Longyearbyen Airport and air temperature manually measured at the sampling site.

5.3 **Water level and discharge**

Longyearelva drains a catchment of 23.71 km^2 out of which approximately 30% is glacier covered (Grønsten, 1998). Runoff in the river is therefore highly influenced by the glaciers in the catchment. On the basis of calculations and measurements conducted by Grønsten (1998) and Sægrov (1995) and observations from fieldwork, the proportions of the different tributaries in Longyearelva were estimated. Water flowing from Larsbreen is thought to

constitute 35% of total discharge in Longyearelva and water from Longyearbreen 50% of total discharge. The 50% was split into two components where 33% of total runoff in Longyearelva flows in the western meltwater stream (water from the small unnamed glacier and water emerging from the western drainage system of Longyearbreen) and 17% emerges from the moraine cave and flows in the eastern meltwater stream where water sampling was conducted. The final 15% of total discharge is thought to come from smaller tributaries after Longyearelva and Larselva confluence.

Figure 5.12 shows variations in water level measured at the gauging station together with air temperature and precipitation during the summer of 2004. The term "ablation period" will hereafter be used to denote the period where thawing of snow, glacier ice and permafrost occurred.

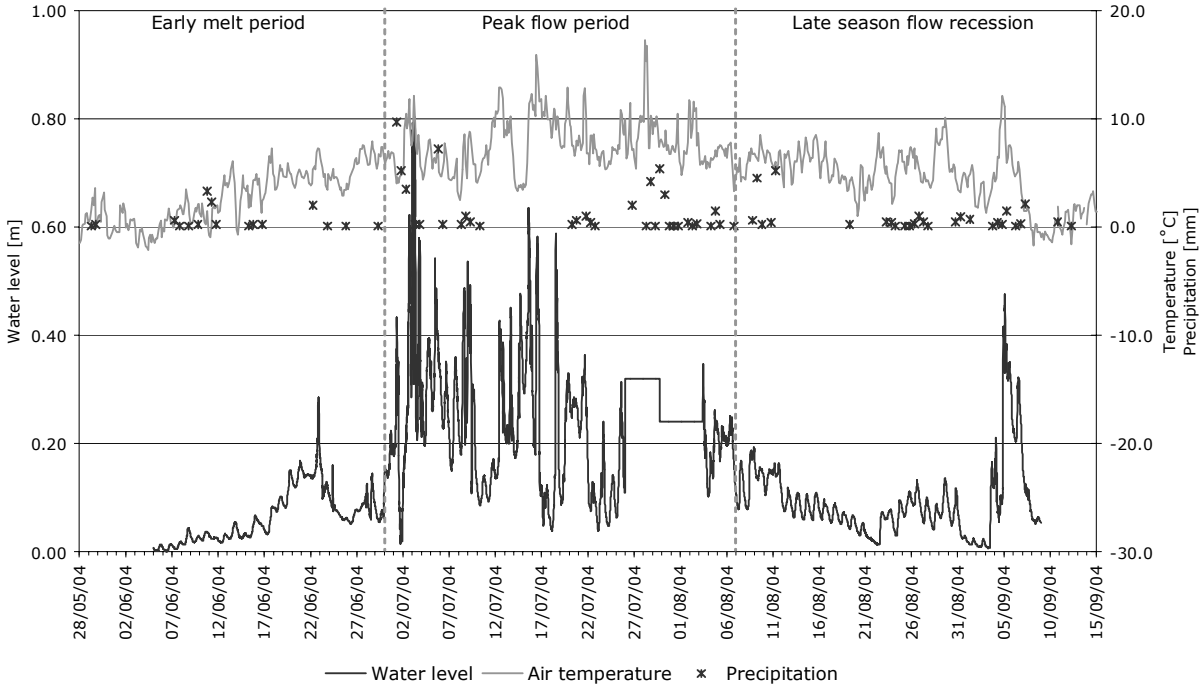

Figure 5.12. Water level in Longyearelva along with air temperature and precipitation events recorded during the ablation period. The ablation period was divided into three sub-periods as suggested by Wadham et al. (1998): Early melt period, peak flow period and late season flow recession.

Water was registered at the gauging station from 5 June to 9 September. This period was subsequently divided into an early melt period (5 to 29 June), a peak flow period (30 June to 6 August) and a late season flow recession (7 August to 9 September) as suggested by Wadham et al. (1998) (see section 3.3.2). During the period from 25 July 22:30 to 3 August 10:10 the gauging station was out of order and an average water level was estimated based on notes from field work, pictures of the river at the sampling site and the meteorological conditions at the time.

The first meltwater was observed flowing from the snowpack in Longyeardalen on 25 May, 5 days after air temperatures had largely been above zero degrees. On 29 May meltwater was first observed at the sampling site and an inspection of the moraine cave on 30 May

revealed water flowing within the channel and out from under the snow covered portal. The first water was registered at the gauging station in Longyearbyen on 5 June, almost two weeks after water had first been observed in the river bed and the adjoining catchment.

In general, energy inputs during the early melt period were dampened because of the high storage capacity of the thawing snowpack. Small-scale fluctuations in water level therefore occurred without an obvious relationship with air temperature as the water level rose slightly in the beginning of the period. The precipitation events occurring between 7 and 11 June fell as snow over most of the catchment and were not recognised in the hydrograph. A marked high in water level occurred from 18 June to 26 June. Temperatures were slightly enhanced, but do not seem to explain the rapid rise in water level. The episode is thought to reflect the release of water from storage either in the snowpack or in channels connecting to the principal drainage system. A distinct peak in water level occurred in the evening of 22 June. This event was possibly related to a rainfall episode (2 mm) that ended at 7:00 on 22 June. The time lag between event and response was long, since snow still covered the entire catchment. After the reservoir had emptied, water level decreased. Warmer temperatures however eventually resulted in enhanced ablation and a renewed increase in water levels.

The peak flow period was characterized by rapid and large water level fluctuations. The peak in water level at 8:40 on 1 July may be explained by a preceding period of higher air temperatures in combination with a major precipitation event (9.7 mm). The rainfall in the early morning on 1 July possibly triggered the release of water from storage. The short time lag (hours) and the rapid increase in water level, reflect the onset of a change in the drainage system. The dampening effect due to temporal storage of water in the snowpack was becoming less significant and response to climatic influences more rapid. Ice ablation from the glacier became more and more important as the transient snow line began to move up-glacier. The local maximum in water level on 1 July was followed by an extraordinary decline of 0.40 m within 12 hours. This event coincided with a temperature drop from 7 to 4°C, which does not seem to explain the dramatic decline in water level however. The episode may instead have been related to temporarily storage of water during a period of lower ablation. Subsequent temperatures rose to a local maximum of about 12°C and water level reached the highest level recorded (0.80 m) on 3 July in the early morning. Several precipitation events were recorded during the high water levels and are thought to have contributed significantly to runoff in combination with the rapid decomposition of the snowpack in the lower part of the glacier. For comparison, the drier and warmer, mostly cloud free days from 11 to 15 July experienced significantly lower water levels. Photographs from the nearby glacier, Larsbreen, document the rapid changes that occurred in the beginning of the peak flow period (appendix A.5). A picture taken on 29 June shows a glacier covered in dirty soaked snow while patches of glacier ice are visible in the lower areas on a picture from 3 July. During the period where the water level logger was malfunctioning, the highest temperatures during the season occurred in combination with a major precipitation event. It is difficult to conclude whether this event resulted in the maximum water level during the ablation period even though the meteorological conditions suggest it. Factors such as a rapid degradation of the snowpack and an emptying of reservoirs as melt water channels connected to the principal drainage system, had less effect at this late stage in the season. Here, the glacier's drainage system is thought to be well developed and the transient snow line beginning to approach its maximum elevation. Multiyear studies of runoff variations in glacial catchments on Svalbard have shown

however, that peak discharge usually occurs in late summer when high air temperatures coincide with rainfall events (Sund, 2004).

From 7 August water levels slowly declined. This period is referred to as the late season flow recession. Diurnal variations were obvious although precipitation events obscured this pattern at times. The river almost ceased to flow on 3 September. A sudden increase in temperature combined with several precipitation events however, resulted in a short period of renewed ablation, peaking on 5 June 02:00, only hours after air temperature had started to decline.

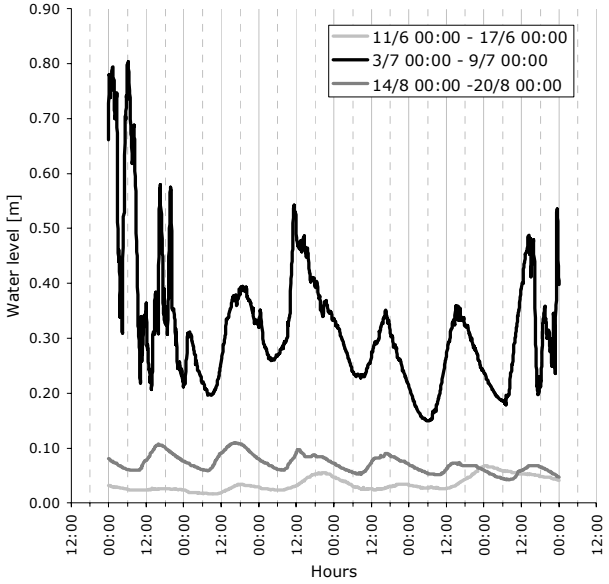

Figure 5.13. Diurnal variations in water level during six day periods in the early melt period (11 June to 17 June), the peak flow period (3 July to 9 July) and the late season flow recession (14 August to 20 August).

Variations during the ablation period in diurnal fluctuations in water level are illustrated in figure 5.13. Fluctuations were insignificant during the early melt period while both the peak flow period and the late season flow recession had clear diurnal fluctuations. The peak flow period had the largest water levels and hence the largest fluctuations. The evolution in drainage patterns during the ablation period in relation to important meteorological parameters is shown in figure 5.14.

The early ablation period, represented by the period from 11 June 00:00 to 17 June 00:00, was a period influenced predominately by snowmelt. Only small variations in runoff were recognised and the possible time lag between temperature and water level varied significantly. The precipitation events occurring during this period were minor and were not recognised in the hydrograph.

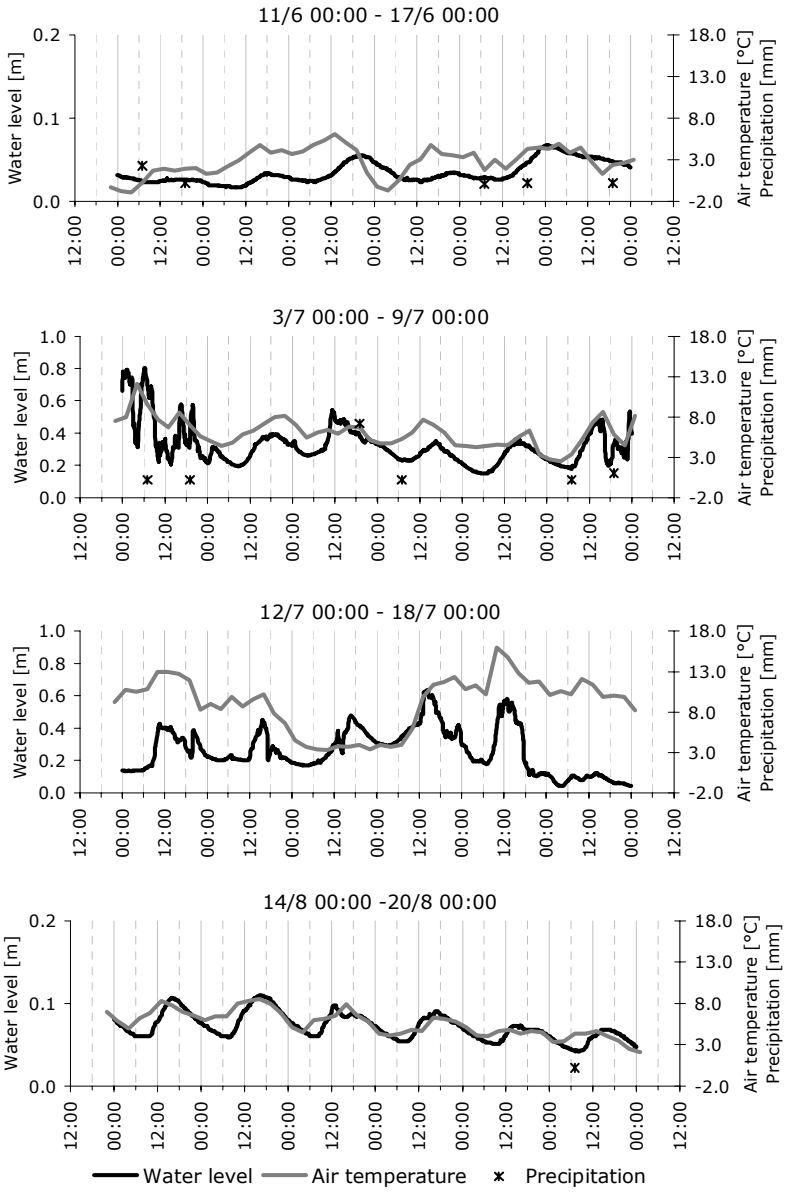

Figure 5.14. Examples of diurnal variations in water level and air temperature for four different 6-day periods during the ablation period. Marked precipitation events reflect precipitation during the preceding three hours. Note change in scale for the two intermediate periods.

The peak flow period is represented in figure 5.14 by a period influenced by precipitation, 3 July 00:00 to 9 July 00:00, and a warm period where no precipitation occurred, 12 July 00:00 to 18 July 00:00. In the first period, diurnal variations in both temperature and water level were evident but occasionally disrupted by precipitation events and possibly the release of snowmelt as the snowpack melted. Diurnal fluctuations of approximately 0.20 m were superimposed on a base flow component of equal size. Maximum runoff occurred predominantly at 18:00 while minimum runoff in Longyearelva took place a 06:00. Time lag between temperature and water level signal can be illustrated by the distinct temperature peak at 13:00 on 6 July followed by a water level peak about 3 ½ hours later. The fact that

the discharge peaks before the air temperature on certain days may be explained by a difference in meteorological parameters at the glacier and at the airport where temperatures were measured. The second period illustrates a complex temperature pattern and water level fluctuations. Temperature fluctuations were however reflected in the water level changes even though the curves were more uneven than those seen for the preceding period. This uneven pattern of the water level curve indicates a pulsation in the runoff rather than a constant flow. The constant temperature low from 14 to 15 June coincided with an air humidity of 100 % in the meteorological data for Longyearbyen airport (appendix A.4). Dense fog laid over the airport during these days, a phenomena often occurring on Svalbard during warm and calm weather. The fact that water levels in Longyearelva still experienced a diurnal maximum on 14 July may indicate that the fog was limited to the valleys and not present on the glaciers in the area, as was often the case.

Diurnal variations were clear in the late season flow recession, illustrated here by the days from 14 August 00:00 to 20 August 00:00. Only one minor precipitation event occurred during this period. Diurnal variations were still in the same order as the base flow component, but both diminished during the 6-day period due to declining air temperatures. Runoff during the late season flow recession experienced a maximum around 18:00 and a minimum at 06:00 similar to during the peak flow period. A water level peak followed the temperature peak at 13:00 on 14 August three hours later. Throughout the period, water level and temperature fluctuated almost simultaneously indicating a fast responsive drainage system for the glaciers in the area.

The calculated discharges for Longyearelva are shown in figure 5.15. Variations in discharge were large, especially in the peak flow period, where the highest discharge of 16.5 $m^3 s^{-1}$ occurred on 3 July.

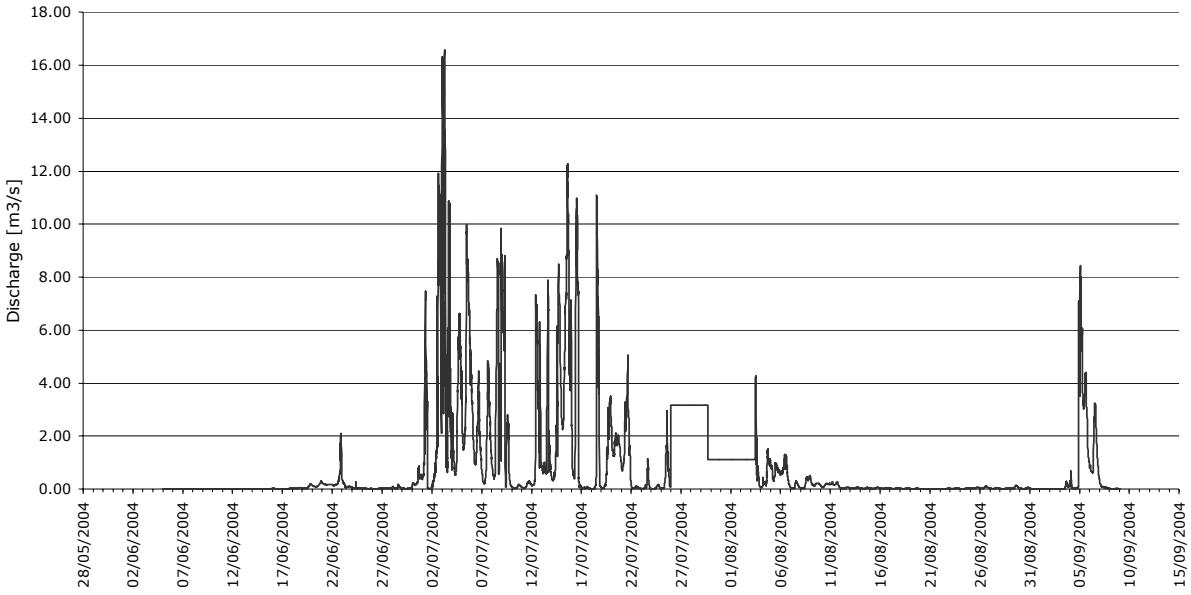

Figure 5.15. Calculated discharges for Longyearelva during the ablation period.

In table 5.1 the total amount of water from the catchment of Longyearbreen is listed for the entire ablation period and the individual sub-periods. 43% of the catchment of Longyearbreen is glacier-covered. 89% of all water draining from Longyearbreen flowed

during the peak flow period characterized by highly variable water levels (standard deviation = 1.28). The late season flow recession had a significant higher total flux than the early melt period primarily because of an exceptional raise in air temperature resulting in a renewed ablation in the beginning of September.

Table 5.1. Statistical summary of discharge [$m^3 s^{-1}$] and flux [m^3] for Longyearbreen during the ablation period of 2004. The numbers in brackets are the relationship between the individual value and the value for the total ablation period.

Period	Min. Q	Max. Q	Mean Q	SD Q	Mean diurnal flux	Total flux
Total ablation period	0.00	8.30	0.43	0.95	37370	3587800 (1.00)
Early melt period	0.00	1.05	0.02	0.07	1980	49610 (0.01)
Peak flow period	0.00	8.30	1.00	1.28	84090	3195480 (0.89)
Late season flow recession	0.00	4.22	0.12	0.42	10080	342710 (0.10)

5.4 **Suspended sediment transport**

The water level measured at the gauging station in Longyearbyen will be used in the following sections as a direct indicator of variations in runoff in the river at the sampling site. Care will be taken in comparing variations below and above a water level of 0.39 m since the relationship between water level and discharge is thought to change at this level (equation 13 and 14). Unless otherwise specified, results presented are from the river at the sampling site.

Nine samples were collected successively in order to reveal short term fluctuations of suspended sediments in the river water. The standard deviation of the data set comprised 5% of the mean value. These 5% are within the estimated uncertainty of the method for determining suspended sediment concentration (SSC) in the collected water.

Figure 5.15 shows variations in suspended sediment concentrations (SSC) and water level during the ablation period with squares indicating time of water sampling. The graph has been divided into the three previously mentioned periods with the ablation period starting 29 May and ending 11 September. Statistical values for the total ablation period and the three sub-periods are listed in table 5.2. The results show an early melt period and a late season flow recession with similar low values of SSC. Mean values of 0.17 and 0.18 $g\,l^{-1}$ respectively were calculated for the two periods. The peak flow period had high and variable SSC with a mean of 3.18 $g\,l^{-1}$ and a standard deviation of 2.73 $g\,l^{-1}$. Calculated mean for the entire population of water samples was 1.32 $g\,l^{-1}$.

The amount of sediment that can be mobilised by water depends on the energy and therefore the velocity of the water. SSC are therefore expected to correlate with water level when sediment sources are abundant (Hodson et al., 1997). In the early melt period, SSC were enhanced after 21 June and on 22 June in particular due to a rise in water level (see figure 5.15).

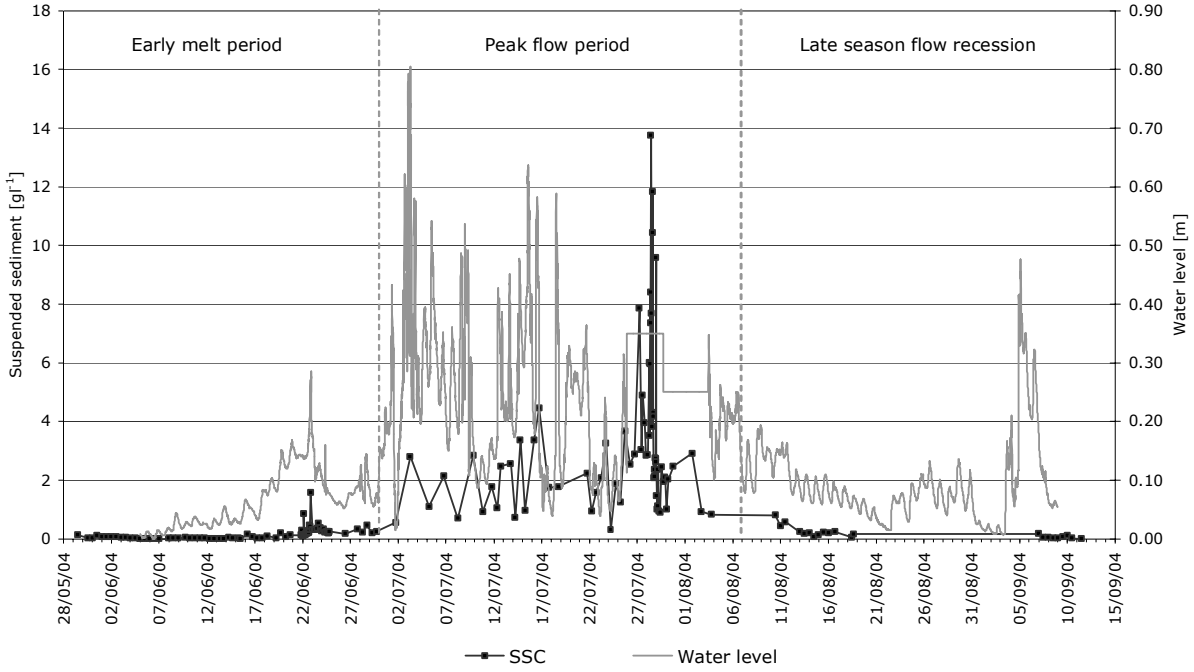

Figure 5.15. Variations in water level and SSC during the ablation period. The individual water samples are marked with squares.

This episode occurred during a three day period with more frequent water sampling (see figure 5.16). The rise in water level was reflected in the measured SSC with the highest values during peak water level. The peak in SSC occurring on 22 June 03:00 was due to the presence of coarser material in the sample collected. The adjacent samples show no evidence of enhanced SSC and the event may have been related to a local slope failure in the river. The maximum SSC measured during the three day period was only documented by one sample. The three preceding samples however, indicated a raise in suspended sediments in the river water and the maximum value is thought to reflect the general conditions at the time of sampling. The relationship between water level and SSC altered during the three days. Low water levels following 22 June subsequently gave rise to a higher load of suspended sediments than before the peak in water level and SSC. This change suggests that the availability of sediments for fluvial transport had improved.

Table 5.2. Minimum, maximum, mean and standard deviations of SSC [g l^{-1}] in river water during the ablation period and the three sub-periods. n = number of samples in each data set.

Period	Min.	Max.	Mean	SD	*n*
Total ablation period	0.00	13.74	1.32	2.23	181
Early melt period	0.00	1.56	0.17	0.21	90
Peak flow period	0.30	13.74	3.18	2.73	69
Late season flow recession	0.00	0.81	0.18	0.20	22

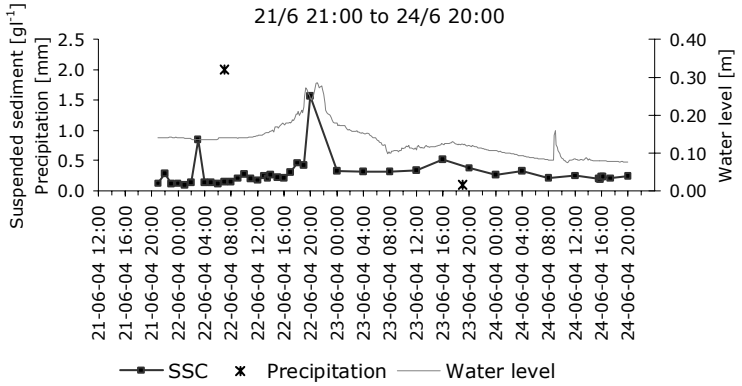

Figure 5.16. SSC, water level and precipitation events from the first period, with more frequent water sampling.

The peak flow period had significantly higher SSC and was also the period where the largest fluctuations occurred. The beginning of the period had low data coverage and it is not possible to see if the raise in discharge in the beginning of July resulted in a raise in SSC. Most marked measured increase in SSC occurred from the evening on 26 July to 29 July 00:00. The event coincided with a period with very high air temperatures and with several major precipitation events. Unfortunately, the water level logger was not working during this period and it is therefore not possible to give detailed information about discharge. Mean water level during the period was, however, estimated to 0.35 m until 29 July 18:00 after which it was lowered to 0.25 m. The marked increase in SSC occurred during a period with more frequent water sampling (see figure 5.17).

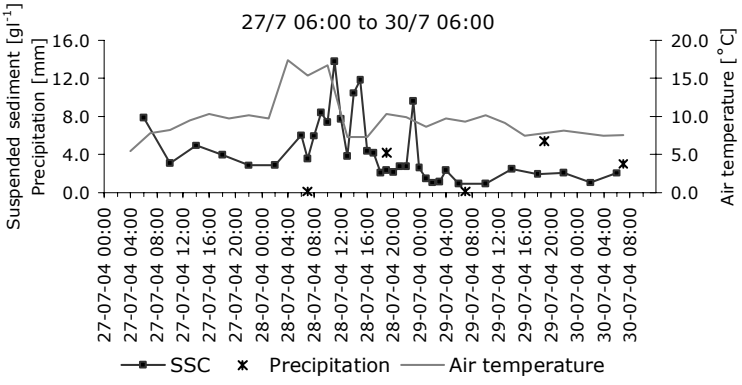

Figure 5.17. SSC, water level and precipitation events from the second period, with more frequent water sampling.

The SSC showed higher variability than the first period with frequent water sampling. Highest SSC measured during the entire ablation period (13.74 g l^{-1}) occurred on 28 July 11:00 during a period where runoff at the sampling site was estimated to be at the highest level during the whole period (see notes from fieldwork in appendix A.6). Lower water levels were observed after 29 July 18:00 where SSC had also lowered considerably. The effect of the precipitation events is unclear possibly because of large local differences in the size of the rainfall. The second largest peak on the SSC curve coincided with heavy rainfall recorded at the sampling site between 12:00 and 17:00 on 28 July, with maximum intensity at 15:00. Rainfall was not, however, registered at the sampling site at the time of the third

major suspended sediment peak. No signal in SSC was observed after the precipitation event recorded at both at Longyearbyen Airport and at the sampling site in the evening on 29 July. During precipitation events, slope failures in the proglacial mountain sides fed the river with abundant amounts of sediment. Because of high water levels, sampling had to be conducted 100 m after the water emerged from the glacier river portal, and sediment sliding from the sides of the valley may therefore have contributed significant to the measure SSC.

On 28 July 02:00 significantly clearer water than the water at the sampling site was observed in the western meltwater stream (see figure 5.18). This was not examined in more detail during high discharge and samples collected in both streams during low discharge gave an ambiguous result (see appendix A.7).

Figure 5.18. Picture taken on 28 July 02:00 looking from the eastern meltwater stream (at the sampling site) towards the western meltwater stream. Debris-covered glacier snout outside the picture to the left.

In figure 5.19 seasonal changes in the relationship between SSC and water level are shown. A general raise in the relationship between SSC and discharge occurred during the early melt period and the majority of the peak flow period. The early melt period was characterised by relatively small fluctuations with a clear change in the relationship between SSC and water level on 22 June 17:00. The relationship between SSC and water level was about 1:1 prior to this episode, while after it was about 3:1 (shown in figure 5.19). No change occurred in the proglacial area that explained this shift. In the peak flow period, large fluctuations were observed in the relationship between SSC and water level. The marked peaks on figure 5.19 were related to periods with low water levels where a relatively high load of suspended sediment was still held in suspension by the water. These peaks were often observed following high discharge periods. During the late season flow recessions the relationship between SSC and water level gradually changed from 3:1 to 1:3 as the water ceased to flow.

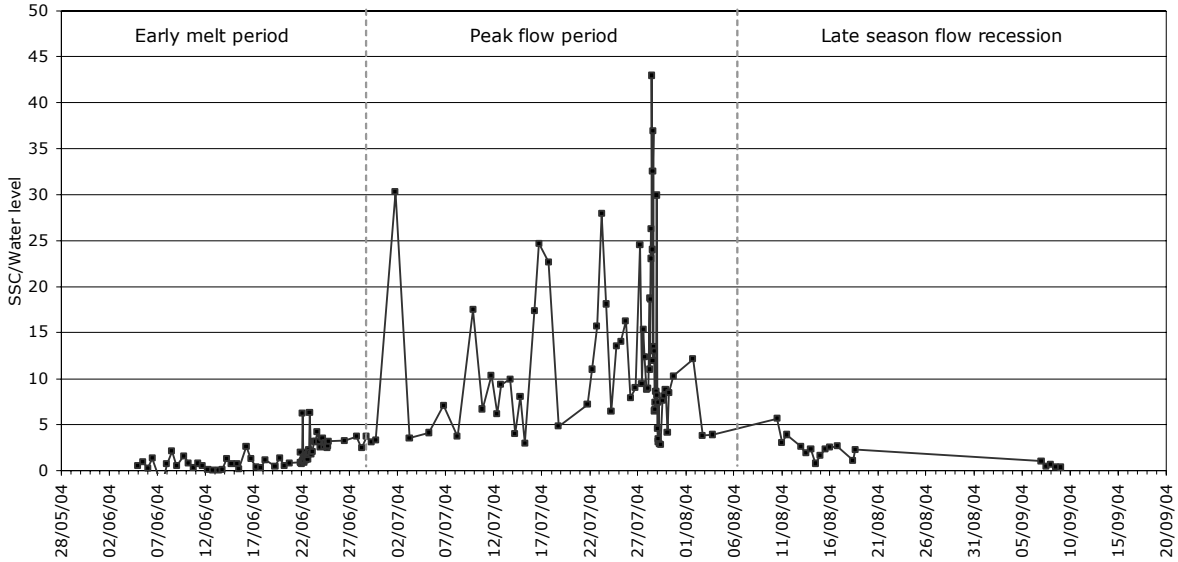

Figure 5.19. The relationship between SSC and water level for 2004. Values of SSC were left out for the beginning and end of the season since no water was recorded at the bridge in Longyearbyen at the time of sampling.

The sources of the suspended sediment were investigated on 18 August, a day with low runoff and little suspended sediment in the water. Meltwater samples were collected at several localities in the catchment of Longyearbreen (see figure 4.9 for location). The values of SSC are listed in table 5.3. Samples were collected at the sampling site at both the beginning (10:00) and the end (16:00) of the fieldwork for comparison. During the four hours, SSC had increased in the water.

Table 5.3. Mean and standard deviation of SSC [g l^{-1}] measured in water samples collected at different localities in the catchment of Longyearbreen between 10:00 and 16:00 on 18 August.

Source	Mean SSC	STD	*n*
Sampling site (10:00)	0.079	0.021	3
Supraglacial channels (on ice)	0.008	0.026	7
Supraglacial channels (on debris)	0.216	0.142	3
Upper lateral channel (east)	0.207	0.001	2
Lower lateral channel (east)	1.288	-	1
Upper lateral channel (west)	0.214	-	1
Westen meltwater stream	0.370	0.005	2
Tværdalen	0.134	-	1
Sampling site (16:00)	0.164	-	1

Water flowing in supraglacial channels on the clear ice had the lowest accessibility to erodible sediments, which was reflected by the low SSC in the water. Coarse sediments were observed in the channels but were too big to be mobilised by the flowing water. SSC increased significantly as the water ran over the debris-covered glacier snout where erodible sediments are abundant.

Water in the eastern lateral channel is thought to be one of the main contributors to the water flowing at the sampling site. Samples from the upper part of the lateral channel had a

relatively high amount of suspended sediment. However, the highest concentration of suspended sediment was measured in the lower part of the eastern lateral channel. The high value reflects the abundance of sediment and the high energy environment governing in this part of the channel. Sediments are delivered to the eastern lateral channel by mass-wasting of sediments from the mountainsides and from water draining from Larsbreen through lateral moraines before entering the channel. This is illustrated in figure 5.20 that also shows the meandering shape of the upper eastern lateral channel. Similar high values of SSC were not observed in the water at the sampling site. This is most likely caused by a change in energy of the water in the less confined subglacial channel rather than an input of sediment poor water.

Figure 5.20. Picture showing the upper eastern lateral meltwater channel. Large rocks cover the channel floor while fine-grained sediments are carried away with the flow (18 August 2004).

The upper western lateral channel had similar values as the eastern lateral channel, while water from the unnamed glacier (Tværdalen) resembled the water from the sampling site. Water from the western meltwater stream carried about twice the amount of sediments as the eastern stream.

The annual sediment yield for Longyearbreen was calculated in three ways resulting in three very different end results. For all estimates, it was assumed that water from the sampling site was representative for the bulk meltwater emanating from Longyearbreen. First, an estimate of annual sediment yield was made by multiplying SSC for the individual samples by discharge measured at the time of sampling (appendix A.8). The area under the graph was calculated and resulted in an annual sediment yield of 8910 $t\,y^{-1}$ (diurnal mean = 90 $t\,d^{-1}$). With a catchment area of 10.68 km^2 this gave a specific sediment yield of 830 $t\,km^{-2}\,y^{-1}$. The second estimate of annual yield was found by multiplying mean discharge (0.43 $m^3\,s^{-1}$) by mean SSC (1.32 $g\,l^{-1}$) and the length of the ablation period (96 days). This method resulted in a significantly smaller annual yield of 4710 $t\,y^{-1}$ (diurnal mean = 50 $t\,d^{-1}$) and a specific sediment yield of 440 $t\,km^{-2}\,y^{-1}$. A third estimate of 3030 $t\,y^{-1}$ was obtained by using the same procedure as for the second estimate but with a mean SSC of 0.85 $g\,l^{-1}$

found by only including two samples a day during periods of frequent water sampling (at about minimum and maximum discharge). This resulted in a diurnal mean of 30 $t\,d^{-1}$ and a specific sediment yield of 280 $t\,km^{-2}\,y^{-1}$.

5.5 **Ions**

Four snow pits were dug on Longyearbreen during the spring of 2004. Snow pit 1 and 2 were dug on 15 April at 355 m.a.s.l. and 450 m.a.s.l. respectively. Snow pit 3 was excavated on 23 April at almost same locality as snow pit 2 while snow pit 4 was dug on 29 April in an altitude of 475 m.a.s.l. Locations of the four snow pits are shown in figure 4.9. Snow pit 1-3 were dug before the initiation of snowmelt, while snow pit 4 was excavated after temperatures had reached zero degrees in the upper 45 cm snow. Concentrations of ions in the four snow pits are shown in figure 5.21 and 5.22 together with snow temperatures and $\delta^{18}O$ values. Variations in $\delta^{18}O$ values will be treated in more detail in section 5.6. All snow pits were located in the ablation area of the glacier.

A statistical summary of the ionic composition of the snowpack is listed in table 5.4. Cl^- (34% of total solute content) and Na^+ (27% of total solute content) were the dominant ions in the snowpack for all snow pits, but Ca^{2+}, SO_4^{2-} and Mg^{2+} also had relatively high concentrations. NO_3^- and K^+ had significantly lower concentrations than the other major ions and, in 17 snow samples, NO_3^- concentration was below detection range. HCO_3^- was not measured directly and has been calculated from the concentrations of the other ions. Uncertainties in these are therefore reflected in the value for HCO_3^-. For many snow samples this uncertainty resulted in negative values for HCO_3^-. Furthermore, calculation of the concentration was not possible for the samples where NO_3^- concentration was below detection range. Only 7 out of 39 snow samples are represented in table 5.4 and the mean concentration in table 5.4 is therefore unreliable.

Snow pit 1 and 2 (figure 5.21) were dug on the same day and showed similar variations in chemical composition. Snow temperature decreased from -5.7°C in the top layer to -8.0°C in the bottom layer in snow pit 1, and from -6.2°C to -9.6°C in snow pit 2. Snow pit 2 was about 10 cm deeper than snow pit 1. The variations in ion content suggest that the lowermost 20 cm of snow were missing in snow pit 1 due to an earlier start to snow accumulation higher on the glacier. Ice layers are expected to be solute-poor compared to the snow because of an exclusion of ions from the ice during refreezing (Raben and Theakstone, 1994, Theakstone and Knudsen, 1996a). In snow pit 1, a 2 cm ice layer was present at 55 cm depth, while several ice lenses were located between 35 and 55 cm depth in snow pit 2. The fact that no obvious decreases in ion concentrations were observed in these depths most likely relates to the fact that the collected material was a mix of both ice and snow within the 10 cm sampling interval. A 10 cm thick layer of coarse grained red snow crystals was found in the lowest part of snow pit 2. This layer had a very high concentration of Ca^{2+}, a trend that was also recognised in snow pit 1 although to a much lower extent. The raise in Ca^{2+} may have been caused by Ca^{2+} rich airborne sediments settling on the glacier surface during early autumn where river beds have dried out and are subjected to significant wind erosion.

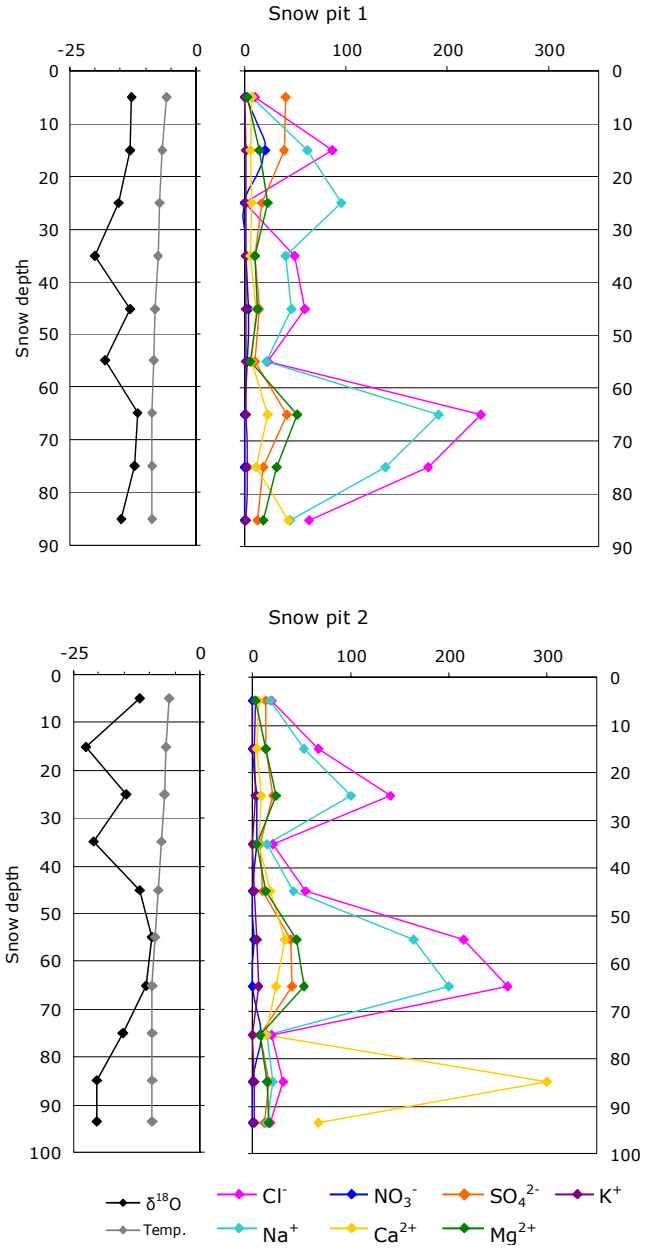

Figure 5.21. Variations in concentration of major ions [µeq l^{-1}], snow temperature [°C] and $\delta^{18}O$ values [‰] in snow pit 1 and 2. Locations of the pits are shown on figure 4.9.

A significant warming of the upper snowpack had occurred between 15 and 23 April. Snow pit 3 (figure 5.22) had snow temperatures decreasing from -3.7°C in the top layer, to -8.8°C in the bottom snow layer. In snow pit 3 three ice lenses were found at 37, 43 and 58 cm depth. Samples of the ice lenses in 43 and 58 cm depth showed a clear decrease in ion concentrations compared to the surrounding snow. Ion concentrations were high in the top 15 cm in snow pit 3 compared to the other snow pits, but otherwise the profile showed similar variations as snow pit 1 and 2.

When snow pit 4 (figure 5.22) was dug at the end of April, snow temperature had already reached 0°C in the upper 45 cm. Snow temperature in the bottom of the snowpack was,

however, still well below zero degrees (-6.7°C). A downward leaching of ions with the first meltwater is expected (Hodgkins and Tranter, 1998b). Of all the snow pits, snow pit 4 had the lowest concentrations of ions in the top 25 cm. A downward movement of ions had therefore, perhaps already initiated. It is difficult to tell if this is the case since no information exists about the original ionic composition of the snowpack.

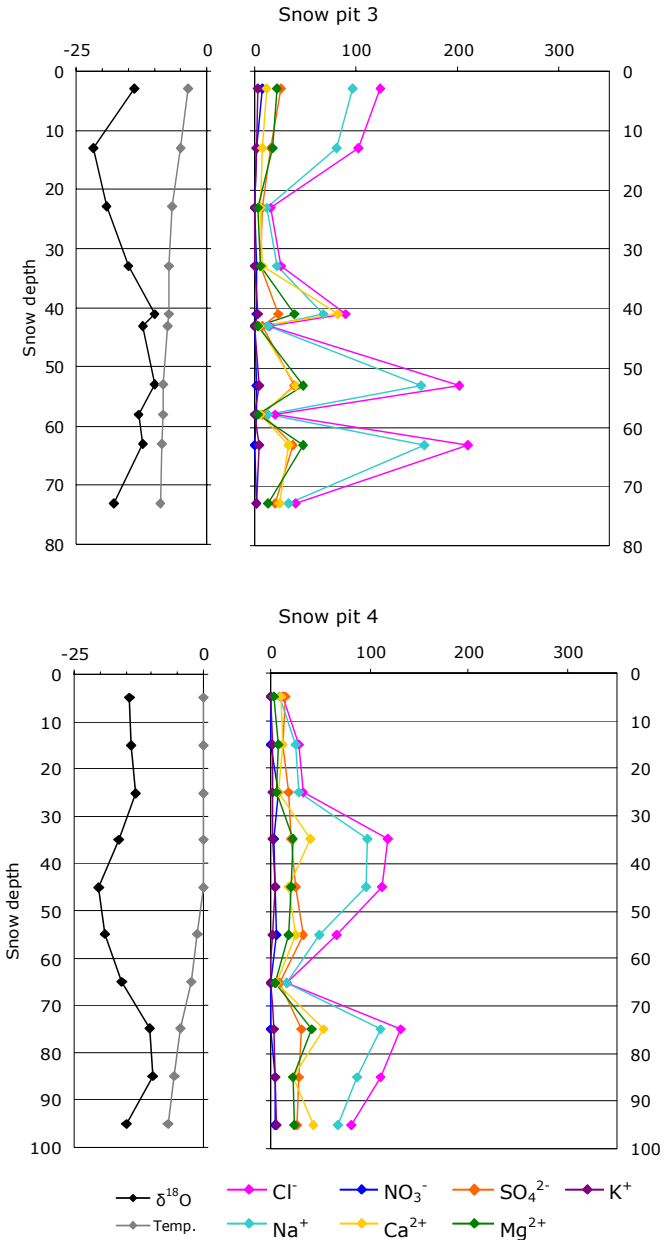

Figure 5.22. Variations in concentration of major ions [µeq l^{-1}], snow temperature [°C] and $\delta^{18}O$ values [‰] in snow pit 3 and 4. Locations of the pits are shown on figure 4.9.

The concentration of sea-salt in precipitation is expected to decrease during the winter as the source of sea-salt becomes more distal due the formation of sea-ice (Humlum et al., 1995). In the winter of 2004 however, sea-ice extent on Svalbard was limited and open sea was only about 10 km from the glacier when the ice extent was at its maximum, as opposed

to 3 km during open sea conditions. Despite this, there was a trend towards the largest concentrations of Cl^- and Na^+ occurring in the early periods of snow accumulation.

In table 5.4 a statistical summary of the ionic composition is presented for snow samples from the four snow pits, snow samples from the scooter track, freshly precipitated snow from the sampling site, a rain sample, clear ice from the wall of the ice cave and debris-rich basal ice from the moulin. Si content in all samples except from the basal ice (0.786 ppm) was below detection range.

Longyearbreen is a major transport route for snow scooters in the winter and spring (see front-page picture). To investigate a possible effect of this on the chemical composition of the snow, four samples were collected from the scooter track. Concentrations of Na^+ and Cl^- in these samples were low compared to the values in the snow pits but still dominant. The samples showed no sign of contamination by anthropogenic activity.

Table 5.4. Mean concentrations and standard deviation (SD) of ions in snow (from snowpits), snow from scooter track on Longyearbreen, freshly precipitated snow collected at the sampling site, rain, clear ice and basal debris-rich ice. Concentrations are in µeq l^{-1}. b.d. = below detection range. n = number of samples.

	Cl^-	NO_3^-	SO_4^{2-}	HCO_3^-	K^+	Na^+	Ca^{2+}	Mg^{2+}
Snow (pits)								
Mean	82	4.2	20	20	2.0	65	27	19
SD	71	4.2	11	27	1.5	55	48	15
n	38	22	39	7	39	39	39	39
Snow (scootertrack)								
Mean	40	6.9	20	-	1.3	32	14	9.1
SD	5.2	0.66	4.6		0.43	4.5	1.0	1.0
n	4	4	4		4	4	4	4
Snow (new)								
Mean	11	3.0	46	14	1.2	18	23	12
SD	7.7	1.0	29	16	1.1	14	29	18
n	5	3	5	2	5	5	5	5
Rain	13	b.d.	13	-	9.1	16	17	7.4
Clear ice (ice cave)	11	-	24	-	1.7	13	57	40
Debris-rich basal ice	20	16	120	311	9.6	26	231	199

Five samples of freshly precipitated snow were collected at the sampling site during or within hours of the individual precipitation event. SO_4^{2-} was the major ion while Na^+ and Cl^- concentrations were similar to that of Ca^{2+} and Mg^{2+}. Samples had a significantly lower content of sea-salts compared to snow samples from the snow pits. Mean SO_4^{2-} concentration for freshly precipitated snow collected at the sampling site was, however, more than twice the mean value for snow from the snow pits. The rain sample shown in table 5.4 was collected 29 July 14:30 close to the sampling site. It is difficult to compare one rain sample to the much larger data set of snow samples since it is evident that large variations in ionic composition of precipitation occurred. The rain sample did however show

similar characteristics as the freshly precipitated snow except for a lower SO_4^{2-} concentration.

Clear glacier ice had relatively low concentrations of Na^+ and Cl^- but high concentrations of Ca^{2+} and Mg^{2+}. This was even more striking for the debris-rich basal ice where SO_4^{2-}, HCO_3^-, Ca^{2+} and Mg^{2+} concentrations were highly elevated due to the incorporated sediments.

Ten samples of river water were collected successively on 16 August 18:00 to evaluate small scale fluctuation of ionic composition of the river meltwater. In table 5.5 mean values and standard deviation for the major ions in the ten samples are listed. The method used for determining Si gave uncertain results and the ion is not shown in the following tables but will be treated in more detail later. The measured concentrations generally showed a small variability that can be explained merely by the uncertainty associated with the analyses (uncertainty of the method was 5% for Na^+ and Mg^{2+}, 10% for K^+ and Ca^{2+} and 5% for the anions). HCO_3^- clearly had the highest value of standard deviation compared to the mean value due to the uncertainty related with the calculation of these concentrations (section 4.5.1).

Table 5.5. Mean concentration, standard deviation (SD) and SD in per cent of the mean value for ten water samples collected without time lag on 16 August 18:00.

	Cl^-	NO_3^-	SO_4^{2-}	HCO_3^-	K^+	Na^+	Ca^{2+}	Mg^{2+}
Mean [μeql^{-1}]	50	21	2062	136	18	688	706	856
SD [μeql^{-1}]	3.7	1.3	15	28	0.30	31	3.5	5.6
SD/mean [%]	7.5	6.2	0.75	21	1.7	4.6	0.50	0.66

In figure 5.23, variation of the major ions in river water from the sampling site is shown during the ablation period. Sampling was stopped during two periods from 4 August to 10 August and 19 August to 7 September. A statistical summary of the ablation period and the three sub-periods can be found in table 5.6.

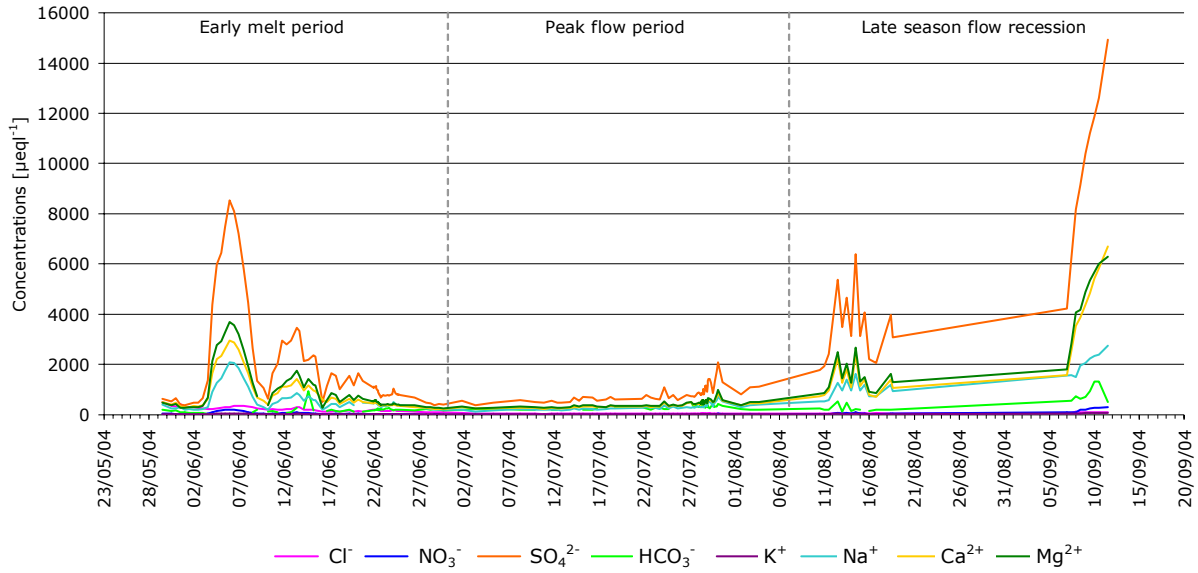

Figure 5.23. Variation in concentrations of major ions in river water during the ablation period.

A distinct seasonal pattern was recognized in most major ions during the ablation season. Values were generally high during the early melt period, where ions seemed to be released from the system in three large peaks decreasing in size. First rapid rise in concentrations occurred during a period of decreasing runoff from the glacier caused by a decrease in air temperature (see appendix A.6 for observations from the sampling site). The temperature low culminated on 5 June after which runoff started to increase slightly. Although less obvious in the meteorological data, notes from the fieldwork suggest that the second peak in concentrations was also related to a period of declining runoff followed by renewed increase. On 15 June, a significant increase in runoff occurred. During the peak flow period solute concentrations were relatively low due to the high influence of dilute icemelt to the meltwater and the low residence time in the drainage system. Concentrations rose again in the late season flow recession as the water ceased to run from the glacier. SO_4^{2-} was the dominant ion throughout the ablation period but Mg^{2+}, Ca^{2+} and Na^+ also had relatively high concentrations. Cl^-, NO_3^- and K^+ had low concentrations compared to other ions during the entire ablation period. Variability of the individual concentrations were high during the early melt period and the late season flow recession while the peak flow period showed more constant values. Generally, the proportionality of the individual ions varied very little during the ablation period (table 5.6). Cl^- however, clearly constituted the largest proportion of the total solutes during the early melt season where snowmelt dominated. A decrease in the proportion of SO_4^{2-} during the peak flow period was also observed.

Table 5.6. Mean values and standard deviations (SD) for concentrations of major ions in river water [µeq l^{-1}] and the proportion of the individual ions in the total solute concentrations [%]. n = number of samples.

	Cl^-	NO_3^-	SO_4^{2-}	HCO_3^-	K^+	Na^+	Ca^{2+}	Mg^{2+}
Total ablation period								
Mean	119	36	1887	267	21	541	814	905
STD	93	52	2452	188	9.4	488	1005	1099
%	2.6	0.79	41	5.8	0.46	12	18	20
n	183	178	183	155	182	181	182	182
Early melt period								
Mean	194	40	1654	182	21	513	697	809
STD	79	41	1805	105	7.5	395	621	790
%	4.7	0.98	40	4.4	0.51	13	17	20
n	90	90	90	75	90	89	89	89
Peak flow period								
Mean	41	8.9	855	306	18	313	423	449
STD	5.6	5.1	315	94	3.3	111	128	136
%	1.7	0.37	35	13	0.73	13	18	19
n	70	65	70	60	70	70	70	70
Late season flow recession								
Mean	61	97	5936	470	35	1380	2452	2661
STD	18	92	3936	373	15	660	1847	1860
%	0.47	0.74	45	3.6	0.27	11	19	20
n	23	23	23	20	22	22	23	23

In the following figures, conductivity and variations in concentrations of each individual ion is shown together with water level (note the different scales on the y-axis). The snow derived fraction of the individual ion is also shown on the figures. These concentrations were calculated from the relationships between Cl^- and the ions in the snowpack (table 5.7) as demonstrated by Wadham et al. (1998). The calculation gives a rough estimate of the snow derived fraction since the preferential leaching of some ions to others is not considered. Correlation coefficients of major ions, water level and SSC during the ablation period are shown in table 5.8 and correlation coefficients for the three sub-periods can be found in appendix A.9.

Table 5.7. Statistical summary of the relationship between ions and Cl^- in the snowpack. SD = standard deviation and n = number of samples.

	NO_3^- / Cl^-	SO_4^{2-} / Cl^-	HCO_3^- / Cl^-	K^+ / Cl^-	Na^+ / Cl^-	Ca^{2+} / Cl^-	Mg^{2+} / Cl^-
Mean [μeql^{-1}]	0.09	0.45	0.28	0.03	0.80	0.66	0.26
SD [μeql^{-1}]	0.11	0.65	0.27	0.02	0.07	1.61	0.13
n	22	38	7	38	38	38	38

Correlation between solutes and suspended sediment concentrations (SSC) was not particularly good for the entire ablation period. When studying the three sub-periods (appendix A.9) it appears that Cl^-, K^+ and Si changed from a negative relationship in the early melt period and the late season flow recession, to a positive relationship in the peak flow period. These three ions were amongst the ions with the best correlations with SSC in the individual periods. The best correlation between ions and SSC occurred during the late season flow recession.

Table 5.8. Correlation coefficients (R) between ions in the river meltwater during the ablation period. Negative values indicate an inverse correlation. Values for the three sub-periods can be found in appendix A.9. SSC = suspended sediment concentrations, Cond. = conductivity and w. l. = water level.

	Cl^-	NO_3^-	SO_4^{2-}	HCO_3^-	K^+	Na^+	Ca^{2+}	Mg^{2+}	Si	SSC	Cond.	W. l.
Cl^-	-	0.31	0.14	-0.44	0.25	0.18	0.11	0.15	0.62	-0.45	0.17	-0.61
NO_3^-		-	0.96	0.22	0.95	0.94	0.95	0.96	0.52	-0.30	0.82	-0.50
SO_4^{2-}			-	0.30	0.96	0.98	0.99	1.00	0.43	-0.24	0.92	-0.42
HCO_3^-				-	0.32	0.24	0.41	0.35	-0.11	0.30	0.26	0.39
K^+					-	0.95	0.96	0.96	0.53	-0.15	0.89	-0.33
Na^+						-	0.95	0.97	0.41	-0.27	0.95	-0.43
Ca^{2+}							-	0.99	0.41	-0.20	0.88	-0.39
Mg^{2+}								-	0.45	-0.22	0.90	-0.41
Si									-	-0.01	0.19	-0.15
SSC										-	-0.33	0.62
Cond.											-	-0.40
W. l.												-

The measured conductivity (figure 5.24) reflects the pattern observed on figure 5.23. Correlation was strong between conductivity and all ions except Cl^-, HCO_3^- and Si. During the entire ablation period correlation coefficients ranged between 0.82 and 0.95 for NO_3^-, SO_4^{2-}, K^+, Na^+, Ca^{2+} and Mg^{2+}.

The concentration of Cl^- (figure 5.24) in the river water differed significantly from the trends seen on the conductivity curve and for the other ions. Concentrations were largest in the earliest melt period with a maximum concentration of 511 $\mu eq\,l^{-1}$ in the first sample collected. Low Cl^- concentrations were measured in the glacier ice (table 5.4) and Cl^- therefore primarily originated from snowmelt. The ion therefore strongly reflected the preferred leaching of ions from the snowpack and the eventual change from snow to icemelt influenced runoff. The first water sample collected clearly illustrated this with a concentration of Cl^- more than 6 times the mean value of the snowpack. The concentration peaks that were prominent in the early melt period were also recognised in the temporal variations for Cl^- although to a much smaller extent. The first peak had a maximum value on 7 June 12:00 and the second on 13 June 18:00, with a minimum value on 10 June 06:00 in between. The peaks were superimposed on an overall gradual decline in concentrations of Cl^- during the early melt period. During the peak flow period, concentrations of Cl^- had a relatively constant value of 41 $\mu eq\,l^{-1}$ (table 5.6). No correlation existed between Cl^- and water level during this period. A slight increase in concentrations was observed in the late season flow recession which was also the period where Cl^- correlated best with the other ions (appendix A.8).

The concentrations of NO_3^-, SO_4^{2-} (figure 5.24), K^+, Na^+, Ca^{2+} (figure 5.25), and Mg^{2+} (figure 5.26) in river meltwater showed similar fluctuations. Correlation coefficients between these ions were between 0.94 and 1.00 during the ablation period (table 5.8) with the best correlation in the early melt period and late season flow recession (appendix A.9). SO_4^{2-} had the highest concentrations of all ions throughout the entire ablation period with a maximum value of 14939 $\mu eq\,l^{-1}$ in the final sample. K^+, which constituted the smallest fraction of the ions mentioned above, in contrast had a maximum value of 66 $\mu eq\,l^{-1}$ in the last sample. The fluctuations in concentrations during the early melt period decreased in size with the first peak occurring on 6 June 00:00, the second peak on 13 June 09:30, with an intermediate minimum on 10 June 06:00 for all the above mentioned ions. This differs significantly from the time of peak observed for Cl^-, where first peak occurred 36 hours later and second peak, 8½ hours later. The snowpack derived fractions of each ion were largest during the early melt period and constituted the largest proportion for NO_3^-, K^+ and Na^+. The peak flow period was characterized by relatively low and stable ion concentrations (table 5.6) slightly increasing during the period. Correlation between the concentrations and water level was poor during this period, especially for NO_3^-, SO_4^{2-} and Na^+ (appendix A.9). A rise in all above mentioned ions occurred in the end of July during a period of enhanced runoff from the glacier. Unfortunately, data coverage was poor after this event. The curves do however indicate a gradual increase in solute content during the late season flow recession and more widespread small scale fluctuations. A prominent increase in concentrations occurred in the end of the ablation period.

HCO_3^- (figure 5.25) was calculated from the concentrations of the major ions measured in the meltwater. The occasional negative concentrations give clear evidence of the uncertainties associated with this method. A general increase in HCO_3^- concentrations occurred during the ablation period. Furthermore, the correlation coefficient between HCO_3^- and the other ions in the meltwater improved as the season progressed (appendix A.9).

Si is shown in ppm and not $\mu eq\,l^-$ (figure 5.26) because Si is not present in the meltwater as an ion and therefore has no charge. Concentrations were very low and uncertainty in the

calibration of the method resulted in an uneven curve with values sometimes below zero. The three peaks in the early melt season were however also recognised for Si.

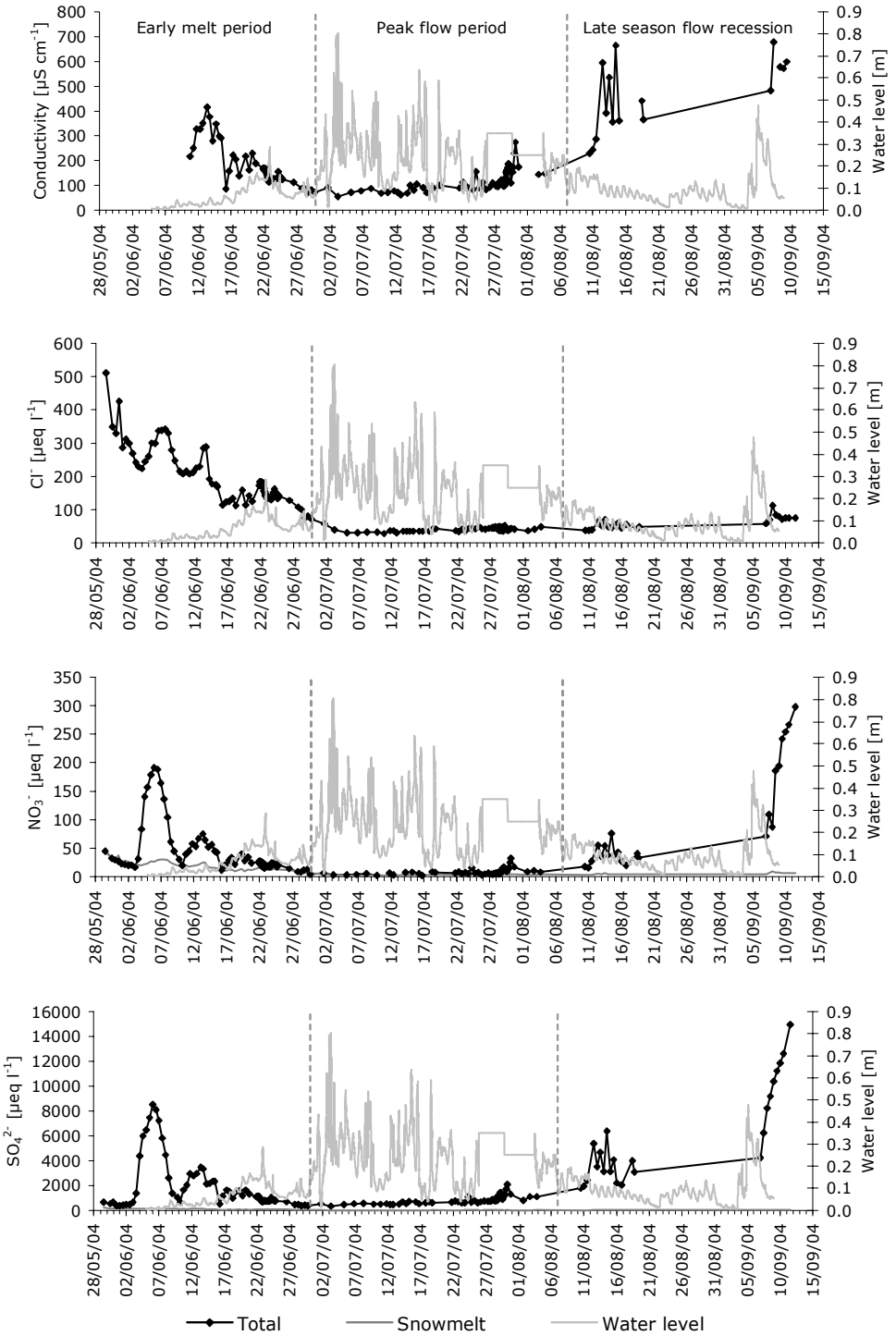

Figure 5.24. Variation in water level, measured conductivity, total concentration and calculated snowmelt derived proportion of Cl^- (only snow), NO_3^-, and SO_4^{2-} during the ablation period. Note change in scale on y-axis.

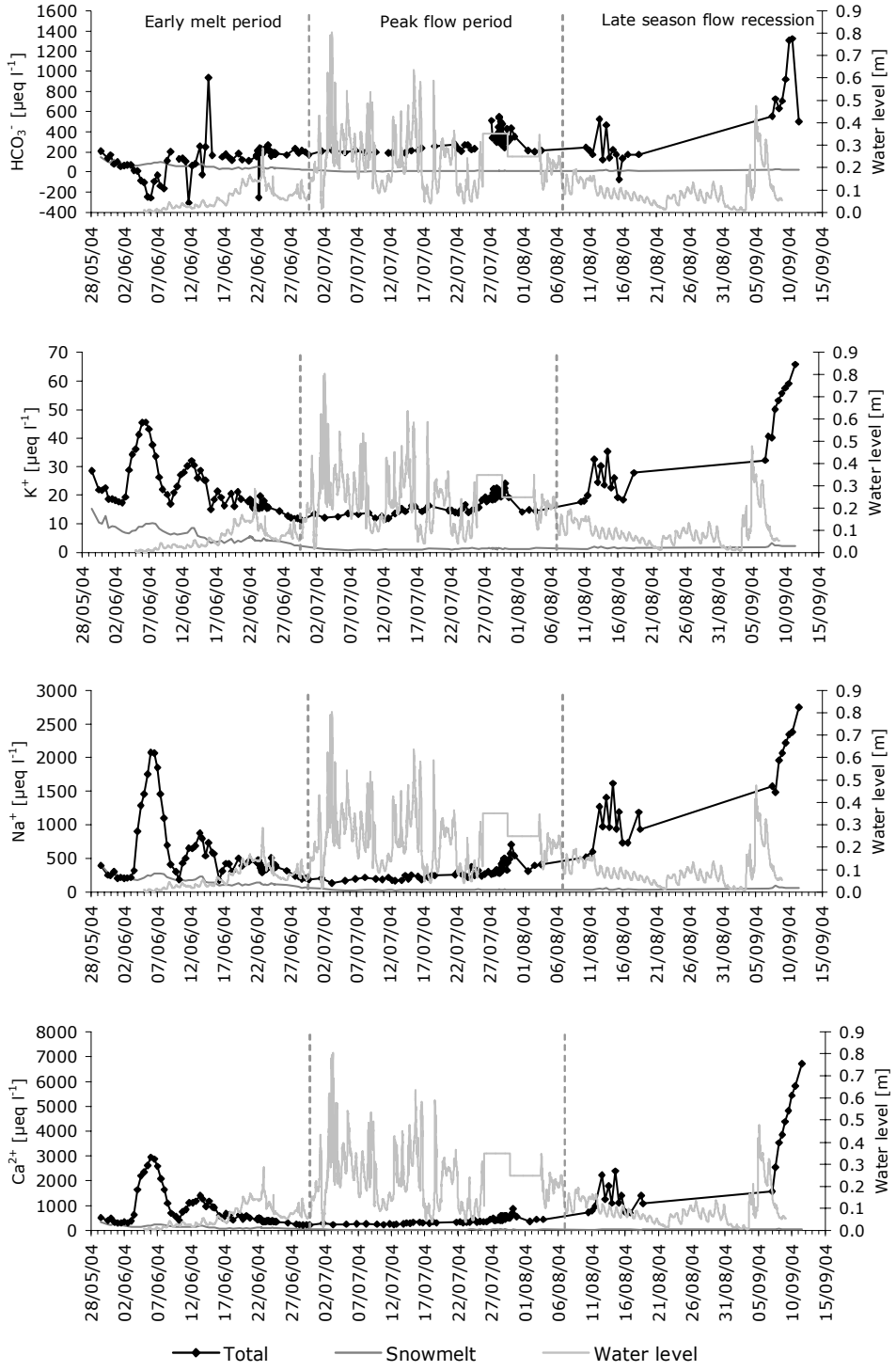

Figure 5.25. Variations in water level, total concentration and calculated snowmelt derived proportion of HCO_3^-, K^+, Na^+ and Ca^{2+} during the ablation period. Note change in scale on y-axis.

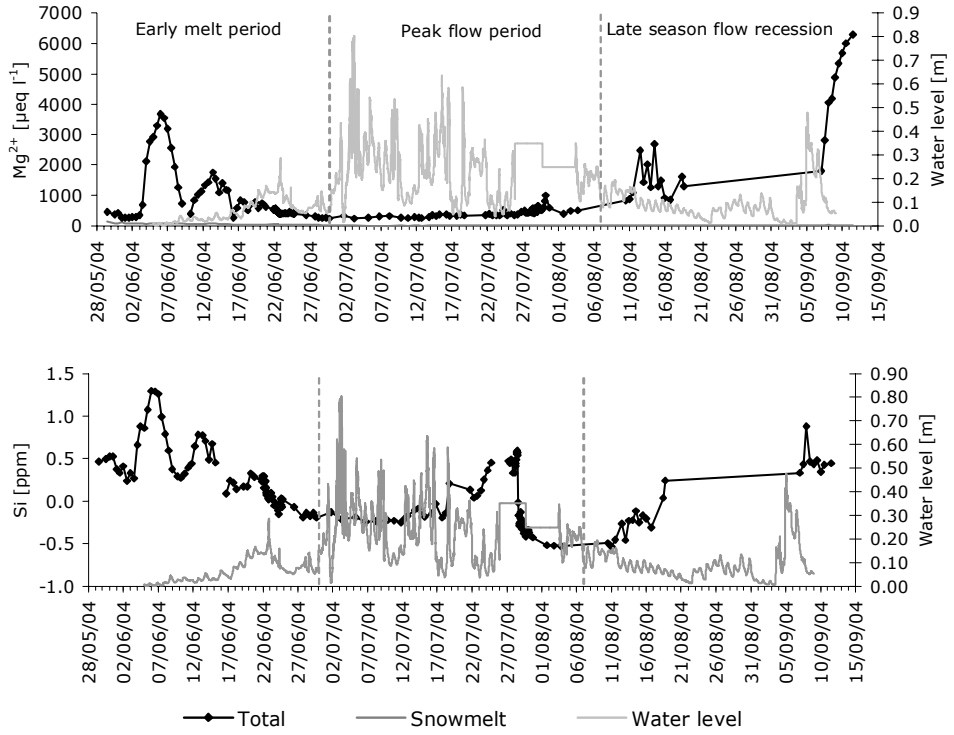

Figure 5.26. Variations in water level, total concentration of Mg^{2+} and Si, and for Mg^{2+} also calculated snowmelt derived proportion during the ablation period. Note change in scale and unit on y-axis.

The results from the first three days of frequent sampling are shown in figure 5.27. Note that precipitation was measured at Longyearbyen Airport with a three hour interval. Fluctuations in water level were large during this period possibly due to the release of water from storage in combination with several precipitation events and relatively high air temperatures (see section 5.4). Water levels and solute concentrations were constant during the first 10 hours of the period. As the water level rose, solute concentrations of the river water dropped to a minimum coinciding with the maximum water level recorded during the period. A small increase in solute concentrations was observed in the late evening on 22 June. This event was possibly related to a significant decline in water levels. Between 23 June 00:00 and 24 June 00:00 the solute content of the meltwater was fairly constant in spite of a continuous lowering of glacial runoff. A peak in solute concentrations occurred on 24 June at 04:00, possibly brought on by the low water levels. No evidence of the rainfall events were detected in the solute concentrations. A time lag of 3-4 hours occurred between fluctuations in solute concentrations and water levels.

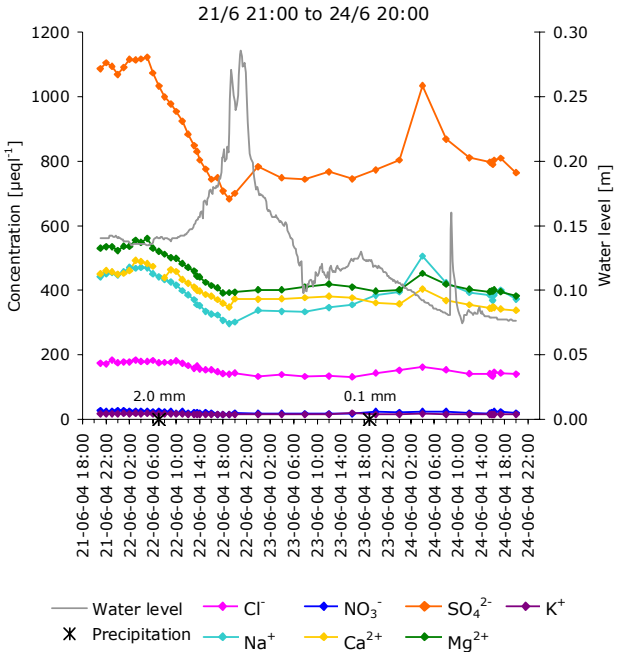

Figure 5.27. Variations in water level and concentration of major ions during the first three day period of frequent water sampling. Precipitation amounts were measured at Longyearbyen Airport every three hours and are shown as crosses on the x-axis with associated values.

A second period with frequent water sampling took place in the peak flow period from 27 July 06:00 to 30 July 06:00 (figure 5.28). Unfortunately the gauging station was out of order during this period and air temperature has instead been applied on figure 5.28 as an indicator of variations in runoff from the glacier. Mean water level during the period was estimated to 0.35 m prior to 29 July 18:00, after which it was lowered to 0.25 m. Maximum runoff is thought to have occurred on 28 July at 11:00 (appendix A.6). A general increase in solute concentrations occurred during the period especially after runoff is thought to have begun declining. The solute increase was uneven, with several fluctuations perhaps reflecting precipitation events. The rain sample presented in table 5.4 was collected close to the sampling site on 29 July 14:30. Solute concentration in this sample was significantly lower than that of the river meltwater, and a dilution of the meltwater is therefore expected if rainwater influenced the chemical composition. A minimum in solute concentrations on 29 July 14:00 coincided with the precipitation event from which the rain sample was collected. From 29 July 14:00 a rapid increase in solute concentrations took place culminating on 29 July 06:00 where the largest concentration of all ions except Cl^- was measured during the peak flow period.

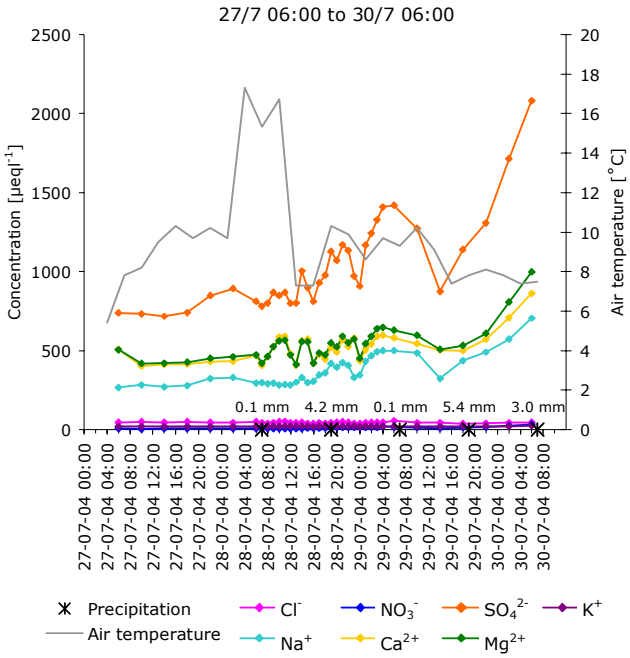

Figure 5.28. Variations in water level and concentration of ions during the second three day period of frequent water sampling. Precipitation amounts were measured at Longyearbyen Airport every three hours and are shown as crosses on the x-axis with associated values.

Distinct diurnal variations were not observed during the two periods with frequent water sampling. Samples collected twice a day during the late season flow recession however gave indication of the diurnal fluctuations that occurred during this period (figure 5.29).

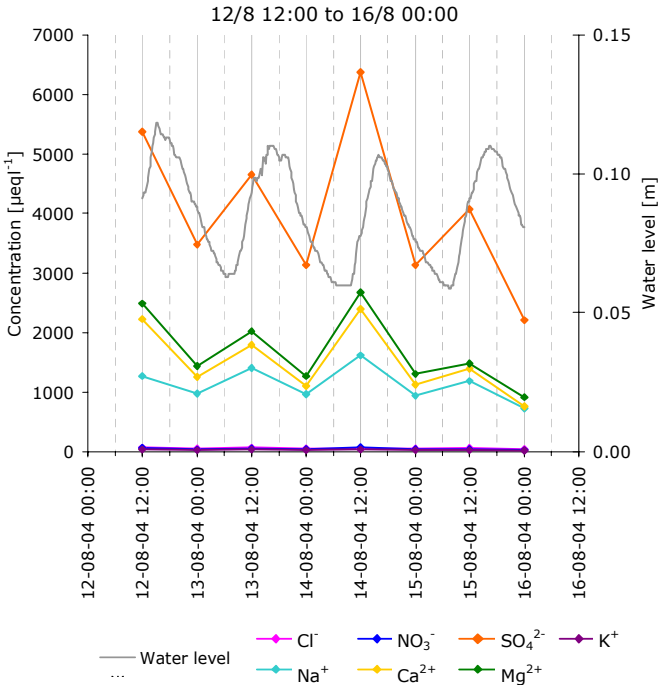

Figure 5.29. Diurnal variations in water level and solute concentrations during a 3½ day period in the late season flow recession. Air temperature varied between 3.9 and 8.5°C and no precipitation events occurred.

Time of water sampling was changed from 06:00 and 18:00 to 12:00 and 00:00 on 10 August based on a change in diurnal cycle observed in previous year's water level measurements from Longyearelva (Ole Humlum, unpublished data). Unfortunately this was not the case in 2004 and samples were therefore not collected at maximum and minimum water level. Diurnal variations were nevertheless still recognizable in the river meltwater and highest concentrations of solutes occurred after periods with low runoff, while lowest solute concentrations were measured after periods with high runoff.

On 18 August sources contributing to the bulk meltwater draining from Longyearbreen were investigated. The localities where water samples were collected are seen in figure 4.9. A statistical summary of the results is presented in table 5.9. For reference, a water sample was collected at the sampling site before (10:00) and after (16:00) field work. During the day a decrease in major ions except Cl^- had occurred, most likely caused by an increase in icemelt from the glacier. Water at the sampling site is thought to originate from the eastern lateral channels, supraglacial channels disappearing into the debris-covered glacier snout and possibly an englacial or subglacial component.

Samples from the supraglacial channels flowing on the clean glacier ice were dilute with the dominant ions Cl^- and Na^+ originating from melting snow higher on the glacier. SO_4^{2-} was almost absent and significantly smaller than elsewhere in the glacial drainage system. The supraglacial channels on the debris-covered glacier snout were fed by water from supraglacial channels on the glacier in combination with debris-rich water from the thawing sediment-covered glacier snout. A considerable increase in concentrations of all ions and SO_4^{2-} and Ca^{2+} in particular gives evidence of the sediment-rich environment. The meltwater streams on the terminus differed significantly in solute content and standard deviation was large for these samples. Considerably higher ionic concentrations were measured in samples collected in slowly flowing water.

Samples were collected both in the upper and lower part of the eastern lateral channel. The upper samples were collected immediately after meltwater from Larsbreen confluences with the channel. This is most likely the reason for the high concentrations of SO_4^{2-}, Ca^{2+}, and Mg^{2+} in a channel that is partly fed by solute-poor supraglacial meltwater. Water draining from Larsbreen on the other hand, drains through an old lateral moraine before entering the drainage system on Longyearbreen. A sample collected further down-stream showed lowered but still relatively high concentrations of ions, probably due to input from solute-poor supraglacial water between the two localities. The western lateral channel had considerably lower ion concentrations and was probably more influenced by supraglacial meltwater water than the eastern lateral meltwater channel.

Water flowing in the western meltwater stream is thought partly to originate from the englacial and subglacial drainage system that is accessible during winter and spring (the ice cave). The water had the highest concentrations of SO_4^{2-}, Ca^{2+} and Mg^{2+} measured in the drainage system on 18 August with SO_4^{2-} as the dominant ion. The negative concentration of HCO_3^- was clearly an artefact and reflects the uncertainties related to the determination of this ion. A more detailed examination of the difference between the eastern and western meltwater stream is shown in appendix A.10. Samples collected concurrently in the streams

show that during the late season flow recession only a minor difference in solute content existed.

Water collected in Tværdalen originates from the unnamed glacier on Nordenskiöld. This water showed similar characteristics as the water from the sampling site.

Table 5.9. Statistical summary of the chemical composition of meltwater from different sources all contributing to water flowing in Longyearelva. Concentrations are in µeq l^{-1}. b.d. = below detection range.

	Cl^-	NO_3^-	SO_4^{2-}	HCO_3^-	K^+	Na^+	Ca^{2+}	Mg^{2+}
Sampling site (10:00)								
Mean	47	43.8	3965	195	28	1180	1415	1628
SD	4.1	2.8	18	21	0.09	10	13	4.3
n	3	3	3	3	3	3	3	3
Supraglacial channels (on ice)								
Mean	20.9	b.d.	8.8	-	0.5	18	12	9.0
SD	11.7		2.8		0.27	9.1	2.3	2.5
n	8	8	8		8	8	8	8
Supraglacial channels (on debris)								
Mean	66	62	1601	544	24	483	1032	609
SD	68		1947		20	583	1082	549
n	3	1	3	1	3	3	3	3
Upper lateral channel (east)								
Mean	40	19	2363	265	16	328	1126	1218
SD	3.0	3.4	19	48	0.05	0.80	3.5	70
n	2	2	2	2	2	2	2	2
Lower lateral channel (east)	26	18	1811	210	23	12	1009	1021
Upper lateral channel (west)	56	b.d.	37	-	4.0	3.4	78	63
Western meltwater stream								
Mean	78	30	5032	-	25	424	2063	2510
SD	3.4	0.8	65			542	25	8.2
n	2	2	2		1	2	2	2
Tværdalen	111	29	3170	-	-	1462	1276	-
Sampling site (16:00)	49	33	3067	-	-	933	1076	1296
Inside moraine cave (15 Sep.)	80	431	19489	2242	75	3417	9047	9702

On 15 September 21:00 water had ceased to run in front of Longyearbreen and the caves from which the eastern and western meltwater stream emanates were investigated. The western cave became too narrow after only a couple of meters. The eastern moraine cave, on the other hand, was similar to the previous years and accessible several 100 m below the glacier. Even though water had frozen near the entrance of the cave, water was still gently flowing deeper inside the cave. The ionic composition of a water sample collected inside the

moraine cave is shown in table 5.9. The sample had the highest concentrations of all ions except Cl^- measured throughout the entire ablation period.

Samples collected from different places along Longyearelva are presented in appendix A.11. The results suggest that solute acquisition of the meltwater predominately took place within the glacial drainage system and not in the proglacial areas.

In table 5.10 the relationships between some of the ions in the river meltwater are shown. Figure 5.30 furthermore shows the relationship between $*SO_4^{2-}$ and $(*SO_4^{2-} + HCO_3^-)$ (* denotes the crustally derived fraction of the ion = total concentration - snowmelt derived proportion).

Table 5.10. Mean values for $*SO_4^{2-}/(*SO_4^{2-} + HCO_3^-)$ and Na^+/Cl^- in river meltwater. Standard deviations are shown in brackets.

	$*SO_4^{2-}/(*SO_4^{2-} + HCO_3^-)$	Na^+/Cl^-
Total ablation period	0.80 (0.10)	6.87 (6.75)
Early melt period	0.81 (0.08)	2.63 (1.17)
Peak flow period	0.73 (0.07)	7.54 (2.35)
Late season flow recession	0.93 (0.03)	21.91 (7.20)

The ratio $*SO_4^{2-}/(*SO_4^{2-} + HCO_3^-)$ gives an estimate of the relationship between chemical weathering by oxidation of sulphides (output anion: SO_4^{2-}) and dissolution of carbonates (output anion: HCO_3^-) (equation 2 and 3) (Raiswell, 1984). A ratio of 0 signifies weathering by carbonation or hydrolysis of carbonates (equation 5, 6, 7 and 10), a ratio of 0.5 (lower dashed line) indicates a predominance of coupled sulphide oxidation and carbonate dissolution (equation 4) while a ratio of 1 (upper dashed line) occurs when the meltwater is exclusively dominated by chemical weathering by sulphide oxidation (equation 2) (Wadham et al., 1998; Hodgkins et al., 1998a). Figure 5.30 shows that oxidation of sulphides clearly dominated in the glacial meltwater, particularly during the early melt period and the late season flow recession. There was a clear excess of Na^+ to Cl^- during the entire ablation period, most pronounced in the end of ablation period.

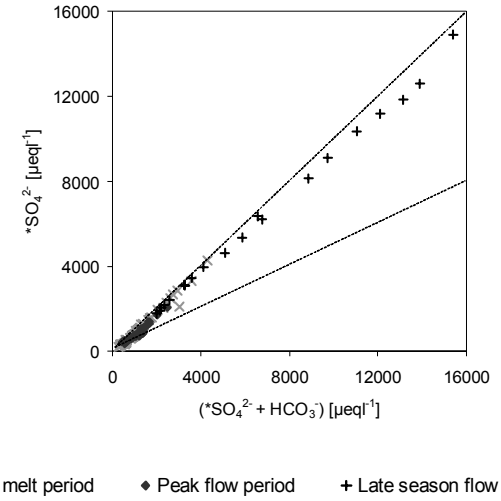

Figure 5.30. Relationship between $*SO_4^{2-}$ and $(*SO_4^{2-} + HCO_3^-)$ in river meltwater.

Previous studies have shown that the chemical composition of sampled meltwater may change if the water is not filtrated directly after sampling (Collins, 1977; Sægrov, 1995; Hansen, 2001). The chemical change is thought to reflect reactions between the water and suspended sediments. Conductivity was calculated from the total solute content measured in the laboratory between 2½ and 6 months later and the linear relationship (R^2 = 0.98) existing between measured conductivity and the total solute content (see appendix A.12). In figure 5.31, the measured conductivity is shown together with calculated conductivity. No systematic change occurred in the relationship between the two data sets during the ablation period.

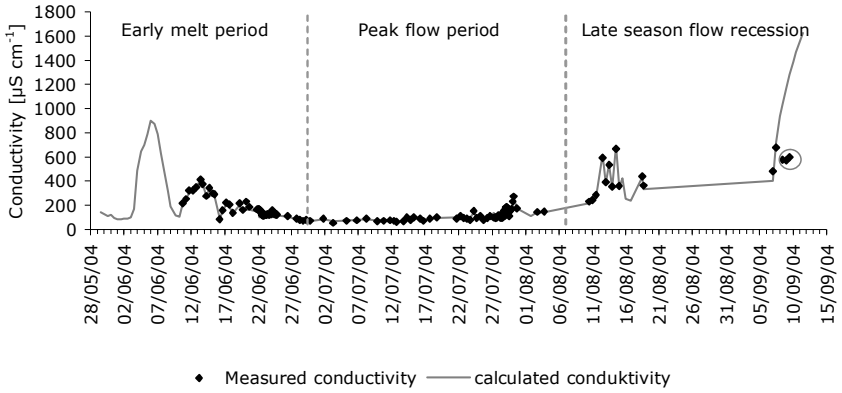

Figure 5.31. Measured conductivity and conductivity calculated from the total solute content using the linear relationship derived in appendix A.12. The three samples marked by the circle were excluded from the data set.

5.6 **Isotopes**

Oxygen isotope variations in the four snow pits are shown in section 5.6 on figures 5.20 and 5.21. Marked variations in the isotopic composition of the snow were observed in all four pits reflecting the sequence of snow layers originating from different precipitation events. The $\delta^{18}O$ values ranged from a low of -22.57‰ measured at a depth of 15 cm in snow pit 2, to -9.36‰ measured at a depth of 85 cm in snow pit 4. Two low values of -20.14‰ and -17.90‰ in snow pit 1 and -22.57‰ and -21.50‰ in snow pit 2 may have originated from the same precipitation events. This supports the hypothesis (see section 5.6) that the lowermost 20 cm in snow pit 2 are missing in snow pit 1. Neither snow pits 3 or 4 resembled any of the other pits but both had variations in $\delta^{18}O$ values in similar range as snow pit 1 and 2. Ice layers in the snowpack are expected to be less depleted of the heavy oxygen isotope than the surrounding snow as a fractionation occurs during the refreezing process (Raben and Theakstone, 1994; Theakstone and Knudsen, 1996a). However no raise in $\delta^{18}O$ values for ice rich layers were observed in snow pit 1, 2 and 4, most probably because intervals with ice layers were sampled together with the surrounding snow. In snow pit 3, where samples of the ice lenses were collected, a slight ^{18}O enrichment was observed in 43 cm depth. This was not the case for the ice layer at 58 cm depth, where a lowering of the $\delta^{18}O$ value occurred.

Table 5.11. Statistical summary for $\delta^{18}O$ values [‰] measured in snow, glacier ice, bottom ice in moraine cave and rain. n = number of samples.

	Min.	Max.	Mean	SD	*n*
Snow (pits)	-22.57	-9.36	-14.90	3.62	43
Snow (freshly precipitated)	-20.25	-12.38	-17.84	2.86	9
Glacier ice	-12.92	-11.37	-12.15	0.78	3
Frozen channel floor	-18.26	-15.09	-16.22	1.77	3
Rain	-13.39	-5.22	-8.32	3.87	4

Snow samples from snow pits and freshly precipitated snow showed similar characteristics (table 5.11). Both had high isotopic variability and minimum values below 20.00‰. Snow from the pits reflects winter accumulation on the glacier, while the freshly precipitated snow was collected at the sampling site in either early or late summer at a minimum temperature of -4°C. The highest value of -9.36‰ was measured in snow from snow pit 2 demonstrating that precipitation episodes with a high ratio of ^{18}O may occur at all seasons on Svalbard.

Samples of glacier ice were collected in the ice cave and are therefore not necessarily representative of the ice at the glacier surface. The glacier ice was generally less depleted in ^{18}O compared to the snow samples with a minimum value of -12.92‰. The data set only included three samples making it difficult to compare directly with the larger set of snow samples. Previous studies on Longyearbreen have found a mean of -13.9‰ for surface glacier ice (Bringedal, 2004). Three samples of ice were collected from pools of refrozen meltwater in the moraine cave. The $\delta^{18}O$ values of this ice were generally lower than for the glacier ice.

Rain collected during the ablation season had the highest $\delta^{18}O$ values measured, with a maximum value of -5.22‰ occurring on 26 July at an air temperature of 12.5°C. Compared to the data set for snow and ice, rain samples displayed the largest variation in isotopic composition (SD = 3.87).

In figure 5.32 the correlation between $\delta^{18}O$ values in precipitation and the air temperature at the time of sampling is shown. The majority of the snow samples were collected during the snowfall events while others were collected within hours of the precipitation events. Measured air temperature is therefore thought to be representative of the individual snow samples. There was a large spread in the data ($R^2 = 0.52$) but in general, high $\delta^{18}O$ values occurred when precipitation fell as rain at high air temperatures while snow samples collected at lower temperatures were more depleted of ^{18}O. The relationship between air temperature and isotopic composition of precipitation in Longyearbyen found by Bringedal (2004) is also shown on figure 5.32 together with the trend line from 2004. The two lines differ significantly, most likely because of the small dataset presented here compared to the more comprehensive study by Bringedal (2004) where 291 precipitation samples were collected over 5 years.

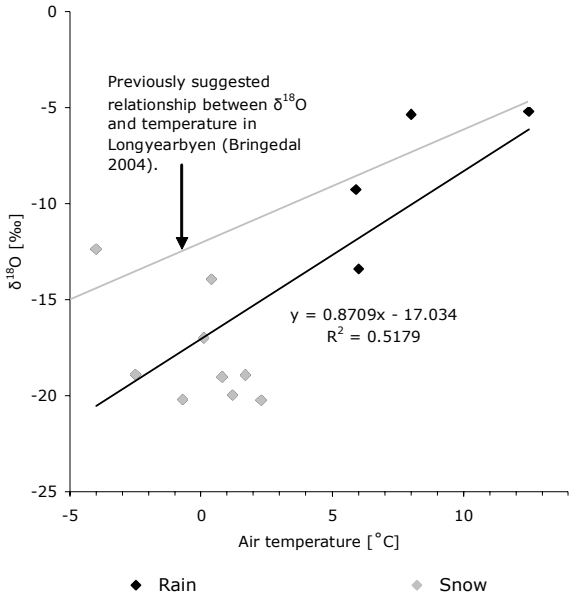

Figure 5.32. Correlation between $\delta^{18}O$ values in precipitation samples and air temperature at the time of sampling. Black line indicates the relationship between $\delta^{18}O$ and air temperature derived from the collected precipitation samples. Grey line indicates the relationship derived by Bringedal (2004).

To evaluate small-scale fluctuation of $\delta^{18}O$ values in the river meltwater, 25 water samples were collected successively on 16 August. Samples had a maximum $\delta^{18}O$ value of -13.25‰, a minimum value of -13.42‰ and a mean $\delta^{18}O$ value of -13.32‰. Standard deviation was only 0.04‰ which is within the uncertainty associated with the analyses.

Figure 5.33 shows variations in the ratio of heavy and light oxygen isotopes in the river water during the ablation period together with water levels measured at the gauging station in Longyearbyen.

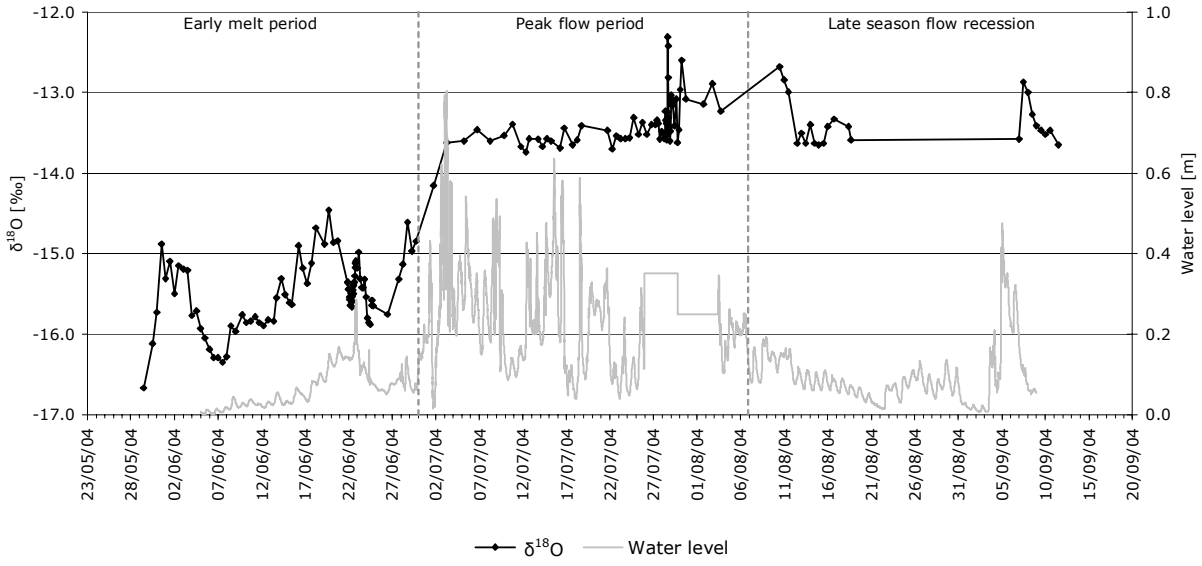

Figure 5.33. Variations in water level measured at the gauging station in Longyearbyen and isotopic composition of river meltwater during the ablation period.

A statistical summery of the entire ablation period, the early melt period, the peak flow period and the late season flow recession is presented in table 5.12.

Table 5.12. Statistical summary of measured $\delta^{18}O$ values in river water during the ablation period and the three sub-periods. SD = standard deviation and n = number of samples.

Period	Min. [‰]	Max. [‰]	Mean [‰]	SD [‰]	*n*
Total ablation period	-16.67	-12.31	-14.42	1.1	182
Early melt period	-16.67	-14.46	-15.50	1.2	89
Peak flow period	-14.15	-12.31	-13.39	0.30	70
Late season flow recession	-13.65	-12.68	-13.37	0.29	23

The early melt period was characterized by meltwater initially with very low $\delta^{18}O$ values, and the lowest value of 16.67‰ was measured in the first sample collected. The low $\delta^{18}O$ values give evidence of the high influence of snowmelt during this period. Large fluctuations occurred during the early melt period. Two peaks in $\delta^{18}O$ values occurred on 31 May 12:00 and 19 June 18:00 and two distinct dips culminated on 7 June 12:00 and 24 June 12:00. The rapid decrease in $\delta^{18}O$ values occurring between 3 June 12:00 and 7 June 12:00 is probably related to a decline in runoff from the glacier observed at the sampling site. The overall variations observed in $\delta^{18}O$ values after 7 June appear to have been related to fluctuations in water level. The glacier meltwater gradually became less depleted in ^{18}O as water level rose with a successive low corresponding to a low in water levels. Between 21 June 21:00 and 24 June 20:00 a period with frequent water sampling took place (figure 5.34). $\delta^{18}O$ values correlated well with water level during the three days, with maximum values at approximately the same time as maximum runoff from the glacier. The small peak observed on 22 June 06:00 may have been caused by rainfall event raising the ^{18}O ratio in the river water. Prior to this event, no obvious relationship between the measured $\delta^{18}O$ values and precipitation was observed possibly due to a long time lag in the drainage system.

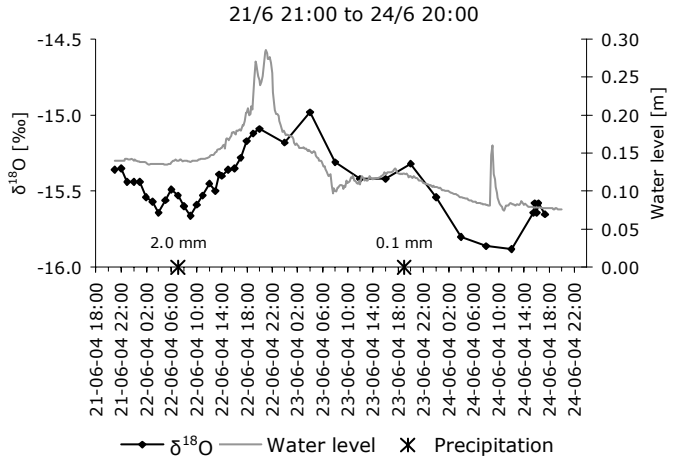

Figure 5.34. Variations in $\delta^{18}O$ values and water level in river water from 21 June 21:00 to 24 June 20:00. Precipitation was measured every three hours at Longyearbyen Airport and is shown as crosses on the x-axis with associated values.

$\delta^{18}O$ values and water levels rose dramatically between 26 June and 3 July at the onset of increased ^{18}O rich icemelt. Photographs taken by a camera monitoring the nearby Larsbreen

show that this episode coincided with the first snow free patches of ice appearing in the lowest part of the glacier (Appendix A.5). $\delta^{18}O$ values for the river water had very little isotopic variability until the 28 July and the peak flow period as a whole had a standard deviation of only 0.30‰ (table 5.12). Small diurnal variations in ^{18}O content of the river water were seen in the days before 28 July. After the 28 July large fluctuations in the relationship between ^{16}O and ^{18}O occurred in the river water. On several occasions distinct peaks occurred on the $\delta^{18}O$ curve signifying water masses in the river significantly enriched with the heavy oxygen isotope. The highest value of -12.31‰ was measured on 28 July at 15:00 during a period with more frequent water sampling. Data from this period is shown in detail in figure 5.35.

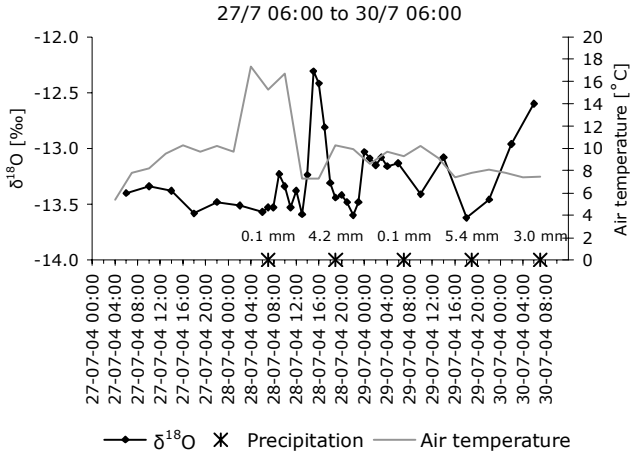

Figure 5.35. Variations in air temperature and $\delta^{18}O$ values in river water from 27 June 06:00 to 30 June 06:00. Precipitation was measured every three hours at Longyearbyen Airport and is shown as crosses on the x-axis with associated values.

Fluctuations in $\delta^{18}O$ values are related to air temperature in figure 5.35, since no water level was recorded during the period. Precipitation was measured at Longyearbyen Airport covering an interval of three hours. Marked events of increased ^{18}O in the water appear to be superimposed on a constant value of -13.5‰ which is slightly higher than at the beginning of the peak flow period. The peaks in $\delta^{18}O$ values correlated well with the precipitation events recorded at Svalbard Airport in combination with observations at the sampling site (see appendix A.6). Rain was recorded at 07:00 and 08:00 on 28 July coinciding with the first minor peak at 09:00 on 28 July. Between 12:00 and 17:00 on 28 July heavy rain was recorded at the sampling site with maximum intensity occurring at 15:00, where also the maximum $\delta^{18}O$ value was measured in the river water. Rain samples were collected at 13:00 and 15:30 and showed a $\delta^{18}O$ value of -5.37‰ and -9.28‰ respectively. These values were considerably higher than the mean of -13.39‰ for the peak flow period and, as observed on figure 5.35, capable of influencing the river water significantly. Several large precipitation events occurred during the following 24 hours and the uneven character of the $\delta^{18}O$ curve most likely reflects this. The largest precipitation event during the period was registered at Longyearbyen Airport at 29 July 19:00. This rainfall was probably related to the peak in $\delta^{18}O$ values on 29 July 14:00 since a significant decrease in intensity of the rainfall was observed at the sampling site by 18:00 where a relatively low $\delta^{18}O$ value was measured. On 30 July 00:00 the rain stopped at the sampling site. However, the same rainfall that was registered at the airport was probably still falling

heavily on the higher parts of the glacier resulting in a marked increase of $\delta^{18}O$ values in the river water. This culminated with the second highest $\delta^{18}O$ value measured during the entire ablation period occurring on 30 June at 06:00 in the morning.

The late season flow recession began with a marked decline of $\delta^{18}O$ values measured in the river meltwater probably related to the ending of a rainfall events (figure 5.10 and figure 5.33). From 12 August 12:00 to 15 August 12:00, diurnal variations in the relationship between ^{18}O and ^{16}O were observed to be superimposed on a constant value of about -13.6‰ (see figure 5.36). Air temperature during the period varied between 3.9°C and 8.5°C and no precipitation events occurred.

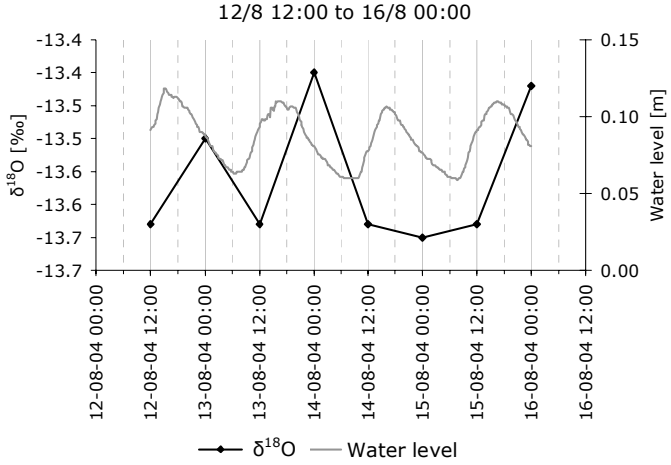

Figure 5.36. Diurnal variations in $\delta^{18}O$ values in river water from 12 August 12:00 to 16 August 00:00.

With the exception of the water sample collected on 15 August 00:00, river water was most depleted in ^{18}O after low runoff from the glacier and less depleted after high discharge. This is as expected, since ^{18}O poor snowmelt temporarily stored in the snowpack has been found to constitute a larger proportion of the meltwater during low ablation as opposed to during high ablation, where icemelt less depleted in ^{18}O dominates (Theakstone, 2003). The late season flow recession ended with a marked decrease in $\delta^{18}O$ values. This was probably related to a precipitation event that ended in the morning on 7 September (figure 5.10 and figure 5.33). The $\delta^{18}O$ values declined to a value of -13.65‰ in the last sample collected similar to the base flow value observed throughout the period.

The different sources of bulk meltwater were investigated on 18 August (table 5.13) where samples of meltwater were collected from localities within the catchment area of Longyearbreen (see figure 4.9).The isotopic composition of the meltwater generally showed little variation within the drainage system. However, the supraglacial streams on the clear glacier surface were nearer to the transient snow line and consequently more influenced by ^{18}O poor snowmelt compared to the supraglacial streams on the glacier snout. Furthermore, two samples collected on the debris-covered glacier snout differed from the rest of the dataset with lower $\delta^{18}O$ values (-11.86‰ and -11.92‰). These two samples were collected in slow flowing pools of water with a high influence of ice ablation from the glacier snout.

Table 5.13. Statistical summary of the isotopic composition of meltwater from samples collected at different localities within the drainage system of Longyearbreen. All samples were collected between 10:00 and 16:00 on 18 August except the last sample collected inside the moraine cave. SD = standard deviation and n = number of samples.

Source	Min. [‰]	Max. [‰]	Mean [‰]	SD [‰]	*n*
Sampling site (10:00)	-13.46	-13.41	-13.42	0.02	5
Supraglacial channels (on ice)	-14.79	-13.66	-14.19	0.38	16
Supraglacial channels (on debris)	-14.16	-11.86	-13.33	1.12	6
Upper lateral channel (east)	-13.97	-13.89	-13.93	0.03	4
Lower lateral channel (east)	-13.91	-13.90	-13.91	0.01	2
Upper lateral channel (west)	-13.90	-13.86	-13.88	0.03	2
Western meltwater stream	-13.55	-13.45	-13.49	0.05	4
Tværdalen	-13.21	-13.18	-13.20	0.02	2
Sampling site (16:00)			-13.59		1
Inside moraine cave (15 Sep.)			-13.72		1

In figure 5.37 variations in $\delta^{18}O$ values and Cl^- concentrations in the meltwater are shown. Both $\delta^{18}O$ values and Cl^- concentrations reflect the influence of snowmelt in the river meltwater (Theakstone and Knudsen, 1996a). Furthermore, the results presented above show, that precipitation events also influenced the $\delta^{18}O$ values. $\delta^{18}O$ values and Cl^- concentrations were well correlated (R^2=0.85) during the ablation period (see figure 5.38).

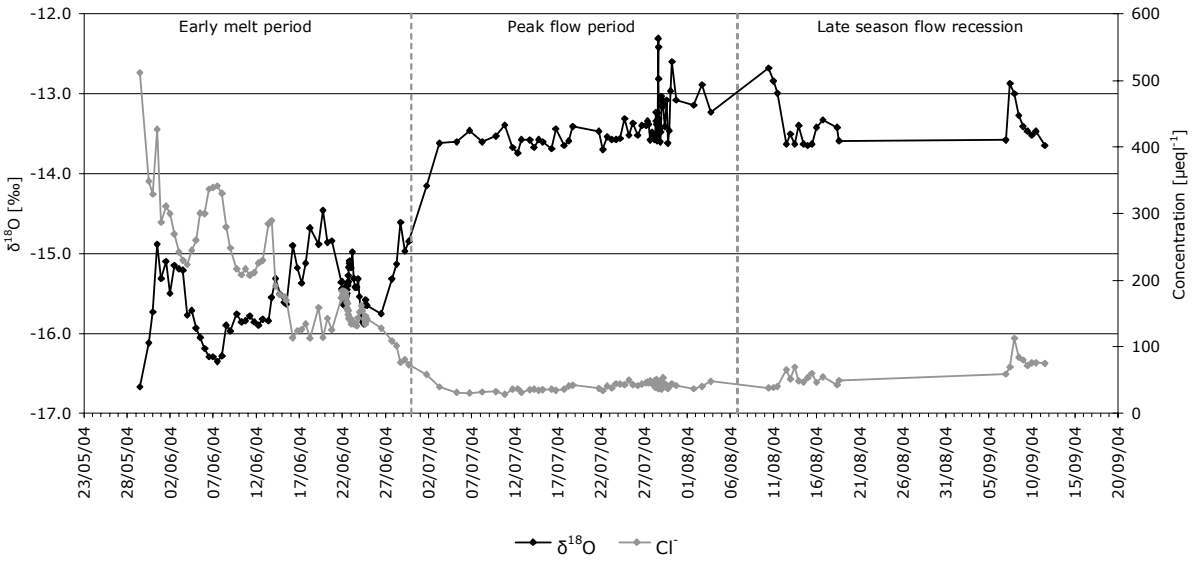

Figure 5.37. Variations in $\delta^{18}O$ values and Cl^- concentrations in river water during the entire ablation period.

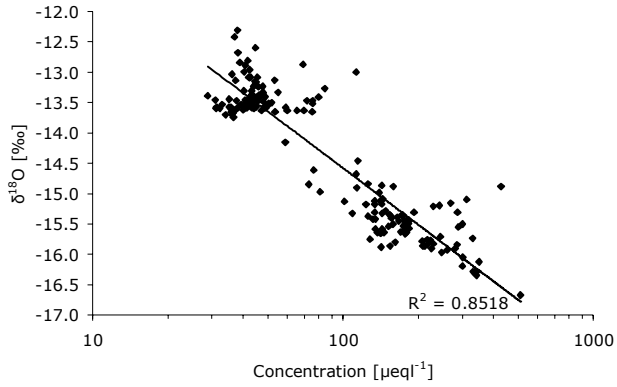

Figure 5.38. Correlation between $\delta^{18}O$ values in river water and measured concentrations of Cl^- during the entire ablation period.

Cl^- concentrations in the river supported the results derived from the $\delta^{18}O$ values. The early melt period was highly influenced by snowmelt and ions were leached from the thawing snowpack as the meltwater in the river became progressively enriched in ^{18}O. The correlation coefficient between $\delta^{18}O$ values and Cl^- during the early melt period (R^2=0.43) was lower than for the rest of the ablation period. High $\delta^{18}O$ values and low Cl^- concentrations recorded during the peak flow period and the late season flow recession give evidence of a river highly dominated by meltwater from ice ablation.

6. Discussion

6.1 GPR

6.1.1 Uncertainties concerning the lengths of the survey lines

The main problem concerning the GPR survey was the large discrepancy between some of the lengths measured by the odometer wheel and the lengths obtained from the handheld GPS. This brought about the question of whether or not it could be justified to assign the lengths obtained from the GPS to all radar lines. However, no jumps in the reflectors were observed in the radar profiles and a more detailed study of the odometer lengths to GPS lengths (Bælum, 2006) supported the assumption that the error in length measurements by the odometer wheel could be treated as constant within each survey line. In the present study, diffraction hyperbolas corresponding to a radar wave velocity of 0.17 m ns^{-1} were found in most radar profiles after correcting the survey line lengths. A radar wave velocity of 0.17 m ns^{-1} has previously been found to be valid for cold glaciers (Ødegård et al., 1997; Murray et al., 2000), indicating a correct step size for the profiles. No change in the shapes of the hyperbolas was observed along the profile as would have been expected had the length error not been constant. There are consequently several good reasons to regard the positions of the survey lines and the individual measuring points (traces) obtained from the GPS as adequately accurate for the purposes of this study. It is therefore reasonable to assume that the majority of the survey lines were positioned within the uncertainty of the GPS (5-9 m in the horizontal plane and 9-15 m in the vertical plane).

6.1.2 The thermal regime of Longyearbreen

On most of the radar profiles a clear basal reflector was observed down to the maximum ice depth of 110 m. In some profiles, however, the deepest western part of the glacier had an unclear basal reflector occasionally obscured by diffraction hyperbolas. Examples of this can be seen in appendix A.3 on profiles, C, E, EF, FG and G. A weak basal reflector is indicated with a thin line in the profiles in figure 5.2.

In the western part of the glacier a large number of reflections were observed near the surface and in the ice compared to the eastern part. An explanation as to why a faint reflector was mainly observed in the western part of the glacier may be that energy loss of the radar wave was too high in the glacier ice and that the wave did not reach the basal reflector. However, this does not seem to be the case for profile EF and FG, where only few reflections were observed in the glacier ice.

Previous studies have shown that zones of temperate ice appear on the radar image as areas with immense scattering of the radar signal as opposed to areas of cold ice that are almost transparent in the radar image (Bamber, 1987, 1988, 1989; Hagen and Sætrang, 1991). The GPR survey conducted on Longyearbreen in 1993 revealed that patches of

temperate ice most likely existed, primarily in the upper western area of the glacier (Appendix A.13, Tonning, 1996). These conclusions were based on the difference between two surveys carried out with 30-80 MHz and 320-370 MHz antennae. The areas of temperate ice interpretation by Tonning (1996) are most likely the same features observed in 2004 in the upper western areas of the glacier.

The relatively small accumulation basins on Longyearbreen are not thought capable of eliminating the winter cold wave and advecting temperate ice from the glacier surface. Temperate ice is therefore only thought to be present if the pressure melting point is reached at depth. Previous studies of glaciers of similar size and thickness as Longyearbreen give an idea of expected temperatures in the glacier. For the nearby glacier, Scott Turnerbreen, temperature gradients observed in two boreholes showed that ice thicknesses of 101 and 95 m were required in order for the ice to reach the pressure-melting temperature in the boreholes (Hodgkins, 1999). On Austre Brøggerbreen the pressure melting point is only reached in a thin basal layer in the thickest central part of the glacier, where ice thickness approach 130 m (Björnsson et al., 1996). Finally, a study of the nearby Tellbreen showed that if temperate ice is present in the glacier, it is in the form of small pockets in the deepest parts where ice thicknesses reach a maximum of 120 m (Bælum, 2006). Longyearbreen has a maximum ice thickness of 110 m and a central trough with thicknesses above 100 m (see section 5.1). Based on previous studies of similar glaciers, there is evidence to suggest that basal ice beneath the thickest parts of Longyearbreen is close to or at the pressure melting point and that water may be present at the bed.

The presence of temperate ice might explain the deepest faint basal reflectors observed in profile C, E and EF. However, it does not explain the poor reflector in profile FG and G where ice depth is thought to be maximum 80 m and therefore considered too thin to reach the pressure melting point. Furthermore, a clear basal reflection was observed in the deepest parts of the glacier in profile CD and D where warm ice most likely would be present if temperate ice was present in shallower depths. On the basis of these observations, the presence of temperate ice does not fully explain the features observed on the radar images.

An alternative explanation for the features may simply be that there is no distinct ice/bed interface in the deepest western part of the glacier. The unclear reflection may be caused by frozen debris-rich basal ice or up-thrusted basal sediments scattering the radar signal resulting in the chaotic pattern observed in several of the radar images. This would explain both the faint reflectors observed in the frontal area where the ice is relatively thin and the scattering of the signal in the upper and thicker parts of the glacier. The incorporation of debris into a basal ice layer implies that temperate ice has been present in the glacier (Benn and Evans, 1998). Studies have shown that Longyearbreen at places has thinned between 20 and 30 m since the end of the Little Ice Age (c. 1920 AD) where it is thought to have had its maximum thickness (Humlum et al., 2005). Assuming a present cold base, a continuous thinning of the glacier might have resulted in a gradual change in thermal regime from polythermal to cold-based. This development is thought to have occurred for many small glaciers on Svalbard (Björnsson et al., 1996; Hodgkins 1999; Bælum, 2006).

The weak basal reflector in the upper western parts of Longyearbreen is therefore interpreted as a frozen layer of debris-rich ice, while the weak reflector in the frontal areas of the glacier is thought to be caused by up-thrusted basal sediments. No evidence of

temperate ice was found, and the glacier is interpreted as being entirely cold-based. This is opposite of the conclusion reached by Tonning (1996).

Several thrust features were observed on the radar profiles. Most prominent was probably the discontinuous basal reflector in profile AB and B where a marginal thrust fault had resulted in an uplift of basal sediments incorporating them into the glacier ice. In profile G continuous dipping reflectors were observed in the radar image, several of which connected to surface features of outcropping up-thrusted debris observed on aerial photographs. Similar thrust faults were observed with 100 MHz GPR equipment on the cold-based terminus of the surge-type glacier Bakaninbreen on Svalbard although to a much larger extent (Murray et al., 1997). The thrust faults seen in the radar profiles are most likely remnants from a more active phase of Longyearbreen, where growth of the glacier resulted in major stress zones in the frozen marginal areas. This implies that the glacier has been cold-based near the margins throughout its entire existence. The findings of undisturbed vegetation at the ice/bed interface about 2 km up-glacier and 150 m from the glacier margin where ice thicknesses are thought to reach 30-40 m (Humlum et al., 2005), correspond well with this assumption. Profiles AB, B and G provide evidence of the powerful process by which basal sediments are incorporated into cold-based glacier ice. It is also clear that water draining in supraglacial channels in the marginal areas have access to sediments.

6.1.3 **Evidence of drainage structures**

Reflections in profile D, interpreted as an incised lateral channel now in an englacial position, was found to correlate well with both the locations of the channel in this area of the glacier and observations of the channel geometry (section 5.1). Reflections from what are thought to be lateral channels incised into the glacier ice were visible on many of the radar profiles in both the western and eastern marginal areas. The reflection patterns from these areas were often very chaotic. This is probably a result of the meandering character of the channels and the presence of sediments both in the actual channel (figure 5.20) and as englacial pockets related to shifts in channel position (Hansen, 2001). Furthermore, thrust faults and the consequent uplifting of basal sediment in the marginal areas may complicate matters. It was also shown in section 5.1 that reflections in the surface ice observed in several of the radar profiles, could be related to the presence of a major supraglacial meltwater channel. Profile G showed that this channel was in contact with uplifted debris before reaching the debris-covered glacier snout.

On several profiles, isolated diffraction hyperbolas were observed in clear glacier ice. These may be related to either englacial channels or rocks incorporated into the ice. Englacial channels have previously been mapped by GPR in studies of cold glaciers (Hagen and Sætrang, 1991; Maijala et al., 1998; Moore et al., 1999). Since the location of the reflection varied considerably from profile to profile and the presence of englacial channels in the centre of the cold glacier ice is unlikely, the reflections observed in the radar images are thought to be related to sedimentary features.

6.1.4 **Comparison with previous GPR survey on Longyearbreen**

The GPR survey conducted on Longyearbreen in 1993 showed similar spatial distribution of ice thicknesses as presented here (see appendix A.13), and there is no evidence to suggest that the subglacial topography has changed considerably since 1993. At 100 m depth, the ice thicknesses appears about 1.2 m thicker in the 2004 study because different radar wave velocities of the ice were applied in the two studies (v_{ice} = 0.17 m ns^{-1} in 2004 and v_{ice} = 0.168 m ns^{-1} in 1993). Maximum ice thicknesses measured in 1993 and 2004 were similar in the uppermost regions of the glacier (profiles A, B and C). In profiles D and E, however, a slight thinning had occurred. A maximum thickness of 115 m was measured in profile D in 1993 as opposed to a maximum thickness of 110 m in 2004. In the lower part of the glacier (profiles F and G) considerable differences existed between the two surveys. Profile F appeared to have thinned about 10 m, while the maximum depth differed by as much as 30 m in profile G. All estimates should be treated with caution, since the uncertainty of the ice thicknesses is thought be 5 to 10 m (section 4.1.2). Comparison of the two GPR surveys show that Longyearbreen has thinned between 0 and 0.15 m water equivalent per year (w.e. y^{-1}) in the upper regions (profile A, B and C), between 0.40 and 0.60 m w.e. y^{-1} in the intermediate areas (profile D and E) and between 0.80 and 2.45 m w.e. y^{-1} in the lower parts (profile F and G) since 1993 (assuming an ice density of 0.9 g cm^3). The estimates of net mass balance in different altitudes on the glacier (profile A to G) are shown in figure 6.1 together with results of mass balance studies from different ice masses on Svalbard (Hagen et al., 2003). The net mass balance on Longyearbreen is low compared to the average mass balance (thick grey line), but largely within the lower dashed line. However, the thinning obtained for profile G is significantly below the trend observed for the glacier and ice masses on Svalbard in general. This may be explained by an underestimation of the ice thicknesses in the 2004 survey due to a weak basal reflector. Furthermore, line G was located in the lower, sediment-rich part of the glacier (figure 5.5), where an increased ice ablation is expected due to a change in albedo (Benn and Evans, 1998).

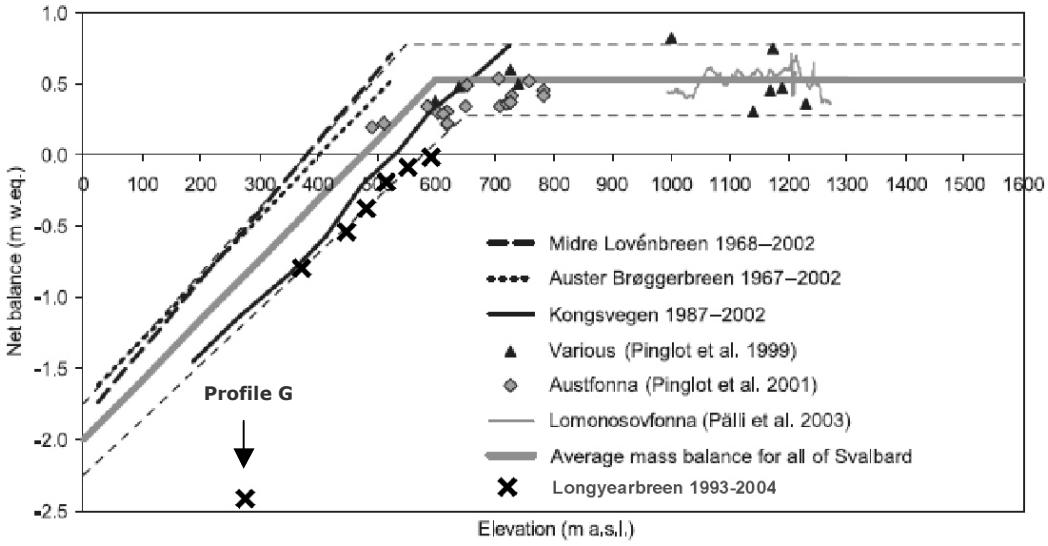

Figure 6.1. Comparison of net mass balance of Svalbard ice masses. After Hagen et al. (2003).

6.2 Discharge

Water level variations measured at the gauging station in Longyearbreen correlated well with personal observations at the sampling site, and the water level measurements are thought to reflect discharge variations from Longyearbreen well.

6.2.1 Variations in discharge during the ablation period

The beginning of the ablation period was highly influenced by snowmelt and temporarily storage of meltwater in the snowpack. A gradual increase in glacial runoff occurred during the early melt period as air temperatures rose and an increasing amount of water was released from the soaked snowpack. Evidence of the release of water from storage was seen between 18 and 26 June where a significant rise in water level took place, unexplained by the meteorological conditions. This episode was followed by a marked decline in water levels as new reservoirs of temporarily stored water built up in the glacial drainage system. During the early melt period the correlation was low between glacial runoff and meteorological input such as air temperature and precipitation.

The transition from a snowmelt dominated runoff in the early melt period to a peak flow period where icemelt contributed significantly to runoff, was extremely rapid as the snowpack on the lower parts of the glacier collapsed and large amounts of temporarily stored water was released. For the remainder of the peak flow period, continuous degradation of the snowpack and the development of the drainage system resulted in chaotic discharge patterns with high water levels and large fluctuations of magnitudes often unexplained by the meteorological data. As the transient snowline moved up-glacier, the temporarily storage of meltwater in the snowpack became less significant and the faster draining icemelt more important. Diurnal variations in runoff were occasionally observed during the peak flow period and the effect of rainfall events was recognized in the hydrograph.

A gradual decline in runoff occurred during the late season flow recession. The transient snowline was by then approaching its maximum height (the equilibrium line altitude, ELA) and the glacial drainage system was fully developed. A strong correlation was consequently found between air temperature and glacial runoff and short time lags were observed. Distinct diurnal variations in discharge were observed as fluctuations in ice ablation were superimposed on a base flow component with a larger proportion of snowmelt.

The variations in runoff observed for Longyearbreen is similar to what has previously been documented for glaciers on Svalbard (Wadham et al., 1998; Hodgkins, 2001). The division of the ablation period in three sub-periods specified by Wadham et al. (1998) could therefore successfully be applied to the runoff. The most distinct feature observed during the ablation season was the rapid transition of the drainage system occurring between 29 June and 3 July. Similar dramatic variations have previously been observed for cold glaciers as opposed to more gradual changes in polythermal and temperate glaciers (Hodgkins, 2001). This difference is explained by an enhanced storage of meltwater in the snowpack caused by the relatively flat and impermeable cold glacier surface, and the rapid drainage of this water through already existing drainage channels (Hodgkins, 2001).

6.2.2 **Annual variations in water flux**

In table 6.1 total flux of water through Longyearelva in 2004 is compared with values from 1995, 1996 and 1997. The relationship between measured water level and discharge was the same for all four years (equation 2 and 3 in section 4.4).

Table 6.1. Calculated annual water flux at the gauging station in Longyearbyen for the ablation period of 1995-1997 (Grønsten, 1998) and 2004.

Year	Ablation period	Calculated annual flux [m^3]
1995	17 Jun. – 25 Sep.	19102200
1996	21 Jun. – 19 Sep.	9669600
1997	04 Jun. – 03 Sep.	22467600
2004	05 Jun. – 09 Sep.	7175600

Even though the ablation periods had similar lengths, large variations in total flux exist from year to year. The total flux for 2004 was considerably lower than the values from 1995 and 1997 but comparable to the value from 1996.

Monthly air temperature and precipitation amounts for the four ablation and accumulation periods are shown in figure A.14.1 in appendix A.14. A possible explanation to the differences in annual runoff may be the increased winter precipitation that preceded the ablation periods in 1996 and 2004. The accumulation of a thicker snowpack would have resulted in a delayed onset of ice ablation since the summer air temperatures were similar for the four periods. Glacier ice has a lower albedo than snow and melting of ice is consequently faster (Benn and Evans, 1998). However, this is not thought to entirely explain the large differences observed in the annual water flux. Mass balance studies on the nearby Larsbreen in 1996 and 1997 showed a winter balance only slightly higher in the accumulation season from 1995-1996 compared to the following year. This does not correspond with the meteorological data. Net balances of -0.25 and -1.20 m w.e. were found in 1996 and 1997, respectively, mainly controlled by a significantly larger loss of mass during the 1997 ablation period (Grønsten, 1998). This suggests that other factors, such as for example wind and radiation patterns may have influenced the ablation significantly.

In table 6.2 the specific discharge (mean diurnal water flux divided by the catchment area) for five glaciers with different thermal regimes are compared. Longyearbreen clearly has the lowest specific discharge with 0.003 m d^{-1}. The value is comparable to the value for the similarly cold-based glacier Scott Turnerbreen, especially if 2004 was a low discharge year compared to normal. The large difference in specific discharges for Erikbreen in 1990 and 1991 illustrates that large annual variations have been reported for this glacier.

Table 6.2. Inferred thermal regime, catchment area, glacierized proportion, terminus altitude, specific discharge, diurnal sediment fluxes and diurnal solute fluxes for five glaciers on Svalbard (after Hodgkins, 1997a).

Glacier	Thermal regime	Catchment area [km^2]	% glacierised	Terminus altitude [m.a.s.l.]	Specific discharge* [$m\,d^{-1}$]	Sediment flux [$t\,d^{-1}$]	Daily solute flux** [$t\,d^{-1}$]
Austre Brøggerbreen	Largely cold-based	31.6	54	40	0.010 (16/6-12/9, '75)	63.9 (09/6-20/9, '77)	20.7 (27/6-20/9, '91)
					0.012 (02/6-24/9, '74)	186 (16/6-12/9, '75)	22.6 (24/6-03/8, '92)
Scott Turnerbreen	Cold-based	12.8	32	230	0.005 (15/6-11/7, '93)	105 (14/6-11/7, '93)	2.5 (14/6-10/7, '93)
					0.006 (20/7-19/8, '92)	126 (20/7-15/8, '92)	
Erikbreen	Polythermal	12.4	75	30	0.007 (01/7-18/8, '91)	22.5 (01/7-18/8, '91)	5.6 (01/7-18/8, '91)
					0.016 (13/7-23/8, '90)	175 (13/7-23/8, '90)	43.7 (13/7-23/8, '90)
Ebbabreen	Polythermal	51.5	52	100	0.012 (29/6-22/7, '85)	624 (29/6-23/7, '85)	105 (29/6-03/7, '85)
Longyearbreen	Cold-based	10.7	43	210	0.003 (05/6-09/9, '04)	30 (05/6-09/9, '04)	2.7 (05/6-08/9, '04)

*Specific discharge for Longyearbreen equals mean diurnal flux (32580 $m^3\,d^{-1}$) divided by the catchment area of 10.68 km^2. **Daily solute flux has been calculated from the solute fluxes found for Longyearbreen by Yde et al. (in prep.) shown in appendix A.17.

Another explanation for the large variations in annual water flux from Longyearbreen may relate to the difficulties that exist in obtaining accurate measurements of water levels in an environment as dynamic as a glacierized catchment. Furthermore, construction work in the river bed before and after the measuring site may have resulted in a change in relationship between water level and discharge since 1997 where equation 13 and 14 were constructed (see section 4.4.1). The appearance of the discharge curve on figure 5.15 suggests that low water levels may have been underestimated when calculating discharges (equation 13), resulting in an almost complete elimination of the base flow component observed in the water level chart (figure 5.12).

The results presented here show that either the ablation period of 2004 was a low discharge year compared to normal, or uncertainties in the stage measurement or stage relationship, have resulted in an underestimation of the water flux in Longyearelva. It is unclear which of these explanations apply, and it may even be a combination of the two. In the following it is assumed that 2004 was a low discharge year, since previous studies have shown that annual variations of similar size have been observed in the past for Longyearbreen (Grønsten, 1998) and Erikbreen (table 6.2). The calculated discharges and the estimate of the total water flux should however be treated with caution. The uncertainties concerning the stage relationship does not influence the fluctuations in water level observed in Longyearelva.

6.3 Suspended sediment transport

In general, variations in the measured SSC corresponded with variations in the measured water level of Longyearelva. There were, however, variations in SSC that could not be explained merely by water level fluctuations and may therefore have been related to changes in the structure of the glacial drainage system.

6.3.1 Sediment sources within the catchment of Longyearbreen

Small isolated peaks were observed in SSC during the two three-day periods with frequent water sampling (see figure 5.16 and 5.17). Since no corresponding signal was observed in the water level data, these events may have been related to a rapid supply of sediments to the meltwater from slope processes in the drainage system and the proglacial area. On a seasonal scale, figure 5.19 illustrates a rapid shift in the relationship between SSC and water level on 22 June. Water samples were collected between 20-50 m from the glacier portal and sediments from the proglacial areas might therefore have influenced the SSC in the river water. Pictures from the sampling site during this period give no evidence of a change in the availability of sediments in the proglacial environment and the change must have taken place within the internal drainage system. This shift may have been caused by the opening of drainage channels through sediments-rich areas previously blocked by ice and snow, or the continuous exposure of snow and ice-free sediments for erosion in the ice-marginal and proglacial areas. A continuous increase in SSC occurred during the early melt period and the peak flow period. The data suggests that no sediment-supply exhaustion occurred during the ablation period.

The highest SSC occurred during periods of high discharge. Unfortunately, no measurements of water levels exist when the largest SSC was measured. The rapid increase and the extraordinary high level of SSC in the water, however, indicate a fast, responsive and abundant sediment source. A distinctive color difference was observed between the eastern and western meltwater stream during a period of high discharge (figure 5.18). The western meltwater stream emanates from the side of the debris-rich glacier snout, whereas the eastern meltwater stream (sampling site) drains below the entire debris-covered frontal part. The eastern stream drains on the glacier surface for a substantially longer distance than the western lateral channel, and consequently has a higher input of sediments from the surrounding slopes. Furthermore, access to fine-grained sediments in the proglacial area is more limited for the western stream. The major sediment sources for the eastern meltwater stream were therefore most likely in the ice-marginal debris-rich parts of the glacier and in the proximal proglacial area. Water samples collected from different places in the glacial drainage system supports this assumption (table 5.3). The principal mechanisms of sediment acquisition by meltwater is thought to be by sediment mobilization within the drainage channels (from the channel floor and to a lesser extent from the debris-rich ice in the sides of the subglacial ice-marginal drainage channel), sliding and slumping of water-saturated sediments from valley sides into the lateral channel and the degradation of sediment-rich ice-marginal areas as the underlying ice thaws. Another factor that may have influenced sediment availability is the thawing of permafrost in the near surroundings of the glacier and possibly in the ice-marginal subglacial channel. Furthermore, the GPR survey presented earlier revealed that supraglacial channels are likely to have access to up-thrusted basal sediments in the lower part of the glacier (see section 5.1). The proportionality of the different factors is thought to change with discharge. Slope processes and degradation of the ice-marginal areas were probably more important during high discharge, whereas sediment mobilization from the drainage channels most likely constituted a larger proportion of the total suspended sediment in the river water during low discharge.

6.3.2 **Comparison with previous studies of SSC in glacial meltwater**

Comparison with previous study conducted on Longyearbreen

Table 5.2 lists a mean SSC in 2004 of 1.32 g l^{-1} with a maximum value of 13.74 g l^{-1}. The values are considerably higher than the mean of 0.5 g l^{-1} and maximum of about 6 g l^{-1} previously measured for Longyearbreen (Etzelmüller et al., 2000). The high mean value can be explained partly by the irregular sampling interval in 2004. The first period with frequent sampling took place during a period in the early melt season, where the suspended sediment concentrations were at their highest. The second period of frequent water sampling was carried out during one of the largest runoff events during the entire ablation period. The two periods of frequent water sampling constitute 43% of the total dataset. Emphasis in the data is therefore on periods with high discharge and correspondingly high SSC. A mean of 0.85 g l^{-1} for the entire ablation period was found by only including two samples a day. Another factor that complicates a direct comparison with the previous studies of SSC for Longyearbreen is that focus has previously been on the beginning and end of the ablation period (Sægrov, 1995). In these periods, results from 2004 rendered a

more comparable mean SSC of about 0.2 g l^{-1} (table 5.2) similar to the 0.3 g l^{-1} found for Longyearbreen in 1993 and 1994 during these periods (Sægrov, 1995). Another important difference between the two studies is the sampling locality. Sampling of water in 2004 took place in the eastern meltwater stream between 20 and 100 m from the glacier portal. Sægrov (1995) sampled water from the western meltwater stream up to 500 m from where the water emanated from the glacier. The data presented here suggest that a significant difference exists between the suspended sediment transport in the two streams, especially during high discharge (figure 5.20 and appendix A.7).

Due to the cold-based thermal regime that was suggested in section 6.1.2, subglacial drainage channels are confined and a distributed drainage system does not exist in the glacier. The availability of erodible subglacial sediments is furthermore limited by the presence of permafrost. The total sediment yield from the glacier is therefore not so much an estimate of the degree of subglacial erosion by the glacier, as an estimate of the degradation occurring in the ice-marginal and proglacial areas (Hodgkins, 1997a). Three rough estimates of the total sediment yield for Longyearbreen were presented in section 5.5 (8910 t y^{-1}, 4700 t y^{-1} and 3030 t y^{-1}). The first two values are thought to overestimate the total sediment yield for Longyearbreen. The former because of the overestimation of particular periods with poor data coverage (see appendix A.8), and the latter because the mean SSC concentration is dominated by the periods of frequent water sampling where SSC were particularly high (see above). The three estimates give a diurnal flux of suspended sediments of 90 t d^{-1}, 50 t d^{-1} and 30 t d^{-1}, respectively. Estimate two and three are significantly smaller than the 61 t d^{-1} and 73 t d^{-1} found by Sægrov (1995) for 1993 and 1994. Measured discharges varied between 1 and 4 $m^3 s^{-1}$ for the periods where sampling took place (Sægrov, 1995) and was therefore significantly larger than the mean discharge of 0.43 $m^3 s^{-1}$ obtained for the ablation season of 2004. A lower sediment yield compared to the values for 1993 and 1994 is therefore expected and the third estimate seems the most reasonable determination of the sediment yield in 2004. Finally, in accordance with the results from 2004, no exhaustion of suspended sediments was observed during the ablation periods of 1993 and 1994 (Sægrov, 1995).

Comparison with studies of SSC in meltwater from other glaciers on Svalbard

The described processes of sediment acquisition and the increased supply of sediment during the majority of the ablation period have previously been documented in studies of SSC in meltwater from cold and largely cold-based glacier (Gurnell et al., 1994; Hodgkins, 1996; Hodson and Ferguson, 1999). These processes differ, however, significantly from the processes that dominate for temperate and to some extent polythermal glaciers. For these two glacier types and for temperate glaciers in particular, evacuation of sediment-rich water from the subglacial distributed drainage system is the most important way of delivering sediments to the meltwater (Gurnell et al., 1994; Hodson and Ferguson, 1999).

A specific sediment yield of 280 t $km^{-2} y^{-1}$ was found to be the most reliable value of the three estimates mention in section 6.3.2. 86 and 150 t $km^{-2} y^{-1}$ were found for the predominately cold-based Austre Brøggerbreen in 1991 and 1992 (Hodson et al., 1998), while the nearby cold-based glacier Scott Turnerbreen had values as high as 1500 t $km^{-2} y^{-1}$ in 1992 (Hodgkins, 1997a). However, the high value for Scott Turnerbreen has been shown

to be considerably higher than has previously been observed for cold-based glaciers (Hodson et al., 1997). In table 6.2 diurnal suspended sediment fluxes for five glaciers on Svalbard with different temperature regimes are listed. The diurnal sediment flux for Longyearbreen is low compared to values for other glaciers except Erikbreen in 1991. This is as expected, considering the low discharge and the cold base of the glacier.

It is obvious that large annual variations in SSC occur for the individual glacier, but also between glaciers with similar characteristics. Previous studies and the data presented here show that the proglacial area is an important sediment source, particularly for cold-based glaciers (Gurnell et al., 1994; Hodgkins, 1996; Hodson and Ferguson, 1999). SSC may therefore vary considerably from study to study because of differences in distances from the sampling site to the glacier margin and the availability of proglacial sediments.

6.4 Ionic and isotopic composition of river water

6.4.1 Composition of the snowpack compared to previous studies

The results of analyses on snow from four snow pits located on Longyearbreen were presented in section 5.6. Mean concentration values from the pits showed that the sea-salt derived Cl^- and Na^+ were the most dominant ions constituting 34% and 27% of the total solute content, respectively. The pits showed large vertical variations in chemical composition. These variations are probably related to the large differences that have previously been documented between precipitation events on Svalbard (Bringedal, 2004) and an alteration of the original chemical stratification of the snowpack during warm spells in the winter. The effect of dry deposition from the atmosphere following precipitation will be discussed in more detail later. Horizontal variations also occurred between the snow pits although they were smaller than the vertical variations. These variations may arise because of local variations in the precipitation pattern and the amount and source of snow transported by wind drift.

Solute content was also measured in snow samples collected from the nearby Tellbreen during the spring 2004 (appendix A.15). Samples from Tellbreen had similarly high standard deviations as observed in the samples from Longyearbreen. Even though the glaciers are only about 13 km apart, differences were observed between the solute concentrations in the snow samples and the snowpack on Tellbreen was 18% more enriched in ions than the snowpack on Longyearbreen. The relationship between the individual ions was similar, with proportion for Cl^- and Na^+ of 39% and 31%, respectively. The Ca^{2+} concentrations, however, were significantly higher in the snow from Longyearbreen. This might indicate a higher amount of Ca^{2+}-rich aeolian dust in the snowpack on Longyearbreen. The $\delta^{18}O$ values were generally higher in the samples from Tellbreen. Snow samples collected on Finsterwalderbreen (see appendix A.1 for location) during the spring of 1995 and 1996 (Wadham et al., 1998) was about 20% more dilute compared to the snow on Longyearbreen. The proportions between the ions were however similar to the observations on both Longyearbreen and Tellbreen, with Cl^- and Na^+ constituting 37% and 31% of total solutes, respectively. Ca^{2+} concentration was relatively high in snow from Finsterwalderbreen with 8% of total solutes. Snow samples from the nearby Scott

Turnerbreen collected in the spring of 1993 (Hodgkins and Tranter, 1998b) differed significantly from the presented studies. Cl^- constituted 56% of total solute content in the snow, while the concentration of Na^+ (31%) was similar to the values observed on Longyearbreen, Tellbreen and Finsterwalderbreen. NO_3^-, Ca^{2+} and Si each constituted less than 1% of all the ions (Hodgkins and Tranter, 1998b).

Except for the snow samples collected on Scott Turnerbreen, the proportions of the ions in snowpacks on different glaciers appear uniform. The difference in total solute content observed between the three glaciers reflects variations in influence of sea-salt derived ions. This is thought to be related to the proximity of a marine source (Humlum et al., 1995). This does however not explain the differences observed, as Scott Turnerbreen is the glacier furthest from the ocean. Local climate and annual variations in dominant moisture source and sea-ice extent is therefore thought to significantly influence the chemical composition of the snow. Relatively large annual variations in the isotopic composition of the snowpack on Longyearbreen have previously been documented by studies of pits dug on the same locality for four consecutive years. Mean $\delta^{18}O$ values were found to vary between -14.49‰ and -12.12‰ in the 2000 to 2003 accumulation seasons (Bringedal, 2004). This is slightly higher than the -14.90‰ found in snow on Longyearbreen in 2004. The variations were thought to arise due to annual variations in dominant moisture source and average air temperature during precipitation events (Bringedal, 2004).

6.4.2 **Ionic and isotopic composition of freshly precipitated snow and rain**

Precipitation samples of freshly precipitated snow and rain were relatively dilute in Cl^- and Na^+ compared to samples of snow from the snow pits. Furthermore, freshly precipitated snow collected at the sampling site during the ablation period, where erodible sediments were exposed, had a higher concentration of SO_4^{2-} compared to snow samples from the glacier. These differences suggest that dry deposition of sea-salts and, when accessible, airborne dust particles may play an important role in ionic enrichment of snow. This has previously been documented in the top snow layers by He et al. (1994). The variations in ionic composition observed in the snowpack might therefore also be related to the amount of time the snow was exposed to the atmosphere following precipitation as well as reflect the source of the precipitation cloud. This effect may be especially pronounced on Svalbard, where precipitation is sparse and snow drift extensive.

Concentrations of ions in the snow samples were highly variable and only few samples of freshly precipitated snow and rain were collected. The data may therefore not represent the general chemical composition of precipitation on Longyearbreen. Previous studies have indeed shown significantly different ionic composition of rain samples with a considerably higher concentration of all ions (Wadham et al., 1998). In order to estimate the degree of post-depositional enrichment of the snow by dry deposition from the atmosphere, a larger set of data therefore needs to be studied.

6.4.3 **Uncertainties concerning the applied methodology**

Unlike all other studies used for comparison, samples collected for this study were not filtrated until 2½ to 6 months after collection. This may have resulted in chemical weathering of the sediment in the bottles. Previous studies on Longyearbreen have documented changes occurring in meltwater that was not filtrated. Studies showed an overall increase in total solute content particularly in HCO_3^-, Ca^{2+} and Mg^{2+}. Results were however ambiguous since a decrease in concentration seemed to occur for several other ions, especially Cl^- and K^+ (Sægrov, 1995; Hansen, 2001). Furthermore, studies have shown that the actual filtration process may alter the chemical composition since desorption of ions from the sediment may occur (Collins, 1977).

Figure 5.31 shows that a linear relationship exists between conductivity measured in the meltwater stream at the time of sampling and the total concentration of solute measured in the water by analyses 2½ to 6 months later. The samples were stored for different periods of time and contained different amounts of suspended sediment (see figure 5.15). Since a linear relationship exists regardless of variations in these two parameters the total change in chemical composition of the meltwater in the bottle is independent of the amount of suspended sediment in the water sample and the period of time the individual bottles were stored prior to analyses. This suggests that either: (1) the water has not reacted with the sediments; or (2) the water has reacted as much as possible and that this is similar in all the bottles; or (3) the degree of chemical reactions in the individual bottle is only dependent on the original concentration of solutes in the water.

In appendix A.12, the relationship between measured conductivity at the time of sampling and total solute content in the collected samples were shown both from 2004 and from a study carried out in 1993 by Sægrov (1995). Samples from this study were filtrated immediately upon collection. In the following discussion it is assumed that the relationship between solute content and conductivity found by Sægrov (1995) is similar to the relationship in the river at the sampling site in 2004. This assumption is concerned with some uncertainty, since the data shows that the chemical composition of the meltwater differed significantly. The discrepancy between the two curves increases with solute concentrations, which contradicts the possibility of none or a constant increase in solute concentration in the samples (situation (1) and (2)). For a given conductivity, the unfiltered samples had a higher concentration of solutes than the filtered samples. Assuming that a higher content of solutes compared to conductivity in 2004 reflects a continued chemical weathering in the bottles, the additional chemical weathering varies between 5% and 18% of total solute content. This would therefore not significantly influence the overall fluctuations in solute concentration observed during the ablation period.

Based on the discussion above, the total solute concentrations measured in the meltwater are thought to reflect the chemical composition of the water at the time of sampling and chemical weathering of sediments subsequent to sampling is thought to be of little importance. This is explained by the relatively fast chemical reactions that occur in the glacial system, resulting in a protecting sediment-coating of low reactive weathering products limiting further denudation (Raiswell, 1984).

The calculation of HCO_3^- was subject to much uncertainty, since the uncertainty for each ion of 5% and 10% (depending of which ion (section 4.4.1)) is reflected in the HCO_3^- concentration. Negative concentrations, resulting from the uncertainties in the determination of HCO_3^-, were found both in samples with low solute concentrations (such as the snow samples presented in table 5.4), but also in more solute rich samples, illustrated on figure 5.25. Since SO_4^{2-} concentrations in the water were very high, uncertainty related with the analysis (5%) had a large influence on the calculations of HCO_3^-. However, the ten samples collected successively (table 5.5) showed that the concentrations of SO_4^{2-} varied little in water that is thought to have had an almost identical chemical composition. The HCO_3^- concentrations observed during the ablation period are therefore not considered to merely reflect the uncertainty of the calculation.

A coal-fired power station equipped with an air filter is present in Longyearbyen only 4 km from Longyearbreen. Pollution from the power station would primarily cause an increase in SO_4^{2-}. However, wind direction is rarely from the power station towards Longyearbreen and SO_4^{2-} concentrations were not increased in the snowpack on the glacier compared to what has previously been measured in snow on Svalbard (Hodgkins et al., 1997b; Wadham et al., 1998). Air pollution from the power station therefore had no significant effect on the chemical composition of the meltwater.

6.4.4 **Ionic and isotopic composition of meltwater during the ablation period**

In the following it will be argued that the ionic composition of the river meltwater is a result of: (1) the preferential leaching of ions from the melting snowpack; (2) the enrichment of the meltwater as it overflows the ice-covered, solute-rich channel floor in the subglacial ice-marginal channel; and most importantly (3) seepage of solute-rich pore water into the meltwater channels from a thawing active layer in the mountain sides, on the debris-covered glacier snout and from lateral moraines. Similar solute provenances have previously been documented for the cold-based glacier, Scott Turnerbreen (Hodgkins, 1998a). The isotopic composition of the river meltwater is thought to reflect variations in the proportions of snow- and icemelt and the occasional influence of precipitation events enriched in ^{18}O.

The early melt period (29 May – 29 June)

Significant variations occurred in both the ionic and isotopic composition of the meltwater in the early melt period. These variations were partly caused by the preferential leaching of ions from the melting snowpack. The effect was most pronounced in the Cl^- concentrations since this ion is thought to originate exclusively from the snowpack. A general decrease of Cl^- concentrations in the river meltwater occurred during the early melt period from values more than 6 times the mean concentration in the snow, to concentrations similar to the snow. This is explained by an increasingly more dilute snowmelt from the depleted snowpack in the lower areas of the glacier and the river bed.

Several features in the ionic composition of the meltwater however suggest the influence of an additional ion source than the melting snowpack. Correlation coefficients were not particularly high between Cl^- and the other ions in the water during the early melt period (a

mean of R^2 of approximately 0.5) as would be expected had the ions originated from the same source. Between the other ions (except HCO_3^-) correlation was however very good with R values ranging from 0.84 to 1.00 (appendix A.9). Even though Cl^- was the dominant ion in the snowpack, this was not the case in river water, where SO_4^{2-} had the highest concentrations during the entire ablation period. Cl^- concentrations were comparable to SO_4^{2-}, Ca^{2+}, Mg^{2+} and Na^+ until the 3 June after which the ions only resembled each other when concentrations were low. Rough estimates of the snowpack derived fractions of each ion are shown together with the total concentrations in figure 5.24, 5.25 and 5.26. It is obvious that the preferential leaching of ions from the snowpack does not explain the concentration peaks observed in the early melt period.

The first peak in ionic concentrations coincided with a significant decrease in the $\delta^{18}O$ values. This increase in solute concentrations and decrease in $\delta^{18}O$ values is thought to be related to a decrease in glacial runoff due to a period of lower air temperatures. On 7 June, renewed increase in runoff occurred and solute concentrations lowered while the $\delta^{18}O$ value of the meltwater rose. A decline in water level was also registered at the sampling site when the second peak in concentrations occurred. This peak was not seen in the isotopes however, and only to a limited extent in the Cl^- concentrations. During the period with more frequent water sampling, a similar trend was observed and as water level rose, the solute content lowered and the $\delta^{18}O$ values increased. The timing and the longer duration of the first peak in Cl^- concentrations differed from what was observed for the other ions. Comparing the peak in Cl^- with the low in the $\delta^{18}O$ value shows a perfect match. The variations in Cl^- and $\delta^{18}O$ values were most likely related to an enhanced influence of ^{18}O depleted, solute-rich snowmelt possibly from a new source area. However, during its passage through the drainage system, this water was significantly enriched in ions.

When water ceased to flow at the sampling site in September, unfrozen water was still stored in pools inside the ice-marginal subglacial channel (the moraine cave). A sample of this water collected on 15 September showed extremely high solute concentrations (table 5.9). Proportions of the four largest ions and Cl^- in this water sample (SO_4^{2-}: 44%, Mg^{2+}: 22%, Ca^{2+}: 20%, Na^+: 8%, Cl^-: 0.2%) show a significant similarity with the mean values of the river water in the early melt period (SO_4^{2-}: 40%, Mg^{2+}: 20%, Ca^{2+}: 17%, Na^+: 13%, Cl^-: 4.7%). The water in the early melt period was however more than 10 times more dilute and had a higher proportion of Cl^- and Na^+. This is consistent with a meltwater source of solute-rich snowmelt in the early melt period and a source of icemelt, and a dilute snowpack in the late season flow recession. Melting of the ice-covered channel floor is not thought to have influenced the $\delta^{18}O$ values of the river meltwater since the degree of melting was low and the mean $\delta^{18}O$ value for the frozen channel floor (-16.22‰) was similar to the snowmelt.

The fluctuations observed in the chemical composition of the meltwater during the early melt period are explained as follows: The earliest samples, with low solute content, showed a similar ionic composition as the snowpack and no additional enrichment of the snowmelt occurred. This implies that either no melting of ice occurred in the subglacial channel or the snowmelt did not drain through the moraine cave but rather originated from melting snow in the proglacial river bed. Water was observed inside the moraine cave on 30 May but may only have contributed a small fraction to the river discharge. As runoff from the glacier declined, solutes from the ice-covered channel floor began to contribute ions to the river meltwater. It seems likely that snowmelt from the proximal river bed would stop earlier and

contribute less to river runoff during periods with low temperatures, whereas snowmelt from the glacier, which had a significantly longer transport distance, continued to flow even when melting of the snow had ceased. Another reason for the enrichment of meltwater may have been an increase in solute uptake from the solute-rich ice in the sub-glacial channel. Uptake of ions from the ice may either have occurred as the meltwater overflowed it or by an onset of melting of the ice caused by a raise of air temperatures in the cave. However, the latter does not correspond with the air temperatures at the sampling site which were largely below zero degrees during the temperature low. As runoff decreased, the ice and water contact time also increased giving the water draining through the moraine cave more time to acquire solutes from the ice. The concentration peaks observed during the early melt period are therefore thought to reflect the enhanced influence of solutes acquired from ice on the channel floor in the moraine cave. As runoff decreased, snowmelt draining through the moraine cave constituted a larger fraction of river runoff and acquired more solutes due to an increased ice contact time. As the early melt period progressed, water runoff increased and contact time between water and the solute-rich ice decreased. At some point, the solute-rich ice would have melted away and the water had access to erodible sediments. The suspended sediment record suggests an increase in sediment availability after 22 June, which may be associated with the disappearance of the protecting channel ice.

An overall increase in $\delta^{18}O$ values occurred during the early melt period. This may reflect variations in the original isotopic composition of the snow and isotopic exchange processes that occur as the meltwater percolates through the snowpack. The latter resulting in meltwater depleted in ^{18}O compared to the residual snowpack (Raben and Theakstone, 1994). Furthermore, variations in $\delta^{18}O$ values similar to those observed in the early melt period have previously been explained by the release of meltwater from storage within the internal drainage system (Theakstone, 2003). It is also possible that ^{18}O enriched ice contributed to glacier runoff early in the ablation period due to thermal heat released, as the snowmelt flowed across the glacier surface. This is an inefficient way of melting ice and thought to be insignificant compared to the large volumes of snowmelt. Therefore, prior to 29 June, icemelt from the glacier surface had little influence on the chemical composition of the meltwater. Cl^- and $\delta^{18}O$ correlated better in the meltwater during the early melt period (R^2=0.43) than in the snowpack (R^2=0.10). This suggests that fractionation of the snowpack occurred simultaneously with the preferential leaching of ions. This would result in a snowmelt, initially enriched in Cl^- and depleted in ^{18}O, but continuously becoming more depleted in Cl^- and more enriched in ^{18}O as the chemical composition of the snowpack altered. This would occur as the snowline moved up-glacier and the drainage system developed. The correlation coefficient between Cl^- concentrations and $\delta^{18}O$ values in the early melt period however suggests that this is not the only reason for the observed variations. The isotopic composition of the river meltwater in the early melt period is therefore thought to reflect: (1) the original composition of the snowpack; (2) the release of water from storage; and (3) an isotopic fractionation of the melting snowpack resulting in a snowmelt initially depleted in ^{18}O progressively becoming more enriched in ^{18}O.

The peak flow period (30 June – 6 August)

Few variations occurred in the chemical composition of the river meltwater during the peak flow period. Solute concentrations were at their lowest during the ablation period and $\delta^{18}O$

values were significantly higher than during the early melt period. Dilute ^{18}O rich icemelt constituted a continuously larger fraction of bulk meltwater as the transient snow line moved up-glacier. SO_4^{2-}, Mg^{2+}, Ca^{2+} and Na^{+} continued to dominate runoff but the proportion of SO_4^{2-} in the river water decreased slightly. Unlike all other ions, HCO_3^{-} maintained similar concentrations during the peak flow period compared to the early melt period. In late July during a period of high water runoff, variations occurred in ionic and isotopic composition of the meltwater. The change in chemical composition occurred during a period with more frequent water sampling. The period was influenced by several rainfall events resulting in an uneven curve for the concentrations and isotopes. On 29 July 14:00, the collected water sample was thought to be highly influenced by rainwater with a significant dilution of all ions and a raise in $\delta^{18}O$ values caused by the solute-poor, ^{18}O rich rainwater which was sampled at the time. After this event $\delta^{18}O$ values lowered and subsequently rose to the second highest value measured during the ablation period. This is thought to have coincided with a major precipitation event and occurred simultaneously with a rapid rise in solute concentrations. A positive relationship therefore existed between $\delta^{18}O$ values and solute content during this event as opposed to the negative relationship observed earlier in the ablation period. Unfortunately, no observations were made on the water runoff and the gauging station was out of order. Solute concentrations may have risen due to a lowered runoff from the glacier. The rainfall event would have had a large influence on the river water during low discharge, resulting in a high ^{18}O ratio. Previous periods with rain however, resulted in an increase in water runoff and as the rain was probably of similar chemical composition as the rain sample presented here, it would have lowered the ion concentrations of the river water. Assuming that the water level rose during the rainfall, a rise in solute concentrations must have been related to an increased input of solute-rich water. An explanation may be that the several days of rain had resulted in a soaking of the thawed active layer in the mountain sides, the sediment-rich frontal area and in the lateral moraines. Solute acquisition by the water is large in the active layer, as sediments are abundant and water:rock contact time is relatively long (Hodgkins, 1998a). The large rainfall event may have resulted in a sudden release of water from the active layer possibly related to slope failures.

The late season flow recession (7 August – 11 September)

Fluctuations in solute content and isotopes during the late season flow recession were clearly related to discharge variations and precipitation events. Diurnal variations were observed between 12 and 16 August in both solute concentrations and $\delta^{18}O$ values. Such fluctuations are often reported in meltwater from temperate and polythermal glaciers (Theakstone and Knudsen, 1996b, Hodgkins, 1997a and Hodgkins and Tranter, 1998b). For these glaciers, a base flow component of snowmelt drains slowly through a distributed drainage network and is diluted during high ablation by an icemelt component draining rapidly through a conduit system with restricted access to erodible sediments (Theakstone et al., 1995b; Hodgkins, 1997a). Longyearbreen is considered to be cold-based throughout (section 6.1.2), and a distributed drainage system does not exist. Diurnal variations in the chemical composition of the river meltwater therefore reflect other mechanisms in the glacial drainage system. No precipitation events occurred during the period where diurnal variations were observed. Variations in ^{18}O content of the water are therefore thought to originate exclusively from an increased proportion of snowmelt in the river meltwater during

low ice ablation where water temporarily stored in the melting snowpack continued to flow. This corresponds with the observed variations in Cl^- concentrations. However, figure 5.24, 5.25 and 5.26 clearly show that variations in the snowpack derived fraction of each ion do not explain the observed diurnal variations in solute concentrations for other ions than Cl^-. The variations therefore must relate to a constant source of solute-rich water that continues to flow with relatively high magnitude during low ablation. The diurnal variations in solute concentrations most likely reflect the leaking of solute-rich water into the glacial drainage system from the thawing active layer on the mountainside, on the lateral moraines and on the debris-covered glacier snout where fine-grained sediments are abundant. As the runoff decreased during the late season flow recession, this component of water became more and more important, hence the rapid rise in solute concentrations observed in all ions except Cl^-. Considerable amounts of solute-rich water were stored during winter in large pools predominantly within the subglacial drainage system where sediments are abundant. It is this refrozen water that is thought to have had such a large impact on the first water that drained through the channel in the early summer.

6.4.5 **Solute provenances**

In the previous section it was suggested that the solute measured in the glacial meltwater draining from Longyearbreen originated from the snowpack, from the thawing ice-covered channel floor and from water seeping through the active layer and into the glacial drainage system. The first two provenances were most important during the early melt period while the latter influenced the river meltwater during the entire ablation period, although most obvious in the late season flow recession, where ice and snow ablation had lowered considerably. The correlation between suspended sediment and solute in the meltwater was low and inverse for most ions. Chemical weathering of the sediment load therefore had little influence on the chemical composition of the river meltwater. The study of sediment provenance showed that the glacial meltwater has access to abundant amounts of sediments both in the supraglacial, lateral and subglacial drainage channels. Chemical denudation of fresh sediments within the drainage system may therefore be an important way of acquiring solute in water stored within the glacial drainage system for longer periods of time. This is the case with water that accumulates in the drainage channels during winter.

Water sampled at different localities within the Longyearbreen catchment gave evidence of the origin of the solute. Samples were collected during the late season flow recession where little suspended sediment was transported by the water. The highest solute concentrations measured in the catchment were in the water emanating from the western meltwater channel (table 5.13). This stream drains englacially and subsequently subglacially for a substantial distance, and flows from below the glacier early in the debris-covered glacier snout. Tonning (1996) concluded that a thin layer of temperate ice was present in Longyearbreen, especially in the upper western area of the glacier. If this is still the case, the high solute concentrations measured in the eastern meltwater stream may be explained by the influence of solute-rich water draining slowly through a distributed drainage network. However, meltwater samples collected from the eastern and western meltwater stream during low discharge showed a similar chemical composition of the meltwater in the two streams (appendix A.10). If meltwater from a distributed drainage system reached the western stream, this would have been even more pronounced in the late ablation season

where drainage through the conduit system was declining. This supports the results from the 2004 GPR study, where no evidence of temperate ice was found in Longyearbreen. The same processes that occur in the eastern lateral channel therefore explain the high solute content in the sample. Only a minor amount of water was observed in the western lateral meltwater channel. Water from the glacier and mountain sides therefore probably reaches the western subglacial drainage channel either via the moulin, through fractures in the ice or towards the lateral border of the glacier.

Water samples collected in the catchment from meltwater sources that were thought to contribute directly to the water at the sampling site, suggest that solute was acquired by the meltwater primarily from two different sources. The first source was illustrated by the high solute content in the water flowing in the upper lateral channel (table 5.13). This is thought to be caused by the entrainment of solute-rich active layer water as the glacier meltwater drained from Larsbreen through lateral moraines and into the meltwater channels on Longyearbreen. Melting of the active layer in the debris-covered glacier snout is also thought to contribute with considerable amounts of solute. The chemical composition of a sample collected on the debris-covered terminus in almost still water is shown in table 6.3. The sample had solute concentrations higher than measured at the sampling site at the time and had the highest Ca^{2+} concentrations measured in the catchment on that day. This suggests that Ca^{2+} was primarily acquired in the debris-covered glacier snout.

Table 6.3. Concentrations of solutes [$\mu eq l^{-1}$] and $\delta^{18}O$ value [‰] in a sample of still water on the debris-covered glacier snout. Concentrations are in $\mu eq\ l^{-1}$.

Cl^-	NO_3^-	SO_4^{2-}	HCO_3^-	K^+	Na^+	Ca^{2+}	Mg^{2+}	$\delta^{18}O$
145	62	3779	544	44	1141	2198	1147	-11.86

The relationships between some of the ions in the meltwater from Longyearbreen were presented in section 5 in figure 5.30 and table 5.10. Figure 5.30 demonstrates that oxidation of sulphides (equation 3) was clearly the most dominant source of protons for chemical weathering in 2004. This is explained by the high content of sulphides such as pyrite in the sedimentary geology of the catchment (Major and Nagy, 1972 and Hjelle, 1993). The predominance of oxidation of sulphides has previously been documented in meltwater from deposits from coal mining consisting of the same sedimentary rocks as present on Longyearbreen (Holm et al., 2003; Schmidt and Jensen, 2005). During the peak flow period, an increase in the coupling of oxidation of sulphides with carbonate dissolution (equation 4) probably explains the enhanced proportion of HCO_3^- in the meltwater. Similar increases in carbonation reactions have previously been documented during high discharge where water from the conduit system constitutes a larger proportion of the bulk meltwater (Sharp et al., 1995). Once a proton source has been established, ions are thought to be acquired by the meltwater through ion exchange of protons for ions on the surfaces of the sediment grains. The high correlation coefficients between NO_3^-, SO_4^{2-}, K^+, Na^+, Ca^{2+} and Mg^{2+} during the entire ablation period suggests similar weathering mechanisms for the ions. Hydrolysis of carbonates (for example equation 10) and magnesium-rich silicates and feldspar (for example equation 8 and 9) are thought to be the dominant chemical processes occurring in the glacial catchment. This would explain the high solute concentrations of Na^+, Ca^{2+} and Mg^{2+}.

6.4.6 **Comparison with previous studies of meltwater composition**

No detailed study of stable isotopes in glacial meltwater has previously been conducted on Svalbard. Multi-year observations of $\delta^{18}O$ values in runoff from Austre Okstindbreen in Norway however, showed similar seasonal and diurnal trends to those presented here (Theakstone and Knudsen, 1996a and 1996b; Theakstone, 2003). Short term variations in $\delta^{18}O$ values of the meltwater in the beginning of the ablation period similar to those observed on Longyearbreen, were also documented in these studies and explained by the release of water from storage within the glacial drainage system (Theakstone, 2003).

Comparison with previous study of meltwater chemistry on Longyearbreen

A study of solute concentrations in meltwater from the catchment of Longyearbreen has previously been conducted in 1993 by Sægrov (1995). A total of 37 samples were collected at an irregular time interval during the two periods 16 June – 7 July and 23 August – 1 September. Water samples were collected 0.5 - 1 km from the glacier portal in the early ablation period and in the western meltwater stream later in the ablation period. A comparison of total solute content and concentrations of selected ions are shown in appendix A.16. The results from 1993 showed an early ablation period where total solute content (figure A.16.1) decreased from 2430 $\mu eq\,l^{-1}$ to a constant level of 640 $\mu eq\,l^{-1}$ in the period from 16 June to 4 July. At the end of the ablation period, solute content had increased significantly to a mean total solute content of 4235 $\mu eq\,l^{-1}$. These overall variations are similar to in 2004, although higher solute concentrations were observed. Unlike for 2004, all ions correlated well with Cl^- during the 1993 ablation period (Sægrov, 1995). The variations in Cl^- concentrations in the early ablation period in 1993 and 2004 were very similar, with values in both years decreasing from concentrations in the range 500-600 $\mu eq\,l^{-1}$ (figure A.16.2). It however appears that the leaching of ions from the snowpack occurred faster and possibly later in 1993. Large, unexplained fluctuations in Cl^- concentrations were observed late in the ablation period in 1993. SO_4^{2-} concentrations (figure A.16.3) were considerably higher in 2004 than 1993 while the concentrations of HCO_3^- (figure A.16.4) were low in the early ablation period in 1993 compared to 2004. However, later in the season similar concentrations of HCO_3^- were observed. In 1993 Cl^- (26%) and Na^+ (23%) were the most important ions in the early ablation period while Mg^{2+} (22%) and SO_4^{2-} (21%) were most dominant later in the ablation period. The proportion of the individual ions were very different in 2004, with Cl^- and Na^+ only constituting 4.7% and 13% respectively in the early melt period and SO_4^{2-} and Mg^{2+} dominating the entire ablation period with 45% and 20% in the late season flow recession.

The discrepancies between the chemical variations observed in the glacial meltwater are potentially explained by four factors. (1) The proportion of sea-salt derived ions in the meltwater was considerably larger in 1993. This might be explained either by a snowpack enriched in ions compared to 2004 or a deeper snowpack and hence more ions. (2) Sampling of river water began later and ended earlier in the ablation period in 1993. The features observed in the early and late ablation period in 2004 may therefore have taken place, but before and after the sampling period. (3) Sampling was conducted in the western meltwater stream. Subglacial storage of refrozen meltwater and solute acquisition of this

water is probably considerably higher in the eastern subglacial meltwater channel, where water drains through a wide channel in the sediment-rich ice-marginal area. (4) Hodgkins (1998a) found that the influence of solute-rich pore water from the active layer constituted a larger proportion of the bulk meltwater during low discharges. The overall dilution of the meltwater in 1993 compared to the meltwater in 2004 may therefore further be explained by the lower runoff recorded from the glacier in 2004. The discrepancies in proportionality of the individual ions in the river meltwater suggest that different solute sources existed during the two ablation periods and that a lower discharge in 2004 does not fully explain the higher ionic concentrations that year. The different chemical composition of the meltwater therefore most likely is a combination of the factors listed above. In order to fully understand the mechanisms resulting in the observed differences, sampling needs to be conducted from both the eastern and western meltwater stream during multiple years.

Even though solute concentrations were considerably lower in the 1993 ablation period, estimates of daily flux were considerably higher than in 2004 due to larger discharge. From 25 June to 13 July 1993, 9 t d^{-1} evacuated from Longyearbreen compared to 4.4 t d^{-1} in the peak flow period and a mean of 2.7 t d^{-1} in 2004 (table A.17.2). The daily flux for Longyearbreen was calculated based on flux estimates shown in appendix A.17. These estimates were derived assuming similar solute content in all water draining from Longyearbreen as was measured in the river water at the sampling site. This is inaccurate, since meltwater samples collected in the two stream showed some discrepancy in chemical composition (table 5.9 and appendix A.10).

Comparison with study of meltwater chemistry on a similar cold-based glacier

Three principal sources of solutes similar to those presented here were reported for meltwater draining from the cold based Scott Turnerbreen on Svalbard (Hodgkins et al., 1998a). Firstly, variations in solute content occurred as the proportion between snow- and icemelt changed during the ablation period. Secondly, a proglacial icing enriched overflowing meltwater with solutes during the early melt season. Lastly, chemical weathering within the thawing active layer in the moraines resulted in solute-rich pore water continuously leaking into the drainage channels of the glacier. The solute-rich active layer water gave rise to diurnal variations in solute content similar to those observed for temperate and polythermal glaciers. The largest volumes of solute-rich active layer water entered the glacial drainage system during high discharge where melting of the active layer was at its highest. The effect on the chemical composition of the meltwater was however, offset by the large volumes of solute-poor icemelt and only evident during low discharge (Hodgkins, 1998a). Table 6.2 shows that Scott Turnerbreen and Longyearbreen had similar mean diurnal solute flux. However, this is only because discharge was significantly higher for Scott Turnerbreen than for Longyearbreen (Hodgkins, 1997b). Mean total solute content in the river water for Longyearbreen was about 3 times the solute content measured at Scott Turnerbreen. In table 6.4 the river meltwater from Longyearbreen (early melt period and peak flow period) is compared with bulk meltwater from Scott Turnerbreen. Water from Scott Turnerbreen was sampled from the onset of surface drainage in the proglacial area (Hodgkins, 1998a).

Table 6.4. Concentrations [µeq l^{-1}] of selected ions in the river meltwater at the sampling site at Longyearbreen (mean value of the early melt period and the peak flow period, 29 May – 7 August, 2004) and Scott Turnerbreen (22 June – 10 July, 1993). In brackets are shown the range of the measured concentrations (Hodgkins, 1998a).

	$*SO_4^{2-}$	HCO_3^-	K^+	Na^+	Ca^{2+}	Mg^{2+}
Longyearbreen	1200 (200-8380)	240 (0-940)	19 (11-46)	420 (130-2080)	580 (210-2950)	650 (230-3680)
Scott Turnerbreen	130 (96-200)	170 (110-260)	9.4 (5.1-19)	210 (110-740)	180 (120-300)	150 (99-290)

Of the total solute flux emanating from Scott Turnerbreen, 29% was thought to be snowpack derived (Hodgkins et al., 1997b) compared to 7% for Longyearbreen (see appendix A.17). The lower discharge for Longyearbreen may partly explain the different solute concentrations since solute-rich pore water is thought to constitute a larger proportion of the bulk meltwater during low discharge (Hodgkins, 1998a). The $*SO_4^{2-}/(*SO_4^{2-} + HCO_3^-)$ ratio for Scott Turnerbreen ranged from 0.33 to 0.62 with a mean of 0.43. This clearly shows that coupled sulphide oxidation, carbonate dissolution and carbonation processes in general were more important at Scott Turnerbreen than for Longyearbreen. Scott Turnerbreen is located in similar lithology as Longyearbreen (Major and Nagy, 1972). Large variations however exist in the transport of weathered sediments onto the glaciers in the area. Frost-weathered coal and fossils from the Aspelintoppen Formation, which is thought to be particularly rich in sulphides, are for example much more abundant on Longyearbreen compared to on Larsbreen (personal observations). The differences in chemical composition of the meltwater from Scott Turnerbreen compared to Longyearbreen might therefore be explained by a lower input of sulphide-rich sediments from the Aspelintoppen Formation.

Comparison with meltwater chemistry studies on glaciers with other temperature regimes

Table 6.5 shows discharge and concentrations of selected ions in meltwater from Longyearbreen, the largely cold-based Austre Brøggerbreen and the temperate Haut Glacier d'Arolla, Switzerland. The meltwater from Longyearbreen has the highest concentrations of SO_4^{2-} and a significantly larger range of HCO_3^-. Austre Brøggerbreen and Longyearbreen both have high Cl^- concentrations in the meltwater compared to Haut Glacier d'Arolla due to the maritime locations of the two glaciers.

Table 6.5. Range of discharge [$m^3 s^{-1}$] and concentration of three selected ions [µeq l^{-1}] for three glaciers with different temperature regime (Tranter et al., 1996).

	Discharge	SO_4^{2-}	HCO_3^-	Cl^-
Longyearbreen (2004)	0.0-8.3	350-14940	0-1320	30-510
Peak flow period (30 Jun. – 6 Aug.)	*0.0-8.3*	*354-2080*	*187-548*	*29-59*
Austre Brøggerbreen (1991 and 1992)	0.5-4.5	10-140	145-520	21-550
Haut Glacier d'Arolla (1989 and 1990)	0.4-7.2	20-240	180-460	0.03-6.7

The river meltwater collected at Longyearbreen obviously differ significantly from data of previous studies of chemical composition of glacial meltwater even during the peak flow period, where the meltwater was most dilute. Most remarkable is probably the high SO_4^{2-}

concentrations measured during the entire ablation period and the comparatively low HCO_3^- concentrations. This signifies a dominance of sulphide oxidation contrary to previous results from cold, polythermal and temperate glaciers, where chemical weathering has been found to be driven primarily by carbonation reactions (Tranter et al., 1996; Hodgkins et al., 1997b; Wadham et al., 1998; Brown, 2002). The meltwater is thought to exhibit this chemical composition because of a relatively low discharge and an extremely aggressive chemical weathering environment caused by the lithology of the sediment in the area. Furthermore, the results illustrate variations in chemical composition of glacial meltwater, from the beginning to the end of the ablation period. Data indicate that large fluctuations occur during the early and late ablation period. Unfortunately, due to logistic reasons, these periods are often neglected when studying meltwater chemistry.

7. Conclusion

Longyearbreen is a small (2.9 km^2) valley glacier characterised by a large debris-covered terminus. A maximum ice thickness of 110 m was found in the GPR survey. The GPR survey revealed no evidence of temperate ice. However, evidence of a former zone of temperate ice was found in the upper and thickest part of the glacier, where a weak basal reflector was interpreted as a basal layer of debris-rich ice. Similar to many small valley glaciers on Svalbard, Longyearbreen is thought to have undergone a change from polythermal to cold-based since the end of the Little Ice Age. Several debris-rich thrust faults in the marginal regions involving the ice/bed interface signify the cold-based conditions that have probably prevailed in these areas during the entire existence of the glacier. No evidence of englacial and subglacial drainage features were observed in the radar images in the upper part of the glacier. Differences in ice thicknesses between the GPR studies conducted in 1993 and 2004 showed that the observed thinning was comparable to other ice masses on Svalbard.

Drainage of meltwater takes place primarily through a major supraglacial channel in the middle of the glacier, but most importantly through two well-developed incised lateral channels. The drainage features are stable and vary little from year to year. The lateral channels become englacial and subsequently subglacial towards the glacier terminus. The western lateral channel is more incised, and drains subglacially for a considerable distance, emerging from the side of the debris-covered glacier snout. The eastern lateral channel disappears into the ice just before the debris-rich frontal area and drains from below the glacier terminus.

Water samples collected from the eastern meltwater stream in 2004 gave valuable information about the seasonal development of the drainage system. The ablation period of 2004 was characterised by relatively low discharges with a mean of 0.43 $m^3 s^{-1}$ and a peak discharge of 8.3 $m^3 s^{-1}$. Runoff variations were generally related to the air temperature and, later in the ablation period, also precipitation events. Three periods were recognised in the ablation period. The first period, the early melt period, where diurnal variations were dampened by the snow cover. An intermediate period, the peak flow period, characterised by large variations in discharge caused by the melting snow cover and a higher influence of ice ablation. Lastly, a period of late season flow recession, where the transient snow line was at its maximum height and clear diurnal variations in discharge were observed.

Suspended sediments in the meltwater generally correlated well with discharge. A peak SSC of 13.74 $g l^{-1}$ was measured during a period of enhanced runoff from the glacier and an average daily sediment flux of 30 $t d^{-1}$ was calculated for the glacier. A change in the relationship between measured water level and SSC in the early melt period was related to ice-free conditions in the subglacial meltwater channel. Confined peaks in the SSC reflected either a development of the drainage system or a rapid input of a large amount of sediment caused by slope failure in the ice-marginal or proglacial areas. The majority of entrained sediment originated from slope processes in the surrounding mountainside, degradation of the sediment-rich ice-marginal areas and mobilization of sediments from the floor and sides of the ice-marginal subglacial channel. The proglacial areas furthermore contributed

significantly to the suspended sediment concentrations, especially during high discharge. Precipitation events increased slope failure and consequently the sediment load of the glacial meltwater.

The record of stable isotopes and solutes in the river meltwater revealed a dynamic system, where rapid changes occurred within short periods of time. The isotopic composition of the river meltwater was clearly influenced by ^{18}O poor snowmelt in the early melt period (mean $\delta^{18}O$ value of -15.50‰). Several smaller fluctuations in the early melt period reflected either the release of water from storage or the onset of draining from different source areas in the catchment. A rapid increase in $\delta^{18}O$ values occurred between 26 June and 3 July illustrating the onset of icemelt in the lower part of the glacier. The remainder of the ablation period had relatively high $\delta^{18}O$ values with a mean of -13.38‰. River meltwater was clearly influenced by precipitation events in the end of the ablation period resulting in distinct peaks in the $\delta^{18}O$ of the river meltwater. Diurnal variations in $\delta^{18}O$ values and Cl^- concentrations in the late season flow recession probably reflected a larger proportion of snowmelt during low ice ablation.

Considerable variations occurred in the solute concentrations of river meltwater during the ablation period. Generally, solute concentration in the water was high, signifying a very aggressive chemical weathering environment in the catchment of Longyearbreen. The early melt period was influenced by the preferential leaching of ions with the first meltwater draining through the snowpack. This effect was most pronounced in the Cl^- concentrations that decreased continuously during the early melt period. All other ions were highly influenced by the enrichment of ions from solute-rich ice in the subglacial drainage channel. This was most obvious during two periods of low discharge, where total solute content at its maximum was as high as 17500 $\mu eq\, l^{-1}$. During the peak flow period river meltwater was most dilute, signifying the large influence of solute-poor icemelt and snowmelt from an increasingly depleted snowpack draining rapidly through the glacial drainage system. Total solute content during this period was fairly constant, with a mean value of 2410 $\mu eq\, l^{-1}$. Towards the end of the ablation period, solute concentrations raised to a maximum value of 31620 $\mu eq\, l^{-1}$ in the final water sample collected.

During the entire ablation period, SO_4^{2-} was the major ion, but Mg^{2+}, Ca^{2+} and Na^+ also had relatively high concentrations. Calculated HCO_3^- concentrations were generally low compared to SO_4^-. The chemical composition of the meltwater reflected an overall dominance of sulphide oxidation with a slight increase in the proportion of coupled sulphide oxidation and carbonate dissolution during the peak flow period. Ion exchange by hydrolysis was the dominant chemical reactions occurring in the glacier catchment. The predominant sources of solute acquisition in the early melt period were from the thawing snowpack but more importantly, from the release of ions from solute-rich ice in the glacial drainage system. As the ablation season progressed, seepage of solute-rich pore water from the thawing active layer into the glacial drainage system became the dominant solute source. This was most evident in the late season flow recession, where solute concentrations increased dramatically as surface ablation on the glacier decreased. Diurnal variations in all other ions than Cl^- were thought to reflect a larger proportion of solute-rich water from the active layer during low discharge.

8. References

Andersen, K. K., Azuma, N., Barnola, J.-M., Bigler, M. and 45 others. (2004). High-resolution record of Northern Hemisphere climate extending into the last interglacial period. *Nature*, 431: 147-151.

Annan, A. P. (1992). Ground Penetrating Radar – Workshop notes. *Sensors & Software Inc*: 126 pp.

Bamber, J. L. (1987). Internal reflecting horizons in Spitsbergen glaciers. *Annals of Glaciology*, 9: 5-10.

Bamber, J. L. (1988). Enhanced radar scattering from water inclusions in ice. *Journal of Glaciology*, 34 (118): 293-296.

Bamber, J. L. (1989). Ice/bed interface and englacial properties of Svalbard ice masses deduced from airborne radio echo-sounding data. *Journal of Glaciology*, 35 (119): 30-39.

Benestad, R. E., Hanssen-Bauer, I., Skaugen, T. E. and Førland, E. J. (2002). Association between sea-ice and the local climate on Svalbard. *Det Norske Meteorologiske Institut*, rep. nr. 07/02: 13 pp

Benn, D. I. and Evans, D. J. A. (1998). Glaciers and Glaciation. *Oxford University Press* Inc.: 734 pp.

Bennet, M. R. and Glasser, N. F. (1999). Glacial Geology – Ice Sheets and Landforms, Wiley, chapter 4 (Glacial Meltwater): 17 pp.

Berge, J., Johnsen, G., Gulliksen, B., Slagstad, D. (2005). Ocean temperature oscillations enable reappearance of blue mussels *Mytilus edulis* in Svalbard after 1000 year absence. *Marine Ecology Progress Series*, 303: 167-175.

Björnsson, H., Gjessing, Y., Hamran, S.-E., Hagen, J. O., Liestøl, O. and Erlingsson, B. (1996). The thermal regime of sub-polar glaciers mapped by multi-frequency radio-echo sounding. *Journal of Glaciology*, 42 (140): 23-32.

Bluth, G. J. S. and Kump, L. R. (1994). Lithologic and climatologic controls of river chemistry. *Geochimica et Cosmochimica Acta*, 58: 2341-2359.

Boon, S. and Sharp, M. (2003). The role of hydrologically-driven ice fracture in drainage system evolution on an Artic glacier. *Geophysical research letters*, 30 (18), 1029.

Bringedal, Å. H. (2004). Oxygen isotopes from the surface of Longyearbreen, central Spitsbergen: palaeoclimatic implications. *Unpublished Ms thesis*. University of Bergen: 108 pp.

Brown, G.H. (2002). Glacier meltwater hydrochemistry. *Applied Geochemistry*, 17: 855-883.

Bælum, K. Mapping of the general shape, depth, and various internal structures of Tellbreen, a glacier on Svalbard, by means of GPR (Ground Penetrating Radar). *Unpublished Ms Thesis*. University of Aarhus.

Collins, D. (1977). Hydrology of an alpine glacier as indicated by the chemical composition of meltwater. *Zeitschrift für Gletscherkunde und Glazialgeologie*, 13, (1/2): 219-238.

Collins, D. (1979). Quantitative determination of the subglacial hydrology of two alpine glaciers. *Journal of Glaciology*, 23 (89): 347-361.

Copland, L. and Sharp, M. (2001). Mapping thermal and hydrological conditions beneath a polythermal glacier with radio-echo sounding. *Journal of Glaciology*, 47 (157): 232-242.

Dansgaard, W. (1964). Stable isotopes in precipitation. *Tellus*, 16 (4): 436-468.

Duplessy, J.-C., Ivanova, E., Murdmaa, I., Paterne, M. and Labeyearsie, L. (2001). Holocene paleoceanography of the northern Barents Sea and variations of the northward heat transport by the Atlantic Ocean. *Boreas*, 30: 2-16.

Elliston, G.R. (1973). Water movement through the Gornergletscher. *International Association of Hydrological Sciences*, 95: 79-84.

Etzelmüller, B., Ødegård, R.S., Vatne, G. Rønnaug, S.M, Tonning, T. and Sollid, J. L. (2000). Glacier characteristics and sediment transfer systems of Longyearbreen and Larsbreen, western Spitsbergen. *Norsk geografisk Tidsskrift*, 54: 157-168.

Fountain, A.G. and Walder, J.S. (1998). Water flow through temperate glaciers. *Reviews of Geophysics*, 36 (3): 299-328.

French, H. (1996). The periglacial environment. 2nd edition. *Longman*: 341 pp.

Førland, E.J., Hanssen-Bauer, I. and Nordli, P.Ø. (1997). Climate statisics & longterm series of temperature and precipitation at Svalbard and Jan Mayen. *Det Norske Meteorologiske Institut*, 21/97: 72 pp.

Grønsten, H.A. (1998). Hydrological Studies and simulations of a high Arctic Catchment Longyearelva, Spitsbergen. *Unpublished Ms thesis*, University of Oslo: 76 pp.

Gurnell, A.M., Hodson, A., Clark, M.J., Bogen, J., Hagen, J.O. and Tranter, M. (1994). Water and sediment discharge from glacier basins: an Arctic and Alpine comparison. *International Association of Hydrological Sciences Publication* 224 (Symposium at Canberra 1994 – *Variability in Stream Erosion and Sediment Transport*): 229-311.

Hagen, J.O. and Liestøl, O. (1990). Long-term glacier mass-balance investigations in Svalbard, 1950-88. *Annals of Glaciology*, 14: 102-106.

Hagen, J.O. and Sætrang, A. (1991). Radio-echo sounding of sub-polar glaciers with low-frequency radar. *Polar Research*, 9 (1): 99-107.

Hagen, J.O., Liestøl, O., Roland, E. and Jørgensen, T. (1993). Glacier atlas of Svalbard and Jan Mayen. *Norwegian Polar Institute, Oslo*, (129): 141 pp.

Hagen, J.O., Kohler, J., Melvold, K. and Winther, J.-G. (2003). Glaciers in Svalbard: mass balance, runoff and freshwater flux. *Polar Research*, 22 (2): 145-159.

Hamilton, G.S. and Dowdeswell, J.A. (1996). Controls on glacier surging in Svalbard. *Journal of Glaciology*, 42 (140): 157-168.

Hamran, S.-E., Aarholt, E. Hagen, J.O. and Mo, P. (1996). Estimation of relative water content in a subpolar glacier using surface-penetration radar. *Journal of Glaciology*, 42 (142): 533-537.

Hansen, O.H. (2001). Internal drainage of some subpolar glaciers on Svalbard. *Unpublished Ms thesis*, University of Bergen: 134 pp.

Hanssen-Bauer, I., Kristensen and M.S., Steffensen, E.L. (1990). The climate of Spitsbergen. *Det Norske Meteorologiske Institut*, 39/90: 40 pp.

He, Y. and Theakstone, W.H. (1994). Climatic influence on the composition of snow cover at Austre Okstindbreen, Norway, 1989 and 1990. *Annals of Glaciology,* 19: 1-6.

Hjelle, A. (1993). Geology of Svalbard. *Norsk Polarinstitutt, Polarhåndbok*, 7: 162 pp.

Hodgkins, R. (1996). Seasonal trend in suspended-sediment transport from an Arctic glacier, and implications for drainage-system structure. *Annals of Glaciology*, 22: 147-151.

Hodgkins, R. (1997a). Glacier hydrology in Svalbard, Norwegian High Arctic. *Quaternary Science Reviews*, 16: 957-973.

Hodgkins, R., Tranter, M. Dowdeswell, J.A. (1997b) Solute provenance, transport and denudation in a high Arctic glacierised catchment. *Hydrological Processes*, 11: 1813-1832.

Hodgkins, R., Tranter, M. and Dowdeswell, J.A. (1998a). The hydrochemistry of runoff from a "cold-based" glacier in the High Arctic (Scott Turnerbreen, Svalbard). *Hydrological Processes*, 12: 87-103.

Hodgkins, R. and Tranter, M. (1998b). Solute in High Arctic glacier snow cover and its impact on runoff chemistry. *Annals of Glaciology* 26: 156-160.

Hodgkins, R., Hagen, J.O. and Hamran, S.-E. (1999). 20th century mass balance and thermal regime change at Scott Turnerbreen, Svalbard. *Annals of Glaciology* 28: 216-220.

Hodgkins, R. (2001). Seasonal evolution of meltwater generation, storage and discharge at a non-temperate glacier in Svalbard. *Hydrological Processes*, 15: 441-460.

Hodson, A.J., Tranter, M., Dowdeswell, J. A., Gurnell, A. M. and Hagen, J. O. (1997). Glacier thermal regime and suspended-sediment yield: a comparison of two high-Arctic glaciers. *Annals of Glaciology*, 24: 32-37.

Hodson, A., Gurnell, A., Tranter, M., Bogen, J., Hagen, J. O. and Clark, M. (1998). Suspended sediment yield and transfer processes in a small High-Arctic glacier basin, Svalbard. *Hydrological processes*, 12: 73-86.

Hodson, A.J. and Ferguson, R.I. (1999). Fluvial suspended sediment transport from cold and warm-based glaciers in Svalbard. *Earth Surface Processes and Landforms*, 24: 957-974.

Hodson, A. Tranter, M. and Vatne, G. (2000). Contemporary rates of chemical denudation and atmospheric CO_2 sequestration in glacier basins: an arctic perspective. *Earth Surface Processes and Landforms*, 25: 1447-1471.

Hodson, A., Tranter, M., Gurnell, A., Clark, M. and Hagen, J.O. (2002). The hydrochemistry of Bayelva, a high Arctic proglacial stream in Svalbard. *Journal of Hydrology*, 257: 91-114.

Holm, A.B., Brandvik, P.J. and Steinnes, E. (2003). Pollution in acid mine drainage from mine tailings in Svalbard, Norwegian Arctic. *J. Phys. IV France*, 107: 625-628.

Humlum, O., Christiansen, H., Hansen, Hasholt, Jacobsen, Nielsen and Rasch (1995). Holocene landscape evolution in the Mellemfjord area, Disko Island, central West Greenland: Area presentation and preliminary results. *Danish Journal of Geography*, 95: 28-41.

Humlum, O., (2002). Modelling late 20^{th}-century precipitation in Nordenskiöld Land, Svalbard, by geomorphic means. *Norwegian Journal of Geography*, 56: 96-103,

Humlum, O., Elberling, B. Hormes, A. Fjordheim, K., Hansen, O.H. and Heinemeier, J. (2005). Late Holocene glacier growth in Svalbard, documented by subglacial relict vegetation and living soil microbes. *The Holocene*, 15 (3): 396-407.

Isaksson, E., Kohler, J., Pohjola, V., Moore, J., Igarashi, M., Karlöf, L., Martma, T. Meijer, H., Motoyama, H., Vaikmäe, R. and S.W. van de Wal, R. (2005). Two ice-core $\delta^{18}O$ records from Svalbard illustrating climate and sea-ice variability over the last 400 years. *The Holocene*, 15 (4): 501-509.

Jania, J., Mochnacki, D. and Gadek, B. (1996). The thermal structure of Hansbreen, a tidewater glacier in southern Spitsbergen, Svalbard. *Polar Research*, 15 (1): 53-66.

Jansson, P., Hock, R. and Schneider, T. (2003). The concept of glacier storage: a review. *Journal of Hydrology*, 282: 116-129.

Justad, G.H., (1997). Morfologiske og sedimentologiske studier av et terrestrisk iskontaktsystem ved Lonyearbreen, Svalbard. *Unpublished Ms thesis*, University of Tromsø: 98 pp.

Kattenberg, A., Gruza, G. V., Jouzel, J., Karl, T. R., Ogallo, L. A. and Parker, D. E., (1996). Observed Climate Variability and Change. In: Houghton, J.T., Filho, L.G.M., Callander, B.A., Harris, N., Kattenberg, A. and Maskell, K. (Eds.), Climate Change 1995 – The Science of Climate Change, *Cambridge University Press*: 134-192.

Lefauconnier, B. and Hagen, J.O. (1990). Glaciers and Climate in Svalbard: Statistical Analysis and Reconstruction of the Brøggerbreen Mass Balance for the last 77 Years. *Annals of Glaciology*,14: 148-152.

Liestøl, O. (1977). Pingos, springs and permafrost in Spitsbergen. *Norwegian Polar Institute, Yearbook 1975*: 7-29.

Maijala, P., Moore, J.C., Hjelt, S.-E., Pälli, A. and Sinisalo, A. (1998). GPR investigations of glaciers and sea-ice in the Scandinavian Arctic. *GPR98 - 7th International Conference on Ground-Penetrating Radar Proceedings*: 143-148.

Major, H. and Nagy, J. (1972). Geology of the Adventdalen map area. *Norsk Polarinstitutt, Skrifter*, 138: 58 pp.

Moore, J.C., Pälli, A., Ludwig, F., Blatter, H., Jania, J. Gadek, B., Glowacki, P., Mochnacki, D., Isaksson, E. (1999). High-resolution hydrothermal structure of Hansbreen, Spitsbergen, mapped by ground-penetrating radar. *Journal of Glaciology*, 45 (151): 524-532.

Murray, T., Gooch, D.L. and Stuart, G.W. (1997). Structures within the surge front at Bakaninbreen Svalbard, using ground-penetrating radar. *Annals of Glaciology*, 24: 122-129.

Murray, T., Stuart, G.W., Fry, M. Gamble, N.H. and Crabtree, M.D. (2000). Englacial water distribution in a temperate glacier from surface and borehole radar velocity analysis. *Journal of Glaciology*, 46 (154): 389-398.

Nienow, P., Sharp, M., Willis, I. (1996). Velocity-discharge relationships derived from dye-tracer experiments in glacial meltwaters: implications for subglacial flow conditions. *Hydrological Processes*, 10: 1411-1426.

Paterson, W. S. B. (2001). The physics of glaciers, third edition. *Butterworth-Heinemann*: 481 pp.

Plewes, L.A. and Hubbard, B. (2001). A review of the use of radio-echo sounding in glaciology. *Progress in Physical Geography* 25 (2): 203-236.

Raben, P. and Theakstone, W.H. (1994). Isotopic and ionic changes in a snow cover at different altitudes: observations at Austre Okstindbreen in 1991. *Annals of Glaciology*, 19: 85-91.

Raiwell, R. (1984). Chemical models of solute acquisition in glacial melt waters. *Journal of Glaciology*, 30 (104): 49-57.

Salvigsen, O., Forman, S.L. and Miller, G.H. (1992). Thermophilous molluscs on Svalbard during the Holocene and their paleoclimatic implications. *Polar Research* 11 (1): 1-10.

Salvigsen, O. (2002). Radiocarbon-dated *Mytilus edulis* and *Modiolus modiolus* from northern Svalbard: climatic implications. *Norsk Geografisk Tidsskrift*, vol. 56: 56-61.

Sensors and Software Inc. (1992-1999). Ground penetrating radar, survey design: 22 pp.

Sharp, M., Tranter, M., Brown, G.H. and Skidmore, M. (1995). Rates of chemical denudation and CO_2 drawdown in a glacier-covered alpine catchment. *Geology*, 23 (1): 61-64.

Simões, J.C. (1990). Environmental interpretation from Svalbard ice cores. *Unpublished Ph.d. thesis*. University of Cambridge, Cambridge: 236 pp.

Schmidt, L.B. and Jensen, L.A. (2005). The environmental impact of acid mine drainage on an Arctic soil-plant system. *Unpublished Ms thesis*, University of Copenhagen: 95 pp.

Snyder, J.A., Werner, A. and Miller, G.H. (2000). Holocene cirque glacier activity in western Spitsbergen, Svalbard: sediment records from proglacial Linnévatnet. *The Holocene*, 10 (5): 555-563.

Stenborg, T. (1970). Delay of runoff from a glacier basin. *Geografiska Annaler*, 52A (1): 1-30.

Sund, M. (2004). NVEs virksomhet på Svalbard. *Hydrologisk månedsoversikt – November 2004*: 50-54.

Svendsen, J.I. and Mangerud, J. (1997). Holocene glacial and climatic variations on Spitsbergen. *The Holocene*, 7 (1): 45-57.

Sægrov, R. (1995). Drenering og glasiofluvial materiatransport i Larsbreen og Longyearbreen, Svalbard. *Unpublished Ms thesis*, University of Oslo: 90 pp.

Theakstone, W.H. and Knudsen, N.T. (1996a). Oxygen Isotope and Ionic Concentrations in Glacier River Water: Multi-Year Observations in the Austre Okstindbreen Basin, Norway. *Nordic Hydrology*, 27: 101-116.

Theakstone, W.H. and Knudsen, N.T. (1996b). Isotopic and ionic variations in glacier river water during three contrasting ablation seasons. *Hydrological Processes*, 10: 523-539.

Theakstone, W.H. (2003). Oxygen isotopes in glacier-river water, Austre Okstindbreen, Okstindan, Norway. *Journal of Glaciology*, 49 (165): 282-298.

Tonning, T. (1996). Bruk av eit geografisk Informasjonssystem på glasiologiske problemstillingar – Døme frå Longyearbreen og Larsbreen på Svalbard. *Unpublished Ms thesis*, University of Oslo: 106 pp.

Tranter, M., Brown, G., Sharp, M. and Gurnell, A.M. (1993). A conceptual model of solute acquisition by Alpine glacial meltwaters. *Journal of Glaciology*, 39 (133): 573-581.

Tranter, M., Sharp; Brown, G.H.; Hodson, A.J. and Gurnell, A.M. (1996). Hydrochemistry as an indicator of subglacial drainage system structure: a comparison of alpine and subpolar environments. *Hydrological Processes* 10: 541-556.

Vatne, G. (2001). Geometry of englacial water conduits, Austre Brøggerbreen, Svalbard. *Norsk Geografisk Tidsskrift*, 55: 85-93.

Wadham, J.L., Hodson, A.J., Tranter, M. and Dowdeswell, J.A. (1998). The hydrochemistry of meltwaters draining a polythermal-based high-Arctic glacier, south Svalbard: I. The ablation season. *Hydrological Processes* 12: 1825-1849.

Yde, J.C. and Knudsen, N.T. (2004). The importance of oxygen isotope provenance in relation to solute content of bulk meltwaters at Imersuaq Glacier, West Greenland. *Hydrological Processes*, 18: 125-139.

Ødegård, R.S., Hagen, J.O. and Hamran, S.-E. (1997). Comparison of radio-echo sounding (30-1000 MHz) and high resolution borehole-temperature measurements at Finsterwalderbreen. *Annals of Glaciology*, 24: 262-276.

Ådlandsvik, B. and Loeng, H. (1991). A study of the climatic system in the Barents Sea. *Polar Research*, 10: 2-16.

Websites:

www.unis.no/research, *University Centre in Svalbard*, 15 March, 2006.
www.forskning.no/Artikler, *Forskning.no*, 15 March, 2006.
http://www.sysselmannen.svalbard.no, *The Governor of Svalbard*, 15 March, 2006.
http://kart.npolar.no, *The Norwegian Polar Institute*, 15 March, 2006.
http://met.no, *The Meteorological Institute of Norway*, 15 March, 2006.

A APPENDIX

A.1 Map of Svalbard with location of glaciers

Figure A.1.1 shows the location of glaciers on Svalbard referred to in the text.

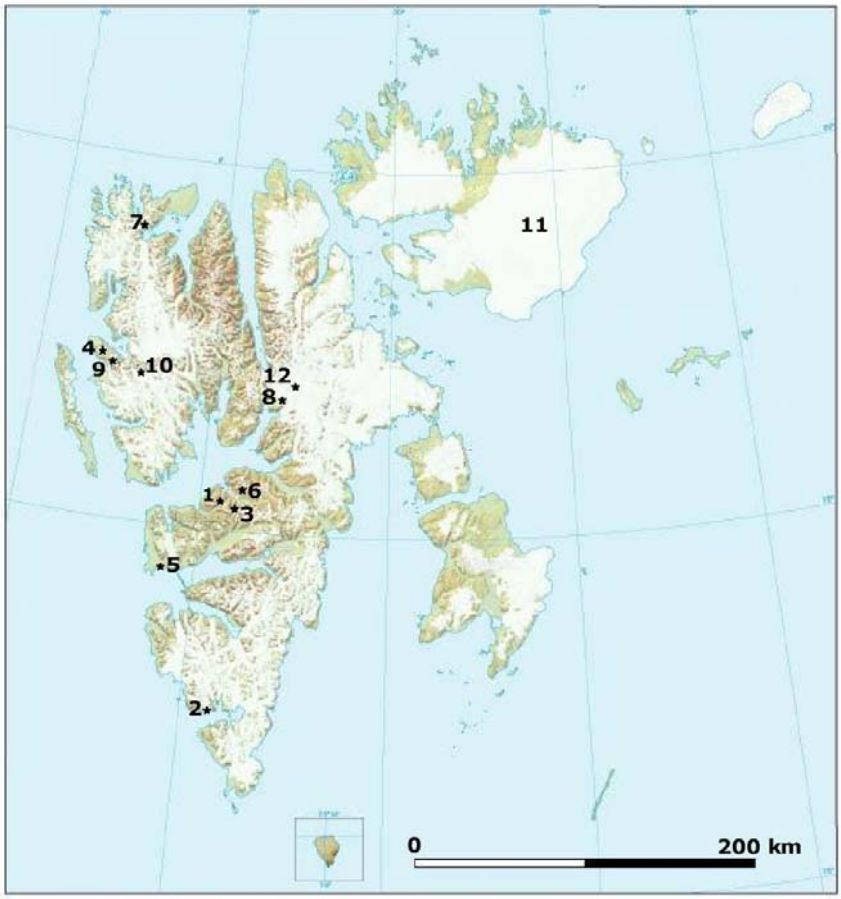

Figure A.1.1. Map of Svalbard with the locations of glaciers referred to in the text: 1. Longyearbreen and Larsbreen, 2: Finsterwalderbreen, 3. Scott Turnerbreen, 4. Austre Brøggerbreen, 5. Erdmannbreen, 6. Tellbreen, 7. Erikbreen, 8. Ebbabreen, 9. Midre Lovénbreen, 10. Kongsvegen, 11. Austfonna, 12. Lomonosovfonna.

A.2 CMP surveys

Figure A.2.1 shows the result of the CMP surveys conducted on Longyearbreen.

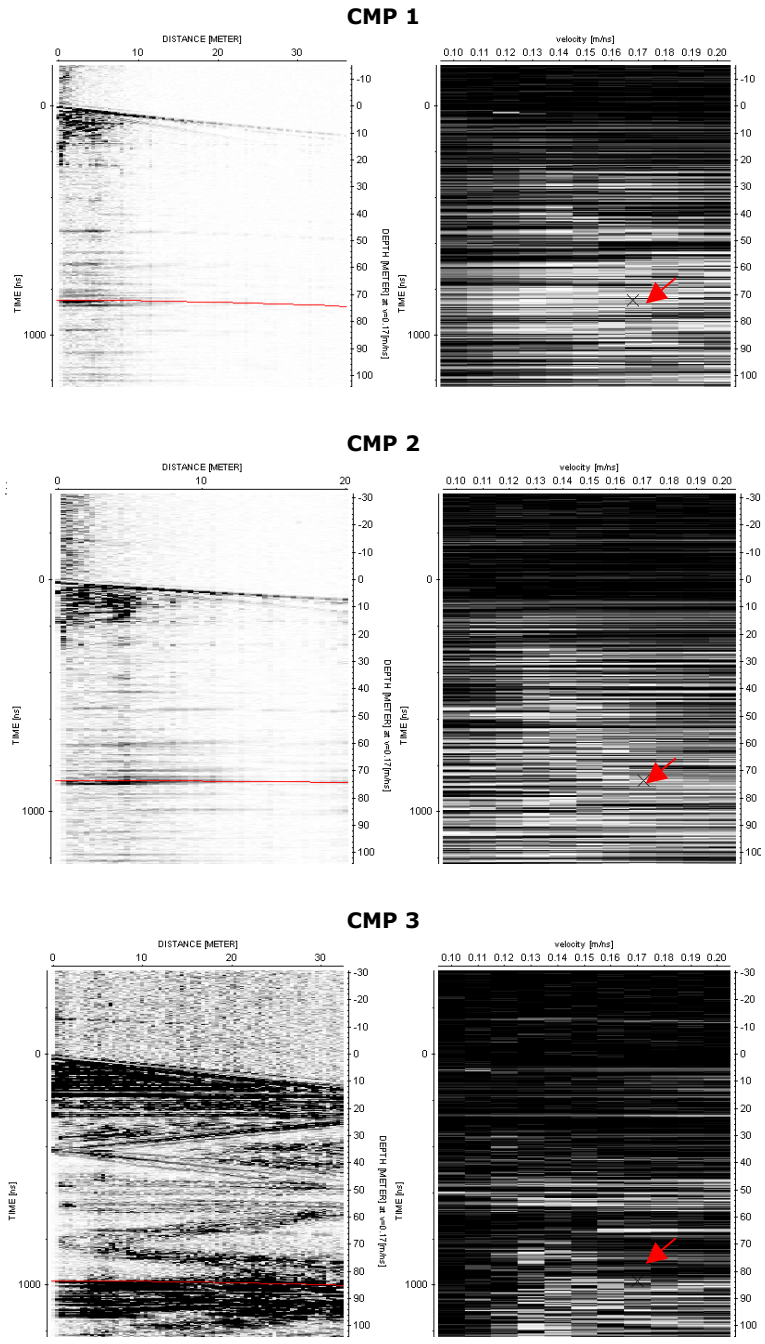

Figure A.2.1. The output of the three CMP surveys conducted on Longyearbreen. The red line on the left picture marks the basal reflector and the black cross on the right picture marks the velocity corresponding to the inclination of the chosen layer boundary.

To the left the original radar image is shown with the chosen basal reflection marked with a red line. The picture to the right shows the output of the radar wave velocity calculations performed by Reflex-Win. The black cross marks the velocity corresponding to the

inclination of the basal reflection chosen. The radar wave velocity in ice for CMP 1 was 0.168 m ns^{-1} while CMP 2 and CMP 3 both had velocities of 0.170 m ns^{-1}. The three CMP surveys are not ambiguous however, since velocities in a large range matched the almost flat laying basal reflector.

A.3 GPR profiles

GPR profiles presented in this study are shown in the following figures. The upper diagram shows the profile without migration while lower diagram is with migration. Where only one profile exists, no migration was considered necessary.

Profile A

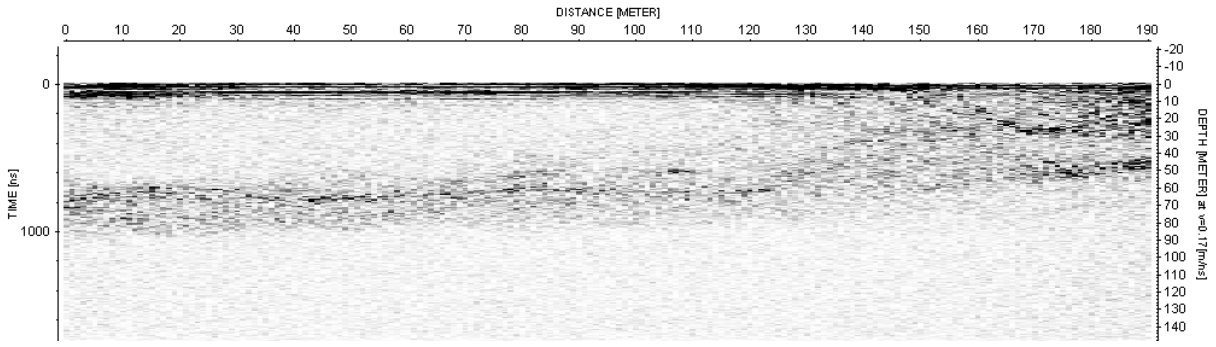

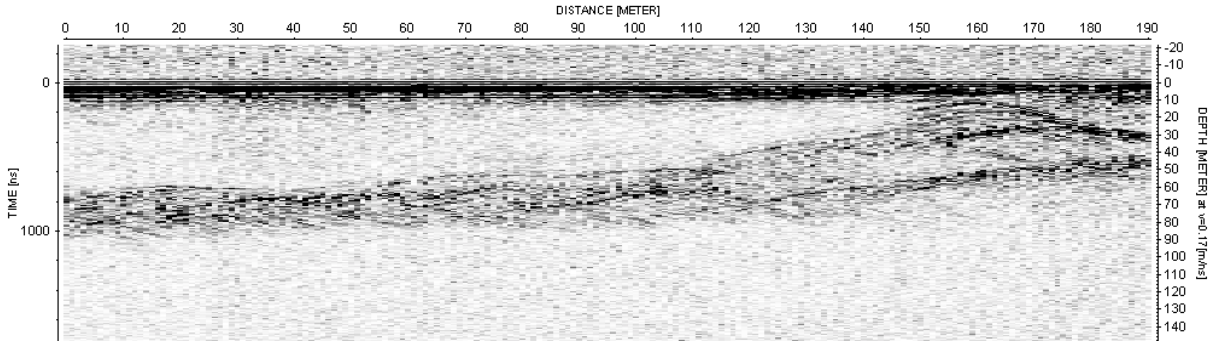

Profile AB

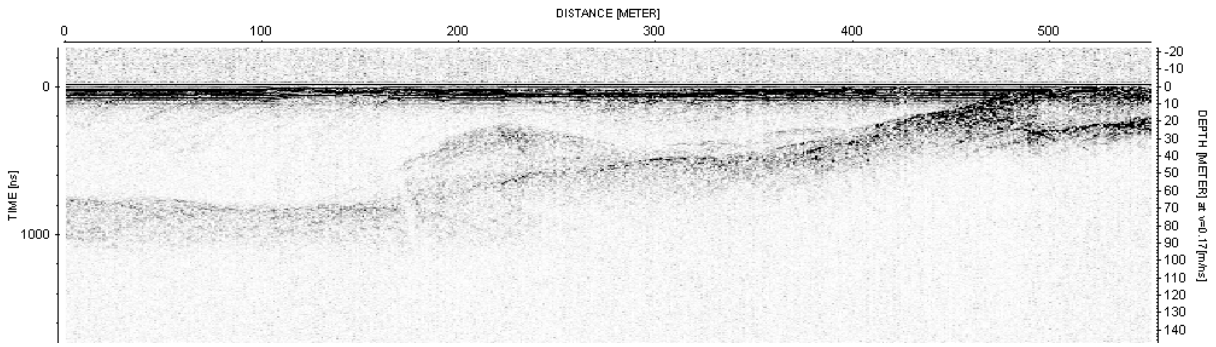

Profile B

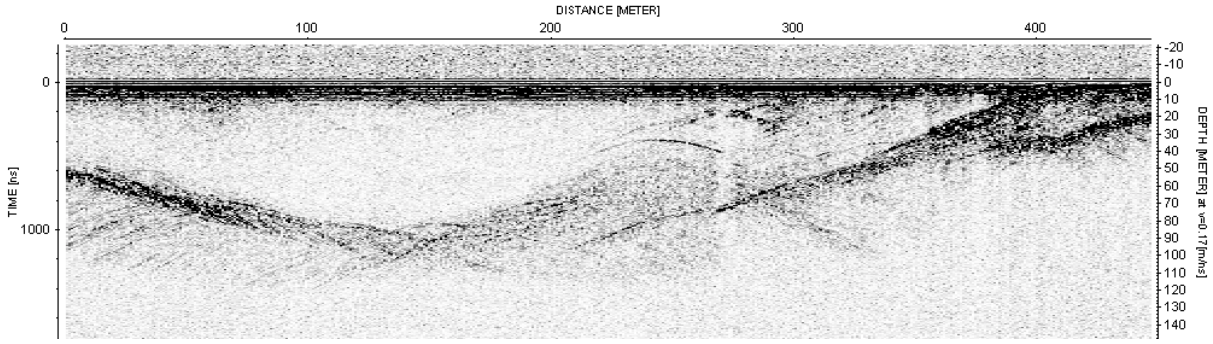

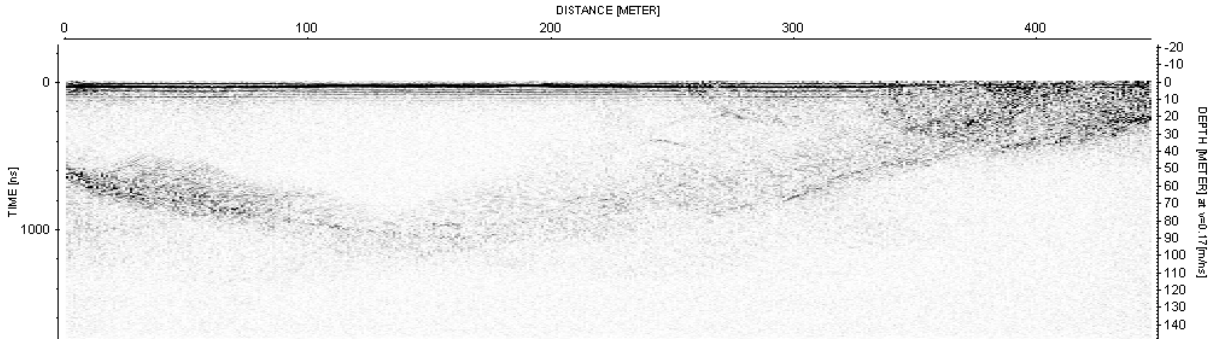

Profile BC

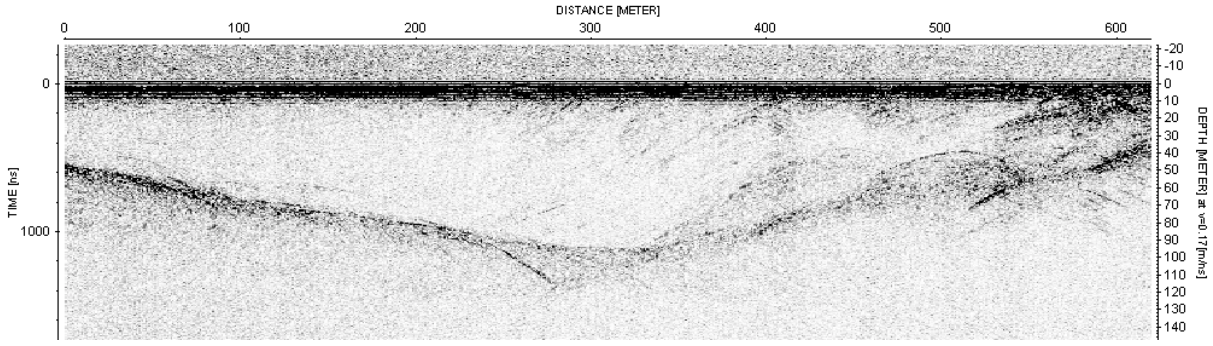

Profile C

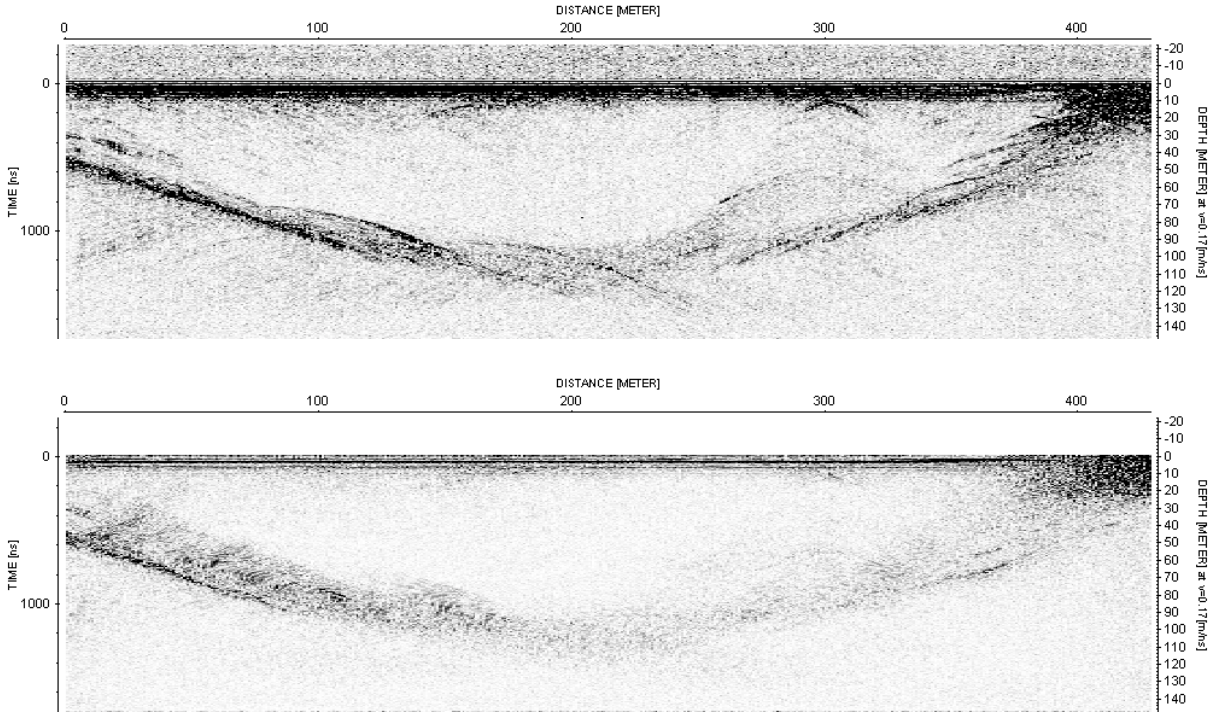

Profile CD

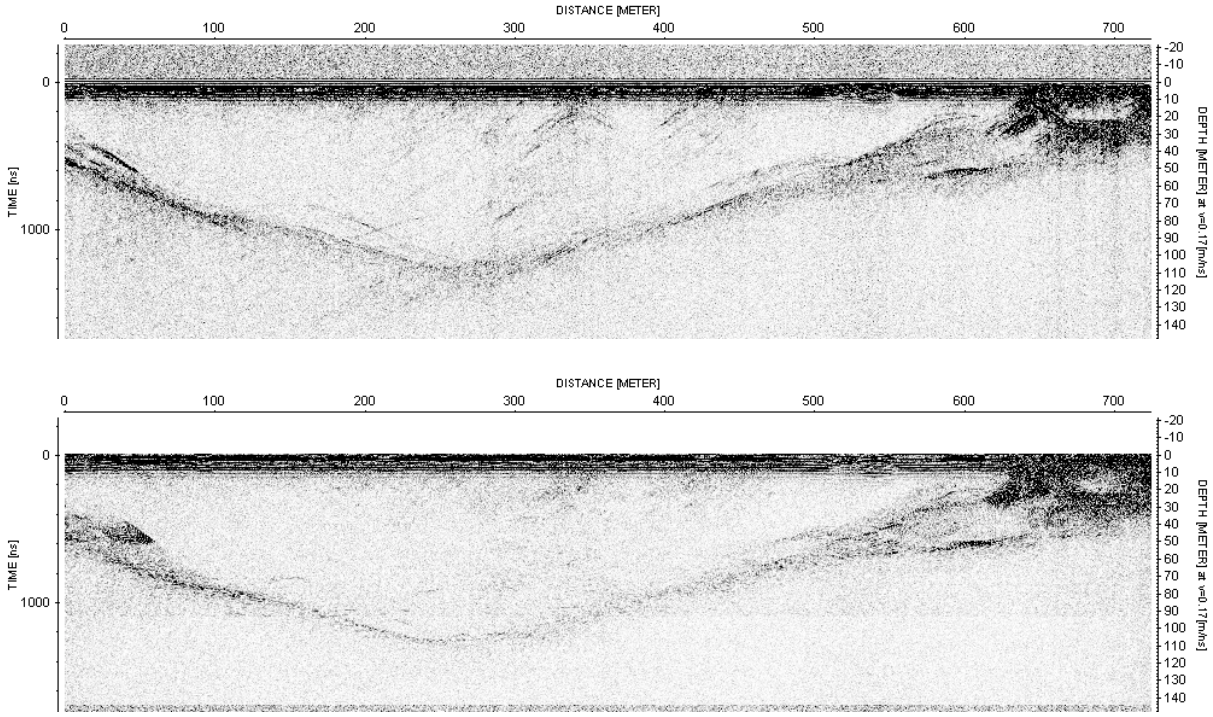

Profile D

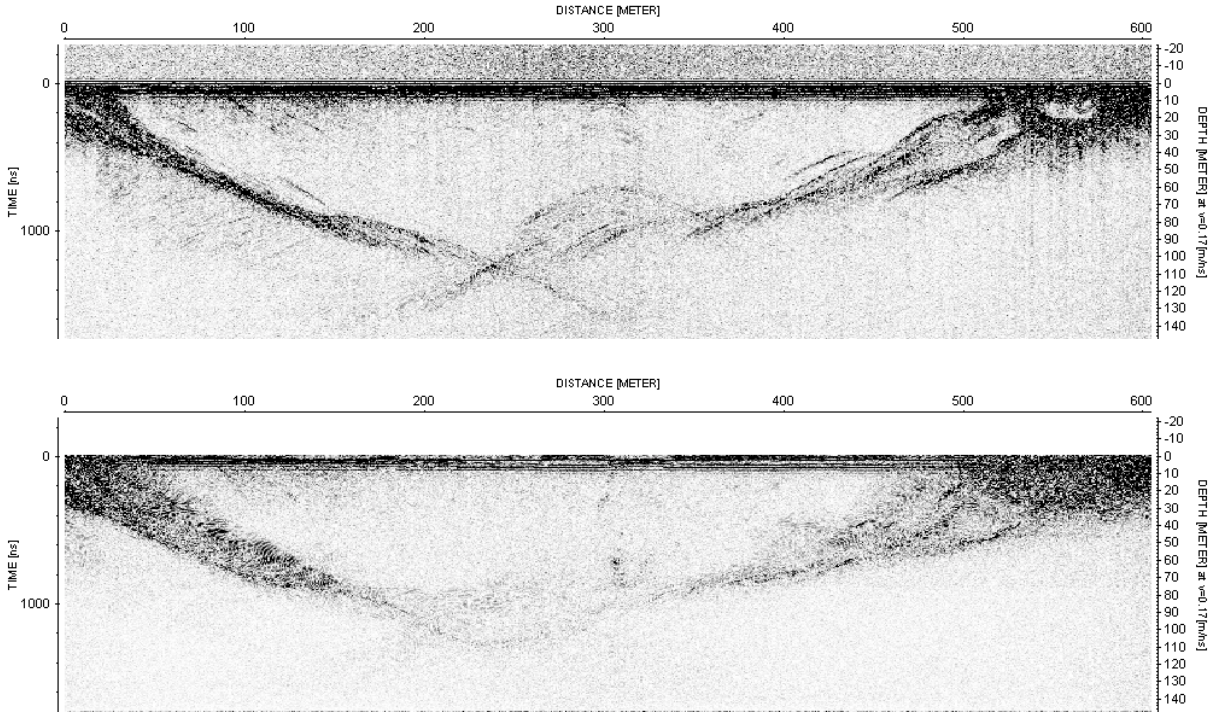

Profile DE

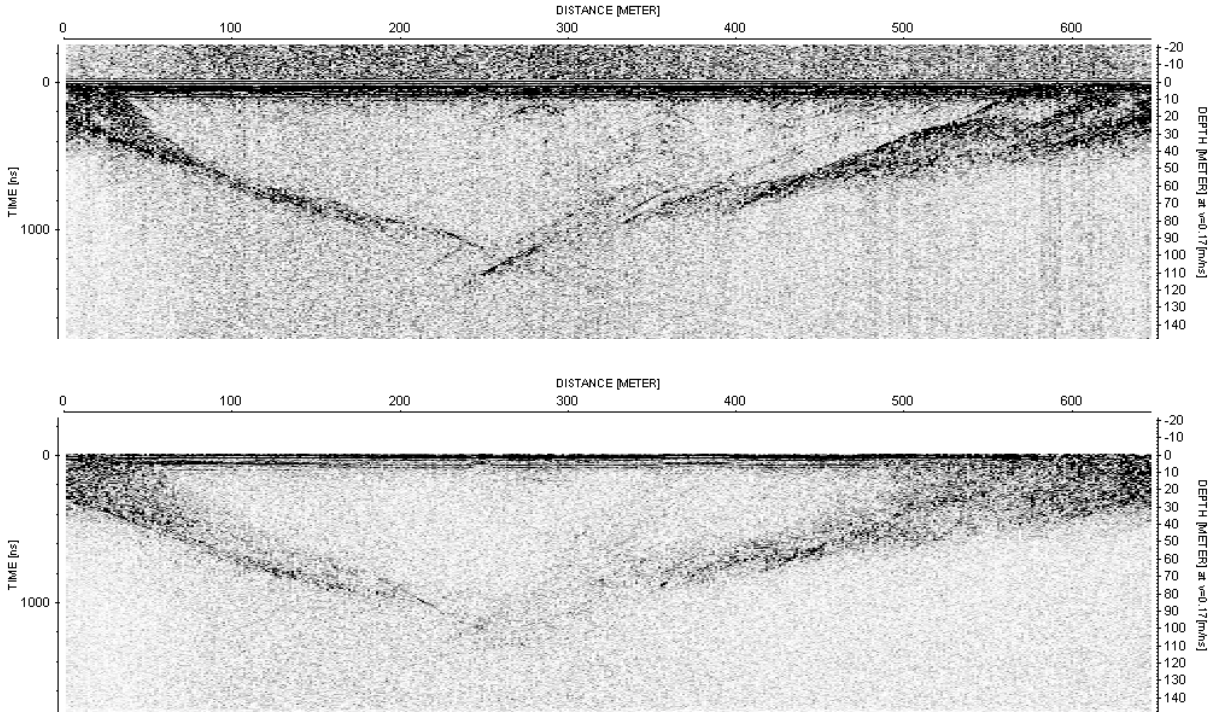

Profile E

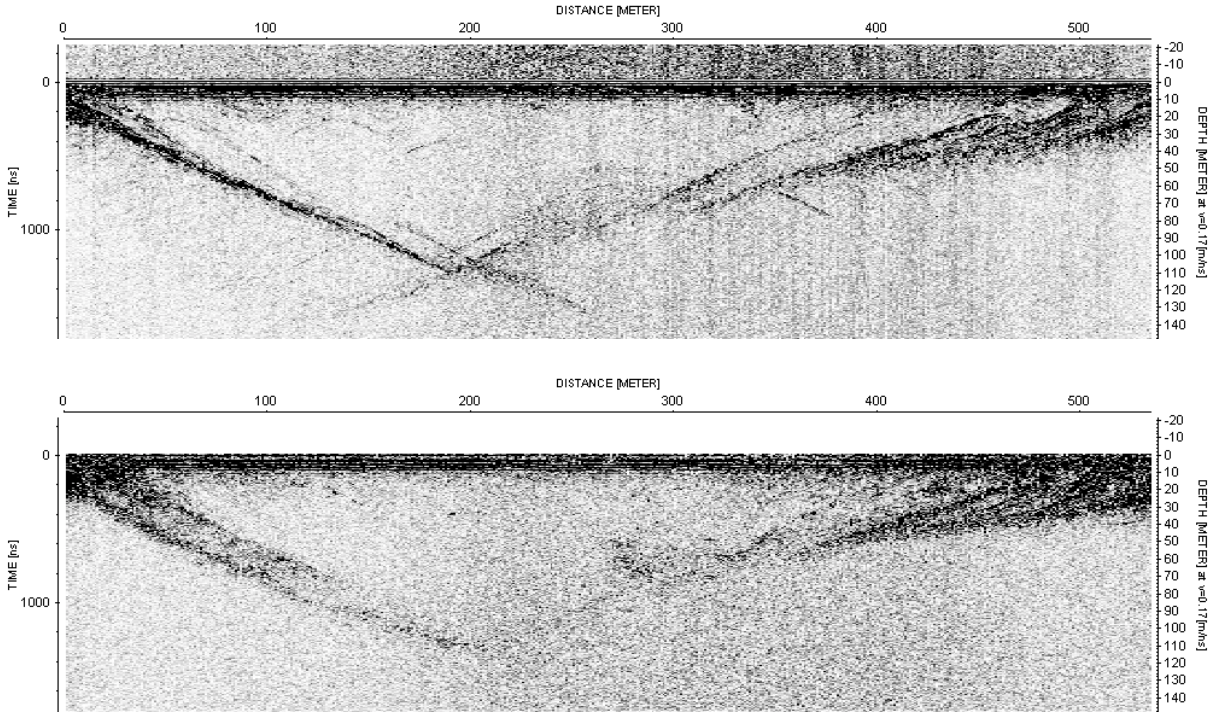

Profile EF

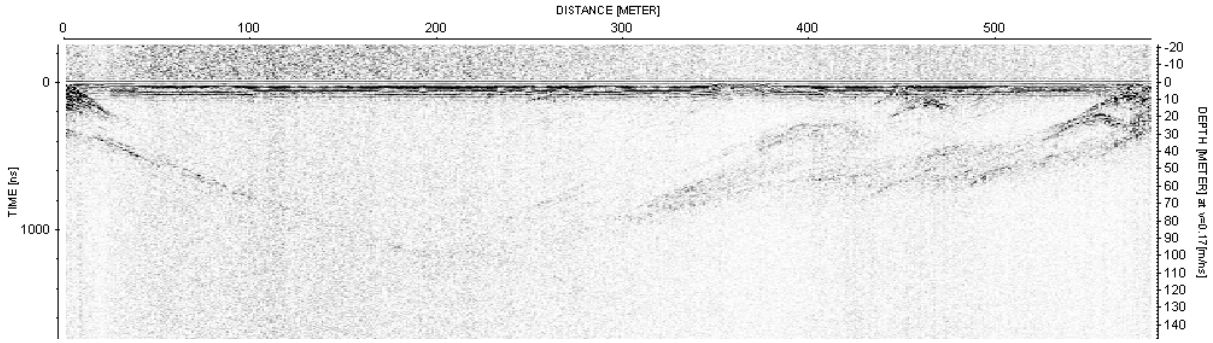

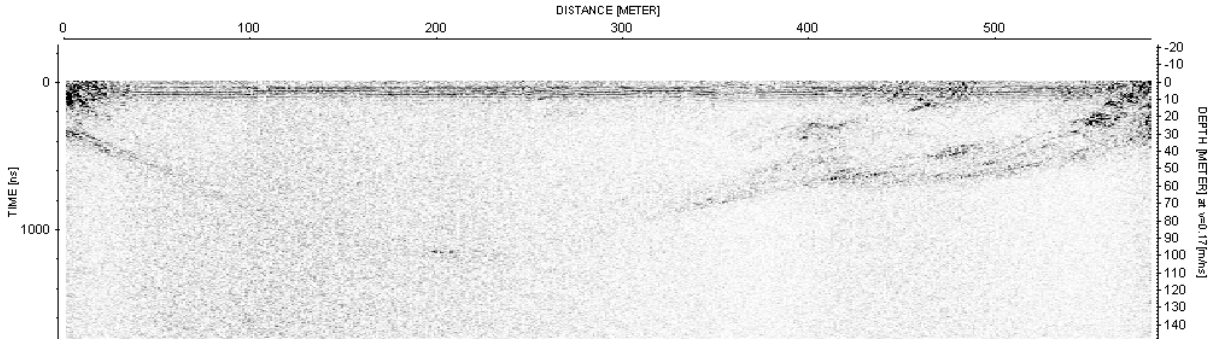

Profile F

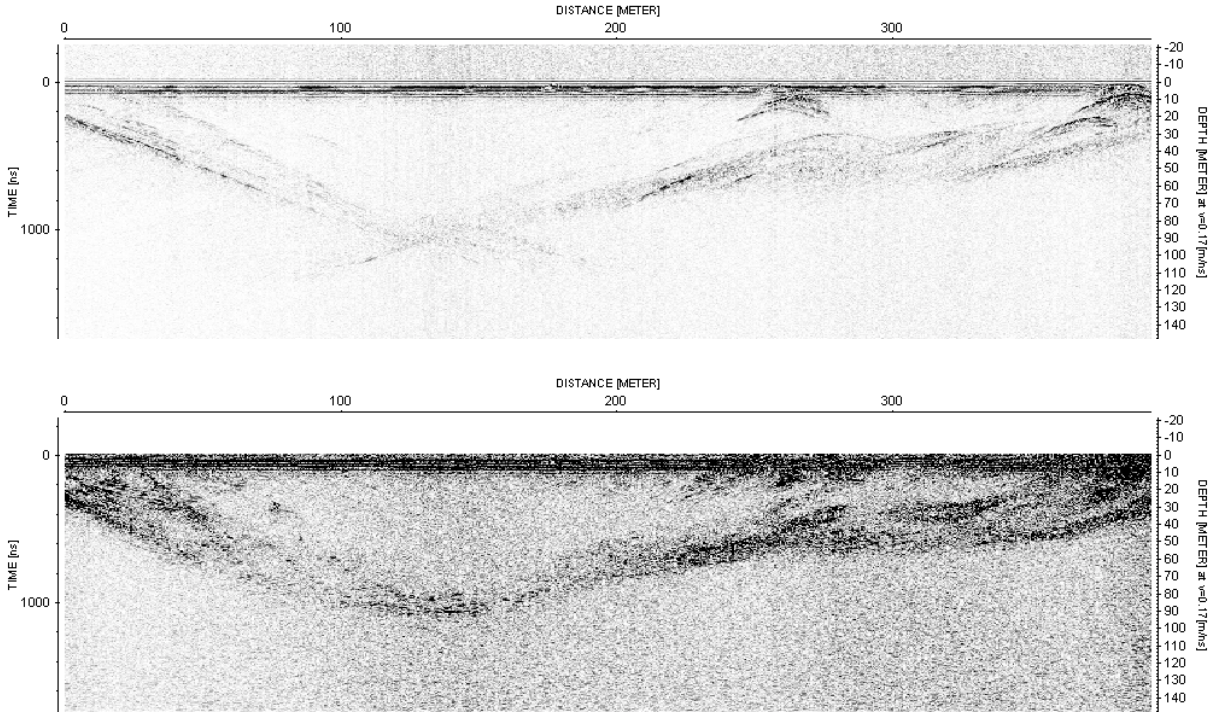

Profile FG

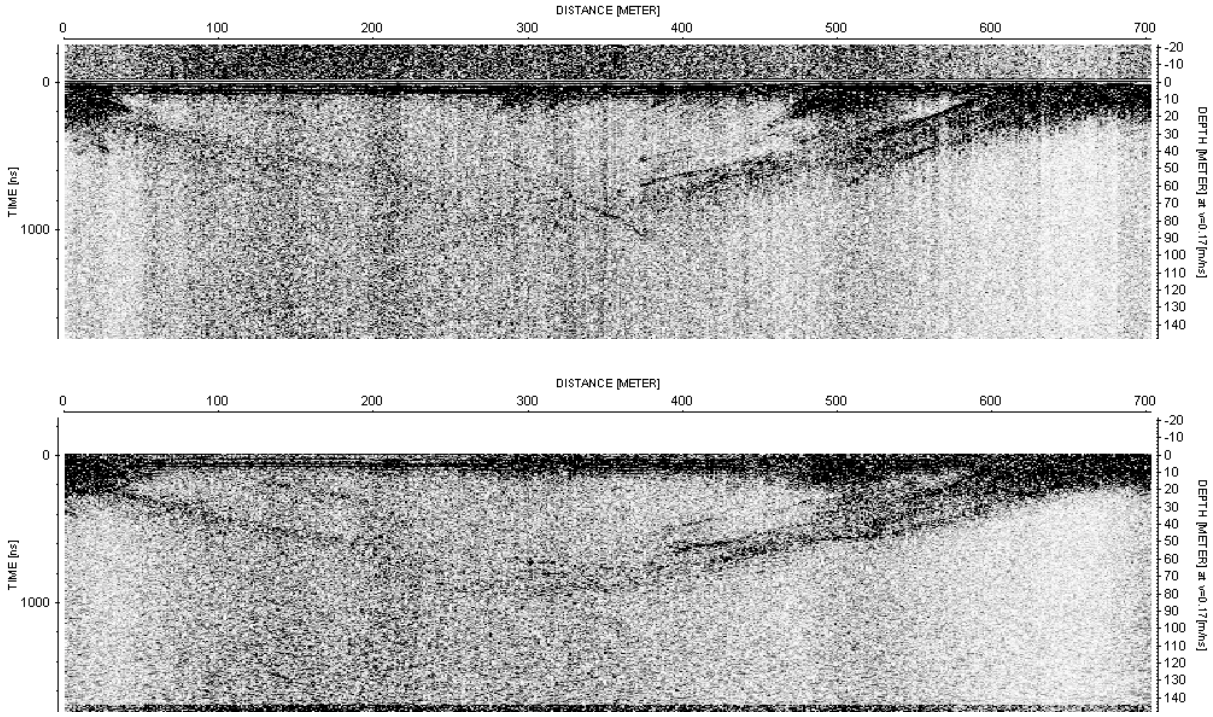

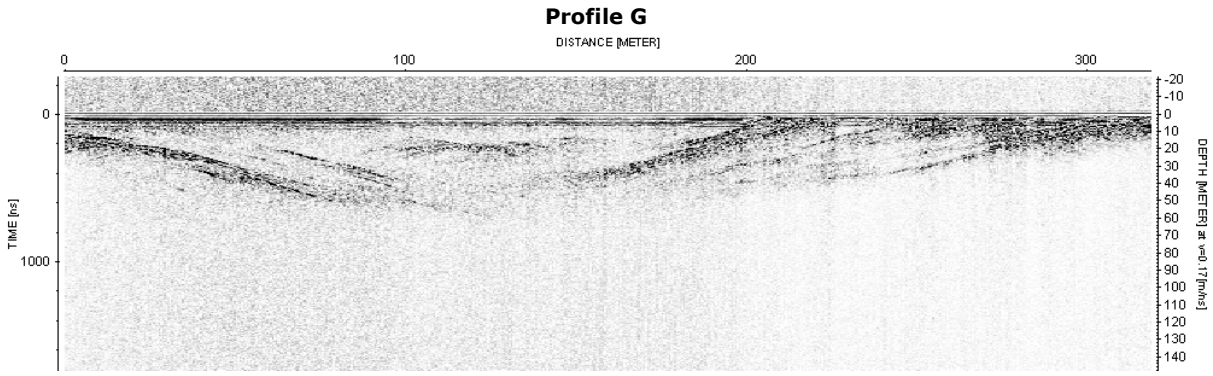

Figure A.3.1. All 13 GPR profiles with and without migration.

A.4 Cloud cover and air humidity

Meteorological data was provided from the meteorological station at Longyearbyen Airport. On figure A.4.1, observed cloud cover and measured air humidity is shown from 15 May to 30 September. Several low values of air humidity, especially in the end of the period, suggest a malfunctioning in the equipment. Generally, air humidity varied between 60 and 100%. 7/8 of the sky was usually covered with clouds and only few clear days were observed during the period shown in figure A.4.1.

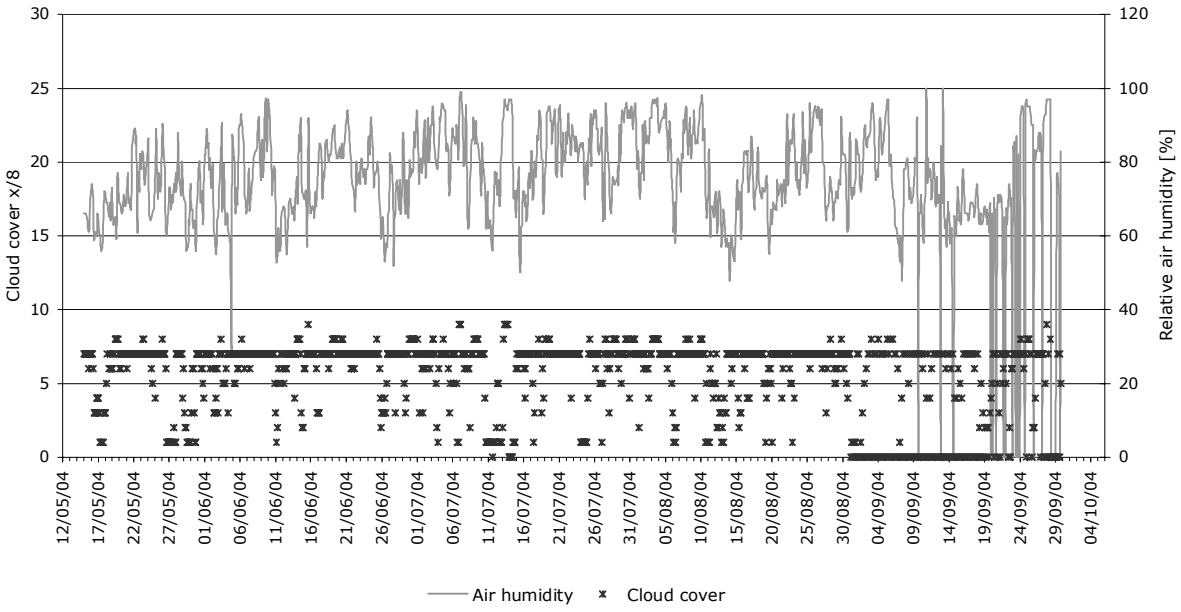

Figure A.4.1. Air humidity and cloud cover recorded at the meteorological station at Longyearbyen Airport from 15 May to 30 September.

A.5 Photographs reporting the onset of ice ablation

Unfortunate an avalanche carried the digital camera monitoring Longyearbreen away and photographs of the nearby glacier, Larsbreen are shown instead. In figure A.5.1, photographs of Larsbreen taken on 29 June and 3 July clearly illustrate the onset of enhanced ice ablation. On the picture from 29 June, Larsbreen is still covered in soaked, dirty snow while on 3 July glacier ice with debris bands are observed in the lower part of the glacier.

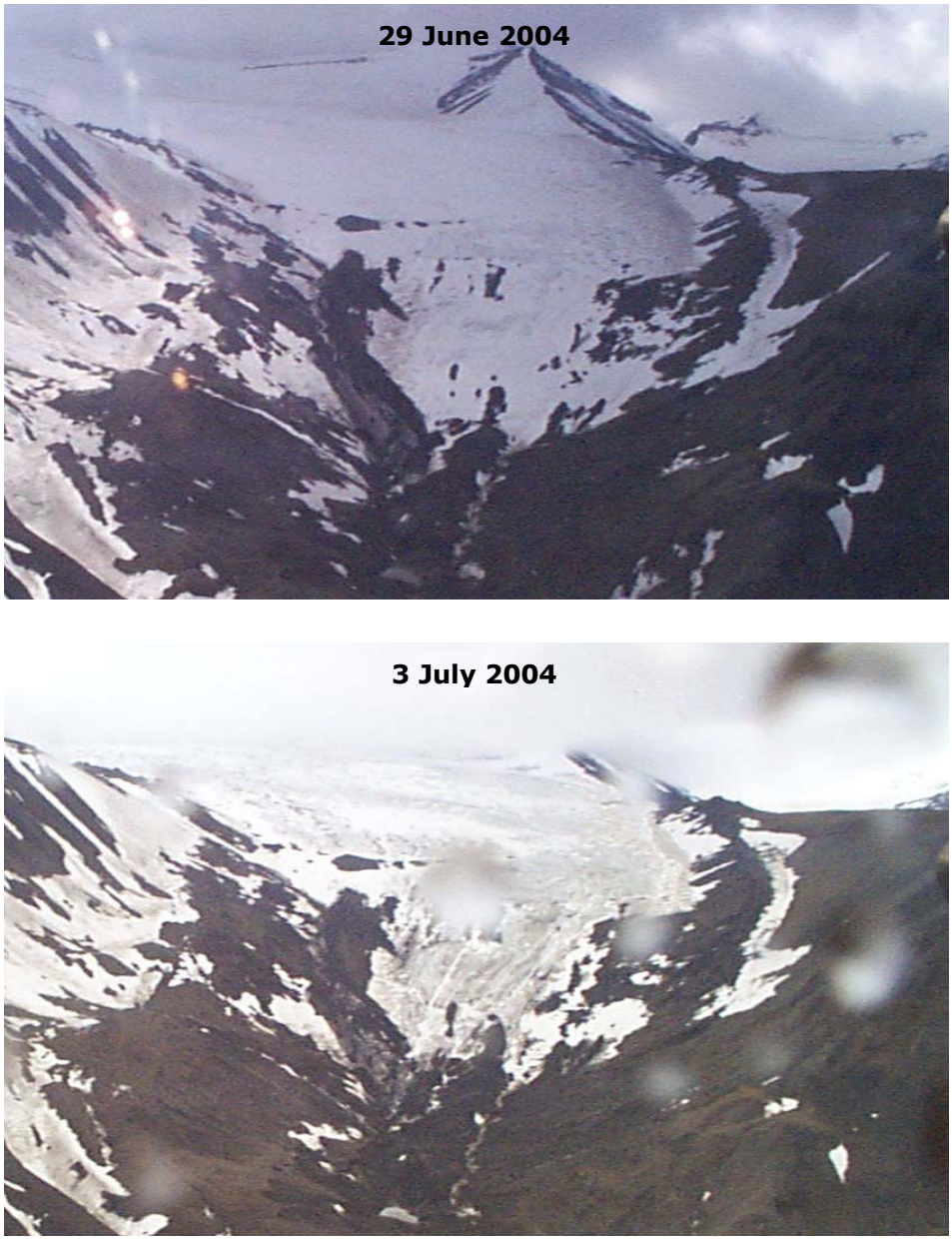

Figure A.5.1. Photographs of the nearby glacier, Larsbreen from 29 June and 3 July. Photographs were taken as a part of a research project at the Department of Geology at the University Centre in Svalbard where digital cameras are used to monitor glaciers in Adventdalen.

A.6 Notes from fieldwork

Below are shown notes of weather conditions and obvious changes in runoff at the sampling site during 2004.

Date and time	Notes
26-05-04 00:00	No water in front of or inside the moraine cave. Meltwater is running under the snowpack in Longyeardalen.
27-06-04 11:30	No water at the moraine cave. Meltwater now runs in a small confined meltwater stream in Longyeardalen.
28-05-04 12:00	Clear sky. Possible to hear the river from Nybyen.
29-05-04 12:00	Clear sky. Water 50 m in front of the moraine cave. Water may originate from melting snow in the river bed.
30-05-04 12:15	Clear sky. Meltwater stream slightly frozen over. Moraine cave dry at entrance. Running water inside cave.
30-05-04 23:40	Clear sky. Meltwater stream almost frozen over. Same water amount. Water flowing from the moraine cave.
31-05-04 12:00	Clear sky. More water in the stream.
01-06-04 00:00	Thin cloud cover, no sun. Stream frozen over. More water
01-06-04 12:00	Light cloud cover, sun. More water, but still ice and snow over the meltwater stream.
02-06-04 00:00	Light cloud cover, no sun. More water.
02-06-04 12:00	Cloudy, light snowfall. Still snow and ice covered stream. Snow bridges have however started collapsing.
03-06-04 00:00	Cloudy, light snowfall. More water.
03-06-04 12:00	Clear sky, sun. Same or slightly less water in the meltwater stream.
04-06-04 00:00	Few clouds, sun on the glacier. Less water
04-06-04 12:00	Cloudy, light wind, snowfall. Less water and the meltwater stream frozen over.
05-06-04 00:00	Light cloud cover, occasionally sun. Snowed the entire day. No wind. Less water.
05-06-04 12:00	Sun. Less water. No sediments in the water.
06-06-04 00:00	Cloudy, no wind. About 1 cm freshly precipitated snow. Same amount of water.
06-06-04 12:00	Cloudy, light wind. About 1½ cm freshly precipitated snow. Less water.
07-06-04 00:00	Snowfall. Wind. About 1 cm freshly precipitated snow. Slightly more water.
07-06-04 12:00	Snowfall. Cloudy, almost no wind. Less water.
08-06-04 00:00	Snowed all day, but now clear weather. Total amount of snow: 2 cm. More water.
08-06-04 12:00	Cloudy, but occasionally sun. No precipitation since yesterday. More water
09-06-04 00:00	Cloudy, light snowfall. A considerable increase in amount of water in the river.
09-06-04 18:00	Cloudy. Light snowfall all day. More water.
10-06-04 06:00	Cloudy, light snowfall. Less water.
10-06-04 18:00	Cloudy. Heavy snowfall since 10:00. More water.
11-06-04 06:00	Cloudy, light snowfall. Starting to clear. Slightly less water.
11-06-04 18:00	Cloudy, light precipitation. Less water.
12-06-04 06:00	Clear sky. Light wind. Slightly less water.
12-06-04 18:00	Clear sky and sun all day, now cloudy and windy. Same amount of water.
13-06-04 09:30	Cloudy. Occasionally sun. Wind. Slightly less water.
13-06-04 18:00	Cloudy. Occasionally sun. Wind. More water.
14-06-04 06:00	Cloudy. Occasionally sun. Strong wind. Same amount of water.
14-06-04 17:00	Cloudy. Occasionally sun. Wind. More water.
15-06-04 06:00	Cloudy. Just started to snow. Same amount of water.
15-06-04 11:30	Snowfall in the morning, then rainfall and now dry. Light wind. Same amount of water.
15-06-04 18:00	Clear sky. Sun. More water.
16-06-05 06:00	Light cloud cover. Last night at 24:00 clear sky. Now much more water in the stream.
16-06-04 18:00	Cloudy all day. Light snowfall. More water.
17-06-04 06:30	Cloudy and windy. Less water.
17-06-04 18:20	Less clouds, slight wind.
18-06-04 06:00	Much more water.
19-06-04 06:00	Cloudy, no wind.
19-06-04 18:00	Cloudy but occasionally sun. More water.
20-06-04 06:00	Fog. More water.
20-06-04 18:00	Cloudy.
21-06-04 21:00	Heavy rainfall.
21-06-04 22:00	Rainfall but less heavy.
21-06-04 23:00	Light rainfall.

Date and time	Notes
22-06-04 00:00	No rain.
22-06-04 01:00	
22-06-04 02:00	Light rainfall.
22-06-04 03:00	Heavy rainfall.
22-06-04 04:00	Heavy rainfall.
22-06-04 05:00	Rain stopped, but still cloudy.
22-06-04 06:00	Cloudy
22-06-04 07:00	Cloudy. The time of lowest water levels in the stream.
22-06-04 08:00	Cloudy but occasionally sun. More water.
22-06-04 09:00	Cloudy.
22-06-04 10:00	Cloudy.
22-06-04 11:00	Cloudy.
22-06-04 12:00	Cloudy.
22-06-04 13:00	Cloudy.
22-06-04 13:30	Cloudy.
22-06-04 14:00	
22-06-04 15:00	
22-06-04 16:00	Sunshine.
22-06-04 17:00	Sunshine.
22-06-04 18:00	More water.
22-06-04 19:00	More water.
22-06-04 20:00	Sunshine.
23-06-04 00:00	Cloudy.
23-06-04 04:00	Cloudy but occasionally sun.
23-06-04 08:00	Cloudy.
23-06-04 12:00	Rainfall from 08:00 until now. Cloudy.
23-06-04 16:00	Nice weather, sunshine for the last couple of hours. Now cloudy.
23-06-04 20:00	Cloudy.
24-06-04 00:00	Cloudy.
24-06-04 04:00	Cloudy.
24-06-04 08:00	Cloudy.
24-06-04 12:00	Cloudy.
24-06-04 16:00	Cloudy.
24-06-04 20:00	Cloudy, slight rainfall.
26-06-04 11:30	Cloudy.
27-06-04 18:00	Sunshine.
28-06-04 06:00	Cloudy, rainfall last evening.
28-06-04 18:00	Cloudy. Wind.
29-06-04 06:00	Cloudy. Wind.
29-06-04 18:00	Cloudy. Wind. Occasional sunshine.
01-07-04 18:00	Cloudy, light rainfall.
03-07-04 06:00	Sun, strong wind. A lot more water in the river.
05-07-04 06:00	Light cloud cover, no wind. Normal river.
06-07-04 18:30	Cloudy, light wind. Same amount of water.
08-07-04 05:30	Low, dense fog. No wind. Less water.
09-07-04 20:30	Low clouds, fog. Light wind. Normal river.
10-07-04 20:00	Cloudy, no wind. Same amount of water.
11-07-04 18:15	Sunshine, clear sky, no wind. Same amount of water.
12-07-04 08:15	Sunshine, clear sky, no wind. Same amount of water.
12-07-04 18:15	Sunshine, clear sky, no wind. More water.

Date and time	Notes
13-07-04 18:00	Sunshine, clear sky, no wind. Same amount of water.
14-07-04 06:00	No wind. Fog from Nybyen and up. Less water.
14-07-04 19:00	No wind. Sunshine. More water.
15-07-04 06:00	No wind. Sunshine now and all night. Slightly less water.
16-07-04 06:00	No wind. Cloudy.
16-07-04 18:00	Cloudy. Strong wind.
17-07-04 17:45	No wind.
18-07-04 06:00	
18-07-04 18:00	Cloudy, but sunshine earlier.
21-07-04 18:00	Cloudy. Rainfall earlier in the day.
22-07-04 06:00	Cloudy. Slight rainfall.
22-07-04 18:00	Cloudy. Occasional sunshine.
23-07-04 06:00	Cloudy. Occasional sunshine.
23-07-04 18:00	Sunshine. More water
24-07-04 06:00	Fog. Cloudy. Less water in the stream.
24-07-04 18:00	Cloudy. Occasional sunshine. Much more water.
25-07-04 06:00	Clear sky. No wind. Almost as much water as last night.
25-07-04 18:00	Clear sky. Much more water.
26-07-04 06:00	Cloudy. No wind. Less water, but still more than normal. Rain just started falling.
26-07-04 18:00	Heavy rainfall since this morning. Now sunshine. Much water in the river.
27-07-04 06:00	Light cloud cover, occasionally sun. Still much water in the river.
27-07-04 10:00	Light cloud cover, occasionally sun. Less water.
27-07-04 14:00	Cloudy
27-07-04 18:00	Cloudy. Less water.
27-07-04 22:00	Cloudy. Wind. More water.
28-07-04 02:00	Clear sky. Still much water in the river.
28-07-04 06:00	Big, dark clouds. Wind. Still much water in the stream, but less than before.
28-07-04 07:00	Cloudy. Slight rainfall. Snow on the top of Nordenskiöld. More water.
28-07-04 08:00	Several rainfalls but occasionally sunshine. Not snow on Nordenskiöld anymore. More water.
28-07-04 09:00	Strong wind. Slight rainfall but interrupted by periods of sunshine. More water.
28-07-04 10:00	Wind. Cloudy. More water.
28-07-04 11:00	Cloudy. Same amount of water.
28-07-04 12:00	Cloudy. Windy. Fog on Longyearbreen.
28-07-04 13:00	Rained the last hour. Fog on Longyearbreen.
28-07-04 14:00	Heavy rain. More water.
28-07-04 15:00	Even heavier rainfall. More water.
28-07-04 16:00	Rainfall. Slightly less water in the river.
28-07-04 17:00	Rainfall. Same amount of water in the river.
28-07-04 18:00	Break in the rain. Clearing. Fog disappearing from Longyearbreen. Less water.
28-07-04 19:00	Cloudy. No rain. Slightly less water in the river.
28-07-04 20:00	Cloudy. Less water.
28-07-04 21:00	Cloudy.
28-07-04 22:00	Cloudy. Rainfall. Windy.
28-07-04 23:00	Now light rainfall but heavy showers of rain during the last hour. More water.
29-07-04 00:00	Sky clearing.
29-07-04 01:00	Clear sky. Less water.
29-07-04 02:00	Clear sky. Less water.
29-07-04 03:00	Clear sky.
29-07-04 04:00	Dark clouds approaching. Still sunny though.
29-07-04 05:00	Cloudy. Light rainfall.

Date and time	Notes
29-07-04 10:00	Cloudy. Light rainfall.
29-07-04 14:00	Heavy rainfall the last couple of hours. Much more water
29-07-04 18:00	Heavy rainfall and strong wind until now. Less wind and rain now. More water.
29-07-04 22:00	Rain.
30-07-04 02:00	Rained until 24:00. Now it seems to be clearing.
30-07-04 06:00	Clearing over the tent, but dark in Longyeardalen.
30-07-04 18:00	Nice weather, light clouds and wind.
01-08-04 18:00	
02-08-04 18:00	Cloudy. Light rainfall. Windy.
03-08-04 18:00	Cloudy. Ocassional sunshine.
10-08-04 12:00	Cloudy, no wind. Significantly less water.
11-08-04 00:00	Rained most of the day.
11-08-04 12:00	Cloudy. Less water.
12-08-04 12:00	Sunshine yesterday in the evening. Now cloudy. Small amount of water.
13-08-04 00:00	Clouds, but sunny. Less water.
13-08-04 12:00	Sunshine and no wind. Same amount of water.
14-08-04 00:00	Clear sky.
14-08-04 12:00	Sun
15-08-04 00:00	Sun all day but now cloudy.
15-08-04 12:00	Sunshine.
16-08-04 00:00	Cloudy, but occasionally sun.
16-08-04 18:00	Sun.
18-08-04 10:00	Cloudy, no wind.
18-08-04 16:00	Cloudy, no wind. Ligt rainfall at 13:00.
07-09-04 00:00	Foggy all day. Rain.
07-09-04 12:00	Cold, windy. Snow on the mountains.
08-09-04 00:00	Cold, clear sky.
08-09-04 12:00	Meltwater stream almost frozen over.
09-09-04 00:00	Cloudy, no wind.
09-09-04 12:00	High clouds, sunny. 1/2 cm new snow. Almost no water. More water in the western meltwater stream.
10-09-04 00:00	Cloudy, no wind.
10-09-04 12:00	Snow. Strong wind going home.
11-09-04 12:00	No water at the usual sampling site. Water still present right in front of the moraine cave.
12-09-04 12:00	High clouds, no wind, nice weather. No water in the eastern stream. Still water in the western stream.

A.7 SSC in western and eastern meltwater stream

A comparison between suspended sediment concentrations in river water in the western and eastern meltwater stream emerging from Longyearbreen is seen in figure A.6.1. No ambiguous result can be drawn from the figure as SSC were similar four out of six times but differed significantly for the last two.

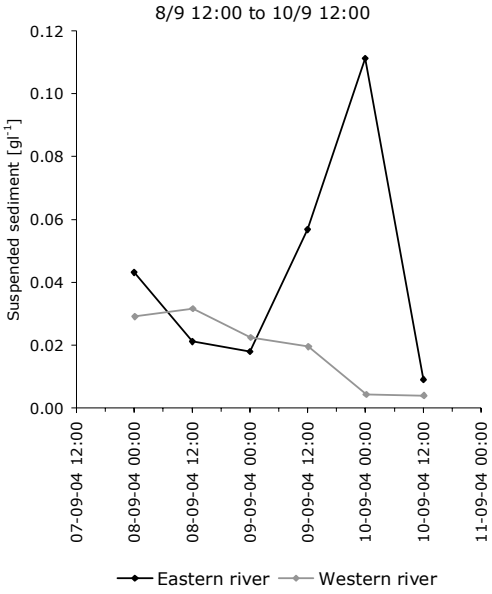

Figure A.7.1. Suspended sediment concentrations in river water in the eastern and western meltwater stream of Longyearbreen over two days.

A.8 Calculation of total sediment flux

The area under the graph on figure A.8.1 was used to calculate the total sediment flux from Longyearbreen during the ablation period. Arrows indicate episodes where the sediment yield was overestimated due to low data coverage.

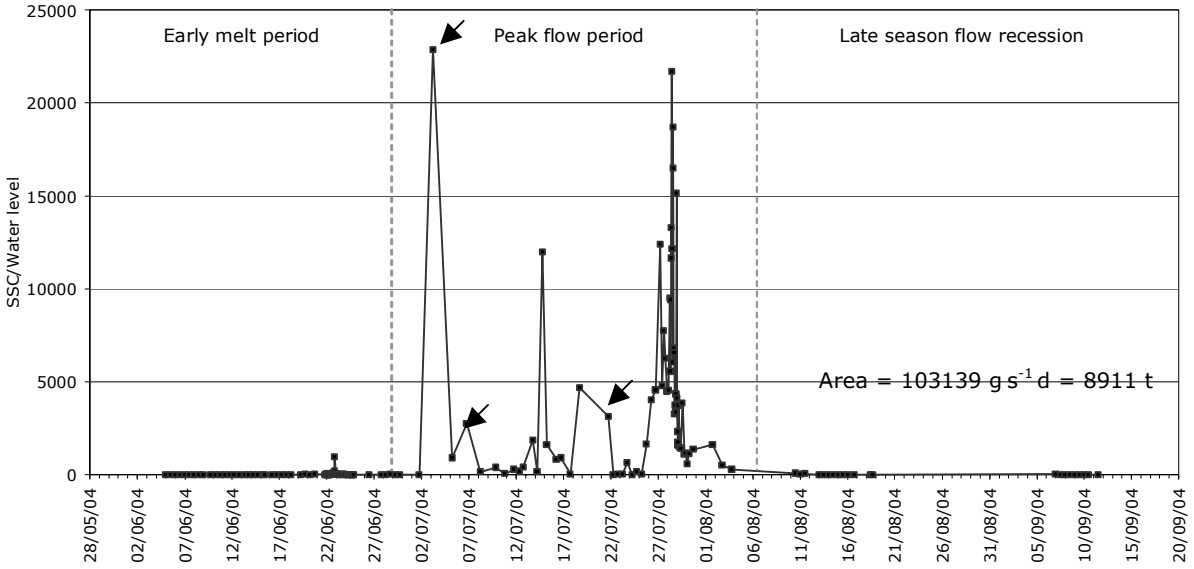

Figure A.8.1. Variations in sediment yield [g s^{-1}] during the ablation period.

A.9 Correlation coefficients

Figures A.9.1, A.9.2 and A.9.3 show the correlation coefficients (R) between ion concentrations, SSC, conductivity and water level for the three sub-periods in the ablation period. The relationships shown here are linear. A coefficient value of 1.00 signifies a perfect linear relationship between the two data sets. Negative correlation coefficients indicate a negative relationship.

Table A.9.1. Correlation coefficients for the early melt period. Cond. = conductivity, w. l. = water level and SSC = suspended sediment concentrations.

	Cl^{-1}	NO_3^-	SO_4^{2-}	HCO_3^-	K^+	Na^+	Ca^{2+}	Mg^{2+}	Si	SSC	Cond.	W. l.
Cl^{-1}	-	0.46	0.46	-0.40	0.68	0.46	0.50	0.47	0.74	-0.39	0.79	-0.53
NO_3^-		-	0.99	-0.55	0.95	0.98	0.98	0.99	0.89	-0.37	0.98	-0.59
SO_4^{2-}			-	-0.56	0.94	0.98	0.99	1.00	0.87	-0.37	0.99	-0.60
HCO_3^-				-	-0.50	-0.50	-0.47	-0.52	-0.47	0.26	-0.07	0.38
K^+					-	0.92	0.95	0.95	0.96	-0.45	0.99	-0.64
Na^+						-	0.97	0.98	0.84	-0.32	0.94	-0.53
Ca^{2+}							-	0.99	0.89	-0.39	0.93	-0.61
Mg^{2+}								-	0.88	-0.38	0.99	-0.62
Si									-	-0.50	0.93	-0.27
SSC										-	-0.39	0.65
Cond.											-	-0.56
W. l.												-

Table A.9.2. Correlation coefficients for the peak flow period. Cond. = conductivity, w. l. = water level and SSC = suspended sediment concentrations.

	Cl^{-1}	NO_3^-	SO_4^{2-}	HCO_3^-	K^+	Na^+	Ca^{2+}	Mg^{2+}	Si	SSC	Cond.	W. l.
Cl^{-1}	-	0.19	0.41	0.41	0.50	0.41	0.52	0.48	0.32	0.19	0.39	0.09
NO_3^-		-	0.92	0.18	0.57	0.91	0.77	0.86	-0.45	-0.23	0.94	-0.05
SO_4^{2-}			-	0.33	0.76	0.99	0.91	0.96	-0.29	-0.06	0.98	0.08
HCO_3^-				-	0.77	0.28	0.70	0.58	0.42	0.78	0.19	0.33
K^+					-	0.73	0.92	0.87	0.15	0.44	0.68	0.35
Na^+						-	0.87	0.92	-0.32	-0.13	0.98	0.07
Ca^{2+}							-	0.98	-0.01	0.32	0.84	0.23
Mg^{2+}								-	-0.11	0.18	0.91	0.16
Si									-	0.57	-0.37	0.11
SSC										-	0.48	0.30
Cond.											-	0.03
W. l.												-

Table A.9.3. Correlation coefficients for the late season flow recession. Cond= conductivity, w. l. = water level and SSC = suspended sediment concentrations.

	Cl^{-1}	NO_3^-	SO_4^{2-}	HCO_3^-	K^+	Na^+	Ca^{2+}	Mg^{2+}	Si	SSC	Cond.	W. l.
Cl^{-1}	-	0.62	0.72	0.67	0.71	0.69	0.71	0.74	0.82	-0.62	0.75	-0.41
NO_3^-		-	0.98	0.82	0.98	0.96	0.98	0.97	0.71	-0.56	0.67	-0.40
SO_4^{2-}			-	0.81	0.99	0.98	1.00	0.99	0.76	-0.63	0.78	-0.50
HCO_3^-				-	0.82	0.77	0.83	0.86	0.71	-0.44	0.67	-0.32
K^+					-	0.99	0.98	0.99	0.82	-0.66	0.80	-0.46
Na^+						-	0.97	0.97	0.77	-0.71	0.87	-0.66
Ca^{2+}							-	0.99	0.74	-0.59	0.75	-0.47
Mg^{2+}								-	0.77	-0.61	0.75	-0.48
Si									-	-0.72	0.67	-0.17
SSC										-	-0.40	0.69
Cond.											-	-0.42
W. l.												-

A.10 Solute content in western and eastern meltwater stream

The difference between the solute content in water draining from Longyearbreen in the eastern (sampling site) and western ("WMS*" on figure 4.9) meltwater stream is illustrated by the two graphs in figure A.9.1 (note the difference in scale). Solute concentrations in the eastern stream are shown with the solid line, while concentrations in the western stream are indicated by the dashed line. The two streams generally had similar ionic composition with NO_3^- and Cl^- showing the largest difference in values proportional to the total concentration. In the end of the period the eastern stream had NO_3^- values about twice as high as those measured in the western stream, while Cl^- concentrations were constantly about 50% higher in the western stream. SO_4^{2-}, Mg^{2+} and Ca^{2+} had the largest concentrations in the western stream to begin with, while the opposite was the case in the end of the period.

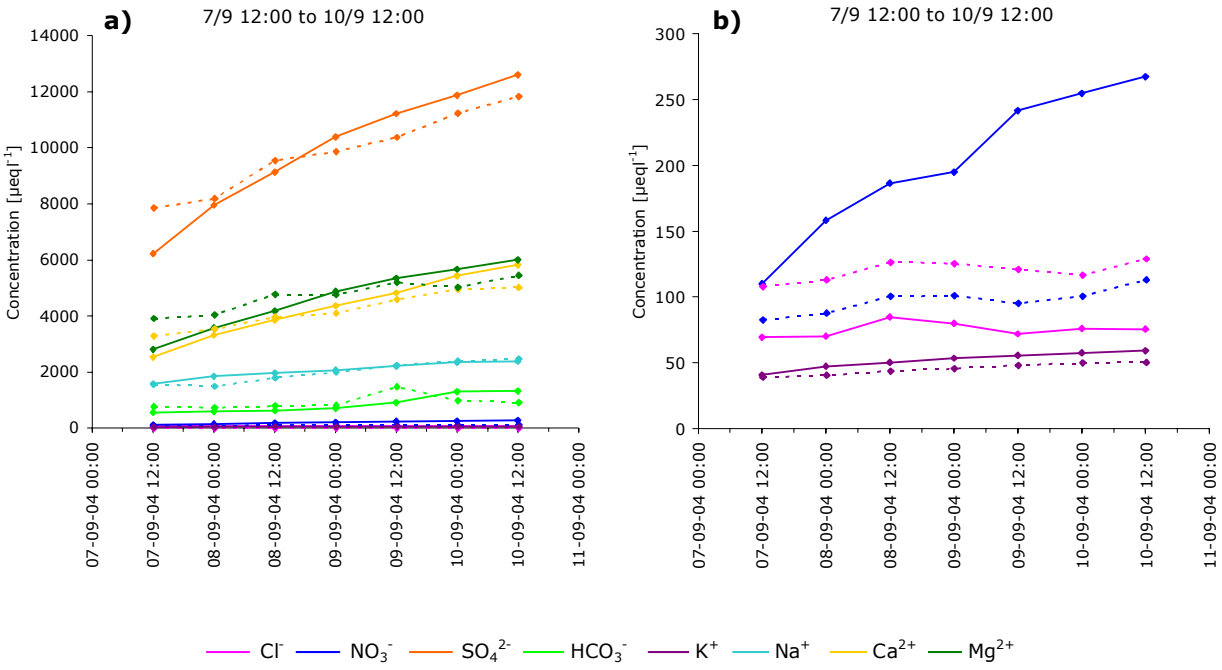

Figure A.10.1. Comparison between the chemical composition of meltwater from the eastern stream (solid line) and meltwater from the western stream (dashed line). a) Variations in the major ions and b) variations in ions with low concentrations.

A.11 Solute acquisition in the proglacial areas

The change in solute content of the meltwater from Longyearbreen was investigated from 13 August to 15 August (figure A.11.1). Samples were collected at three localities: the sampling site, after meltwater from the eastern and western meltwater stream confluence ("LE" on figure 4.9) and just before water from Larsbreen meets Longyearelva ("LE*" on figure 4.9). In general, the samples did not differ significantly from each other. There was however, a trend towards a slight increase in concentrations as the water flowed in the river, except for Na^+ and NO_3^- where samples from the sampling site usually had the highest concentrations measured.

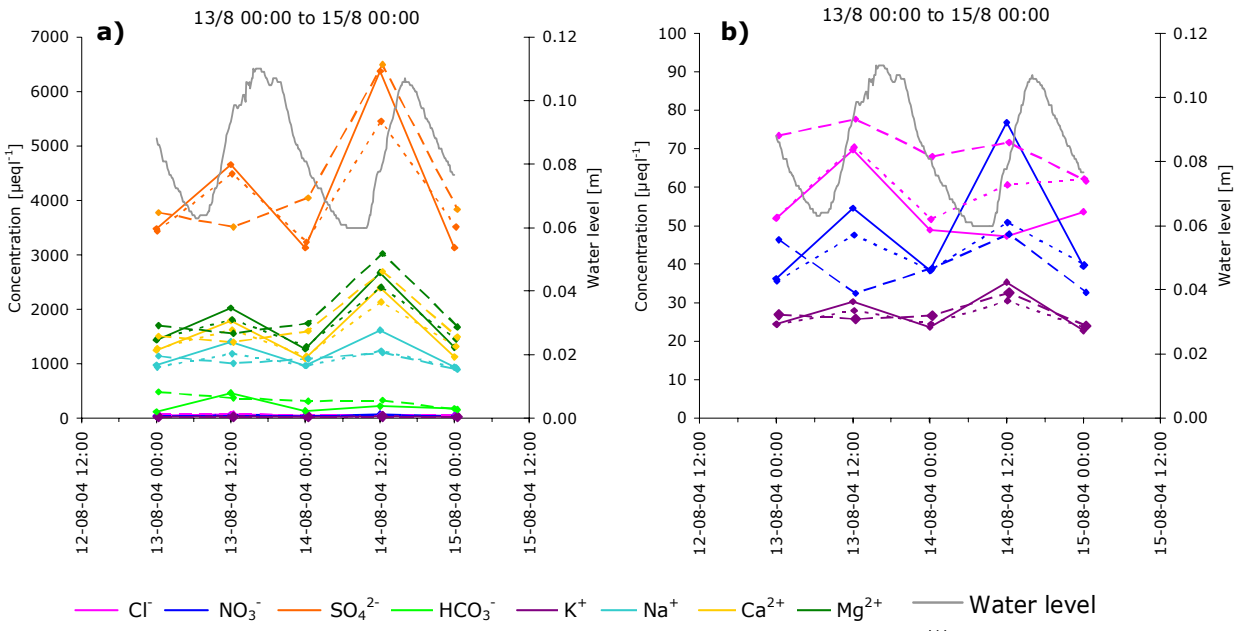

Figure A.11.1. The change in chemical composition of meltwater as it flowed down stream. The figure shows water from the sampling site (solid line), water from after the eastern and western meltwater stream had confluenced in front of Longyearbreen (dashed line) and water from Longyearelva just before it confluenced with Larselva (long dashed line). a) Variations in the major ions and b) variations in ions with low concentrations.

A.12 Conductivity versus total solute content

The relationship in the river meltwater between conductivity measured at the time of sampling, and total solute content obtained by analyses between 2½ and 6 months later, were investigated in order to evaluate the possible change in chemical composition of the meltwater prior to filtration (see figure A.12.1). Apart from three data points that were excluded, there was a very good correlation between the two datasets (R^2 = 0.9753). The three conductivity measurements that did not correlate with the rest of the data set were the last three measurements to be conducted. Unlike for the rest of the data set these measurements were conducted using a different instrument that was probably out of order.

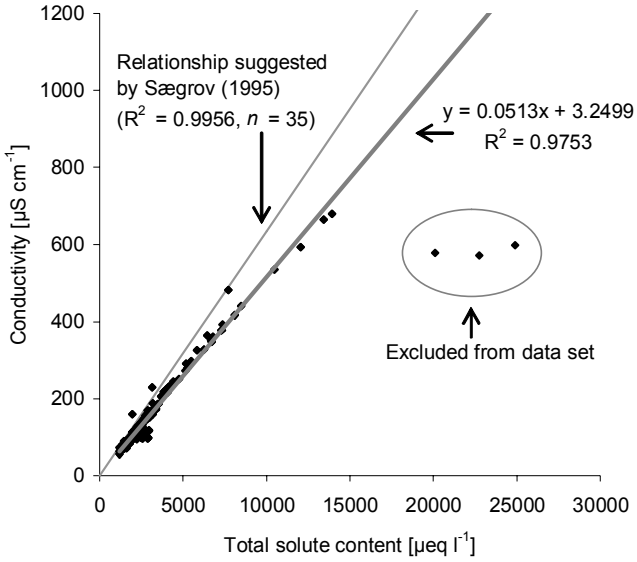

Figure A.12.1. The relationship between measured conductivity and total solute content in the river meltwater. Three measurements were excluded from the dataset. The light grey line indicates the relationship calculated by Sægrov (1995) for meltwater from Longyearbreen.

The discrepancy between the two curves was not constant and varied between 0 and 200 µS cm^{-1}. This equals a maximum difference in total solute content of about ~ 3500 µeq l^{-1}.

A.13 GPR survey, 1993

Figure A.13.1 shows the position of the survey lines from the 1993 study compared to the position of the survey lines in 2004. The positions of the individual lines correlated well and generally, the survey lines were no more than 25 m apart.

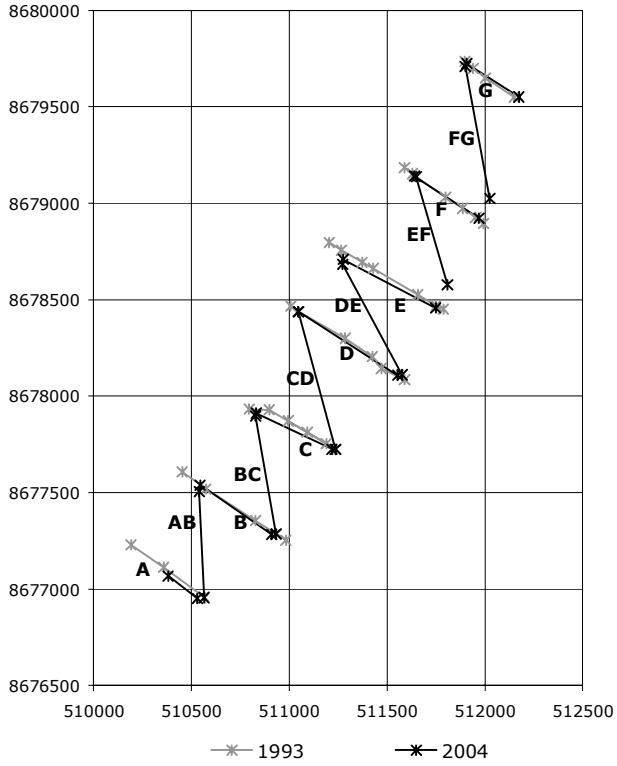

Figure A.13.1. The position of GPR survey lines in 1993 (Tonning, 1996) and 2004 (UTM coordinates are in datum ED50).

Ice depth measurements in radar profiles from the GPR survey conducted on Longyearbreen in 1993 (Tonning, 1996) are shown in figure A.13.2. Radar wave velocity was 0.167 m ns^{-1} for this study as opposed to 0.17 m ns^{-1} in 2004. This results in an estimation of ice thicknesses about 1.2 m thinner at 100 m depth for the study in 1993 compared to the study in 2004.

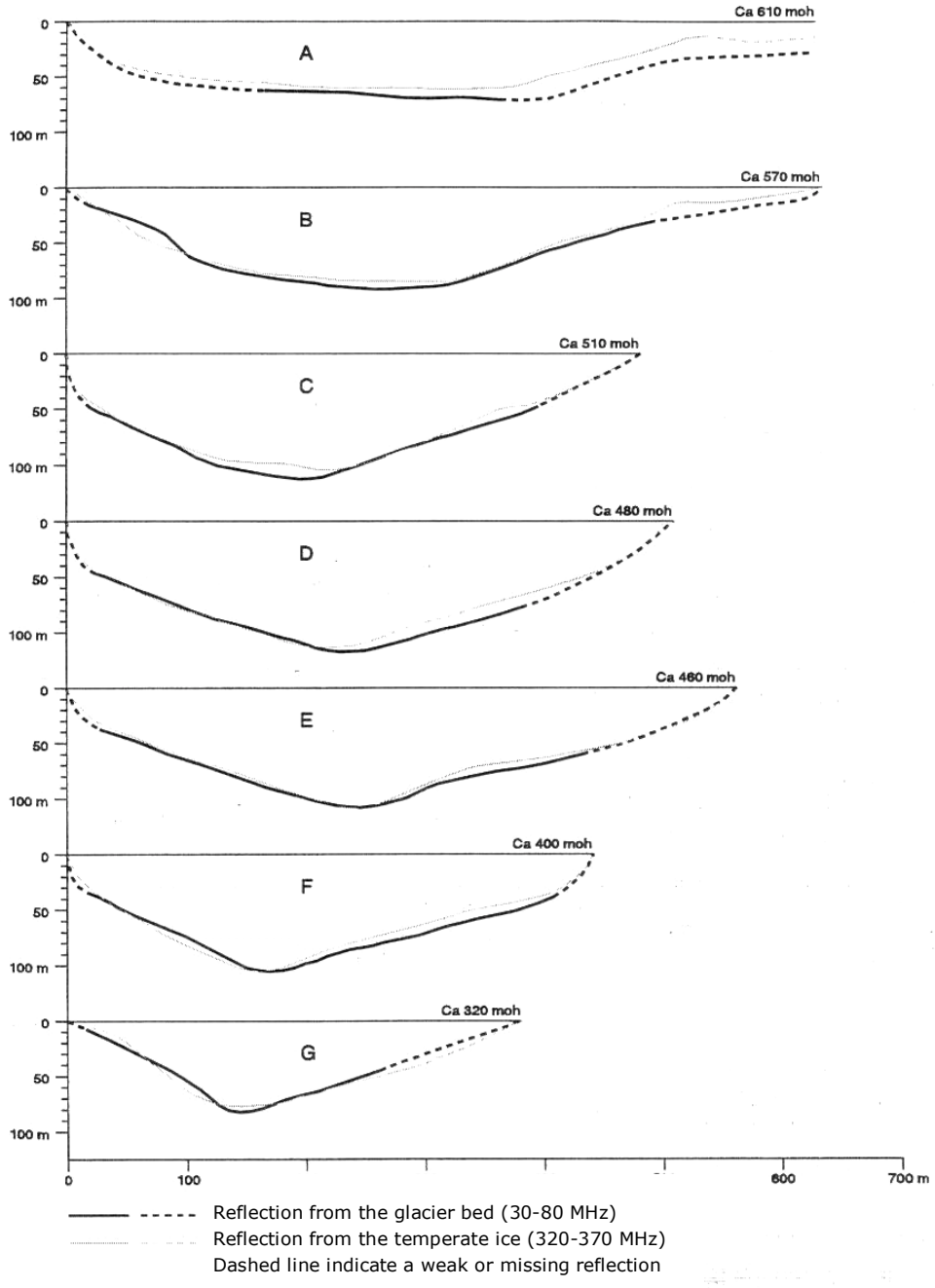

Figure A.13.2. Ice thicknesses measured in the GPR survey conducted on Longyearbreen in 1993 (Tonning, 1996).

A.14 Monthly air temperature and precipitation levels, 1995-1997 and 2004

Figure A.14.1 compares monthly air temperature and precipitation amount for the accumulation and ablation periods of 1995, 1996, 1997 and 2004. The four ablation seasons had similar air temperatures, although 2004 was generally warmer. Winter precipitation (Oct.-Apr.) was higher for the accumulation periods 1995-1996 and 2003-2004 with 161 and 106 mm respectively, compared to 1994-1995 and 1996-1997 with 62 and 84 mm respectively. Summer precipitation (May-Jul.) was high for 2004 (72 mm) while 1995, 1996 and 1997 had similar values of 52, 56 and 58 mm respectively.

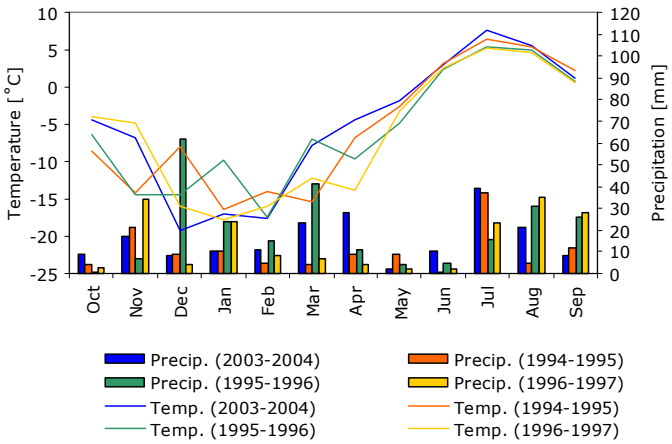

Figure A.14.1. Monthly air temperature and precipitation data from the meteorological station at Longyearbyen Airport (Grønsten, 1998 and http://met.no/).

A.15 Snow samples from Tellbreen

Table A.15.1 lists mean values for ionic and isotopic composition of snow samples collected in a snow pit on the nearby Tellbreen in the spring of 2004. Snow samples had higher concentrations of sea-salt derived ions Cl^- and Na^+ than those measured in the snowpack on Longyearbreen despite the slightly more inland position of this glacier.

Table A.15.1. Mean values of ionic and isotopic composition of snow samples from Tellbreen.

	Cl^-	NO_3^-	SO_4^{2-}	HCO_3^-	K^+	Na^+	Ca^{2+}	Mg^{2+}	$\delta^{18}O$
Mean	111	9.5	30	-	2.4	88	9.7	21	-12.7
SD	90	11	27	-	1.7	71	3.7	17	3.6
n	5	3	5	-	5	5	5	5	5

A.16 Comparison of solute in river meltwater in 1993 and 2004

Figure A.16.1, A.16.2, A.16.3 and A.16.4 show variations in total solute content, Cl^- ,SO_4^{2-} and HCO_3^- concentrations during the ablation period 1993 and 2004.

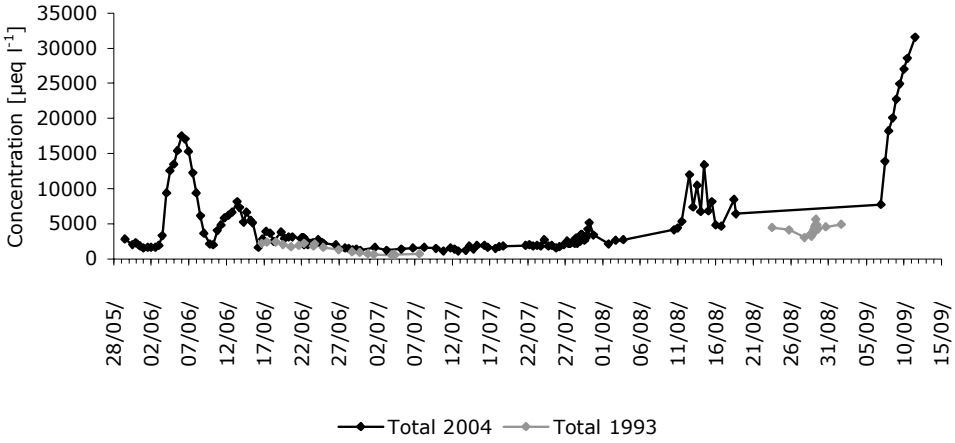

Figure A.16.1. Variations in total solute content in river meltwater in 1993 and 2004.

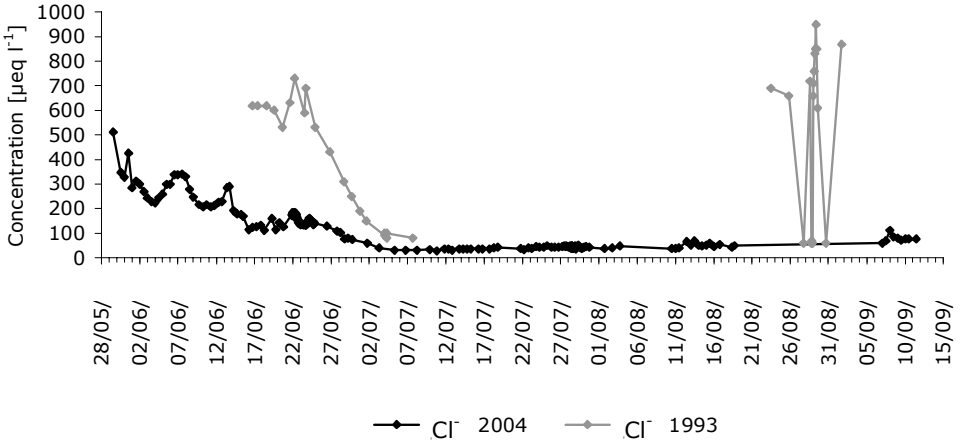

Figure A.16.2. Variations in Cl^- concentrations in river meltwater in 1993 and 2004.

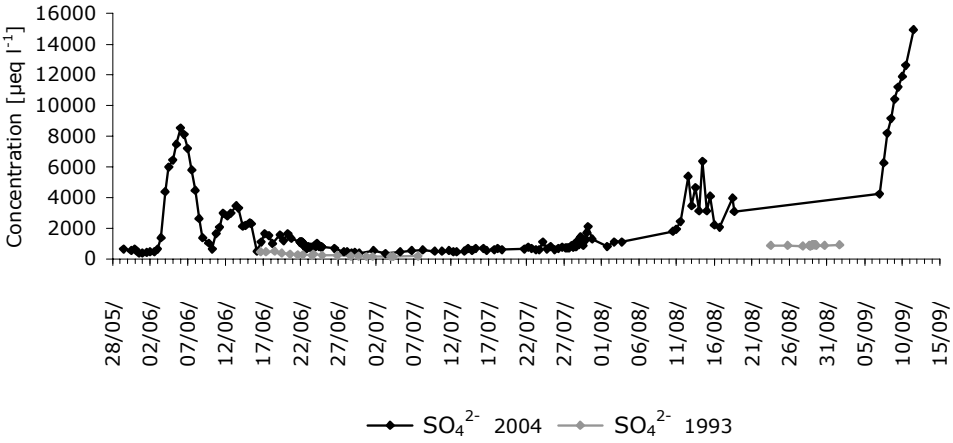

Figure A.16.3. Variations in SO_4^{2-} concentrations in river meltwater in 1993 and 2004.

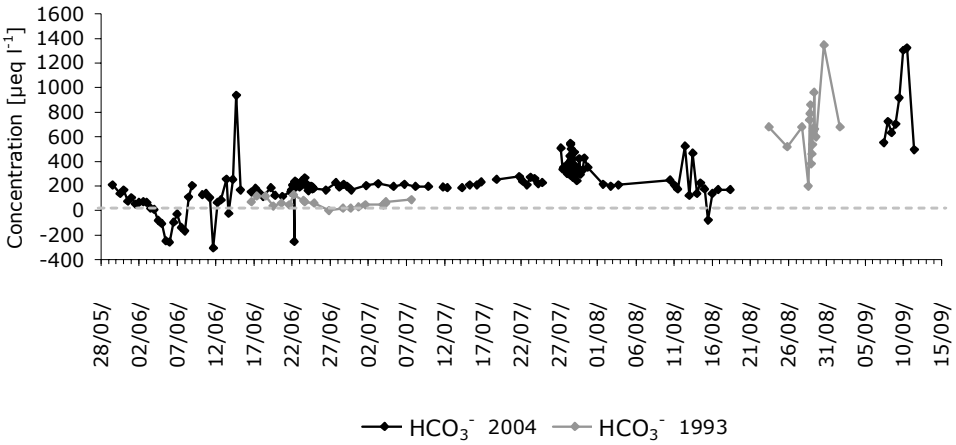

Figure A.16.4. Variations in HCO_3^- concentrations in river meltwater in 1993 and 2004.

A.17 Solute flux for Longyearbreen

Flux calculations for the ablation period of 2004 were carried out by Yde et al. (in prep.) by log-log regression between discharge and solute concentrations over different time intervals during the ablation period (5 June – 8 September). Table A.17.1 lists estimates of solute flux for the entire ablation period and the three sub-periods, together with the correlation coefficients between the model and measured ion concentrations.

Table A.17.1. Flux calculations and correlation coefficients between the model and measured ionic concentrations (Yde et al., in prep.). Also listed is the snowpack derived fraction of each ion obtained by the relationship between the ions and Cl^- in the snowpack.

	Cl^-	NO_3^-	SO_4^{2-}	HCO_3^-	K^+	Na^+	Ca^{2+}	Mg^{2+}
Flux [kg]								
Early melt period	315	72	2331	776	39	479	457	311
Peak flow period	4604	1128	101224	51882	2050	17405	21899	14317
Late season flow recession	438	294	23693	5433	189	2887	4326	2824
Total	5357	1494	127248	58091	2277	20771	26681	17452
Correlations coefficient (R)								
Early melt period	0.75	0.89	0.87	-0.02	0.87	0.85	0.89	0.88
Peak flow period	0.60	0.36	0.88	-0.10	0.08	0.67	0.56	0.56
Late season flow recession	0.80	0.89	0.88	0.86	0.86	0.83	0.91	0.91
Flux, snowpack derived [kg]	5357	482	2410	1500	161	4286	3536	1392

Table A.17.2 shows total and diurnal solute flux for the 1994 ablation period. The values have been calculated based on the flux calculations presented in table A.17.1.

Table A.17.2. Total and diurnal flux calculations based on table A.17.1.

	Total solute flux [t]	Diurnal solute flux [$t\,d^{-1}$]
Early melt period	4.8	0.2
Peak flow period	214.5	4.4
Late season flow recession	40.1	1.3
Total	259.4	2.7